VNIVERSITAT DE VALÈNCIA

Facultat de Química

MINIATURIZED LIQUID CHROMATOGRAPHY: FROM LAB TO PORTABLE TOOL FOR ENVIRONMENTAL, BIOLOGICAL AND NANOPARTICLES SAMPLES

Thesis presented to obtain the PhD degree under the “Doctorado en Química (R.D. 99/2011)

Sergio Cortés Bautista

Supervisors:

Profa. Dra. Pilar Campíns Falcó

Profa. Dra. Carmen Molins Legua

Valencia, july 2023

VNIVERSITAT DE VALÈNCIA Facultat de Química

DEPARTAMENTO DE QUÍMICA ANALITICA

Dra. Pilar Campíns Falcó y Dra. Carmen Molins Legua, ambas Catedráticas del Departamento de Química Analítica de la Facultad de Química de la Universidad de Valencia.

CERTIFICAN

Que la presente memoria titulada “Miniaturized liquid chromatography: from lab to portable tool for environmental, biological, and nanoparticles samples”, constituye la Tesis Doctoral de Sergio Cortés Bautista para optar al grado de Doctor en Química, que ha sido realizada en los laboratorios del Departamento de Química Analítica de la Universitat de Valencia, bajo nuestra dirección y supervisión.

Y para que así conste a los efectos oportunos, firman el presente certificado en Valencia, a 28 de julio de 2023

CAMPINS FALCO, MARIA PILAR (FIRMA)
Firmado digitalmente por CAMPINS FALCO, MARIA PILAR (FIRMA)
Fecha: 2023.07.28 13:54:13 +02'00'

MOLINER MARTINEZ, YOLANDA (FIRMA)
Firmado digitalmente por MOLINER MARTINEZ, YOLANDA (FIRMA)
Fecha: 2023.07.28 14:20:30 +02'00'

Fdo. Dra. Pilar Campíns Falcó
Directora de la tesis

Fdo. Carmen Molins Legua*
Codirectora de la tesis

*Firmado en su lugar por Yolanda Moliner Martínez (directora del departamento de Química Analítica) por baja laboral.

This thesis was carried out within the MINTOTA research group in the Department of Analytical Chemistry at the University of Valencia. Additionally, a three-month research stay took was successfully conducted at the Centre for Microbiology and Environmental System Science in the Department of Environmental Geosciences at the University of Vienna.

The completion of the thesis has been possible thanks to the financial support provided by the Ministry of Science and Innovation in the form of a predoctoral grant (PRE2018-086709).

VNIVERSITAT DE VALÈNCIA

universität wien

Agradecimientos

A través de estas líneas, me gustaría expresar mi sincero agradecimiento a todos aquellos que han sido parte fundamental en el desarrollo de esta investigación y en mi trayectoria académica.

Quisiera comenzar expresando mi más sincero agradecimiento a mis directoras, Pilar y Carmen, por confiar en mi desde el primer momento brindarme la oportunidad de formar parte del equipo de MINTOTA. Su dedicación y voluntad para compartir sus conocimientos han sido de gran ayuda en cada etapa de mi desarrollo académico. En esta línea, también quería agradecer a Rosa y Yolanda que siempre han estado ahí, dispuestas a colaborar y ayudar en todo lo posible.

Así mismo, agradezco a Frank y al resto de compañeros del “Deparment of Environmental Geosciences” en Viena por abrirme las puertas a su grupo de investigación durante mi estancia doctoral.

También quiero expresar mi agradecimiento a mis compañeros y amigos de trabajo, tanto de MINTOTA como de GIGAPC, por haber contribuido a crear un ambiente laboral excepcional. Que lo que “los gatos” ha unido no lo separe el hombre.

Del mismo modo, quiero agradecer de corazón a mi familia y amigos quienes han sido una fuente inagotable de amor y compresión a lo largo de este camino. Gracias por estar siempre ahí.

Resumen

La conciencia pública acerca de los problemas ambientales y la salud ha aumentado notablemente en las últimas décadas. La sociedad muestra mayor preocupación por el medio ambiente y por el impacto negativo de sus prácticas en este, exigiendo así soluciones más sostenibles. Asimismo, los gobiernos y organizaciones internacionales están promoviendo políticas públicas que fomentan la adopción de enfoques sostenibles en la industria y otros sectores, estableciendo leyes y regulaciones ambientales cada vez más estrictas.

La química analítica ha tenido y tiene que adaptarse para cubrir estas nuevas necesidades, aproximándose a las bases y principios de la química sostenible y química verde. A pesar de que ambos enfoques tienen puntos de intersección, la química sostenible considera a su vez la conservación de los recursos naturales, los aspectos económicos y sociales relacionados con la producción y uso de procesos y productos químicos, mientras que la química verde esta más centrada en la reducción de la toxicidad y los residuos generados en los procesos químicos.

Dentro de las diferentes estrategias que la química analítica ha seguido para lograr metodologías más respetuosas con el medioambiente, la miniaturización de los procesos analíticos ha tenido especial relevancia debido a los grandes beneficios que ofrece, como el menor consumo de disolventes, reducción en la generación de residuos, menor coste económico, y simplicidad. A su vez, la miniaturización ha contribuido a la portabilidad de la instrumentación analítica, facilitando la transición de los equipos convencionales de laboratorio a equipos que permitan el análisis en el punto de necesidad e *in-situ.*

La cromatografía líquida (LC) es una técnica de separación fundamental en muchos métodos analíticos y particularmente en aquellos en los

que se trabaja con muestras de matrices complejas. La miniaturización en cromatografía líquida (minLC) parte de la reducción del diámetro interno de la columna analítica, y, por tanto, del resto de componentes del sistema cromatográfico. Surgió en el último tercio del siglo XX cuando se empezó a trabajar con columnas con diámetros internos inferiores a 1 milímetro y observando como a medida que se reducía el tamaño de la columna, la eficacia aumentaba. Desde entonces este campo se ha ido desarrollando hasta la actualidad, pudiendo encontrar columnas analíticas con diámetros internos de unas pocas decenas de micrómetros, trabajando a flujos del orden de microlitros o incluso nanolitros por minuto. Consecuencia directa de la miniaturización en LC, las cantidades de disolvente y muestra requeridos, así como de residuos generados son mínimos. Por otro lado, la reducción del diámetro interno supone una reducción de la difusión radial de los analitos en el sistema cromatográfico que se traduce en un aumento de la sensibilidad. Además, estos sistemas facilitan el acoplamiento con los detectores de masas (MS), mejorando la eficiencia de ionización cuando se emplean fuentes de ionización por electrospray (ESI). Existen diferentes niveles de miniaturización en LC que dependen del diámetro interno de la columna analítica, sin embargo, cuando se habla de minLC se suele hacer referencia concretamente a la LC capilar (capLC) y nano (nanoLC) que emplean columnas analíticas con diámetros internos con rangos comprendidos entre 0.5 – 0.15 mm y 0.15 – 0.01mm respectivamente. Estos dos tipos de LC se han utilizado en diversos campos como el análisis medioambiental, forense y alimentario. Sin embargo, la bioquímica ha sido el área que ha recibido mayor atención, especialmente en el caso de la nanoLC.

Uno de los problemas de la minLC son los pequeños volúmenes de inyección que admite. Se puede incrementar la sensibilidad aumentando el volumen de muestra procesado. Para ello se pueden utilizar técnicas de precolumnas acopladas (*switching column*) o la microextracción en fase sólida

en tubo (IT-SPME). En esta última, la fase extractiva se encuentra inmovilizada en un capilar (inicialmente a partir de un fragmento de una columna de cromatografía de gases). Estos capilares pueden obtenerse comercialmente con la fase extractiva inmovilizada o pueden utilizarse capilares de sílice fundida sin tratar para posteriormente sintetizar la fase en el laboratorio. La IT-SPME combina automatización con miniaturización, siendo a la vez sencilla, versátil, de bajo costo, y permitiendo un fácil acoplamiento a técnicas de LC. Actualmente la IT-SPME-LC es una técnica establecida y se pueden encontrar en la bibliografía aplicaciones para todo tipo de muestras como medioambientales, alimentarias, industriales, y forenses, entre otras. Por contra, el acoplamiento a minLC no se ha explorado en profundidad y su aplicación está más acotada a muestras ambientales. El binomio IT-SPME acoplado a minLC es una de las principales especializaciones del grupo “Miniaturización y Métodos Totales de Análisis” (MINTOTA), grupo en el cual se ha realizado esta tesis y que ha realizado valiosas contribuciones en este campo desde 2006. La IT-SPME-minLC es una técnica de gran interés ya que mejora la eficiencia de la columna analítica y la sensibilidad, permite etapas de lavado de la muestra, es fácilmente acoplada en línea, y reduce a su vez el consumo de disolventes y residuos generados.

Una aplicación llamativa de la IT-SPME acoplada en línea a minLC con detector de fila de diodos (DAD) es el estudio de dispersiones de nanopartículas metálicas (MNPs). En las MPNs la luz incidente provoca oscilaciones de la banda conductora de electrones dando lugar a la absorción de la luz en la región UV-vis del espectro. Este fenómeno es conocido como resonancia localizada del plasmón de superficie (LSPR) y puede ser medido mediante detectores ultravioleta-visible (UV-vis). El análisis de MNPs mediante IT-SPME-minLC-DAD da lugar a perfiles cromatográficos en los que se observan dos picos cromatográficos correspondientes a dos grupos de nanopartículas existentes en la dispersión. El primero de los picos corresponde con las MNPs polarizadas, las cuales presentan una débil interacción

con la fase extractiva del IT-SPME y su separación está gobernada por mecanismos de exclusión por tamaño en la columna analítica. Por otro lado, el segundo pico cromatográfico se corresponde con las NMPs no polarizadas que interactúan con la fase extractiva de IT-SPME por medio de un efecto hidrofóbico. Esto permite caracterizar las dispersiones en función de la relación de las áreas de ambos picos. Además, se ha demostrado como el área de los picos está relacionada con la concentración de las MNPs en la dispersión, permitiendo su cuantificación. En esta tesis se ha demostrado la capacidad de la IT-SPME-minLC-DAD en la caracterización de MNPs así como la posibilidad de utilizar la técnica para el seguimiento de ensayos plasmónicos.

La miniaturización ha permitido el desarrollo de equipos de LC portátil que permiten el análisis de muestras complejas en el punto de interés, como por ejemplo en el control de aguas medioambientales o en ensayos clínicos donde una respuesta a tiempo real ayuda a establecer un diagnóstico rápido. A diferencia de otros instrumentos portátiles como los electroquímicos o los espectrofotométricos, estos han evolucionado lentamente debido a las dificultades relacionadas con la miniaturización de sus componentes, particularmente de los sistemas de bombeo que deben generar flujos muy pequeños y estables, a la vez que deben soportar las presiones generadas por la columna analítica.

Los primeros equipos de LC portátil fueron introducidos en la década de 1990, sin embargo, estos no cumplen con los requisitos actuales para ser considerados instrumentación portable. No fue hasta esta última década cuando surgió una nueva ola de LC portátiles con características acordes a la idea contemporánea de portabilidad. La mayoría de estos sistemas han sido desarrollados en el laboratorio y no han sido comercializados haciendo difícil su reproducción. En 2019, la compañía Axcend lanzó al mercado el

primer minLC portátil, el Axcend Focus LC con un sistema de cartuchos intercambiables que contienen el detector y la columna analítica. Desde la fecha de su lanzamiento se han publicado varios artículos en los que se estudian sus prestaciones en diferentes campos. En esta Tesis, el rendimiento de dicho equipo de minLC portátil ha sido evaluado y comparado con el de otros equipos de minLC de sobremesa.

El objetivo general de esta Tesis ha sido generar nuevo conocimiento entorno al binomio nanoescala-LC a través del acoplamiento IT-SPME a minLC (tanto capLC como nanoLC), demostrando las ventajas de la técnica en relación a la LC convencional. Para ello, se establecieron los siguientes objetivos específicos:

1) Desarrollar nuevas configuraciones para el acoplamiento en línea de la IT-SPME a minLC.
2) Demostrar los beneficios potenciales de las NPs como fases en el acoplamiento mencionado.
3) Proponer nuevas estrategias que aporten métodos de coste efectivo para evaluar contaminantes emergentes.
4) Dar evidencias de la sostenibilidad de la técnica en estudio a la vez que incluir la huella de carbono como figura de mérito de una metodología dada.
5) Demostrar como la miniaturización puede contribuir a la portabilidad de la LC.

Durante el desarrollo de la Tesis se ha estudiado la miniaturización enfocada a la LC aplicada al análisis de muestras medioambientales, biológicas, y nanopartículas. Los sistemas de cromatografía líquida miniaturizada se acoplaron en línea a microextracción en fase sólida en tubo (IT-SPME) empleando diferentes configuraciones. Del mismo modo, se han evaluado las posibilidades de la LC portátil para el análisis en el punto de necesidad

discutiendo sus fortalezas y debilidades. Además, se ha utilizado el criterio BETTER, propuesta por F. Rahimi et. al., y la herramienta HEXAGON, propuesta por el grupo MINTOTA, con el fin de evaluar la portabilidad en el primer caso, y los métodos propuestos desde un punto de vista de la química sostenible y verde en el segundo. Concretamente, se han estudiado las siguientes técnicas: IT-SPME-capLC-DAD, IT-SPME-nanoLC-DAD, y minLC-UV-LED portátil. Los resultados obtenidos durante la tesis se pueden clasificar en función de la matriz objeto de estudio ya sean medioambientales, biológicas o de nanopartículas.

Con respecto a las muestras medioambientales, se evaluó el rendimiento de un minLC portátil comercial con detector de diodo emisor de luz ultravioleta (LED UV) (255 nm) para el análisis de diferentes analitos de interés en muestras de agua y los resultados se compararon con los obtenidos mediante IT-SPME-capLC-DAD y IT-SPME-nanoLC-DAD de sobremesa. El minLC portátil ofreció cromatogramas con una mejor resolución de pico en un menor tiempo de análisis, permitiendo la detección de un mayor número de compuestos en ventanas de tiempo más cortas. Sin embargo, su sensibilidad es limitada en comparación con los equipos de sobremesa, además de que, al trabajar a una única longitud de onda, la identificación de los compuestos se basa únicamente en el tiempo de retención. Por otro lado, se estudió el impacto de diferentes parámetros ambientales como la humedad, temperatura, y viento en la respuesta cromatográfica. El criterio BETTER se utilizó para comparar el minLC portátil estudiado con otros desarrollados recientemente obteniéndose para algunos criterios resultados mejorados. De manera similar, se utilizó la herramienta HEXAGON para comparar desde el punto de vista de la sostenibilidad y la química verde los LC de sobremesa con el LC portátil obteniéndose resultados favorables para este último en el contexto de los análisis planteados.

Para demostrar la aplicabilidad de la técnica se analizaron diferentes biocidas en aguas residuales y otras aguas superficiales. En el primer caso se detectó y cuantificó sorbato potásico y pirimetanil, obteniéndose resultados comparables a los de los equipos de sobremesa. El imazalil, que fue cuantificado por IT-SPME-nano/capLC-DAD, no fue detectado mediante minLC portátil ya que este no absorbe a la longitud de onda del LED UV utilizado. Además, se analizaron muestras de aguas superficiales mediante minLC portátil con el fin de determinar los pesticidas diurón e isoproturon. Se optimizó una etapa previa de extracción en fase sólida que permitió alcanzar los valores de las normas de calidad ambiental establecidos por la legislación para ambos pesticidas, sin detectar ninguno de ellos en las muestras analizadas. En esas mismas aguas y en la línea con el análisis *in-situ* y a tiempo real de muestras ambientales, se estudiaron las posibilidades de un analizador para el seguimiento de nitrato en aguas de pozo, comparando los resultados con los obtenidos por una fibra óptica portátil y un espectrofotómetro de sobremesa. Las determinaciones se basaron en la medida de la absorbancia nativa del nitrato. Se determinaron nitratos en las aguas obteniéndose resultados similares a los proporcionados por el espectrofotómetro de sobremesa. No se observó influencia de la turbidez y los ácidos húmicos en las condiciones de trabajo. Como aplicación, se siguió la concentración de nitratos en una planta de tratamiento de aguas obteniéndose resultados adecuados y comparables a los proporcionados por la fibra óptica portátil.

La IT-SPME-nanoLC-DAD también se aplicó a muestras biológicas, más concretamente, a la determinación de paracetamol en muestras de orina. Se realizó un tratamiento mínimo de la muestra que consiste en la desproteinización en medio ácido, centrifugación, y extracción mediante SPE. Los resultados se compararon con los proporcionados por cromatografía líquida de ultra alto rendiminto (UHPLC) acoplada a un detector de

espectrometría de masas de tiempo de vuelo cuadrupolo (QTOF) con interfase de ionización por electrospray (ESI) y por análisis directo en tiempo real (DART) acoplado a QTOF. El paracetamol se determinó en la orina recogida a diferentes horas tras la ingesta de 1 g del compuesto. En comparación con el DART-QTOF, el IT-SPME-nanoLC-DAD y el UHPLC-ESI-QTOF proporcionaron una mayor sensibilidad y reproducibilidad. Sin embargo, el DART-QTOF permitió realizar el análisis en el menor tiempo. Con respecto a la cuantificación del paracetamol en las diferentes muestras de orina, se obtuvieron resultados comparables entre las técnicas estudiadas. Los tres equipos se compararon utilizando la herramienta HEXAGON concluyendo que la técnica IT-SPME-nanoLC-DAD es superior para esta aplicación, generando una menor cantidad de residuos, empleando menos reactivos, reduciendo la huella de carbono, y a un menor coste económico.

También, se demostró que es posible discriminar y asegurar la calidad de una dispersión dada de AgNPs y AuNPs para la realización de un ensayo plásmonico mediante IT-SPME-capLC-DAD y IT-SPME-nanoLC-DAD. El uso del IT-SPME permitió estudiar la proporción en la dispersión inicial de dos grupos de NPs, polarizadas y no polarizadas, en función de sus interacciones con la fase extractiva del IT-SPME, y cuya separación se explica mediante exclusión por tamaños y efecto hidrofóbico. Se estudió la degradación de dispersiones de AgNPs y AuNPs comerciales (tanto con recubrimientos de fosfato como citrato) en función del tiempo y de la concentración de ácido a partir de los perfiles cromatográficos obtenidos. La disminución en el área de los picos cromatográficos se relacionó con un desplazamiento del plasmón hacia longitudes de onda mayores, lo cual indica un fenómeno de agregación. En ambos casos, la estabilidad de las dispersiones de AuNPs fue superior a las de AgNPs. Se estudió la agregación inducida por espermina y ácido acético relacionándose la disminución del área de los picos cromatográficos con la concentración, obteniéndose una sensibilidad mayor a la proporcionada por espectroscopía UV-vis. Tanto la capLC

como la nanoLC acopladas a IT-SPME con DAD permitieron la medida del LSPR de AuNPs desnudas a partir de la relación entre las áreas de los picos cromatográficos, demostrando la posibilidad de determinar la funcionalidad de las dispersiones a partir de los perfiles cromatográficos en menos de 10 min en todos los casos.

Como aplicación, se determinó espermina en orina, como biomarcador de cáncer, mediante IT-SPME-capLC-DAD. La concentración de espermina se correlacionó linealmente con la disminución del área del pico cromatográfico permitiendo su cuantificación. Se determinaron orinas de voluntarios sanos y con cáncer, obteniéndose concentraciones de espermina en concordancia con la bibliografía.

Por último, con objeto de conocer mejor las transformaciones que tiene lugar en las AgNPs en sistemas medioambientales, se estudió la sulfuración y disolución en un sistema de flujo continuo bajo diferentes condiciones de flujo, fuerza iónica, oxígeno, y concentración de sulfuro. La presencia de sulfuro provocó un aumento inicial en la disolución de las AgNPs que se relacionó con la formación de una capa de Ag_2S amorfo, pues es más soluble que las AgNPs. Empleando flujos más altos y tiempos mayores, la disolución de las AgNPs en medio sulfuroso termina disminuyendo por debajo de la del ensayo sin sulfuro, lo que indica la formación del Ag_2S cristalino menos soluble. La presencia de oxígeno produce un aumento de la solubilidad de las AgNPs por la formación de una capa más soluble de Ag_2O alrededor de la nanopartícula. Para fuerzas iónicas superiores, obtenidas a partir de distintas concentraciones de $NaNO_3$, la disolución de las AgNPs disminuye, como consecuencia de la compresión de la doble capa eléctrica. Finalmente, el ensayo realizado a diferentes flujos mostró una correlación positiva con la disolución de las NPs.

Abstract

In the last years, the world is becoming more aware of the environmental issues and its impact on the planet, embracing more sustainable and environmentally friendly lifestyles. This has sparked a pressing need in various areas, including analytical chemistry, which must adapt its methodologies to align with this trend.

In this context, the miniaturization of LC is presented alternative to conventional LC systems, not only improving its performance and sensitivity, but also from an environmental point of view, reducing the solvents required, waste generated, and operational costs. It involves a scaling down of the dimensions of LC systems, including columns, flow rates, and detection systems. As a result, minLC has gained significant attention and holds great promise for various fields, including pharmaceutical analysis, biomedical research, and environmental monitoring. The advancements in miniaturization have made it possible to bring the portability to LC systems, which is particularly relevant for point-of-need determinations such point-of-care (POC) applications or environmental monitoring.

In the same vein, the miniaturization of sample treatment techniques Is progressively replacing conventional procedures which involves high number of steps and large volumes of solvents. Among the miniaturized sample preparation techniques, such as SPME, LLME, and microextraction by packed sorbent (MEPS), have been widely employed. IT-SPME is a type of SPME that combines miniaturization with automation, fulfilling various of the requirements of green ans sustainable analytical chemistry while allowing for easy coupling to minLC systems.

In the framework of development of this thesis, the capabilities of minLC, both nano and capLC, were studied for the analysis of different ma-

trices of analytical interest, including environmental, biological, and nanoparticles samples. For this purpose, the minLC was coupled on-line to IT-SPME demonstrating the potential benefits in terms of sensitivity, versatility, rapidity, solvent usage, and waste generation for the analysis of different environmental water and urine samples. Also, the technique has allowed the assessment of NPs from the chromatographic profiles for its usage in further monitoring of plasmonic assays and to follow also them, providing better selectivity and sensitivity than the monitoring by means of UV-vis spectrophotometry. Moreover, the possibilities the portable LC were evaluated and compared with LC systems. As for the comparative studies, the HEXAGON tool and the BETTER (portaBle fiEld Testing sTandard frameWoRk) criteria were employed for the evaluation of greenness and sustainability of the method and portability, respectively. Finally, the stability of the AgNPs in presence of several agents was studied in-flow in order to approximate to environmental conditions.

Index

p.

CHAPTER 1 : INTRODUCTION 1

1.1 The analytical context: recent trends 3

1.2 Miniaturized liquid chromatography 10

1.2.1 On-line sample treatment configurations 17

1.2.2 Miniaturization of detectors 22

1.3 Portable liquid chromatography 25

1.3.1 Instrumentation 34

1.3.1.1 Pumps 36

1.3.1.2 Injectors 38

1.3.1.3 Analytical columns 41

1.3.1.4 Detectors 42

1.3.2 Applications of portable LC 45

1.4 Studied matrices and analytes 46

1.4.1 Environmental samples 47

1.4.1.1 Pesticides *48*

1.4.1.2 Legislated nitrogen compounds 52

1.4.2 Biological fluids 53

1.4.2.1 Acetaminophen in urine 54

1.4.3 Metallic nanoparticles 56

1.4.3.1 Noble metal nanoparticles dispersions 61

1.4.3.2 Metallic nanoparticle transformations 63

CHAPTER 2 OBJETIVES 67

CHAPTER 3 : METHODOLOGY 73

3.1 Reagents 75

3.2 Instrumentation 79
3.2.1 UV-vis spectrometry 79
3.2.2 DART-MS and ICP-MS 82
3.2.3 Capillary liquid chromatography 83
3.2.4 Nano liquid chromatography 84
3.2.5 Miniaturized portable liquid chromatography 85
3.2.6 Ultra high-performance liquid chromatography 85
3.3 Sample treatment 86
3.3.1 Solid phase extraction 86
3.3.2 In-tube solid phase microextraction 87
3.4 Synthesis procedures 89
3.4.1 Synthesis of IT-SPME capillaries 89
3.4.2 Synthesis of naked AuNPs 90
3.5 Experimental conditions 90
3.5.1 UV-vis spectroscopy 90
3.5.2 DART-MS 93
3.5.3 ICP-MS 93
3.5.4 Chromatographic conditions 96
3.6 Analysed samples 100
3.6.1 Fruit washing residual water 100
3.6.2 Well water and different surface waters 100
3.6.3 Urine samples 101
3.6.4 Noble metal nanoparticles dispersions 101
CHAPTER 4 : RESULTS AND DISCUSSION 103
4.1 Environmental samples 105
4.1.1 Benchtop and portable minLC 105

4.1.1.1 Optimization of chromatographic conditions 105

4.1.1.2 Figures of merit 109

4.1.1.3 Determination of biocides in wastewaters 117

4.1.1.4 Evaluation tools for benchtop and portable miniaturized liquid chromatography 121

4.1.1.5 Conclusions 126

4.1.2 Determination of legislated nitrogen compounds by portable instruments in different water sources *127*

4.1.2.1 Determination of nitrate, nitrite, and ammonium 127

4.1.2.2 Determination of dissolved organic nitrogen 131

4.1.2.3 Determination of phenylurea pesticides by portable miniaturized liquid chromatography 134

4.1.2.4 Conclusions 137

4.2 Biological samples 138

4.2.1 Determination of acetaminophen in urine 138

4.2.1.1 Optimization of chromatographic conditions and figures of merit of IT-SPME-nanoLC-DAD *138*

4.2.1.2 Optimization of chromatographic conditions and figures of merit of UHPLC-ESI-QTOF 141

4.2.1.3 Optimization of method conditions and figures of merit of DART-QTOF 142

4.2.1.4 Analysis of urine samples 144

4.2.1.5 Evaluation tool 147

4.2.1.6 Conclusions 151

4.3 Nanoparticles samples 151

4.3.1 IT-SPME-minLC-DAD for the assessment of MNPs dispersions and plasmonic assays 151

4.3.1.1 Characterization of MNPs dispersions by IT-SPME-minLC-DAD 152

4.3.1.2 Study of the MNPs degradation overtime by IT-SPME-minLC-DAD 153

4.3.1.3 MNPs assessment and plasmonic assays monitored by IT-SPME-minLC-DAD 154

4.3.1.4 Conclusions 164

4.3.2 Sulfidation transformation study of solid AgNPs 165

4.3.2.1 Conclusions 172

CHAPTER 5 : GENERAL CONCLUSIONS 173

REFERENCES 179

ANNEXES 217

A1. Abbreviations 219

A2. List of figures 225

A3. List of tables 233

A4. PhD contribution to publications 237

CHAPTER 1:

INTRODUCTION

1.1 The analytical context: recent trends

Analytical chemistry is a scientific discipline that plays a key role in our society, covering different fields including pharmaceuticals, environmental assessment and monitoring, forensics sciences, food analysis, and industry, among others. Its main objective is to develop methods for the characterization, identification, and quantification of substances in any kind of sample matrices. In this regard, accurate and reliable analytical techniques are essential for ensuring product quality, human health, and environmental safety.

Over the last decades, analytical chemistry has undergone significant advancements driven by the society needs and the increasing demands for green, sustainable, and environmentally friendly methodologies (see **Figure 1**). Traditional analysis techniques have provided valuable insights and served as basis for our understanding of chemical composition and properties, nevertheless, these methodologies often require bulky instrumentation, extensive sample preparation, high amount of reagents and solvents used, and time-consuming analysis procedures. These limitations have sparked the need for faster, sensitive, reliable, and environmentally friendly alternative methodologies.

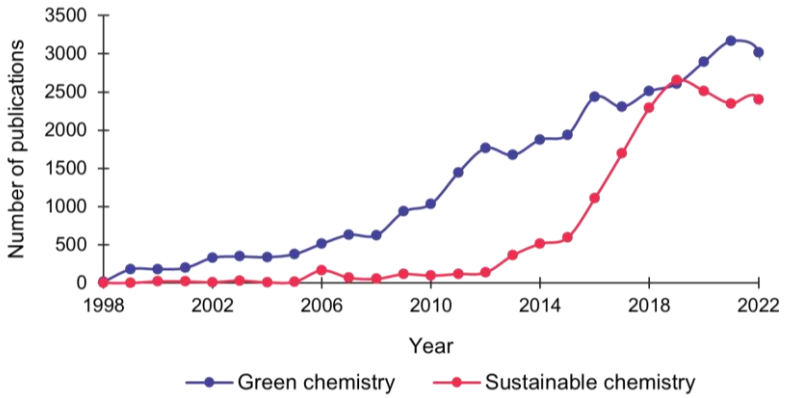

Figure 1. Number of publications in the Web of Science database in the last 25 years with topics “green chemistry” and “sustainable chemistry”. Consulted in June 2023.

In this context the requirements for “sustainable” and “green” chemistry must be addressed. Both terms have been used interchangeably to refer to environmentally friendly methodologies. However, although they are connected, there are differences between them. In 1999, Hutzinger clarified these differences, pointing out that green chemistry focus on the "design, manufacture, and use of chemical processes that have little or no pollution potential or environmental risk" while sustainable chemistry refers to the "maintenance and continuation of an ecologically-sound development” [1].

The idea of sustainability first appeared in the 1970s when several artists produced critical writings highlighting the need to integrate nature conservation into economic development [2]. One decade later, in 1987, the World Commission on Environment and Development, published a report titled “Our common future”, better known as “Brundtland Report”, stating the need for an strategy that unite the development and the environment. In this report the term “sustainable development” was described for first time as the “development that meets the needs of the present without compromising the ability of future generations to meet their own needs” [3]. Sustainable chemistry also prioritizes the consumption of resources, including energy, at a rate that allows for natural replenishment, while ensuring that waste generation is slower than the pace at which it can be effectively managed [4].

The green chemistry emerges in the 1990s as a response to the high industrial emissions. It supposes a shift in perspective of environmental solution strategies, from lowering emissions at “the end of the pipe” towards those focused on active prevention and mitigation at the source. These ideas were translated into a list of 12 principles by Anastas and Warner in 1998 with the ultimate aim to significantly reduce the influx of chemicals into the environment [5].

Although there are fundamental differences between greenness and sustainability, these also overlaps to some extent, and can be simultaneously

applied leading to the green and sustainable chemistry. More recently, the concept of "white chemistry" has emerged with the aim to integrate the functional and practical aspects of chemical within the framework of green chemistry [6].

In 2013, Gałuszka et al. proposed a list of 12 principles aiming to the develop greener analytical methods [7]. These principles are listed below.

(1) Direct analytical techniques should be used.

(2) Minimal sample size and number are goals.

(3) *In-situ* measurements should be performed.

(4) Integration of all analytical processes to save energy and reagents.

(5) Automated and miniaturized methods should be selected.

(6) Derivatization should be avoided.

(7) Generation of minimal waste with proper management.

(8) Multi-analyte or multi-parameter methods are preferred.

(9) The use of energy should be minimized.

(10) Reagents obtained from renewal source should be preferred.

(11) Toxic reagents should be eliminated or replaced.

(12) The safety of the operator should be increased.

To assess the greenness and/or sustainability of a method, different tools have been developed including the National Environmental Methods Index [8], Analytical Eco-scale [9], Green Analytical Procedure Index [10], RGB additive Color Model [11], the HEXAGON tool introduced by MINTOTA [12–14], and the Analytical GREEnness Metric [15].

An essential movement towards the sustainable and green analytical chemistry is the shift from conventional to miniaturized analytical systems. In analytical chemistry, miniaturization does not only refer to the reduction of the instrument size, but also to every step in the analytical process. The miniaturization of analytical instrumentation is closely related to green chemistry, and therefore, its growth has been accompanied by an increasing demand from society for more environmentally friendly methodologies. From the 12 principles of green analytical chemistry [7], the principles 2 (minimize sample size), 6 (miniaturize analytical methods), 7 (generate minimal waste), 9 (reduce the energy usage), and 12 (increase the safety of the operator) are direct consequences of miniaturization.

One significant milestone for the system miniaturization was the introduction of the microelectrochemical systems (MEMS) technology in the late 1980s [16]. MEMS offered the means to fabricate miniaturized components and sensors, enabling the development of integrate analytical devices with reduced dimensions. This breakthrough revolutionized the field by providing opportunities for on-chip sample handling, manipulation, and detection. Another notable advancement was the development of microfluidic systems in 1990s, allowing the accurate manipulation and control of very small volumes of fluids within miniaturized channels [17]. These platforms offered numerous benefits, including rapid analysis, reduced reagent consumption, and improved portability. Today, miniaturization has become prevalent in every stage of the analytical process, covering sample preparation like solid phase microextraction (SPME), stir bar sorptive extraction (SBSE), dispersive liquid-liquid microextraction (DLLME), and single-drop microextraction (SDME); the analytical separation such as LC, gas chromatography (GC), and capillary electrophoresis (CE); and detection techniques such as atomic and molecular spectroscopy, mass spectrometry (MS), and electrochemical techniques.

Regarding LC, Its wide applicability, high sensitivity, reproducibility, and rapid separation, together with the features derived from miniaturization such as minimal waste generation and solvent consumption, low injection volumes, and sensitivity enhancement makes minLC a powerful analysis technique in various fields.

The increasing social demand for real-time monitoring devices to address on-site challenges together with systems miniaturization, has catalyzed the development of PI. Consequently, there has been a substantial surge in the utilization of PI in diverse scientific areas [18,19].

PI can be defined as devices which have been designed to be light weight and compact to be hand transported [20]. According to Eren, PI is characterized by the following of finely tuned design features [21]:

(1) Limited size and weight.

(2) Limited sized batteries.

(3) Low power consumption.

(4) Trade-off between the instrument cost and its performance.

(5) User friendly interface options.

(6) Operation in diverse environmental conditions.

(7) Data processing and data communication.

Portable equipment has gained prominence due to its potential benefits, including cost-effectiveness and reduced carbon footprint. In the last two decades, the number of publications and citations about with the topic “portable instrumentation” in the Web of Science database have increased showing its growing interest (**Figure 2**). From the more than 25000 results regarding this topic, the 15 % belongs to the field of chemistry. Despite the recent prominence of portable instrumentation in the field of chemistry, it has been a subject of interest for many years. The earliest report can be traced

back to 1957 when T. K. With utilized a portable Wood light source for the analysis of porphyrins [22]. Portable devices present a promising alternative to conventional laboratory equipment in diverse fields, thanks to their versatility and wide range of applicability.

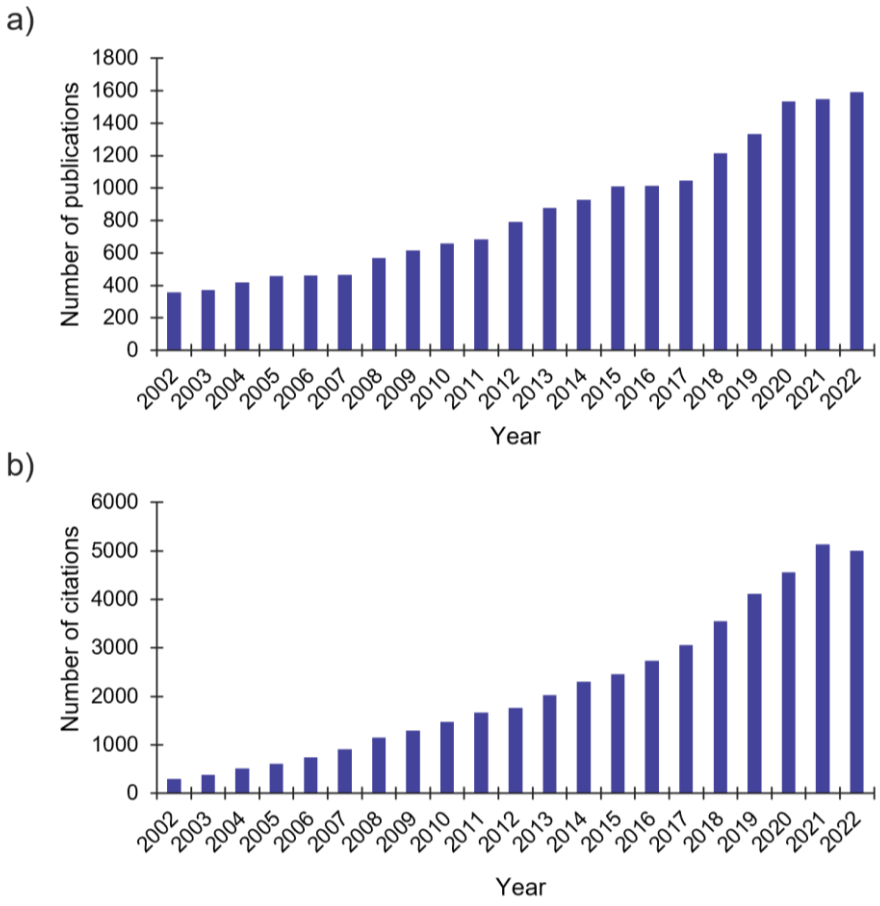

Figure 2. Evolution of the number of publications (a) and number of citations (b) for the topic "portable instrumentation" using the Web of Science database. Consulted in June 2023.

Portable liquid chromatography has evolved slowly due to difficulties related to the miniaturization, and it has not been since the last decade that it has gained more interest. Even so, the works related to the topic "portable liquid chromatography" are scarce when compared to other scientific areas such as spectrometry, spectroscopy, or electrochemistry (**Figure 3**).

Portable LC is of special interest when working with complex samples and a previous separation is needed. The usefulness of these systems is unquestionable in numerous areas, including environmental monitoring, point-of-care analysis in hospitals, and providing real-time feedback in industrial, clinical, or forensic scenarios. [23].

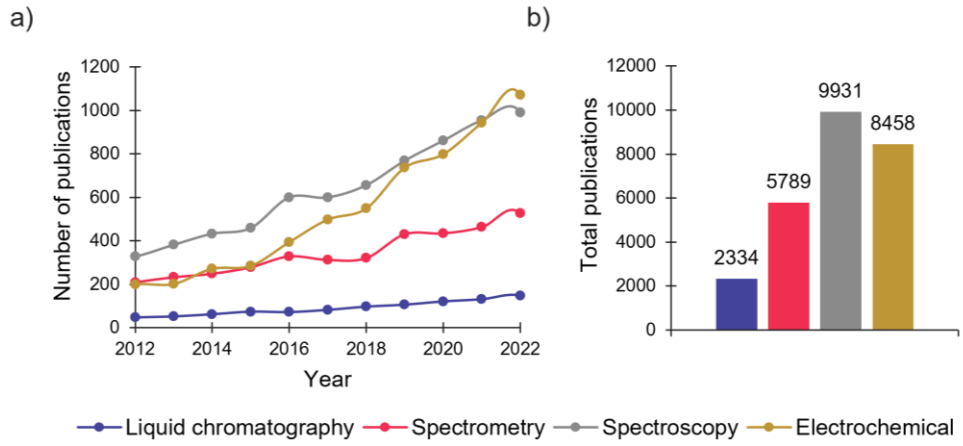

Figure 3. Evolution (a) and total number of publications (b) in the last 10 years with the topic "liquid chromatography", "spectrometry", "spectroscopy", and "electrochemical" and refined by "portable". Consulted in June 2023.

In this thesis, the capabilities of miniaturized LC (minLC) are studied in different matrices, including environmental, biological, and NPs dispersions. The figures of merit were compared to those provided by other well stablished analytical techniques. Furthermore, the Axcend Focus LC, the first commercially available miniaturized portable LC, was employed to investigate the possibilities, strengths, and needs of portability applied to LC. The HEXAGON tool and the BETTER criteria were used as assessments tools to evaluate the greenness and sustainability of the procedures and the instrument portability, respectively.

1.2 Miniaturized liquid chromatography

The history of liquid chromatography (LC) dates back to the year 1906 when Mikhail Tsvet separated the different carotenoids and xanthophylls of a plant using calcium carbonate as adsorbent and a mixture of petrol ether/methanol as mobile phase. He called the technique chromatography, from the Greek words *chroma* and *graph* which means colour and write respectively [24]. LC allows to separate different compounds of a mixture attending to its interactions between two phases, one stationary and one mobile. The essential instrumentation for a liquid chromatograph consists of 1) a solvent delivery unit, which includes the solvent reservoirs and a pumping system, which drives the mobile phase through the system, 2) an injector to introduce the sample into the chromatographic system, 3) an analytical column containing the stationary phase where the separation takes place, and 4) a detector to register the obtained signal. Since its conception, LC has been refining, greatly increasing its applicability and becoming an indispensable technique for multi component analysis of complex samples.

Currently exist a high variety of types of LC according of the i.d. of the analytical column (**Figure 4**). Attending to the nature of the stationary/mobile phase, the reverse phase (RP) LC, where the mobile and stationary phase are polar and non-polar respectively, is the most popular choice due to its high range of applicability and commercial availability. However, other forms of LC such as hydrophilic interaction chromatography, ion-exchange chromatography and normal phase chromatography are also used. According to how the stationary phase is organised into the column there are: packed, monolithic, wall-coated open tubular, and porous layer open tubular column. Regarding to the column internal diameter (i.d.), authors have classified the several types of liquid chromatography. The most popular classification was first proposed by Chervet, et al. [25], the denominations for each column i.d. and flow rate are shown in **Table 1**.

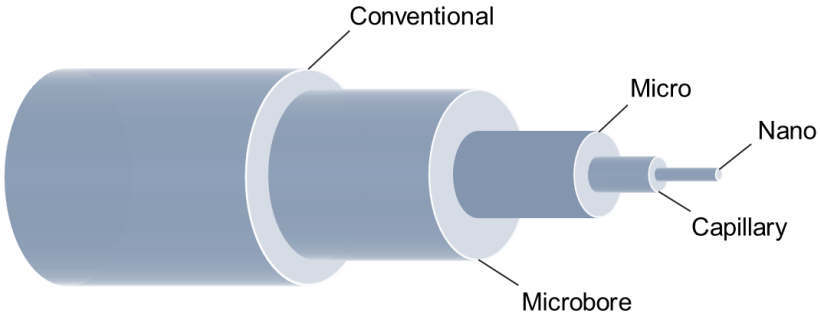

Figure 4. Size comparison of analytical columns for the different levels of miniaturization.

Table 1. Liquid chromatography denominations attending to the analytical column internal diameter and flow rate [25].

Denomination	Column i.d. (mm)	Flow rate (μL min^{-1})
Conventional LC	4.6 – 3.2	2000 – 5000
Microbore LC	3.2 – 1.5	500 – 100
Micro LC	1.5 – 0.5	100 – 10
Capillary LC	0.5 – 0.15	10 – 1
Nano LC	0.15 – 0.01	1 – 0.1

Miniaturized LC, namely capillary and nano LC (capLC and nanoLC respectively), is gaining interest in last years (**Figure 5)**, partly due to the increasing demand for more sustainable analytical, as well as the advantages it offers over conventional LC, encompassing reduced sample volumes required and enhanced sensitivity. MinLC has established itself in various fields of applicability such as: biochemistry, pharmacology, food sciences, environmental sciences, and toxicology (**Figure 6**). Compared to conventional LC, for minLC (specially for nanoLC) most of the applications (> 50 %) are related to the field of biochemistry (proteomics, lipidomics, metabolomics, among others). The increased sensitivity and low sample volumes required along with the variety of add-ons which can be easily incorporated such as immobilized enzyme reactors, enrichment columns or selective trapping makes minLC a powerful tool for low concentration peptide and protein

separations [26]. Biochemistry is followed by pharmacology and food science, while environmental sciences and toxicology represent the minor part of the applications. Nevertheless, with the recent advances in miniaturized instrumentation, new portable instruments which allow the in-situ analysis are being developed, which is of particular interest for environmental, forensic, and clinical analysis.

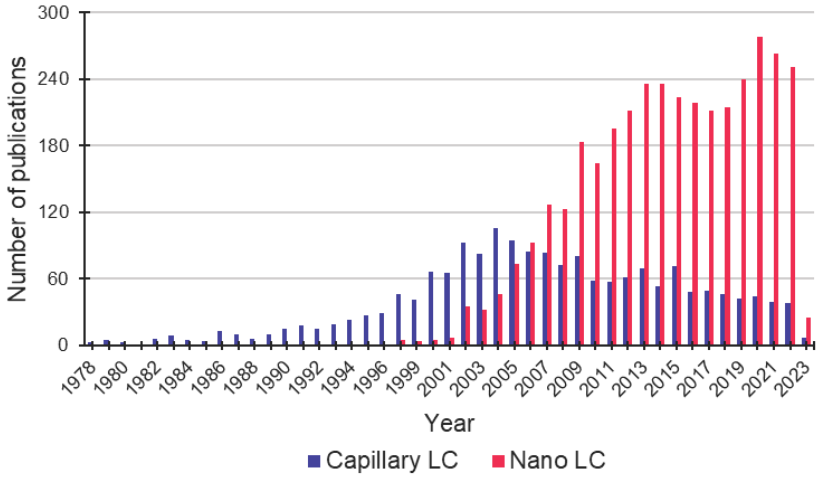

Figure 5. Number of publications reported over the last 45 years with the search topic “Capillary LC” and “Nano LC”. Source: Scopus database.

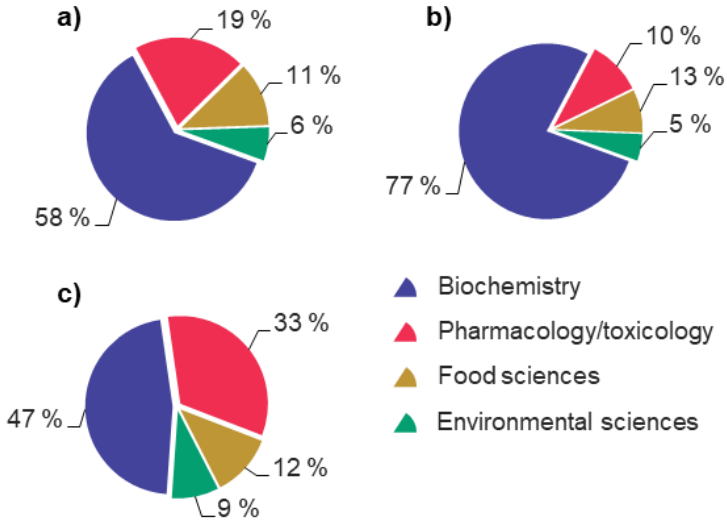

Figure 6. Percentage of publications reported in the Scopus database according to the field of application for the topics a) capillary LC, b) nano LC, and c) HPLC.

Miniaturized LC arises as a consequence of the reduction of the i.d. of the analytical column, which at the same time implies a reduction in the flow rate and all other system components by the next down-scaling factor $(d_1/d_2)^2$, where d_1 and d_2 are the i.d. of both analytical columns. The firsts applications of miniaturized LC were reported by Hovarth, et al. in 1967 , who determined different nucleotides on pellicular ion exchangers using analytical columns with i.d. of 1.0 mm and studied the band broadening effect on capillary columns with i.d. of 0.276 mm [27,28]. In the following years the i.d. of analytical columns were further minimized [29–31] demonstrating how decreasing the i.d. of the columns enhances the separation efficiency. This is due to the reduction of the eddy diffusion (term A in the Van Deemter equation), which is caused by the "wall effect" described by Knox and Parcher [32] and the more rapid diffusion of the analytes in lower i.d. colums. Later, in 1996, Chervert et al [25], established the instrumental requirements for nanoLC and demonstrated how conventional high performance liquid chromatography (HPLC) can be modified to suit the nano scale. Nowadays, the are several commercially available analytical columns with i.d. down to a few μm (nanoLC) with a high variety of lengths, particle sizes, and stationary phases.

One of the main drawbacks of miniaturized LC is the band broadening. The reduction in the i.d. of the analytical column produces a quadratic decrease in the peak volume and, therefore, dead volumes related to the connectors, injection system, and detectors becomes more notorious. This produces the above mentioned extra column band broadening, adversely affecting the efficiency [33]. Numerous studies have been conducted to investigate peak broadening in miniaturized systems and strategies to minimize this effect [34–39], particularly in relation to capillaries and end fittings. Another difficulty related to the usage of miniaturized LC instruments, especially when dealing with very small scales such as nanoLC, is to locate and stop possible leaks in the system as well as the readily clog formation.

Despite this, miniaturized LC provides major benefits over conventional LC. Firstly, the most noticeable is the reduction in the volume of solvent used and waste generated. Given the down-scaling factor, from a conventional analytical column with 4.6 mm of i.d. to a capillary one with 0.5 mm of i.d. translates into a 100-fold reduction in the flow rate. This makes a big difference from the point of view of the green chemistry. The smaller amount of stationary phase required allows to work with more expensive and complex materials increasing the range of applicability. Likewise, the injection volume is drastically reduced being especially attractive for applications where the amount of sample is scarce. In the case that higher sensitivity is needed, larger sample volumes can be injected by using different on-line sample preconcentration configurations such as switching trap columns and in-tube solid phase micro extraction (IT-SPME).

A further benefit of the miniaturization is the increase in the sensitivity. The dilution of the sample in the chromatographic system, *D*, can be expressed as follows (**equation 1**):

$$D = \frac{C_0}{C_{max}} = \frac{\varepsilon \cdot \pi \cdot r^2 \cdot (1+k) \cdot \sqrt{2\pi \cdot L \cdot H}}{V_i} \quad (1)$$

here C_0 is the initial analyte concentration, C_{max} is the analyte concentration at its peak maximum, ε is the column porosity, r is the column radius, k is the retention factor, L is the column length, H is the column plate height, and V_i is the volume of sample injected [40]. Decreasing the column i.d. reduces the radial diffusion and therefore the sample chromatographic dilution in inverse proportion to r^2. However this enhance in sensitivity is countered by the lower injectable volume which is proportional to the amount of stationary phase in the column [41]. It should be noted that **equation 1** is only applicable to the isocratic elution mode; however, it can be extrapolated to gradient elution, albeit with some degree of approximation.

Finally, nanoLC makes the coupling to MS easier, as nano-electrospray ion sources (nESI) are much more effective transferring ions to the detector than conventional electrospray. The reduction in sample introduction causes the emission of very small charged droplets which desolvate more efficiently to individual ions, resulting in an increase of sensitivity [42].

Along with the miniaturization of the analytical column, the other components of the LC must be adjusted to suit the down-scaling. These will be briefly discussed below.

Solvent delivery units comprise a solvent reservoir, a degasser, and a pumping system. The later must be capable of producing stable and accurate flow rates, withstanding the backpressures generated by the column. Reciprocating and syringe pumps keep being the most popular choice. Early reciprocating pump designs were based on a single piston driven by an electric motor in and outside the mixing valve sucking and pushing out the mobile phase. The pulses produced by the single piston can be compensated by incorporating a second piston in series or parallel. In the other hand, syringe pumps use a stepper motor to cause a positive displacement in the piston transferring the mobile phase without pulses through the chromatographic system. The limited volume of the syringe is not necessarily a problem as long as the total syringe volume is greater than the needed to perform a chromatographic run. Also, a second syringe can be used to refill the mobile phase while the other is dispensing it. Commercial solvent delivering units capable of generate flow rates in the order of $nL \cdot min^{-1}$ in split-less mode are commercially available. However, it is worth noting that many other units still require the use of a flow splitter, resulting in most of the solvent being discarded.

Regarding the injection systems, switching injection valves remains being the most used. These are capable of introducing a fixed volume of sample determined by an external loop into the chromatographic system

without affecting the pressure. Sample loop volumes are typically between 5 µL and 1000 µL, however, these volumes are too high for capillary and nano columns. The maximum sample volume that can be injected without loss of efficiency is determined by the **equation 2**:

$$V_{s,max} = 0.36 \cdot \sqrt{Ld_p} \cdot d_c^2 \cdot (k+1) \quad (2)$$

where *L* is the column length, d_p is the particle diameter, d_c is the column diameter, and *k* is the retention factor [43]. As an example, for a packed column with dimension 50 mm × 0.3 mm and 3 µm of particle size, the maximum injection volume is approximately 20 nL. To reach these low volumes partial loop injection or timed injection can be used. Also, new injection valve models have internal sample loops of a few nanolitres consisting of a grove in the rotor of the injection valve. For example, the VICI Valco C4N internal sample injector is available from 20 nL down to 4 nL with both, manual and automated actuation.

Regarding detection system, there are a wide variety of choices, however, absorbance-based detectors and mass detectors are the preferred option due to its easy miniaturization and its applicability. These will be discussed in detail in the **section 1.2.2**.

In the last years, miniaturized LC has established as a topic of interest in the field of the analytical chemistry. **Table 2** shows the main reviews with the topic of miniaturized LC in the last 10 years. As can be seen in the **Table 2,** there are reviews about the fundamentals of the evolution of the instrumentation [44–46], the analytical columns and mass spectrometry [33,47,48], on-line pre-treatment configuration advancements [49], automatization and miniaturization and its applications in the field of proteomics [50,51] as well as food analysis [52,53], and pharmaceutical analysis [54,55]. Miniaturized LC has been applied in fields such as food science [56–58],

pharmaceutical [59,60], environmental [61–63], biochemistry [64,65] and others.

Table 2. Main reviews with the topic of miniaturized liquid chromatography instrumentation and applications in the last 10 years

Title	Topic	Year	REF
From conventional to miniaturized analytical systems.	Instrumentation	2014	[44]
Instrument platforms for nano liquid chromatography	Instrumentation	2015	[45]
A review of portable high-performance liquid chromatography: the future of the field?	Instrumentation	2020	[46]
Evolution in miniaturized column liquid chromatography instrumentation and applications: An overview	Instrumentation / applications	2015	[33]
Miniaturized liquid chromatography focusing on analytical columns and mass spectrometry	Instrumentation	2020	[47]
Nano liquid chromatography columns	Instrumentation	2019	[48]
Recent advances in on-line upfront devices for sensitive bioanalytical nano LC methods	Instrumentation	2021	[49]
Advances in microscale separations towards nanoproteomics applications	Applications	2017	[50]
Nano-liquid chromatography-mass spectrometry and recent applications in omics investigation	Applications	2020	[51]
Capillary-liquid chromatography (CLC) and nano-LC in food analysis	Applications	2013	[52]
Nanoscale separations based on LC and CE for food analysis: A review	Applications	2019	[53]
Current applications of miniaturized chromatographic and electrophoretic techniques in drug analysis	Applications	2014	[54]

1.2.1 On-line sample treatment configurations

Most of the analytical methods require a first step of sample treatment The main objective of this analytical step is to eliminate possible interferents

as well as preconcentrate the analyte in the sample. Standard treatment techniques such as solid phase extraction (SPE), head-space sorptive extraction (HSSE), thermal desorption, or liquid-liquid extraction (LLE) require various steps, reagents, and a considerable volume of solvents. According to a survey undertaken on sample preparation techniques [66], the 65 % of the responders required at least 3 sample preparation techniques per sample, while in average, 80 samples are analysed per instrument and week. In this context, the combination of miniaturization extraction procedures, such as SPME, combined with automation open the door to more sustainable methodologies.

When working with miniaturized LC, on-line sample preparation based on switching columns configurations are often used. In these, both, the analytical column, and an extractive column are connected into a switching valve. The sample is first passed through the extraction column for a selected time and flow rate, making the analytes being retained while the rest of the matrix is discarded. Then, switching the valve position makes the mobile phase to elute the analytes from the extractive column to the analytical column. In this way, higher volumes that those required for direct injection can be processed allowing, if needed, to increase the detectability. Moreover, it eliminates possible interferents and particles that could shorten the lifetime of the analytical column. On-line sample preparation techniques minimize the number of steps and solvent consumption being in line with the principles of green chemistry [67].

Column switching systems can be classified in trap columns [68] and IT-SPME [69,70] (**Figure 7**). Trap columns are commercially available with different bed materials and sizes. For nanoLC, most of the applications use RP packed columns with i.d. ranging from 75 µm to 300 µm and lengths between 5 µm and 20 µm and are widely used in omics applications [49].

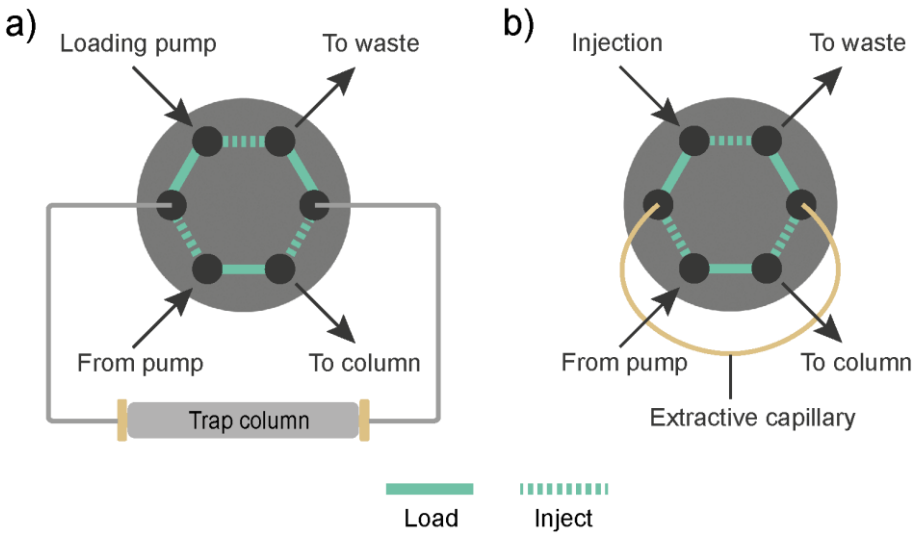

Figure 7. Schematic representation of switching column configurations using a) trap column and b) IT-SPME capillary.

In the other hand, IT-SPME uses a capillary packed or coated with the extractive phase in place of the injection loop or in the sampling circuit in automatic injection. IT-SPME capillaries are segments of open tubular columns, often gas chromatography columns, which are filled with the extractive phase. The main disadvantage of the technique is the low extraction efficiency (< 30 %) [71], in this regard, the development of new extraction phases to improve selectivity and extractive capacity are being pursued. Depending on the application and target compounds different extractive phases can be used. These can classified in packed phases such as: phenylboronate monoliths, octylsilane and octadecylsilane (C8 and C18 respectively) monoliths, restricted access materials, monolithic molecularly imprinted polymers, and immunosorbent monoliths; and coated phases such as: carbon-based nanomaterials and polymers reinforced with nanoparticles (NPs) [72,73].

The simplicity of the on-line coupling, the high preconcentration achieved, and its adaptability makes IT-SPME an interesting technique to be

used in a variety of fields. **Table 3** lists the reported IT-SPME-minLC conditions for different applications in the last 10 years. As can be seen, there are forensic sciences, biomedical, industrial, and environmental applications, being the later the most frequent. The length of the capillaries used in these applications varies from 10 cm to 43 cm. The choice of capillary length depends entirely on the method employed. Longer capillaries offer higher sorption capacity, but they also require more time for analyte desorption, leading to peak broadening. When it comes to the i.d. of the capillaries, the most popular options are 0.32 mm for capLC and 0.10 and 0.075 mm for nanoLC.

Regarding the extractive phases, polydimethylsiloxane (PDMS) based modified with diphenyl groups are the preferred choice since these are commercially available and provides suitable results. Other phases are also used, for example, magnetic in-tube solid phase microextraction (MIT-SPME) was explored using SiO_2 supported with Fe_3O_4 [74]. The adsorption properties of the sorbent together with the application of an external magnetic field enhances the extractive capacity. The application of the variable magnetic fields results in a extraction capacity on the target analytes between 70 % and 100 %, which is higher than those achieved by IT-SPME. Also, tetraethyl orthosilicate (TEOS) and methyltriethoxysilane (MTEOS) polymers functionalized with different metal and metal oxide NPs were tested showing an improvement in the extraction efficiency for SiO_2 NPs [75] and the serial coupling of two capillaries with CuO NPs and TiO_2 NPs [76].

Table 3. Conditions of the reported applications of IT-SPME coupled to Cap/NanoLC in the last 10 years (from 2013 to 2023)

REF	Application	Technique	Capillary dimensions	Capillary extractive phase	Inj. v. (µL)
[77]	Industrial	IT-SPME-CapLC-DAD-MS	43 cm x 0.32 mm	35 % diphenyl 65 % PDMS	2000
[78]	Industrial	IT-SPME-CapLC-µESI-MS	43 cm x 0.32 mm	5 % diphenyl, 95 % PDMS	2000
[79]	Environmental	IT-SPME-CapLC-DAD	40 cm x 0.32 mm	5 % diphenyl, 95 % PDMS	4000
[74]	Environmental	MIT-SPME-NanoLC-DAD	15 cm x 0.075 mm	SiO_2 supported Fe_3O_4 NPs	100
[80]	Environmental	MIT-SPME-CapLC-DAD	35 cm x 0.32 mm	SiO_2 supported Fe_3O_4 NPs	3000
[81]	Industrial	IT-SPME-CapLC-DAD	43 cm x 0.32 mm	35 % diphenyl 65 % PDMS	1000
[82]	Biomedical	IT-SPME-CapLC-DAD	30 cm x 0.32 mm	5 % diphenyl, 95 % PDMS	4000
[83]	Biomedical	IT-SPME-CapLC-FLD	40 cm x 0.32 mm	SWCNTs and MWCNTs functionalized PDMS	20
[75]	Environmental	IT-SPME-NanoLC-DAD	20 cm x 0.075 mm	TEOS-MTEOS-SiO_2 NPs	500
[84]	Forensic	IT-SPME-NanoLC-DAD	12 cm x 0.1 mm	SiO_2 supported Fe_3O_4 NPs	8
[85]	Environmental	IT-SPME-CapLC-DAD	70 cm x 0.32 mm	35 % diphenyl 65 % PDMS	30
[86]	Forensic	IT-SPME-CapLC-DAD	90 cm x 0.32 mm	35 % diphenyl 65 % PDMS	2000
[76,87]	Environmental	IT-SPME-NanoLC-DAD	15 cm x 0.075 mm	Two serial TEOS-MTEOS modified with TiO_2 and CuO NPs respectively	200
[88]	Biomedical	IT-SPME-Cap/NanoLC-DAD	20/15 cm x 0.32/0.075 mm for cap/nanoLC	35 % diphenyl 65 % PDMS (Cap LC), TEOS-MTEOS-SiO_2 NPs (NanoLC)	20
[13]	Environmental	IT-SPME-Cap/NanoLC-DAD	20/1 cm x 0.32/0.075 mm for cap/nanoLC	TEOS-MTEOS-SiO_2 NPs	50

1.2.2 Miniaturization of detectors

Detection systems for minLC are the same as those used in conventional LC. In the **Table 4** some examples of detection systems applied to minLC are listed.

Table 4. Examples of different detection systems for miniaturized LC.

REF	Analytes and sample	LC scale	Detection system	LOD [a]
[89]	Pesticides in apples	NanoLC	DBDI-MS	0.15 $\mu g \cdot L^{-1}$
[90]	Antidepressants in blood	CapLC	DAD-API-ES-MS	0.027 $\mu g \cdot L^{-1}$
[91]	Lipids in yeast	NanoLC	nESI-MS	$fmol \cdot L^{-1}$
[92]	Parabens in urine	CapLC	ESI-MS/MS	0.016 $\mu g \cdot L^{-1}$
			DAD	8 $\mu g \cdot L^{-1}$
[57]	Benzimidazoles in milk	CapLC	DAD	2.2 $\mu g \cdot L^{-1}$
[93]	Drugs in pharmaceuticals	NanoLC	DAD	38 $\mu g \cdot L^{-1}$
[94]	Phenol standards	CapLC	On-column UV-LED	183 $\mu g \cdot L^{-1}$
[95]	Glycopeptide antibiotics in feed	CapLC	AD	4 $\mu g \cdot L^{-1}$

[a] Average LODs for the different analytes

Ultraviolet-visible (UV-vis) detectors are stablished as a standard for capillary and nanoLC due their low cost, simplicity, and range of applicability. Miniaturization of those detectors entails the minimization of dead volumes to avoid the peak broadening. Also, sensitivity when using on-column detection is negatively affected due to the shorter path length. To overcome this, Z-shaped and U-shaped flow cells are used [90,96] (**Figure 8**). Chervet, et al (1991) reported a 14-fold increase in sensitivity compared with on-column detection [97], however, it must be noted that longer path lengths increases the system dead volume causing peak broadening. UV-vis absorbance techniques have limits of detection (LODs) in the order of $\mu g \cdot L^{-1}$. Diode array

detectors (DAD) are often used since it allows to select the best wavelength for each compound while gives full wavelength UV-vis spectra allowing to identify a compound at the same time that allows to discern if a chromatographic peak corresponds to a single compound or a combination of analytes. Light emitting diodes (LED) are gaining interest due to its long life, high stability, bright output, low weight and size, low electricity consumptions, and low price [98,99]. These features makes UV-LED detectors highly attractive for its use in miniaturized systems [94,100]. However, these are limited by the use of fixed wavelengths.

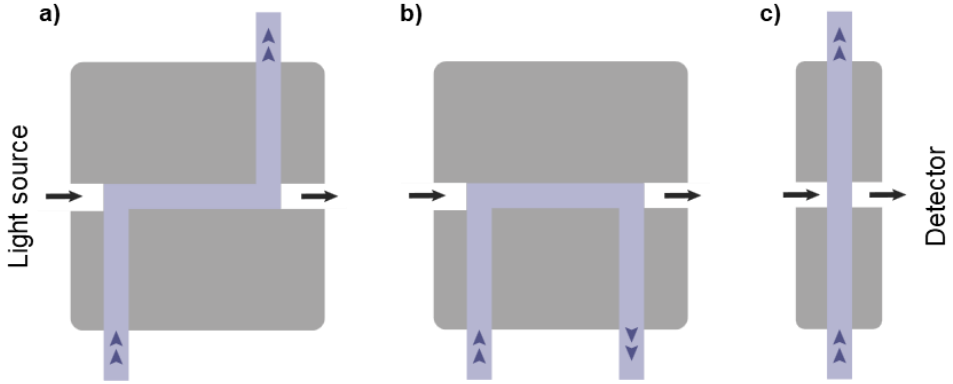

Figure 8. Different flow-cells for UV-vis detection. a) Z-shaped, b) U-shaped, and c) on-column detection.

Mass spectrometry is widely used in both conventional and miniaturized LC due to its high sensitivity, accuracy, precision, and the capabilities of identify compounds from its m/z ratio. Also, the possibility to work with two mass analyzers operating in sequence (tandem MS or MS/MS) allows a more reliable identification of the compounds giving also structural information which is of great interest for protein sequencing in biomedical applications [101]. In this regard, the most used MS/MS techniques are triple quadrupole (QqQ) for known compounds and quadrupole-time-of-flight (Q-TOF) for unknowns.

Electro spray ionization is the most popular interface when coupling minLC to MS. It generates gas-phase ions which are transferred to the MS. The ions are produced by applying a high voltage into the liquid creating charged droplets. As the solvent evaporates the charge density increase until a coulomb explosion occurs generating the gas-phase ions. The efficiency of the ESI depends on different parameters such as the solvent composition, temperature, tip geometry, voltage applied, and flow rate [102,103]. Nano ESI interfaces and the correlation of the flow rate with the droplet size were first described by Wilm and Mann in 1994 [104]. It has been proved how the reduction in the flow rates produces an increase in the ion transfer efficiency and hence in the sensitivity [105]. Reducing the flow rate on the capillary results in lower sized charged droplets which require a lower number of fissions events and solvent evaporation promoting a more efficient ion formation. nESI interfaces flow rates are typically below 20 nL min^{-1}, so the coupling with minLC becomes easier than with conventional LC. This fact, combined with the lower radial diffusion of minLC produces a significant increase in the sensitivity compared to conventional LC.

Among the MS interfaces, direct analysis techniques which reduce or eliminate the sample preparation step are also employed being direct analysis in real time (DART) one of the preferred choice [106–108]. The technique uses an atmospheric pressure ion source where the desorption is carried out by means of a hot gas stream (helium or nitrogen) and the ionization takes place by the reaction between the analyte and the reactive species produced by electronically or vibronically excited gas (**Figure 9**). The technique has some drawbacks compared to LC-MS or GC-MS such as its limited sensitivity, lower accuracy and precision, and the matrix effect derived from the sample components competition for reagent ions or binding of target analytes to the matrix. However, DART offers various advantages over LC-MS or GC-MS such as the shorter analysis times, ease of use, and rapid feedback, making it a potential alternative for POC analysis.

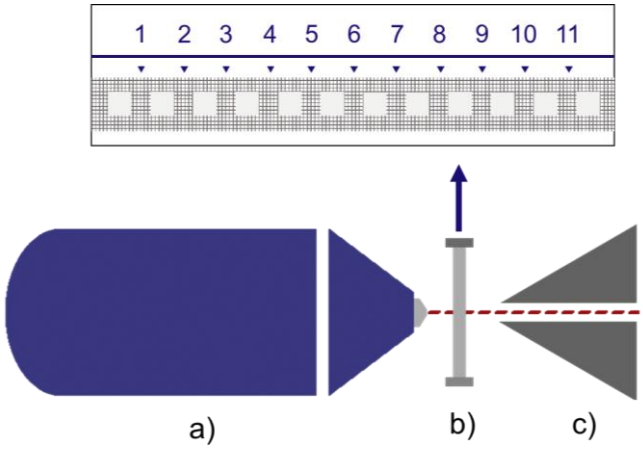

Figure 9. Schematic representation of a DART-MS system where a) is the DART ion source, b) is the sample mesh holder, and c) is the MS detector.

1.3 Portable liquid chromatography

Portability is one of the challenges in analytical chemistry. The increasing demands of methods that allow the analysis *in-situ* to be used in monitoring and point-of-care applications has promoted the develop of different portable instruments. Nowadays, there are well stablished portable instrumentation such as spectrophotometers, refractometers, spectrofluorometers, and electrochemical devices [18]. However, portable LC has evolved slowly compared to these instrumentation due to difficulties related to its miniaturization.

The first liquid chromatograph reported as portable was the OB-4 or Milichrom, developed by Baram et al. in 1983 [109]. The system consists of a single syringe pump for driving the mobile phase through a micro-LC column (0.8 ~ 1.0 mm i.d.) to a microspectrophotometer detector. The system dimensions (length × width × height) and weight were 70 × 50 × 30 cm^3 and 42 kg, respectively. Nevertheless, this system is far away from the contemporary idea of portability. **Figure 10** shows a timeline with relevant portable LC contributions and their main features are described along this section.

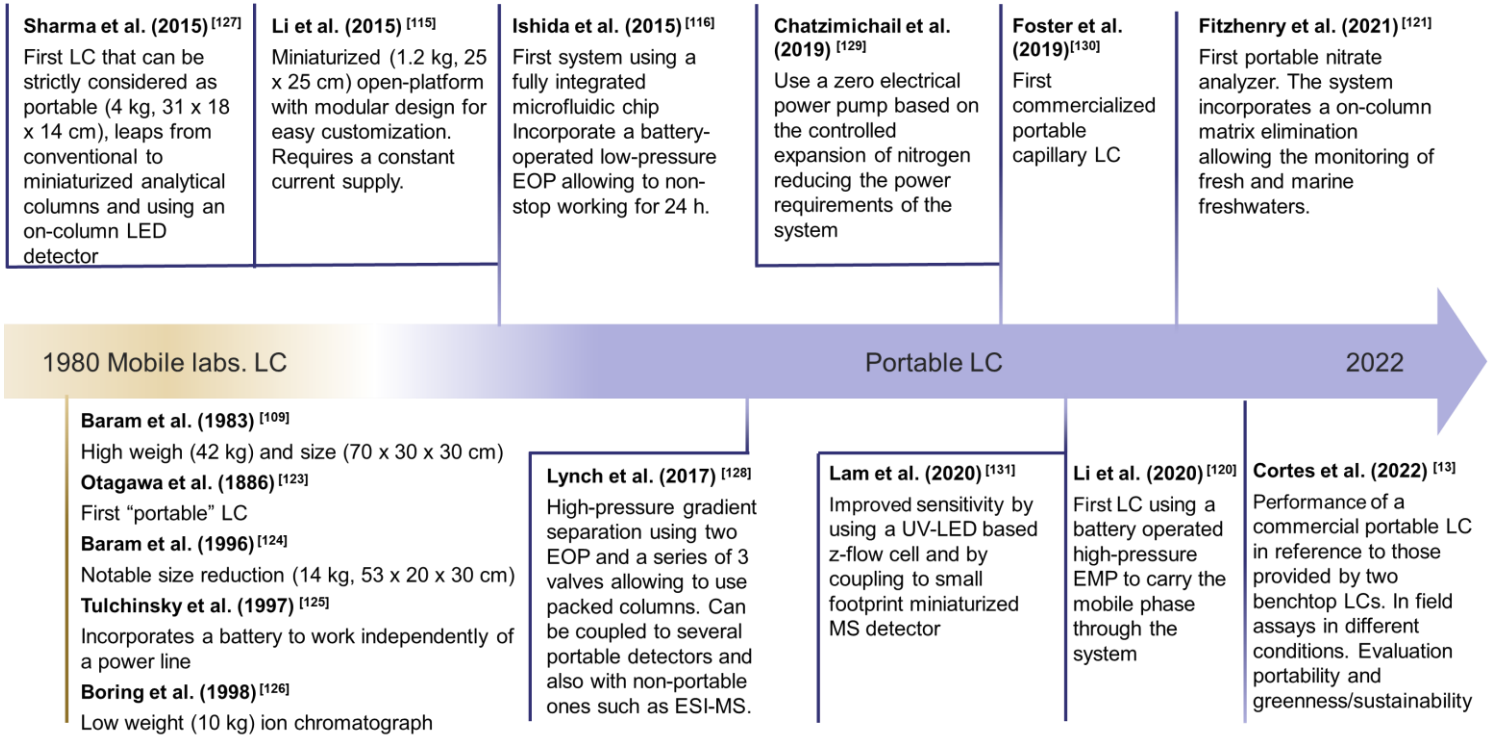

Figure 10. Timeline with the different developed portable LC and its main features.

Otagawa et al. in 1986 [110] developed a portable LC applied to the analysis of primary aromatic amines in coal derivatives. The sample was injected by means of an automated sample injector (20 µL) and driven to a conventional reversed phase analytical column (30 × 4.6 mm, 10 µm) by means of a reciprocating pump. The system worked either using a battery or a direct current power supply. The weight and dimensions of the system were not reported, and the flow-rate stability and the resolution were poor. Later, Baram et al. [111] presented an improved version of the OB-4. They significantly reduced the weight of the system from 42 kg to 14 kg. They used a two-syringe pump (2.5 mL) allowing to work in gradient mode with a maximum pressure of 7 MPa. A microbore analytical column (60 × 2 mm, 5 µm) thermostated by means of a column heater was used. The detection was performed by using a UV-vis spectrophotometric detector. As an application proof the authors determined different pesticides, polycyclic aromatic hydrocarbons (PAHs), phenols, and phthalates. The analysis time ranged from 10 to 30 min with suitable limits of detection (LODs) and good column efficiency and peak resolution. Two years later, Tulchinsky et al. (1998) [112] described a gradient field-portable LC system named MINICHROM, weighing 9.5 kg with a modular design intended to be used by personnel with minimum training. The main advantage of the systems was the incorporation of a battery, which allowed to work for up to 8 h. Also, this was the first high pressure (maximum pressure 35 MPa) portable LC developed, which increased the number of available columns. The latest portable LC developed in the decade was presented by Boring et al. (1998) [113]. It consists of a 10 kg (28 × 43 × 15 cm^3) capillary supressed conductimetric ion chromatograph. It uses a single syringe pump with an electrodialytic sodium hydroxide generator, so the system can work either in isocratic or gradient elution mode. LODs obtained were in the order of low $\mu g \cdot L^{-1}$ and the average peak efficiencies were 80000 plates m^{-1}. This was the first time that an on-line sample pre-treatment

step using a preconcentration column as a loop was used in a portable LC. The main issue of this system was its complexity, being hard to be reproduced by other laboratories. It was constructed for working with a direct current power supply limiting its portability. Although the systems described above were built to be incorporated into portable laboratories rather than for direct field measurements, these served as a basis for the later developed portable chromatographs.

It was not until 2015, after notable advancements in pumps, detectors, and column technology, that a new wave of portable LC surged. In 2015, Sharma et al. [114] developed a hand-portable gradient capillary LC with a total weight and dimensions of 4 kg and 31 × 18 × 14 cm^3, respectively. Two nanoflow syringe pumps (74 µL) controlled by a micro-stepper motor were used to generate steady flow rates lower than 1 $\mu L \cdot min^{-1}$ in gradient elution mode. The maximum working pressure was 55 MPa allowing to work with a high range of columns. A V-shaped stop-flow injector (60 nL) was used. This was the first time that a portable LC incorporated an on-column LED detection, which became a common option due to the advantages it offers to portable systems. The system applicability was tested for the determination of a mixture of phenols. The separation was achieved with good peak shapes, high efficiencies (150000 plates m^{-1}), and reproducible peak retention times in less than 20 min.

Li et al. (2015) [115] described a modular, open platform medium pressure capillary LC with the aim of being easily reproducible and customized. It used low-cost commercialized components to facilitate its accessibility. The total weight was further lowered to 1.2 kg with a breadboard dimensions of 25 × 25 cm. Two micro-syringe pumps (100 µL) were used to generate a continuous gradient. A stop-flow nano injector (20 nL) was used. On-column LED detection was chosen. A 180 × 0.1 mm reversed phase monolithic column was used to separate a mixture of 4 dyes. The separation was performed in less than 8 min with good peak relative retention time deviations and LODs below $\mu g \cdot L^{-1}$. However, the limited maximum pressure achieved (17 MPa) does not allow working with small particle packed columns, compromising the system efficiency (around 70000 plates m^{-1}). Also, the system did not have a built-in battery, which is essential for any portable system.

A portable LC with a battery-operated compact electroosmotic pump was developed by Ishida et al. (2015) [116]. The weight and dimensions of the system were 2 kg and 26 × 18 × 21 cm^3, respectively, being the lightest battery-operated portable LC. The analytical column and an electrochemical detector were integrated into a microfluidic chip. To the date, no portable chromatograph had ever integrated its fluidic system in a chip. Microfabricated devices minimize the solvent usage and the system dimensions being therefore highly attractive for portable instruments. Despite the innovation, the low maximum pressures achieved by the electroosmotic pump (0.7 MPa) limited the analytical column choice and forces to work with lower flow rates increasing the analysis time.

Two years later, Lynch et al. (2017) [117] described a 3 kg (20 × 20 × 17.5 cm^3) portable LC. To minimize the solvent volume and pump size the authors used an electroosmotic pump (EOP) capable of produce $\mu L \cdot min^{-1}$ flow rates with a pressure of 12 MPa. A novel method of producing gradient elution mode using dual electroosmotic pumps and a series of three valves

was described. The system was designed to be able to work with different detection systems such as absorbance or ESI-MS, broadening its applicability. The flow-rate consistency of the system presented certain challenges. As the system was still in its prototype stage, ongoing investigation is being conducted to address the issues related to flow-rate fluctuations.

One of the obstacles when developing a portable LC is to enable battery operation for at least a full working day (8 h). To achieve this, the power requirements, especially those associated to the pumping system, must be minimized. Also, reducing the electrical consumption contributes to lower the carbon footprint. Chatzimichail et al. (2019) [118] reported for the first time a compact portable LC using a zero electrical power pneumatic pump, hence, only a small battery was required for the pressure sensors and detector. These pumps are compact, cheap, simple and, pulse free. These are based on the controlled expansion of a pressurized gas, in this case nitrogen, which pushes the mobile phase through the chromatograph. Linear dependence of pressure with flow rate must exist to get characteristic analyte retention times. The longevity of the pump due to the decrease in the pressure must be controlled. In this system, predictable flow rates in the range of 50 to 1000 $nL \cdot min^{-1}$ were obtained and the pressure drops with consecutive runs were minimal, requiring more than 10000 analyses for the pressure to decrease by 10 % of its initial value. A big limitation of these pumps is their inability to work in gradient elution mode, limiting its applicability.

The Axcend Focus was the first commercialized capillary/nano portable LC [60]. The instrument consists of a compact and cased system with a weight and dimensions of 7.8 kg and 32.0 × 23.1 × 20.1 cm^3. Two high-pressure syringe pumps (max pressure of 70 MPa) allow to generate flow rates in the range of 0.8 to 5 $\mu L \cdot min^{-1}$. An on-column LED detector and a capillary analytical column are comprised in an exchangeable cartridge. Cartridges with different columns and detection wavelength are commercially available

and can be easily installed in the instrument. The system is battery operated allowing to work for more than 10 h away from a d.c. power supply.

Lam et al. (2020) [119] improved the sensitivity of portable LC by using a UV-LED based z-flow cell. Also, proved that the sensitivity can be further improved by coupling it to a small footprint miniaturized MS detector. The system proposed by Li et al. (2020) [120] comprises a battery-operated electrolysis micropump (EMP), a highly integrated LC microchip and an LED-based absorbance detector. As is show in **Figure 10** indicates, Fitzhenry et al. (2021) [121] developed the first portable nitrate analyser, which incorporated an on-column matrix elimination allowing the monitoring of fresh and marine freshwaters.

Our research group MINTOTA evaluated the performance of an Axcend Focus on reference with those provided by two lab LCs (capillary and nano) coupled to DAD. In addition, responses of the portable LC for in-field analysis in several conditions were tested. Besides, two evaluation tools, BETTER criteria (portaBle fiEld Testing sTandard framework) for portability [46] and HEXAGON pictogram [12,122] for sustainability and greenness were applied for comparison purpose.

1.1.1 Criteria for portability

Sharma et al. (2015) [114] proposed a series of requirements that a portable instrument must meet to be considered portable. It establishes different requirements such a minimum weight and size, possible power sources, sustainability related issues, among others. The detailed list is shown below:

(1) Contain all necessary units in a single unit.

(2) Solar or battery operated with > 8 h of autonomy.

(3) Easy operable with minimal supervision.

(4) Rugged enough to withstand changes in temperatures or humidity.

(5) Needs short warm-up times.

(6) Uses low amounts of toxics reagents.

(7) Customized for capillary column use with a non-splitting flow mode and injection, and low dead volumes.

(8) Integrated with a small detector with high sensitivity

(9) Capable of binary gradient generation and competitive in performance to benchtop instruments.

Table 5 shows the portability related characteristics of developed portable LCs, including weight, dimensions, power source, operation time and solvent usage. As it can be seen in this table the mentioned characteristics varies in greatly for the different portable LC.

Table 5. Portability related characteristics of developed portable LC

REF	Weight	Dimension (L x W x H)	Power source	Operation time	Solvent usage [a]
[109]	42 kg	70 x 50 x 30 cm^3	D.c. power supply	Not applicable	10 – 300 mL
[123]	n.a.	n.a.	Battery	n.a.	100 – 500 mL
[124]	14 kg	52 x 20 x 30 cm^3	D.c. power supply	Not applicable	5 – 50 mL
[125]	9.5 kg	41 x 25 x 23 cm^3	Automobile accumulator	n.a.	50 – 1200 mL
[126]	10 kg	28 x 43 x 15 cm^3	D.c. power supply	Not applicable	1 mL
[127]	4 kg	31 x 18 x 14 cm^3	Battery	8 h	5 – 250 µL
[115]	1.2 kg	25 x 25 cm^2	D.c. power supply	Not applicable	2 µL – 70 mL
[116]	2 kg	26 x 18 x 21 cm^3	Battery	26 h	5 mL
[128]	3 kg	20 x 20 x 17.5 cm^3	Laptop USB port	Laptop battery	50 – 800 µL
[129]	6.7 kg	33 x 29 x 14 cm^3	Battery	13 h	25 – 600 µL
[130]	7.8 kg	20 x 23 x 32 cm^3	Battery	12 h	400 – 2400 µL
[131]	2.7 kg	24 x 18 x 16 cm^3	Battery	n.a.	2400 µL
[120]	1.8 kg	20 x 16 x 16 cm^3	Battery	9.3 h	10 mL
[121]	13 kg	60 x 37 x 27 cm^3	Battery	n.a.	350 mL

[a] Total solvent volume assuming non-stop use for a full working day (8 h)

More recently, Rahimi. et al. (2020) [46] developed a criteria to assess LC portability named BETTER criteria. This evaluates different characteristics related to portability such as: the system cost, performance, robustness, operation time, portability, and weight. For each of these, a value from 1 to 5 is given (being 5 the optimum value) and it is represented in a pictogram. This criteria have been used to assess most of the developed portable LCs [46]. This allows a rapid visual evaluation and more objective comparison of the portability of LC systems. More information about the different assessments and criteria can be found in [132]. This criteria aim to serve as a framework that facilitates the comparison between different instruments. Its purpose is to streamline and simplify the process of evaluating and contrasting the various instruments. From the comparison of the different portable LC, Rahimi et al. concluded that even though each of them brings different improvements over the chromatographic separation, there are several areas where more attention is required, such as to offer sufficient performance in a cost-competitive manner and to ensure robustness and stability in the field [46].

To date, portable LC systems meet some of the grade 2 and 3 criteria [13,46,133] for almost all assessments, while grade 4 and 5 criteria are deemed a challenge to be met by next generation devices; indeed, no instrument reported to date reaches grade 5 in any category. Further improvements are needed for in-field analysis in both non-chromatographic and chromatographic characteristics (system cost, cost/test, weight, and performance) as well as in other requirements for in-field analysis (portability, robustness, and sample introduction).

1.3.1 Instrumentation

Ideally, a portable LC sought to minimize the solvent consumption and waste generation while having the dimensions and weight suitable for

hand-transporting (see **Figure 11**), but also maintaining the main figures of merit of conventional benchtop systems. Although the limitations of miniaturized instrumentation make this goal difficult to achieve, several portable LCs have been developed to date to overcome these challenges. Each of them proposes different advances and alternatives either in system instrumentation or portability.

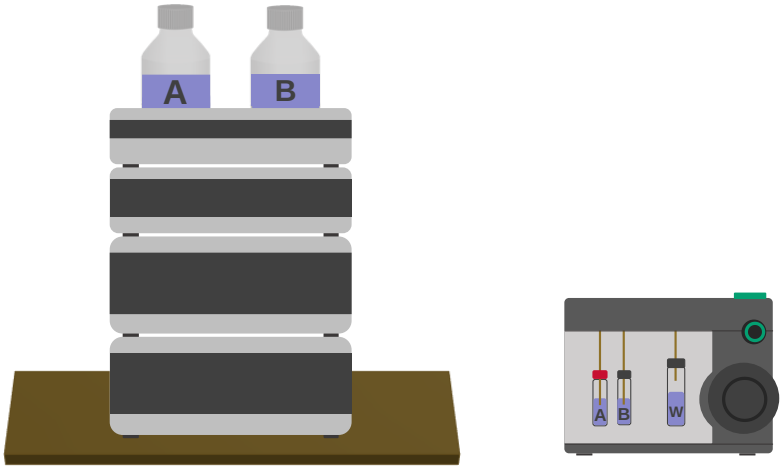

Figure 11. Size comparison between a benchtop (left) and portable LC (right)

Generally, a portable LC consist of 1) a pumping system, to pump the mobile phase through the chromatographic system; 2) an injector, to allows introduce the sample into the system; 3) an analytical column, where the analytical separation is performed; and 4) a detector, which provides the analytical signal (**Figure 12**). Optimally, all these parts must be compactly housed in a solid case minimizing at the same time the number of mobile parts. Furthermore, the construction of the LC platform must be simple enough to be reproduced and to allow its customization.

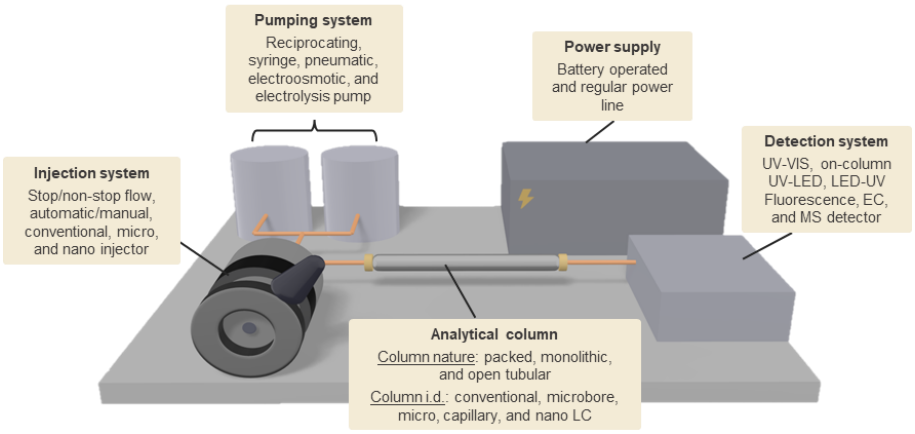

Figure 12. Schematic representation of a portable LC platform showing the different possibilities for injector, pumping system, analytical columns, power supply, and detection system.

1.3.1.1 Pumps

Every LC system needs a solvent delivery unit comprising the mobile phase reservoirs and the pumping system. The later must be capable of generating precise, reproducible, and controlled small flow rates. Pumps that meet these requirements are complex and expensive, hence flow splitting units are widely used for benchtop LCs. In the case of portable LCs, the portability is impaired by the usage of splitters and therefore, the development of appropriate pumps is an added difficulty.

The capabilities of different pumping systems have been tested in several studies being the most popular option the syringe pumps (see T**able 6**). In these pumps, a stepper motor produces a positive displacement of a piston, which constantly transfers the mobile phase at a selected flow rate. The volume of mobile phase delivered per run is limited by the syringe capacity, which is typically low. To address this, some syringe pumps use a second working syringe, which maintains the flow rate while the first syringe is refilled. Miniaturized syringe pumps are commercialised at a relatively low

cost, being able to produce flow rates in the order of $\mu L \cdot min^{-1}$ and hence these are widely used for the construction of portable LC.

Another kind of pumping systems are the reciprocating (or piston) pumps (see **Table 6**). The simplest design of these pumps is based on a single piston, which is driven by an electric motor in and outside the mixing valve, sucking and driving out the mobile phase. The main disadvantage of these pumps is the periodic pulses produced that result in a higher noise in the baseline. To solve this, dual piston pumps (in parallel and serial) are used reducing the pulses by superposition of each piston pulse profile. However, these are more complex and have higher number of moving parts, which are not appropriate for portable instruments.

Besides syringe and reciprocating pumps, more recently, electroosmotic and electrolysis based electrochemical pumps have also been used for chip-based LC as **Table 6** shows. Electroosmotic pumps are compact systems that allow the generation of high-pressure, continuous, and pulse-free electroosmotic flow by applying an external electric field to charged surface (generally silica, PDMS or poly(methyl methacrylate) (PMMA)). Nevertheless, the generation of an electric field requires bulky instrumentation that conflicts with portability. On the other hand, electrolysis pumps use the pneumatic power generated by the electrolysis of a water solution to carry the mobile phase through the chromatographic system. Extra caution must be taken when working with electrolysis pumps since dissolved gas in the solvents may lead to the formation of bubbles adversely affecting the column and detector performance.

One last kind of pumping systems are pneumatic pumps (see **Table 6**). These pumps use the controlled expansion of a pressurized gas as a driver of the mobile phases. Its application to conventional LC is minimal, however it can be an interesting option for portable LC as it makes use of the

latent energy of the pressurized gas and hence the battery requirements are highly reduced.

Table 6. Pumping system specifications for portable LC.

REF	Hydraulics	Nº of pumps	Elution mode	Max pressure
[109]	Syringe (2.5 mL)	One	Isocratic/gradient	5 MPa
[110]	Reciprocating	One	Isocratic	n.a.
[111]	Syringe (2.5 mL)	Two	Isocratic/gradient	7 MPa
[112]	Reciprocating (dual piston)	Two	Isocratic/gradient	35 MPa
[113]	Syringe (0.5 mL)	One	Isocratic/gradient	n.a.
[114]	Syringe (74 µL)	Two	Isocratic/gradient	55 MPa
[115]	Syringe (32.5 µL)	Four	Isocratic/gradient	17 MPa
[116]	Electroosmotic	Two	Isocratic/gradient	0.75 MPa
[117]	Electroosmotic	Two	Isocratic/gradient	14 MPa
[118]	Pneumatic	One	Isocratic	20 MPa
[60]	Syringe	Two	Isocratic/gradient	70 MPa
[119]	Syringe (20 µL)	Two	Isocratic/gradient	> 3.5MPa
[120]	Electrolysis	One	Isocratic	n.a.
[121]	Syringe	Three	Isocratic	n.a.

1.3.1.2 Injectors

In contrast to the solvent delivery units, injectors have not presented a major obstacle in adapting to portable equipment. Stop-flow injectors were utilized, allowing for direct sample introduction at the column head, thereby reducing dead volume (**Table 7**). Alternatively, injection valves were employed for continuous-flow injection. Typical injection valves (6-way) possess two positions: load and injection. In the load position the injected sample goes through the sample loop to the waste while, the mobile phase goes directly to the column. In this step, the sample loop is filled. After that, the valve is switched to the inject position and the mobile phase now goes through the loop carrying the sample to the analytical column. Injection

valves are commercially available in different formats attending to the loop position (internal or external), automation (manual or automated), and sample volume (from few nL to mL).

As commented in the **section 1.2**, the reduction of the i.d. of the analytical column must be accompanied by a reduction in the injection volume (**equation 2**) to avoid an efficiency loss [49]. To overcome this, latest portable minLC opted for VICI Valco nano injectors where sample is loaded in the groove of the injector with volumes down to 4 nL.

Another obstacle that portable LC must overcome is the sample pre-treatment step, which must match the requirements associated to the portability. When working with benchtop nanoLC, on-line sample preconcentration is often used [49]. In many cases, a trap column placed in a switching valve where the sample is first loaded by means of an auxiliary pump (**Figure 7 a**) is used. Then, switching the valve positions makes the mobile phase elutes analytes to the analytical column. This system allows to inject larger volumes of sample, preconcentrating the analyte at the same time that washes salts off. In-tube solid phase microextraction (IT-SPME) is another alternative to the use of trap columns. IT-SPME uses an extractive capillary as a loop, typically a gas chromatography column which can be bought either untreated, so the stationary phase can be synthesized in the laboratory, or with the stationary phase of interest already bounded (**Figure 7 b**). In a first step the sample is injected in the valve preconcentrating the analyte in the extractive capillary. Then, the switching of the valve makes the mobile phase elute the analyte to the analytical column. The use of IT-SPME improves the sensitivity and selectivity, simplifying the pre-treatment step [134].

To the date, reported applications using portable LC employ off-line sample pre-treatment techniques. In reference [63] a protocol based on miniaturized solid phase extraction (SPE) was developed, which can be carried

out on-site, as it involves neither extensive sample manipulation nor additional instrumentation (for solvent evaporation, for instance). The proposed method is suitable to quantify the tested methylxanthines at $\mu g \cdot mL^{-1}$ levels in environmental waters and provides satisfactory linearity and precision, similar to that obtained by IT-SPME-CapLC approach, although the sensitivity attainable is slightly lower. Further advantages of the SPE/nanoLC approach are the better resolution, lower analysis times, and a very significant reduction in solvents consumption. This work represents a pioneer study in the application of portable nanoLC systems for the analysis in-situ of organic pollutants in different kinds of water samples.

The incorporation of the on-line preconcentration techniques described above can suppose a significant improvement in portable LC without compromising their portability.

Table 7. Injectors specifications for portable LC.

REF	Injection mode	Volume	Control
[109]	Stop-flow	n.a.	Auto
[110]	Continuous-flow	20 µL	Auto
[111]	Stop-flow	1 - 100 µL	Auto
[112]	Continuous-flow	20 µL	Manual
[113]	Stop-flow	100 nL	Auto
[114]	Stop-flow	60 nL	Auto
[115]	n.a.	20 nL	Manual
[116]	Continuous-flow	20 nL	Manual
[117]	Stop-flow	60 nL	Manual
[118]	Continuous-flow	2 µL	Manual
[60]	Stop-flow	40 nL	Manual
[119]	Stop-flow	100 nL	Automated
[120]	Stop-flow	1 µL	Manual
[121]	Stop-flow	195 µL	Automated

1.3.1.3 Analytical columns

The downscaling of LC has been closely related to the dimensions of the analytical column, particularly to its internal diameter. It is observed that the reduction of the i.d. of the analytical column produces an increase in the column efficiency resulting in a better chromatographic resolution and improved sensitivity [47].

Mainly, we can find two kinds of analytical columns according to how the stationary phase is filled into the column. On one hand, packed columns are made up of highly packed particles, which constitute or support the stationary phase while the mobile phase goes through the interparticle spaces. As well as the internal diameter, the particle size has also been reduced achieving high efficiency sub-2-micron particle size packed analytical columns. However, working with these columns results in high backpressures, which are hard to withstand for several miniaturized pumps. As alternative, monolithic columns can be used. These columns consist of a continuous unitary porous material with a surface which can be functionalized in countless ways. The high permeability of these columns overcomes the backpressure problems derived from packed columns. Also, the easy fabrication and versatile surface chemistry allow to develop methods with higher selectivity and performance. However, packed columns are still the most widely used and there is a high commercial availability covering multiple i.d., lengths, particle sizes, and stationary phases (see **Table 8**). Nonetheless, in the last few years, various studies proved the possibilities of monolithic columns in the field of portable LC as **Table 8** indicates.

Micro pillar array columns (µPAC) are a novel kind of micro-structured LC columns fabricated by means of lithographic etching where a series of highly ordered pillars coated with an outer porous shell are placed over a silicon chip bed. The main advantage of these columns is the highly homogenous separation paths, which result in a reduction of peak broadening. Also,

the open structure of these columns provides low flow resistance and high permeability lowering the back-pressures and allowing to work with longer columns with its respective increase in efficiency [135]. To date, µPAC columns have applied to omics analysis in benchtop instruments. With the increasing commercial availability, these columns can expect to be a potential improvement in portable LC applications.

1.3.1.4 Detectors

There are a wide range of detectors compatible with LC, such as: UV-vis, fluorescence, refractive index, light scattering, electrochemical (EC), conductivity, and mass spectrometry detectors. Among these, absorbance-based detectors were the most successful when applied to portable LC due to its ease of miniaturization, sensitivity, selectivity, flexibility, and robustness. First portable LC used spectrophotometers with standard light sources such as deuterium or mercury lamps, which are relatively large and require high-power supplies. Also, flow cells add an extra-column dispersion resulting in band broadening. The development of nano flow cells together with U and Z shaped optical paths significantly decreased the band-broadening while inreased the sensitivity. In [119] an Agilent high-sensitivity capillary detection cell (HSDC) was housed in customised 3D printed detector assembly, together with a 255 nm UV-LED light source and a UV broadband photodiode as the detector element. This HSDC was originally developed to overcome the sensitivity limitations of standard on-column detection in capillary electrophoresis. It is a coin-sized cell (~ 11 g), with a z-shaped flow-through channel (100 µm x100 µm rectangular channel) that has a cell volume of 12 nL and specified path length of 1.2 mm. Two pin holes (2 mm i.d.) in the central position are set on both sides of the HSDC to align with the light source. The flow channel is made entirely of black fused-silica and is designed to ensure 100% transmission of light, with the reflective interior functioning as a light pipe, to minimize stray light.

A major step in the way of miniaturization takes place with the incorporation of light emitting diodes as a light source (**Table 8**). These sources greatly reduce the power supply at the same time that are smaller, more compact, and require less warm-time than standard light sources. With the introduction of capillary columns, the dead volumes generated by the flow-cells became even more noticeable. To overcome this, many portable LC opted for on-column detection configurations, which do not make use of flow-cells eliminating the associated dead volumes. In these, the radiation produced by the LED must be directed narrowly and focused into the capillary window while the slit size must be small enough to avoid the interference of stray light. Main disadvantage of on-column detection is the limited sensitivity, which depends on the internal diameter of the column, however, the benefits that bring to portability generally make them the preferred choice.

EC detectors were also used in portable LC, which measure the electrical current produced by a redox process. The flow-cells and electrodes can be easily miniaturized and hence incorporated in the microfluidic system. Unlike absorbance detectors these can be miniaturized without performance loss. EC detectors have a wide detection range, high selectivity, and high sensitivity but are only responsive to a specific analyte class, so their applications are limited to those substances presenting redox properties.

When working with conventional LC, MS is the preferred detection technique for most applications. MS first obtain the organic molecular ions in a gas phase to later be separated in function of their mass charge ratio (m/z). These molecular ions can be further broken by applying an electronic collision energy (tandem MS). The limits of detection achieved by MS detectors are in most of cases superior to other techniques as well as the selectivity, however, the most interesting feature is the structural information they provide making possible the structural elucidation and compound identification. These instruments are expensive, complex, and large so the incorporation

to portable LC is challenging [119,136]. Many efforts have been done to miniaturize them and some have been successfully commercialized but, even so, the total weight is high and require an external power supply, so its application is restricted to in-situ monitoring stations.

Table 8. Column and detector specifications for the different portable LC.

REF	Column type	Column dimensions	Detector
[109]	IE micro packed column	1.0 × 20 – 50 mm	Multi λ UV
[110]	RP conventional packed column	4.6 × 30 mm, 10 µm	EC
[111]	RP microbore packed column	2.0 × 60 – 80 mm, 5 µm	Multi λ UV
[112]	RP conventional packed column	4.6 × 100 mm, 5 µm	Fixed λ UV
[113]	IE capillary packed column	0.18 × 500 mm	Conductivity
[114]	PEGDA capillary monolithic column	0.15 × 165 mm	On-column UV LED
[115]	RP nano monolithic column	0.1 × 180 mm	On-column LED UV
[116]	RP micro-chip packed column	0.8 × 30 mm, 3 µm	Micro EC
[117]	RP nano packed column	0.75 × 100 mm, 3 µm	Fixed λ UV
[118]	RP micro, capillary, and nano packed and monolithic columns	0.15 × 30 mm, 3 µm 0.15 × 70 mm, 5 µm 0.15 × 80 mm, 5 µm 0.1 × 150 mm	LED UV
[60]	RP capillary packed column	0.15 × 100 mm, 2 µm	On-column LED UV
[119]	RP capillary packed column	0.3 – 0.15 × 100 mm, 5 µm	LED UV
[120]	RP micro-chip packed column	0.5 × 40 mm, 5 µm	On-column LED UV
[121]	AE conventional column	4.0 × 50 mm, 9 µm	LED UV

1.3.2 Applications of portable LC

Nowadays, portable instrumentation is a valuable tool in different fields of analytical chemistry such as environment [137], health [138] and food and drinks industry [139]. **Figure 13** shows the different percentages of the most common areas for portable instrumentation in general. It is remarkable its use in health and environment fields.

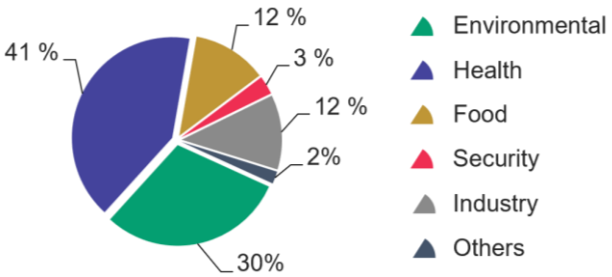

Figure 13. Percentage of different applications for portable instrumentation. Source: Web of Science, consulted in January 2023.

Most of the portable LC are lab-made and have never been commercialized [13]. This results in a limited number of applications as, in most of cases, only one scientific work is derived from each portable LC. The MiLiChrom-4 (Microcolumn Liquid Chromatographs) was one of the few commercialized portable-LC [111]. There are several reports showing its capabilities in different areas, but its high weight (14 kg) and the fact of not being battery operated makes it difficult to truly consider it as portable. Abonamah et al. (2019) [140] utilized a commercial nanoLC (Easy NanoLC Thermo) coupled to ESI-MS detector for on-site detection of fentanyl and its derivatives. As for the previous LC, its higher weight, 37 kg, makes hard to consider it as portable. There are several works where the Easy Nano-LC is utilized for different determinations, however, most of them use it as a benchtop nanoLC.

Recently, the Axcend Focus LC (weight 8 kg), a new fully portable capillary LC has been commercialized [60]. **Figure 14** shows a schematic representation of the system, which integrates the analytical column and a

single or dual LED on-column detector in a cartridge in the fluidic circuit. In the few years since its commercialization various works have tested its possibilities in different applications for in-situ or point of care analysis, such as: determinations of pharmaceutical and illicit drugs in tablets [60], synthetic cathinones [141], biocides in fruit washing residual waters [13], caffeine in environmental waters [63], caffeine and chlorogenic acids in dietary supplements [142,143], scopolamine in beverages [144] and, even educational demonstrations [145].

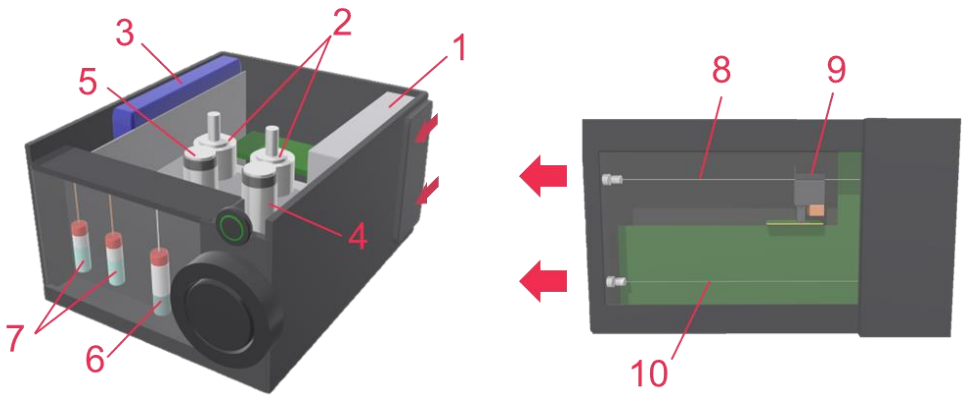

Figure 14. Schematic representation of the Axcend Focus LC (left) and the interchangeable cartridge (right). 1) Interchangeable cartridge, 2) Syringe pumps, 3) battery, 4) injection valve, 5) mixing valve, 6) waste vial, 7) solvent vial, 8) analytical column, 9) on-column UV-LED detector, and 10) to waste capillary.

In this Thesis, the capabilities of a portable Axcend minLC (LED 255 nm) were studied for in-field analysis and its figures of merit were compared with those obtained for benchtop capLC and nanoLC. Also, for objective evaluation the of the instrument and method the BETTER criteria and HEXAGON tool were used.

1.4 Studied matrices and analytes

In the development of the thesis, miniaturized LC, both benchtop and portable systems, has been applied for the analysis of various matrices, in-

cluding environmental samples, biological samples, and nanoparticle dispersions. In this section, different aspects of each matrix will be discussed in relation with the undertaken work.

1.4.1 Environmental samples

The increasing consumption and production of organic compounds have led the contamination of water bodies, biota, soil, and air in the environment. There are diverse pathways and sources by which a contaminant can enter the ecosystem, being the agriculture, industry, and human residues the main routes. Among the organic contaminants, persistent organic pollutants (POPs) are a topic of concern since these persist in the environment and bioaccumulate having toxic effects on humans and the ecosystem [146–148].

To address this situation, several regulations have been adopted to establish a list of pollutants to be monitored and controlled by analytical methods, as well as the maximum allowed concentrations of these. It is worth noting that this list remains open to updates and modifications. The EU Water Framework Directive outlines selected priority substances with the purpose of protect the inland surface waters, transitional waters, coastal waters, and groundwater [149]. Included in these priority substances are heavy metals and its compounds; VOCs; PAHs; and different pesticides families. There are also contaminants of emerging concern (CECs) which have been detected in environmental systems, may have adverse effects on the ecosystem and are not regulated under current legislation. This group include pharmaceuticals, personal care products, licit and illicit drugs, endocrine disruptors, newly registered pesticides, surfactants, high technology rate earth elements, natural and engineered nanomaterials, among others [150]. In the last few years, CECs, are receiving high attention, reflected in the numerous reviews reported [151–156].

Historically, GC and LC have been the go-to methods for determination of pollutants in the environment. GC coupled with mass spectrometry (GC-MS) has typically been used to identify volatile and non-polar pollutants, while LC coupled with MS is useful for detecting more polar micropollutants [33]. However, due to stricter environmental regulations and the need to detect emerging pollutants, there is a growing demand for faster, more cost-effective, and environmentally friendly methods of analysis that produce less waste. Additionally, the need to detect certain substances at ultra-low levels requires highly sensitive methods and in-situ solution. To meet these challenges, miniaturized LC techniques have emerged as a promising tool for achieving these goals.

1.4.1.1 Pesticides

Pesticides are a group of substances including herbicides, insecticides, rodenticide, fungicides and, in general, any other kind of substance used for pest control. These can be classified in function of its chemical nature being there six main groups 1) organophosphorus pesticides, 2) organochlorines, 3) carbamates 4) pyrethroids, 5) triazines, and 6) urea derivates. The main use of pesticides attends to increase the agriculture out-put since these greatly prevents losses from weeds and insect pests in the crops. Also, pesticides are utilized in health care for example to contain infection spread or in forestry to protect trees from weeds, insect, and diseases.

Despite pesticides are supposed to be lethal only to the target pests, pesticides can be toxic to other non-target organism being insecticides and herbicides those with the higher toxicologic risk [157]. Also, the high persistence and mobility of some of these substances causes to move off the site of application reaching surface and ground water [158] and consequently, bioaccumulating in the food chain [159]. To prevent this, there are several regulations for its application and concentration limits in environmental and

drinking waters [160–162] .The legal limit in drinking water is generally 0.1 $\mu g \cdot L^{-1}$ for the individual and 0.5 $\mu g \cdot L^{-1}$ for the total pesticides while, for surface waters, the environmental quality standard is variable for each pesticide, ranging from $ng \cdot L^{-1}$ to $\mu g \cdot L^{-1}$. **Table 9** shows a list of the studied pesticides and some properties.

Table 9. Classification, octanol-water partition coefficient, and structure of the studied pesticides. $LogK_{ow}$ were obtained from PubChem database.

Analyte (Abrev.)	**Class**	**logK_{ow}**	**Structure**
Fluometuron (FMT)	Phenylurea	2.42	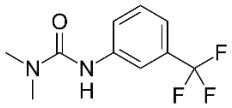
Isoproturon (IPT)	Phenylurea	2.87	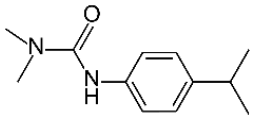
Imazalil (IMZ)	Imidazole	3.82	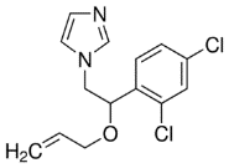
Metribuzin (MBZ)	Triazines	1.7	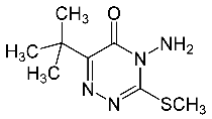
O-phenyl phenol (OPP)	Hydroxyphenyls	3.09	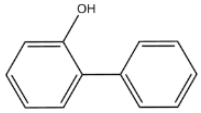
Potassium sorbate (PS)	n.a.	-1.72	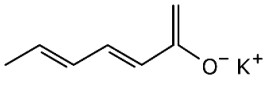
Pyrimethanil (PMA)	Anilinopyrimidine	3.52	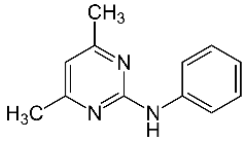
Tribenuron methyl (TBN-m)	Sulfonylurea	0.78	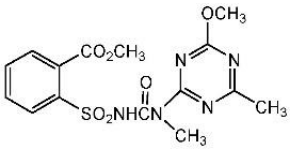

1.1.1.1 Drugs

Drugs are substances that, when ingested, cause a physiological or psychological change in the individual. This term, therefore, includes many substances, including pharmaceuticals, licit and illicit drugs, endocrine disruptors, estrogens, and new psychoactive substances, among others. Pharmaceutical drugs have been widely used for the treatment of all kinds of diseases, increasing the lifetime as well as the life quality of humans and animals. However, the increasing production of these substances along with the lack of specific guidelines for its regulation causes them to end up in the environment (specially in aquatic one due to their low volatility) from different effluents: human and animal, industrial and hospitals [163]. These substances have been found in sewage treatment plants, surface waters, sea waters, ground waters and drinking waters at concentrations usually ranging $ng \cdot L^{-1}$ to $\mu g \cdot L^{-1}$ [164]. Despite these substances are unlike to pose a risk for acute toxicity at these concentrations, toxicological information of long-term low-level exposure is lacking [165,166].

The European Commission, in the Directive 2008/105/EC, published a list of different compounds (9 classified as pharmaceutical drugs) to be controlled in surface waters since these are known to present an environmental risk [167]. Recently, the European Commission, has developed a strategy to address the impact of pharmaceutical drugs (both, human and veterinary) in its full lifecycle in the environment [168]. Since many of these substances are known to cause long-term environmental risk at very low concentrations, for example, paracetamol, one of the most widely used drugs, was proved to pose a risk on reproductive system of marine mussels (and hence in its population survivability) at 40 $ng \cdot L^{-1}$ concentrations for 24 days exposure [169].

Table 10 shows a list of the different drugs studied and its properties. Acetaminophen (APAP), which is a popular analgesic and antipyretic pharmaceutical; and caffeine (CAF), proxyphylline (PPF), theobromine (TBM), and theophylline (TPL), which are methylxanthines with mild stimulant properties were analysed.

Table 10. Classification, octanol-water partition coefficient, and structure of the studied drugs. LogK_{ow} were obtained from PubChem database.

Analyte (Abrev.)	**Class**	**logK_{ow}**	**Structure**
Acetaminophen (APAP)	Analgesics and antipyretics	0.46	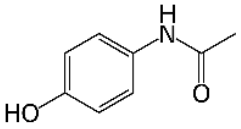
Caffeine (CAF)	Methylxanthines	-0.07	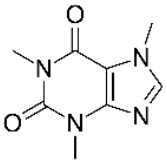
Proxyphylline (PPF)	Methylxanthines	-0.27	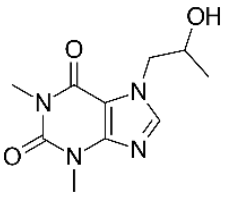
Theobromine (TBM)	Methylxanthines	-0.78	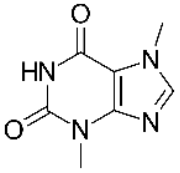
Theophylline (TPL)	Methylxanthines	-0.02	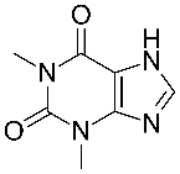

1.4.1.2 Legislated nitrogen compounds

Nitrogen can be found in natural water as dissolved inorganic N (DIN) in the form of ammonium, nitrite, and nitrate species, and organic N (DON), including amino acids, nucleotides, and nitrogen-containing pesticides, such as phenylureas, among others [170,171]. DON only contributes to a relatively small portion of the total dissolved nitrogen (TDN) in surface waters. The TDN is the sum of DIN and DON (see **equation 4**).

$$TDN = DIN + DON = (NH_3/NH_4^+ + NO_3^- + NO_2^-) + DON \quad (4)$$

All these compounds, particularly ammonium and nitrate, play an important role in water quality and, therefore, are regulated by different European legislations as **Table 11** shows.

Table 11. European legislation concerning the N compounds in water

Sample	**Legislation**	**Legislated concentration ($mg \cdot L^{-1}$)**
Drinking water	European legislation EEC/98/83	Nitrite: 0.5 Nitrate: 50 Ammonium: 0.5
Aquatic environment	Water Framework Directive 2000/60/E Directive 2008/105/EC Directive 2013/39/EC RD 817/2015 (Spain)*	Nitrite: 3 Nitrate: 50 **Rivers***: ammonium (0.3 – 1), nitrate (10 – 25) **Transitional waters*:** ammonium (0.15 – 1), nitrate (7.5 – 11), nitrite (0.1 – 0.2), Total N (5 – 10). **Coastal*:** ammonium (0.03 – 0.1), nitrate (0.06 – 2), nitrite (0.02 – 0.04).
Wastewater	Directive 91/271/EEC Directive 98/15/EC SWD (2019) 700 final	Diuron (0.0002 – 0.0018) Isoproturon (0.0001 – 0.0010)

Nitrate is the main DIN specie and can enter the environment either from natural or anthropogenic sources. Its concentration in the natural waters

have drastically increased over the 20th and 21st century primarily due to the increment in nitrogen based fertilizers which usage has steadily increased from ~10 Mt in the 1960, to ~70 Mt and over 100 Mt in 2000 and 2020 respectively [172]. Part of the nitrogen used in fertilizer drains from the fields to contaminate surface and groundwater having several health problems and promoting the eutrophication of surface waters [173–176]. Other minor nitrate and nitrite sources in the environment are the domestic sewage discharge, explosives fabrication, or the alimentary and cosmetic industry.

To control the levels of nitrate a series of legislation have been developed (see **Table 11**). Council Directive 98/83/EC relative to the quality of water intended for consumption set the maximum concentration of nitrate at 50 $mg \cdot L^{-1}$ in drinking water [160]. As well, the World Health Organization (WHO) in its Guideline for drinking water set a reference value of concentration 50 $mg \cdot L^{-1}$ for nitrate [177]. For environmental waters, the Water Framework Directive 2000/60/EC regulates both surface and groundwater and stablishing a monitoring and action plan for nitrate vulnerable zones [178,179]. The maximum concentration levels depend on the type of water body. The Real Decreto 817/2015 (Spain) stablishes a guideline value for nitrate between 10 – 15 $mg \cdot L^{-1}$, 7.5 – 11 $mg \cdot L^{-1}$, and 0.06 – 2 $mg \cdot L^{-1}$ for rivers, transition waters, and coastal waters respectively [180].

1.4.2 Biological fluids

All biological materials obtained from living or deceased organisms are referred to as biological samples. These materials include tissues, cells, and different biological fluids, being of relevance the blood, urine, and saliva. There exist guidelines for the collection, processing, and storage of these samples, indicating the best practices which result in best quality specimens for research purposes [181].

Regarding, biological fluids, these are complex samples that contains different proteins, phospholipids, organic compounds and salts requiring appropriate processing, including stages of separation, purification, enrichment, and chemical modification [182]. In most cases, a sample preparation step is required to reduce matrix effects and eliminate potential interferents. Conventional approaches such as protein precipitation followed by centrifugation, LLE or SPE are widely used in bioanalysis [183,184]. Also, more advanced techniques based on microextraction such as SPME [185], DLLME [186], on-fiber SPME [187], or IT-SPME [82,88] are emerging aiming to reduce the amount of solvent required as well as the sample volume .

Separation step is commonly performed using LC coupled with DAD, MS, or MS/MS detectors. The latest is of special interest due to its selectivity, sensitivity, and capability for identification and structural elucidation. UHPLC-ESI-MS/MS is a powerful and essential technique in the analysis of biological samples in both clinical and forensic laboratories [188]. Miniaturization plays an important role when working with these matrices, offering advantages such as the small sample required to perform the analysis, the lower solvent used and waste generated, and the enhanced sensitivity when coupled to nESI sources [51].

1.4.2.1 Acetaminophen in urine

Acetaminophen, also known as paracetamol, is a widely commercially available over-the-counter medication that is used as an analgesic and antipyretic agent. Properly dosed, it can effectively reduce fever and alleviate mild to moderate pain. However, the accessibility of this medication, combined with the lack of knowledge about its toxicity, causes APAP overdose to be a leading cause of drug-induced injury, particularly acute liver failure . In some European countries, reported cases of liver failure caused by APAP range from 2% in Spain to 57% in the UK . Deliberate self-harm has also

contributed to a rise in the incidence of APAP-induced hepatotoxicity, particularly in the UK [189].

APAP is metabolized by the liver and, in adults, undergoes conjugation with glucoronide by glucoronyl transferase comprising the 57 % of its urinary metabolites while sulphonyl transferase leads to the sulphuration process leading to the formation of acetaminophen-sulfate (APAP-sulf) accounting for 30-44 % of the metabolites. A little fraction of the ingested APAP is metabolized by the cytochrome P450, leading to the APAP hydroxylation, and resulting in metabolite N-acetil-p-benzoquinona imina (NAPQI) (5 – 10 % of the urinary metabolites) which is highly toxic for the hepatic tissues being the main responsible of APAP induced hepatoxicity (**Figure 15**). Less of the 5 % of the ingested APAP is excreted by the urine unchanged [190]. Recommended maximum dosages are 4 g per day and 50 - 75 $mg \cdot Kg^{-1}$ per day for adults and children respectively. Single dosages over 7.5 g for adults and 150 $mg \cdot Kg^{-1}$ are considered potentially toxic and may produce hepatic injures [191].

To identify cases of APAP overdoses, serum and urine determinations are performed. The Runack-Mathew nomogram plots the APAP concentration against the time since ingestion, allowing to diagnose a possible liver toxicity. In the literature there have been reported different techniques for APAP determination in biological fluids such as spectroscopy techniques including colorimetry [192–194], Fourier transform infrared spectroscopy (FTIR) [195], Raman spectrometry [196], and fluorescence spectroscopy [197,198]; electrochemical techniques like differential pulse voltammetry (DPV) [199] and square wave voltammetry (SWV) [200,201] which are gaining interest in the latest years due to its simplicity, low-cost, in-situ analysis possibility [202]; and chromatographic techniques such as LC-UV [203], LC-MS/MS [204–206], and to a lesser extent GC-MS/MS [207] due to APAP low volatility.

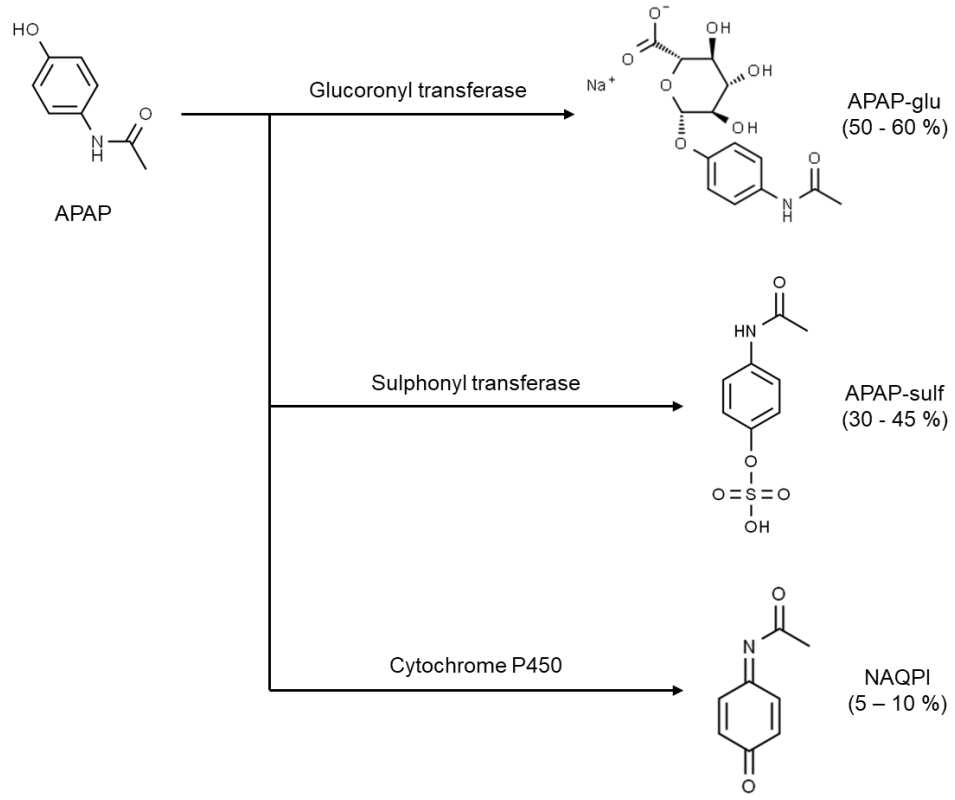

Figure 15. Schematic representation of the APAP main metabolic pathways.

In this Thesis, the IT-SPME-nanoLC-DAD is proposed as a simple, fast, and cost-effective technique for the determination of APAP in urine sample. The obtained results were compared to those obtained by UHPLC-QTOF and DART-QTOF. Furthermore, the HEXAGON tool was used to compare greenness and sustainability of all three methodologies.

1.4.3 Metallic nanoparticles

Nanomaterials are defined by the International Organization of Standardization in ISO/TS/ 80004 as: “the material with any external dimension in the nanoscale or having internal structure or surface structure in the nanoscale, being the nanoscale range between 1 nm and 100 nm”. A more technical and wider definition is proposed by the European Commission in

2022/C299/01 establishing a nanomaterial as: “a natural, incidental or manufactured material consisting of solid particles that are present, either on their own or as identifiable constituent particles in aggregates or agglomerates, and where 50 % or more of these particles in the number-based size distribution fulfils at least one of the following conditions: 1) one or more external dimension of the particle are in in the size range from 1 nm to 100 nm; 2) the particle has an elongated shape, such as a rod, fiber or tube, where two external dimensions are smaller than 1 nm and the other dimension is larger than 100 nm; and 3) the particle has a plate-like shape, where one external dimension is smaller than 1 nm and the other dimensions are larger than 100 nm”.

Metallic NPs are a class of nanomaterials which are composed of pure metals such as silver, gold, magnesium, titanium, copper, zinc, iron, among others, as well as its compounds as metal oxides, sulfides, phosphates, or hydroxides [208]. Noble metal NPs has a number of specific characteristics that differentiate them from macroscopic metals being the main feature its high surface area to volume ratio favouring its interaction with other particles. Other properties of metallic NPs are the large surface energies, quantum confinement, plasmon excitation, increased number of kinks, and a the most important feature, their high surface is to volume ratio [209]. These unique properties lead to a growing interest in their synthesis, characterisation methods [210–212] as well as its applicability in biomedicine as nanocarrier [213], imaging [214], or in cancer therapy [215]; environmental remediation [216]; and industry [217,218].

Metallic nanoparticles (MNPs) synthesis can be done following a top-down approach, starting from the bulk macroscopic material which is reduced to the nanoscale by different methods such as mechanical milling, evaporation/condensation, laser pyrolysis, ionic/electronic radiation. On the other

hand, the synthesis can be done by a bottom-up approach from smaller molecules and/or atoms by means of chemical methods such as chemical/electrochemical precipitation, atomic/molecular condensation, vapor deposition, sol-gel process, laser pyrolysis; and biological methods using bacteria, plant extracts, fungus, and algae [219].

Characterization of metallic NPs is important to predict its behaviour and determinate its biological and toxicological effects. Chemical and physical information such as shape, size, size distribution, surface charge, porosity, among others, can be obtained by different characterization techniques, being the most used the absorbance spectroscopy, transmission electron microscopy (TEM), scanning electron microscopy (SEM), dynamic light scattering (DLS), atomic force microscopy (AFM), x-ray diffraction (XRD), FTIR, and LC (**Table 12**). The different techniques are comprehensively reviewed by Mourdikoudis, et al. (2018) [220].

Noble metal NPs (NMNPs) such as silver and gold NPs (AgNPs and AuNPs respectively) are becoming more and more used in areas such as food sciences, cosmetics, and biomedicine (**Figure 16**). These are of special interest in sensing and imaging applications due to their optical properties, particularly its surface plasmon of resonance (SPR) [221–223]. The SPR is produced due to the collective oscillation of the conduction electrons at the interface of metals and dielectric materials under the resonant excitation of electromagnetic radiation. When the SPR is confined in the surface of nanometric structures as it is in the surface of AgNPs and AuNPs (with particle size smaller than wavelength) , the incident light is scattered producing a localized surface plasmon of resonance (LSPR) resulting in high extinction coefficients in the visible region [224] (**Figure 17**). It must be noted that not only macroscopic materials do not exhibit LSPR band, but also nanoparticles with sizes below 2 nm [225]. LSPR frequency is dependant of the nanoparticle size, shape, dielectric constant, medium, and material nature [226,227].

Table 12. Main techniques used for nanoparticle characterization.

Technique	Principle	Information provided	REF
TEM	Electrons are transmitted through a thin sample to form an image	Morphology Size Shape Crystallinity	[228]
SEM	Electrons are scanned over the surface of a sample to form an image	Surface morphology Size Shape Crystallinity	[229]
XRD	X-rays are diffracted by a crystalline sample to produce a diffraction pattern	Crystallinity Phase identification Particle Size	[230]
DLS	Light is scattered by particles in Brownian motion	Hydrodynamic diameter Size distribution Zeta potential	[231]
UV-vis	UV-vis light is absorbed/transmitted by molecules in solution	Quantification LSPR	[232]
FTIR	Infrared light is absorbed and reflected by molecules	Chemical composition Functional groups Surface modifications	[233]
AFM	Probe scans the surface of the sample	Surface morphology Roughness Mechanical properties	[234]
LC	The analytes are separated based on the different interactions with a mobile and stationary phase	Quantification Size	[165, 166]

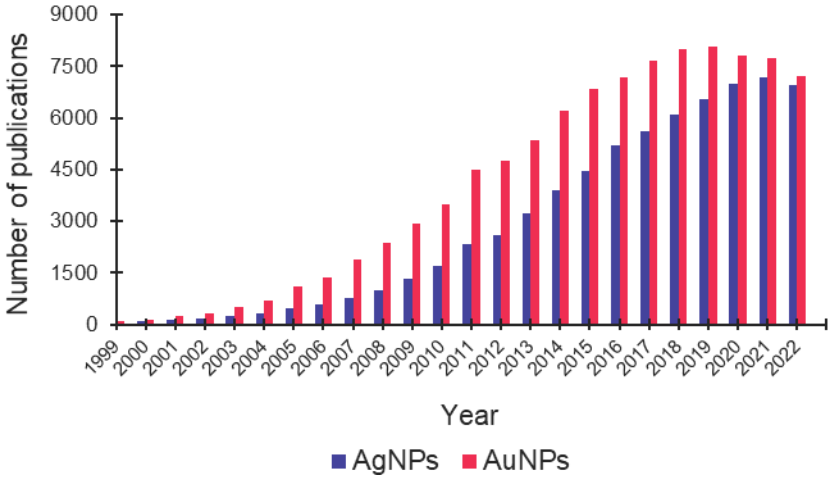

Figure 16. Evolution of the number of publications with time using the following searching topics in the Web of Science database: “AgNPs” or “silver nanoparticles” (blue bars) and “AuNPs” or “gold nanoparticles” (red bars).

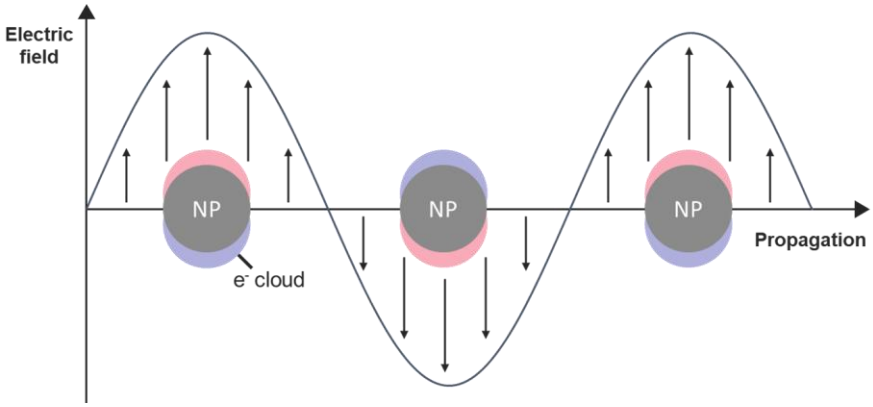

Figure 17. Schematic representation of the LSPR showing the oscillation of the free conduction electron in metallic nanoparticles under resonant excitation of electro-magnetic radiation.

AgNPs and AuNPs are widely used in textile coverings [237,238], food processing and packaging [239,240], and cosmetics [241,242] due to its antibacterial and anti-inflammatory property. In addition, these NPs are of vital importance in nanomedicine being successfully used in cancer control [243], diabetes treatment diabetes treatment [244], drug delivery [245,246] biosensing and imaging [247–249], among other many uses.

1.4.3.1 Noble metal nanoparticles dispersions

A dispersion is defined by the IUPAC as a “material comprising more than one phase where at least one of the phases consists of finely divided phase domains, often in the colloidal size range, dispersed throughout a continuous phase” [250]. Depending on the states of the dispersed and continuous phase there exist different types of dispersions. In these where the dispersed phase consists of a solid in the sub-micron scale and the continuous phase is a liquid are classified as colloids. In the case of metallic NPs, after its synthesis, these are dispersed in a liquid phase to obtain colloidally stable NPs dispersions that can be further utilized in the fabrication of useful components and devices.

The stability of metallic NPs dispersions is controlled by two main factors. On the one side, the particle size should be in the sub-micron scale, so the thermal fluctuations in the fluid can overcome the effect of gravity, preventing sedimentation or flotation. On the other hand, to prevent the formation of aggregates, repulsive interactions between nanoparticles should be higher than attractive ones [251]. The thermal motion in the fluid makes the nanoparticles to collide, interacting in the immediate vicinity by London-Van-der-Waals attractive forces, resulting in aggregates that ultimately sediment [252]. For most solvents, including conventional ones like water, their dispersing capacity is not sufficient to produce stable dispersions of nanoparticles and stabilizing agents are required. Generally, the stabilization of the dispersion is achieved by means of a capping which modify the nanoparticle surface in two possible ways: 1) by the inclusion of surface long-chain steric ligands producing steric repulsion between the nanoparticles, and 2) by formation of a charged surface coating resulting in electrostatic repulsive interactions [253,254]. There is a wide variety of possible capping agents, including polymers such as polyethylene glycol (PEG), polyvinylpyrrolidone (PVP), polyvinyl alcohol (PVA), and chitosan; salts such as PBS and citrate;

and surfactants such as cetyltrimethylammonium bromide (CTAB) or sodium dodecyl sulfate (SDS), among others.

Noble metal nanoparticles dispersions, such as AgNPs and AuNPs, have garnered significant attention for their potential applications in sensing application. In recent years, numerous reviews on this topic have demonstrated its relevance [255–261]. Of particular scientific interest are sensors based on the LSPR, or plasmonic sensors, where the presence of the analyte produces a change in the composition, size, shape, medium, or aggregate state of the nanoparticles, which translates in a shift in the LSPR or, in other words, an observable colour change that can be measured with UV-vis spectrometers. There are a series of properties which AgNPs and AuNPs poses which make them ideal for LSRP sensing. The high extinction coefficient derived from their intense LSPR band, along with their high surface-to-volume ratio, results in a significant increase in sensitivity. Furthermore, noble metal nanoparticles are easy to synthesize, chemically stable, biocompatible, and allow for a wide variety of surface modifications to increase their selectivity [262].

Among the various types of plasmonic sensors, those which benefits of the aggregation of AgNPs and AuNPs as a readout have gained widespread use in diverse fields, such as biological [263–265], clinical [266,267], food sciences [268,269], and environmental applications [270,271]. In these, the selective interaction between the NPs surroundings and the analyte by means of mainly hydrogen bonds and electrostatic interactions induce the aggregation of NPs resulting in a visible colour change from red to blue and from yellow to brown for Au and Ag nanospheres respectively (**Figure 18**). However, these assays can be limited by the lack of reproducibility of both, the NPs dispersions which is affected by the solvent, pH, atmosphere, temperature and, and the matrix; and the aggregation profile which depends on the size distribution, shape, and dielectric environment of the starting NPS

[262]. In this sense, analysis to evaluate the size and stability of the NPs is key to obtain reliable results.

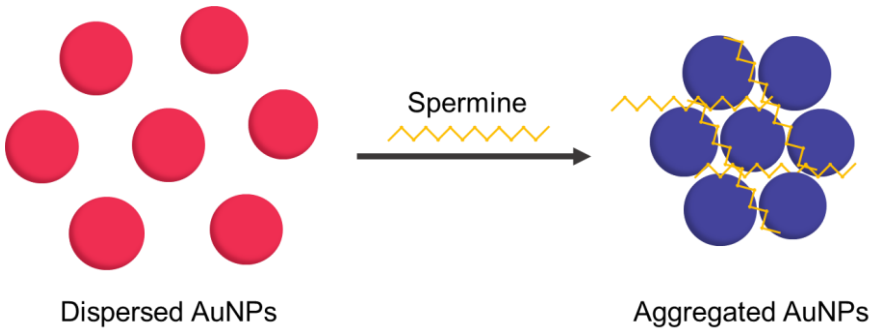

Figure 18. Schematic representation of the AuNPs induced aggregation by spermine. The spermine stabilizes the aggregation thanks to the affinity of its amino groups for the nanoparticle surface. The aggregation produces a shift in the AuNPs LSPR resulting in a colour change from red to blue [266].

In this thesis, the capabilities of IT-SPME-nanoLC-DAD and IT-SPME-capLC-DAD will be studied for the evaluation and characterization of AgNPs, AuNPs, and its mixtures. Also, the LSPR responses obtained from acid aggregation plasmonic assays will be monitored by the mentioned techniques.

1.4.3.2 Metallic nanoparticle transformations

The increasing consumption of metallic and metal oxide NPs has led to a corresponding increase in their release into the environment. NPs can originate from numerous sources, including natural events such as volcanic activity, dust storms, forest fires, and soil erosion caused by wind or water; accidental anthropogenic sources such as vehicle exhaust, fuel cells, welding, and certain industrial processes; and intentional anthropogenic sources such as engineered NPs used in industry, groundwater remediation, drug delivery, diagnosis, and imaging [272]. Understanding the transformations of NPs is essential to comprehending their fate, transport, and implications for the environment.

The physico-chemical properties of the NPs (size, shape, zeta potential, chemical composition, and surface area, charge, and modifications and the medium conditions (e. g. ionic strength, temperature, microorganism, substances present in matrix, etc.) are the main factors driving the NPs transformations, which can be classified depending on whether a physical, chemical, or biological process is involved (**Figure 19**). In the environment, water sources are complex matrices that contains varying properties, diverse organic and inorganic substances, and a wide range of microorganisms, resulting in intricate and diverse transformation pathways [273–275]. Some of these transformations can increase the toxicity of NPs, such as CuO NPs, which have been shown to increase their solubility in low ionic strength media having potential impacts on aquatic organisms [276].

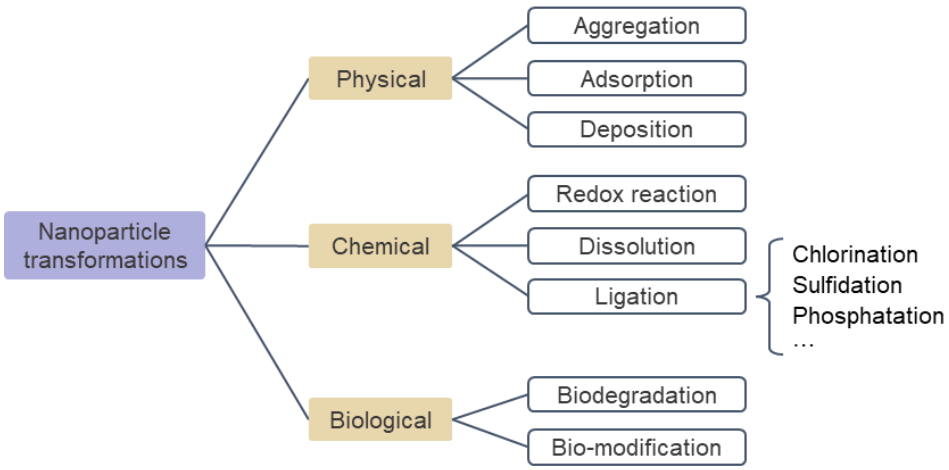

Figure 19. Tree diagram of the different NPs transformations in the environment.

The study of AgNPs is of special relevance due to its generalised use and its potential toxicity. The toxicity has been proved in different studies [277–279] and it has been related to the indirect liberation of Ag^+ ions [280] . These have a high affinity for thiol groups present in cysteine residues within respiratory and transport proteins. The interaction between Ag^+ ions and these proteins can lead to significant biological effects, including the uncoupling of respiration from ATP synthesis through the inhibition of enzymes like

NADH dehydrogenase. Additionally, the binding of Ag^+ ions to transport proteins can result in proton leakage and the collapse of the proton motive force [281]. These findings highlight the potential for Ag^+ ions to influence cellular processes and contribute to the toxic effects of silver exposure. However other studies point to a direct toxic effect of the AgNPs in the microorganism [282,283] . Overall, the toxicity of AgNPs on the organisms are not fully understood.

AgNPs can undergo various transformations in the environment, with the most relevant ones being oxidative dissolution, sulfidation, chlorination, and reduction of Ag^+ ions to AgNPs (as illustrated in **Figure 20**). In the case of oxidative dissolution, the AgNPs are first converted to Ag_2O via an oxidizing agent, typically dissolved O_2 or H_2O_2. The formed Ag_2O shell rapidly dissolves in water, releasing the Ag_+ ions. During this process, some reactive oxygen species (ROS) may form, which can have toxic effects such as oxidative stress and inflammation and can further dissolve the AgNPs [284].

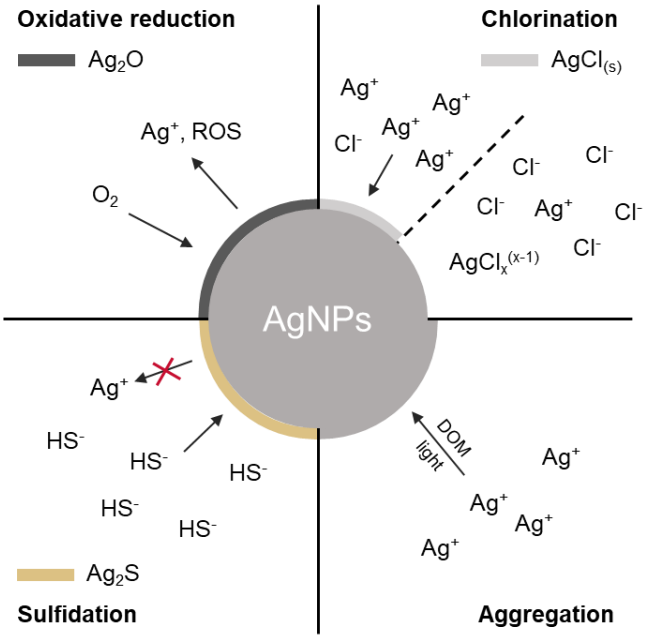

Figure 20. Graphical resume of the main AgNPs transformations in the environment.

Sulfidation is an important process that occurs under anoxic conditions due to the rapid oxidation of HS^-. The sulfidation mechanism involves the formation of an Ag-Ag_2S core-shell in the NPs, which significantly reduces toxicity due to the negligible dissolution of Ag_2S compared to Ag^0. Under aerobic conditions, sulfidation can occur at high HS^- concentrations by the indirect formation of Ag_2S nanobridges or the direct conversion of AgNPs to Ag_2S. [285,286]

The presence of Cl^- in the medium can lead to the formation of $AgCl_{(s)}$ or silver (I) chloride complexes, depending on the concentration ratios of Cl^-/Ag^+. At low Cl^-/Ag^+ ratios, $AgCl_{(s)}$ is formed in the surface of the AgNPs while at higher Cl^- concentrations, the formation of $AgCl_x^{(x-1)}$ is favoured. The presence of Cl^- greatly decreases the toxicity of the AgNPs due to the formation of a $AgCl_{(s)}$ layer in the surface of the NPs which not only decrease the Ag^+ concentration but also prevents the further dissolution of the NPs [287,288].

Finally, under sunlight radiation, dissolved organic matter (DOM) can reduce Ag+ while stabilizing the newly formed AgNPs [289,290]. The decrease in the concentration of dissolved Ag+ results in a reduction of its toxicity.

Given the importance of understanding the behaviour of AgNPs in the environment, this thesis investigates the dissolution and sulfidation rates of these NPs using a continuous flow system (CFS) as a function of different parameters, such as pH, ionic strength, flow rate, presence of oxygen, and sulfide concentration.

CHAPTER 2

OBJETIVES

Since its introduction, LC has been extensively employed for the analysis of various sample types in multiple scientific fields, establishing itself as one of the preeminent analysis techniques of the present time. However, new societal needs require a redirection of the technique towards sustainability and green analytical chemistry. In this regard, miniaturized liquid chromatography has progressively gained importance over the years, positioning itself as a greener, more sustainable, and highly sensitive alternative. Furthermore, derived from miniaturization, the portability of LC is presented as a potential solution for point of need analysis of complex samples where a separation step is necessary. Nevertheless, compared to other techniques such as spectroscopic, portable LC has evolved slowly due to the challenges associated with miniaturizing of its components.

In view of this, the general objective of the thesis aims to generate novel knowledge regarding the synergy between the nanoscale and LC, through the utilization of IT-SPME coupled with minLC. The study utilizes cutting-edge trends in analytical chemistry, expertise in miniaturized LC and its integration with IT-SPME, nanomaterials, an analysis of the initial research, and the environment as action framework.

The thesis, in turn, pursues the following specific objectives:

(1) Develop new configurations for the on-line coupling of IT-SPME to minLC.

(2) Demonstrate the potential benefits of nanoparticles/nanomaterials as phases in the mentioned coupling.

(3) Propose new strategies to develop a cost-effective model for evaluating emerging contaminants.

(4) Seek to provide evidence of the sustainability of the studied technique while incorporating at least carbon footprint as a performance indicator of a given procedure.

(5) Demonstrate that the technique can contribute to the portability of LC.

The development of the thesis has been possible thanks to the MCI-AEI and EU-FEDER (project CTQ2017-90082-P). The author thanks to the Spanish MCI for his predoctoral grant FPI (PRE2018-086709).

The results obtained in this thesis have led to the publication of 3 scientific articles and a chapter of Encyclopaedia, with 2 additional articles currently in preparation:

(1) S. Cortés-Bautista, R. Navarro-Utiel, A. Ballester-Caudet y P. Campins-Falcó. Towards in field miniaturized liquid chromatography: Biocides in wastewaters as proof of concept. *J. Cromatogr. A.* **2022.** https://doi.org/10.1016/j.chroma.2022.463119. Impact Factor JCR (2023): 4.100

(2) L. Sanjuan-Navarro, S. Cortés-Bautista, Y. Moliner-Martínez y P.Campins-Falcó. In-tube solid phase microextraction coupled to miniaturized liquid chromatography for both, noble nanoparticle assessment and sensitive plasmonic assay development. *Anal. Chim Acta*. **2021.** https://doi.org/10.1016/j.aca.2021.338665. Impact Factor JCR (2023): 6.911

(3) S. Cortés-Bautista, H. R. Robles-Jimárez, I. Carrero-Ferrer, C. Molins-Legua, P. Campins-Falcó. Portable determination for legislated dissolved nitrogen forms in several environmental water samples as a study case. *Sci. Total Environ.* ***2023***. https://doi.org/10.1016/j.scitotenv.2022.161131. Impact Factor JCR (2023):

(4) S. Cortés-Bautista, P. Campins-Falcó. Portable liquid chromatography, in: Encyclopaedia of Analytical Chemistry, Wiley. **(In edition)**

(5) S. Cortés-Bautista, C. Molins-Legua, P. Campins-Falcó. Miniaturized liquid chromatography in environmental analysis. A review. **To be published.**

(6) S. Cortés-Bautista, R. Navarro-Utiel, P. Campins-Falcó. Direct analysis in in real-time mass mass spectrometry for rapid determination of acetaminophen in urine samples. **To be published.**

Additionally, the results were presented at the following conferences:

(1) XXXVIII Biennal meeting of the Royal Spanish Society of Chemistry (RSEQ2022) in Granada. S. Cortés-Bautista, R. Navarro-Utiel y P. Campins-Falcó. Direct analysis in real time-mass spectrometry for the rapid determination of acetaminophen in urine samples. 2022. (Poster communication with award).

(2) XXIII International Symposium on Advances in Extraction Technologies (ExTech2021) in Alicante. S. Cortés-Bautista, R. Navarro-Utiel & P. Campins-Falcó. Nano-liquid chromatography: from lab to portable equipments. **2021.** (Poster communication)

(3) XXII Meeting of the Spanish Society of Analytical Chemistry (SEQA2019) in Valladolid. S. Cortés-Bautista, P. Campins-Falcó, C. Molins-Legua. Portable instrumentation: validation for in-situ monitoring. **2019.** (Poster communication)

CHAPTER 3:

METHODOLOGY

3.1 Reagents

The European Regulation (EC) No 1278/2008 on classification, labelling and packaging of substances and mixtures, also abbreviated as “CLP regulation” standardises the warnings on products containing chemical substances. It introduces a labelling system for hazardous chemicals by using a hazard pictogram (**Figure 21**)

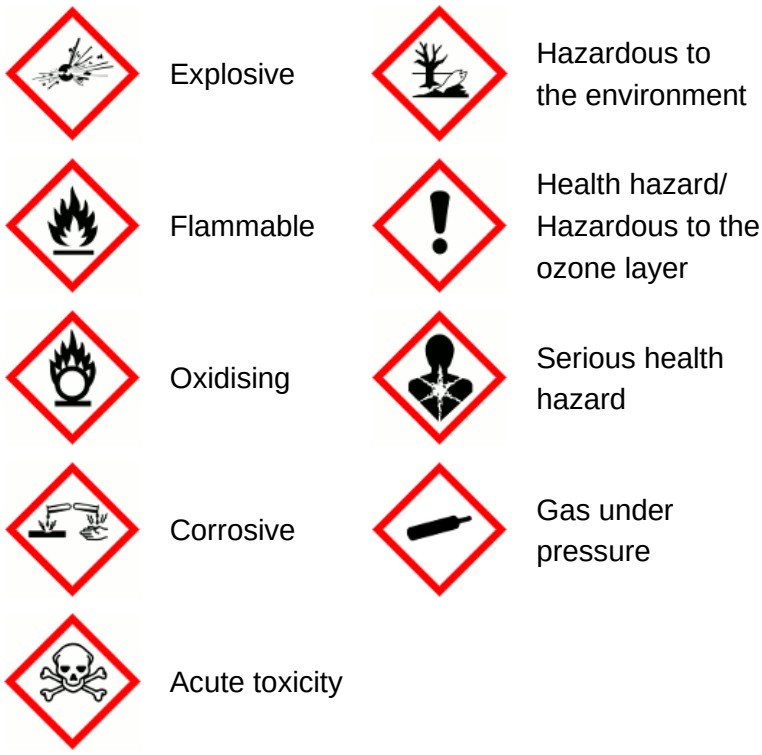

Figure 21. Hazard pictograms according to the CLP regulation (EC) No 1268/2008

The reagents and chemicals used during the thesis are aphetically listed in **Table 13** stating the supplier and its classification according to the CLP hazards pictogram.

Table 13. List of the chemicals used during the thesis, supplier, and hazard identification. The suppliers are the following: Merck (Rahway, NJ, USA), Panreac (Barcelona, España), Scharlau (Barcelona, España), Sigma (St. Louis, MO, USA), and VWR Chemicals (Radnor, PA, USA).

Chemical (CAS)	**Supplier**	**Hazard identification**					
							
Acetaminophen (103-90-2)	Sigma				X	X	
Acetic acid (64-19-7)	VWR	X	X				
Acetonitrile (75-05-8)	VWR	X				X	
AgNPS (20 and 40 nm) (citrate buffer) (7740-22-4)	Sigma					X	
Ammonium acetate (631-61-8)	Panreac						
Ammonium chloride (12125-02-9)	Sigma					X	
AuNPs (20 and 40 nm) (citrate buffer) (7740-57-5)	Sigma						
AuNPs (20 and 40 nm) (PBS) (7740-57-5)	Sigma						
Caffeine (58-08-2)	Sigma					X	
Dimethyl phthalate (131-11-3)	Sigma						
Fluometuron (2164-17-2)	Sigma					X	
Formic acid (64-18-6)	Sigma	X	X	X			
CTAB (57-09-0)	Sigma		X		X	X	X

Chemical (CAS)	Supplier	Hazard identification					
							
Hexamethylene tetramine (100-97-9)	Sigma	X				X	
Humic acid mixture (1415-93-6)	Sigma					X	
Hydrazine sulfate (10034-93-2)	Sigma		X	X			X
Hydrochloric acid (7647-01-0)	Sigma		X			X	
Hydrogen carbonate (144-55-8)	Panreac						
Hydrogen peroxide (7722-84-1)	Merck						
Imazalil (35554-44-0)	Sigma		X	X	X		
Iron (III) chloride (7705-08-0)	Sigma		X			X	
Isoproturon (34123-59-6)	Sigma			X			X
Luminol (521-31-3)	Sigma					X	
Nitric acid (7697-37-2)	Sigma	X	X	X			
N,N-dimethyl-*p*-phenylenediamine (99-98-9)	Sigma			X			
Manganese dioxide (1344-43-0)	Sigma						
Methanol (67-56-1)	VWR	X		X			X
Metribuzin (21087-64-9)	Sigma				X	X	
O-phenylphenol (90-43-7)	Sigma		X		X	X	

Chemical (CAS)	Supplier	Hazard identification					
							
Potassium nitrate (7440-09-07)	Sigma						
Potassium phosphate dibasic (7758-11-4)	Merck						
Potassium sorbate (24634-61-5)	Sigma					X	
Proxyphylline (603-00-9)	Sigma					X	
Pyrimethanil (53112-28-0)	Sigma				X		
Sodium carbonate (497-19-8)	Merck					X	
SDS (151-21-3)	Panreac	X	X			X	
Sodium hydroxide carbonate (144-55-8)	Merck		X		X		
Sodium hypochlorite (7681-52-9)	Sigma						
Sodium nitrate (7631-99-4)	Sigma					x	
Sodium phosphate monobasic (7588-80-7)	Merck						
Sodium thiosulfate (7772-98-7)	Scharlau						
Spermine (71-44-3)	Sigma		X				
Tetraethyl orthosilicate (78-10-4)	Sigma	X				X	
Theobromine (83-67-0)	Sigma					X	X

Chemical (CAS)	Supplier	Hazard identification					
							
Theophyllin (58-55-9)	Sigma			X			
Thymol (89-83-8)	Sigma		X			X	
Tribenuron-methyl (101200-48-0)	Sigma				X	X	X
Tryptophan (73-22-3)	Sigma					X	
TEOS (2031-67-6)	Sigma	X					
Tyrosine (60-18-4)	Sigma					X	

3.2 Instrumentation

3.2.1 UV-vis spectrometry

For the acquisition of UV-vis molecular absorption spectra, a conventional benchtop spectrophotometer, Cary 60 UV-vis (Agilent Technologies, Santa Clara, CA, USA), was used. Either plastic or quartz cuvettes with 1 cm optical pathlength were employed (**Figure 22 a**). The analytical signal was recorded using the Cary WinUV (Agilent Technologies) data acquisition software. On the other hand, a portable spectrophotometer consisting of a Maya200 Pro spectrophotometer (OceanOptics, FL, USA) coupled to an optical fiber (300 µm core and 2 m length) was used (**Figure 22 b**). An on-line water analyser UV500 (Thesthys, Grenoble, France) was used for in-situ nitrate determination (**Figure 22 c**). The working conditions for the different spectrophotometer are summed up in the **Table 14**.

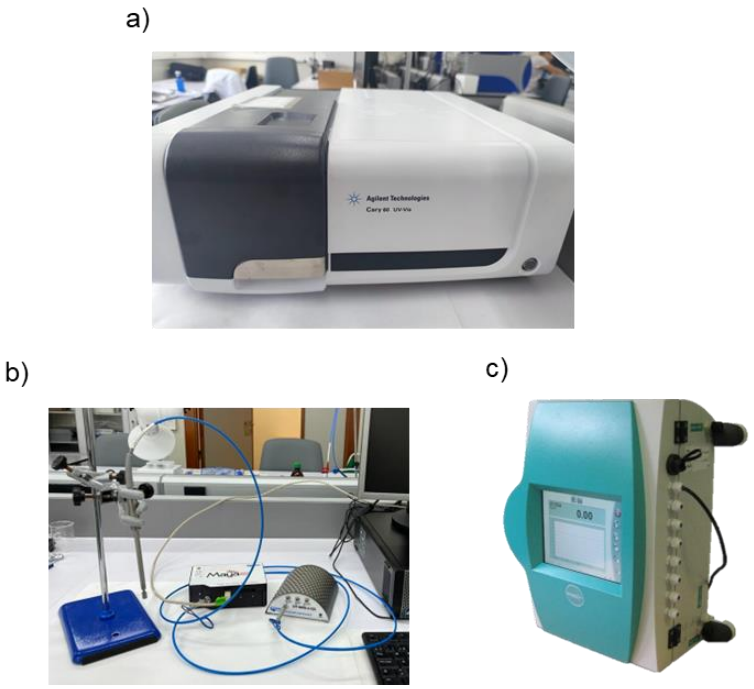

Figure 22. a) Ocean Optics optical fiber portable spectrophotometer, b) Thesthys UV500 nitrate analyzer, and c) Agilent Cary60 UV-vis spectrophotometer

Table 14. Working conditions for the different UV-vis spectrophotometer.

	Cary 60 UV-vis	**Maya200 Pro**	**Analyzer**
Slit (µm)	100	1.5	n.a.
Spectral resolution (nm)	3.52	<1.5	n.a.
Scan range (nm)	200 – 1100	190 – 1100	180 – 750
Energy consumption (W)	2.5	150	n.a.
Size (cm3)	48 × 57 × 20	15 × 20 × 5	42 × 42 × 23
Weight (Kg)	18	0.96	15
Detector	Hamamatsu S10420	Two silicon diode detectors (sample and reference)	n.a.

For fluorescence measurements, a portable optical fiber equipment was used. It consists of a LED lamp at 255 nm for excitation (SMA 905 connection), 600 μm core fiber optic and 2 m length and a Maya200Pro spectrometer from Ocean Optics. A laboratory benchtop fluorescence equipment Agilent Cary Eclipse was also employed (**Figure 23**). **Table 15** lists some characteristics of the used spectrofluorometers.

Figure 23. Benchtop Agilent Cary Eclipse fluorescence spectrometer.

Table 15. Working conditions for the different UV-vis spectrophotometer.

	Maya200Pro spectrofluorometer	**Agilent Cary Eclipse Spectrofluorometer**
Slit (μm)	100	5
Spectral resolution (nm)	3.52	< 1.5
Scan range (nm)	200 – 1100	190 – 1100
Energy consumption (W)	2.5	150
Size (cm3)	15 × 11 × 49 cm	60 × 64 × 27 cm
Weight (Kg)	0.96	31
Detector	Hamamatsu S10420	Photomultiplier R928

For measuring chemiluminescence the signals were recorded by portable tube luminometer from (Berthold Technologies, Bad Wildbad, Germany).

3.2.2 DART-MS and ICP-MS

An Ion Sense DART SVP ion source (Saugus, MA, USA) interface was coupled to an Agilent 6547 LC/QTOF (**Figure 24 a**). The sample introduction was performed by means of an automated Linear Rail Enclosure in which a disposable IonSense QuickStrip wire mesh sample holder is placed (**Figure 24 b**). Ions were transferred to the QTOF by means of a ceramic tube (4.75 mm i.d. and 87 mm length) vacuum interface. An agilent MS40+ mono stage rotary vane pump was used to generate the rough vacuum in the interface.

a)

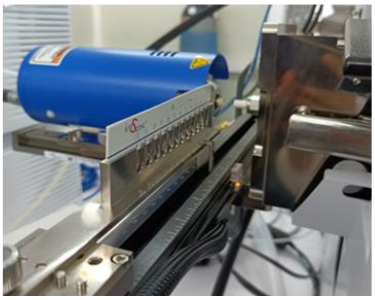

b)

Figure 24. a) Ion Sense DART SVP ion source interface and b) Quick Strip sample holder.

The elemental analysis of Ag^{+} was performed by means of ICP-MS 7900 (Agilent Technologies) equipped with an ASX-500 series autosampler (Agilent Technologies) (**Figure 25**). The ICP-MS was equipped with a quartz cyclonic spray chamber and a MicroMist nebulizer (Agilent Technologies).

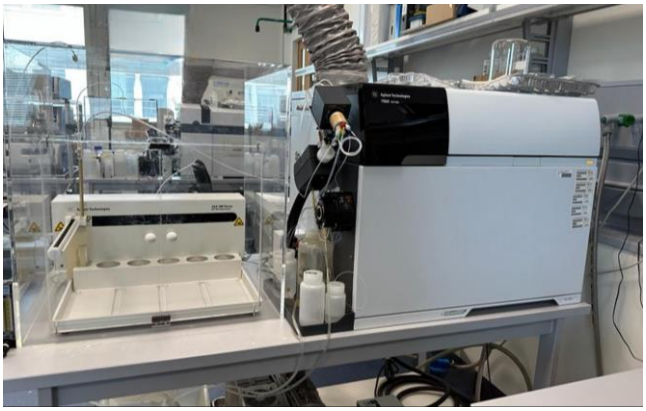

Figure 25. Agilent 7900 ICP-MS detector with an ASX-500 autosampler.

3.2.3 Capillary liquid chromatography

A capLC equipped with an Agilent Infinity 1260 capillary pump (Agilent, Waldbronn, Germany) which allows to work in the range of 1 – 20 μL min^{-1} was used (**Figure 26**). The detection was performed by means of a Agilent Infinity 1200 DAD using a 80 nL flow cell. The wavelength scan range was set from 190 nm to 800 nm, and the chromatographic profile was monitored at different wavelengths depending on the analyte. For the analytical separation, different capillary analytical columns were used. In the case of environmental determination of selected contaminants, ZORBAX SB-C18 (150 × 0.5 mm, 5 μm and, 35 × 0.5 mm, 5 μm) (Agilent) columns were used. On the other hand, for the characterization of NPs dispersions a Jupiter C18 (50 × 0.5 mm, 5 μm) (Phenomenex, Torrance, CA, USA) was used. For the injection a 6-way Rheodyne 7721-i (IDEX Health and Sciences, Rohnert Park, CA, USA) was used. In this, the sample loop was replaced with a capillary with an extractive phase to perform the IT-SPME (see **section 3.3.2** for more information). For data acquisition the Agilent ChemStation software was used.

Figure 26. Agilent 1260 infinity series capillary LC equipped with a Rheodyne 7721-I injection valve for sample injection.

3.2.4 Nano liquid chromatography

The nano liquid chromatograph consists of an Agilent Infinity 1260 nano pump allowing to work from 0.01 µL min^{-1} to 4 µL min^{-1}. As detection system, an Infinity 1200 Agilent DAD with a flow-cell of 80 nL was used. The working range was set in the range from 190 to 400 nm, and the chromatographic profile was monitored at different wavelengths depending on the analyte. The analytical separation was carried out using two analytical column of different dimension: (1) a ZORBAX SB-C18 (50 × 0.075 mm, 3.5 µm) and (2) a ZORBAX SB-C18 (150 × 0.1 mm, 3.5 µm) (Agilent). As injection system, a two-valve system was employed using a Rheodyne 7725i 6 ports – 2 positions and an automatic VICI C2N 10 ports – 2 positions. In the latter, a extractive capillary was incorporated to perform the IT-SPME. More information about the injection configuration and extractive capillary can be found in the **section 3.3.2**. For data acquisition the Agilent ChemStation software was used.

3.2.5 Miniaturized portable liquid chromatography

A portable miniaturized Axcend Focus liquid chromatograph (Axcend, Provo, UT, USA) was used (**Figure 27**). The system was equipped with two high-pressure syringe pumps capable of deliver mobile phase in the ranges from 0.5 μL min^{-1} to 10 μL min^{-1} with a maximum working pressure of 410 bar. The detector consists of an on-column fixed wavelength LED with a working wavelength of 255 nm. The analytical column was a C18 (100 × 0.15 mm, 1.7 μm) which was incorporated along with the detector inside an inter-changeable cartridge. Samples were load manually into a sample loop with a volume of 40 nL. Chromatograms were obtained by means of the Axcend Focus v2 software.

Figure 27. Axcend Focus portable miniaturized LC.

3.2.6 Ultra high-performance liquid chromatography

On one side, an Agilent 6546 LC/QTOF (Agilent Technologies) equipped with an ESI interface was used. The chromatographic separation was carried out by means an Agilent 1290 Infinity II series equipped with an Eclipse Plus C18 RRHD (2.1 × 50 mm, 1.8 μm) at 35 °C (**Figure 28**).

Figure 28. Agilent 6546 LC/QTOF equipped with an ESI interface. The analytical separation was carried out using an Agilent 1290 Infinity II series UHPLC.

3.3 Sample treatment

3.3.1 Solid phase extraction

Isoproturon and diuron were extracted by means of SPE prior to its LC analysis. The cartridge consists of a Strata C18-U cartridge with 55 μm of particle size, 70 Å of pore diameter, and 100 mg of phase (Phenomenex). First, the C18 cartridge was conditioned with 1 mL of MeOH followed by 1 mL of H_2O. Then, up to 25 mL of the sample was manually passed through the cartridge, followed by 1 mL of 2:8 MeOH:H_2O, after the analyte is eluted in 200 μL of MeOH separated in three fractions of 100, 50 and 50 μL for the first, second and third one, respectively. These solutions were measured just after the extraction step.

Urine samples at different times (0 h, 2 h, 5 h, 6 h, and 7 h) after 1 g of APAP ingestion were collected. Then, 100 μL of each sample was deproteinized with 300 μL of formic acid 1 % (v/v) and 700 μL of water. The solution sample solution was centrifugated for 20 min at 15000 rpm and 1 mL of the supernatant was processed by SPE (**Figure 29**). For the SPE a Strata C18-

U cartridge with 55 µm of particle size, 70 Å of pore diameter, and 100 mg of phase (Phenomenex) was used. The SPE included four steps: 1) cartridge activation and conditioning with 1 mL of methanol (MeOH) and 1 mL of ultrapure water respectively, 2) loading with 1 mL of treated sample, 3) washing with 1 mL of ultrapure water, and 4) elution of the analyte in 0.5 mL of methanol. Samples were refrigerated and stored at 4 °C.

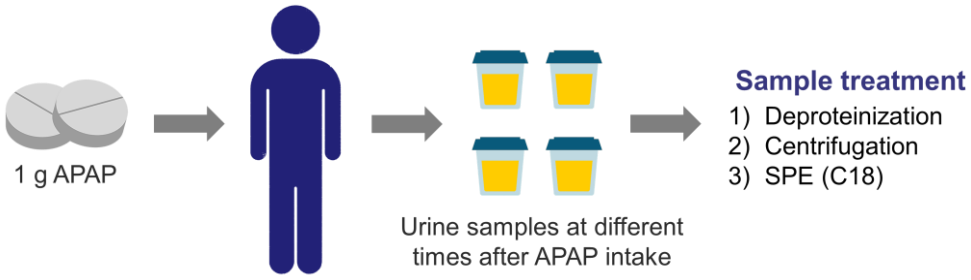

Figure 29. Schematic representation of the APAP sample collection and treatment.

For the spermine extraction in urine samples, C18 silica cartridges (100 mg, Phenomenex, EEUU) were used. First, the cartridges were activated with 1 mL MeOH and 1 mL of $NaHCO_3$ 0.5 M at pH 12. Then, the cartridges were loaded with 1 mL of the urine sample. Before elution of spermine, a clean-up step with 2 mL of $NaHCO_3$ 0.5 M, 1 mL of ACN, and 2 mL of H_2O was carried out. Finally, the spermine was eluted using 500 µL of HAc 5 % separated in two fractions (250 µL each).

3.3.2 In-tube solid phase microextraction

The IT-SPME was coupled to both, cap and nanoLC. In the case of capLC the extractive capillary was replaced by the sample loop in a 6 – way and 2 – port injection valve. The sample is injected in the load position, so it goes through the extractive capillary where the analytes are retained and preconcentrated while the rest of the matrix goes to waste. After this, the injection valve is switched to inject position making the mobile phase to go

through the extractive capillary eluting the analyte to the analytical column (**Figure 7 b**).

This configuration was used for the extraction of AuNPs and AgNPs dispersions, and contaminants in environmental waters. In the case of AuNPs and AgNPs a commercial capillary coated with 35 % PDMS of 20 cm length, 0.32 mm of i.d., 3 μm of thickness, and 16 μL of internal volume was used. On the other hand, for contaminants in water samples, a 20 cm segment of an untreated fused silica capillary with 0.32 mm of i.d. and 16 μL of internal volume (Análisis Vínicos, Tomelloso, Spain) was coated with TEOS-MTEOS and SiO_2 NPs and was used as extractive capillary.

For the nanoLC a two-valve configuration was used (**Figure 30**). The sample is first injected in a 6 – way and 2 – port which is used to transfer the sample to a second injection valve by means of a 15 cm length, 0.1 mm of i.d. and 800 nL of internal volume untreated fused silica capillary. The extractive capillary is mounted in this second 10 – port and 2 – way injection valve. Switching the position of the second valve, makes the retained analyte to be eluted to analytical column by the mobile phase (**Figure 31**). For the analysis of contaminants in water an APAP in urine samples a 15 cm segment of an untreated fused silica capillary with 0.075 mm of i.d. (Análisis Vínicos) was coated with TEOS-MTEOS-SiO_2

a) b)

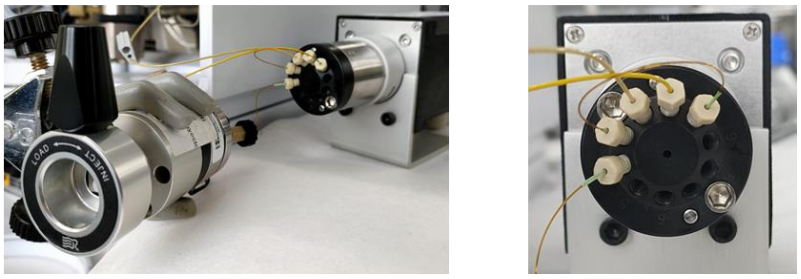

Figure 30. a) Two-valve injection system where a first valve is used for trespassing the sample to the second valve where the IT-SPME takes place and b) close-up of the second valve where the IT-SPME capillary can be seen.

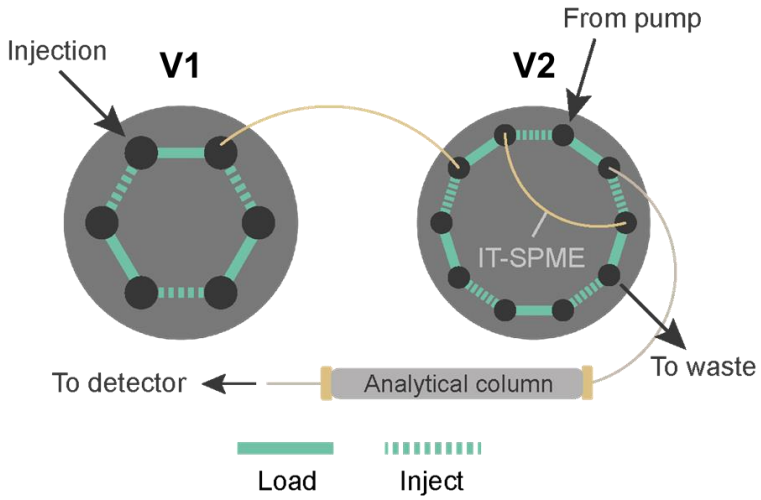

Figure 31. Schematic representation of the two-valve configuration IT-SPME used. V1 and V2 are 6 – port and 2 – way, and 10 – port and 2 – way injection valves respectively. The extractive phase for the IT-SPME consist of a TEOS-MTEOS polymer enhanced with SiO_2 nanoparticles.

3.4 Synthesis procedures

3.4.1 Synthesis of IT-SPME capillaries

TEOS-MTEOS-SiO_2 IT-SPME capillaries were synthetized following the sol-gel procedure described by Serra-Mora et al. (2017) [75]. First, segments of 20 cm length of fused silica untreated capillaries were activated filling them with a 0.1 M NaOH solution and heating at 40 °C for 2 h. Then, they were filled with a 0.1 M HCl solution, left to stand for 30 min at room temperature, and heated at 60 °C for 2 h. 40 °C. Then the capillaries were flushed with water and filled with approximately 200 µL of the coating mixture. This was prepared adding 0.65 g of PEG and 1 mg of SiO_2 (0.05 $mg \cdot L^{-1}$) to a solution containing 1 mL of TEOS, 1 mL of MTEOS, and 0.5 Ml of water and mixed in a vortex. After that, 20 Ml of NH_4OH 0.1 M is added as a catalyst. Once filled, the capillaries were heated at 40 °C for 2 h and then heated

overnight at 120 °C. Finally, the capillaries were flushed with H_2O and acetonitrile (I) enough times to clean and ensure there is no further bleeding from the capillaries.

This procedure was followed for either, nano (0.075 mm i.d.) and cap (0.32 mm i.d.) IT-SPME capillaries. Those were cut off with a ceramic cutter to obtain the desired length.

3.4.2 Synthesis of naked AuNPs

AuNPs synthesis was carried out following the procedure described by Jornet-Martinez et al. (2014) [266]. An aqueous solution of H_2O_2 0.5 – 1.2 mM and $HAuCl_4$ 0.5 mM treated 12 h with Chelex to eliminate metal traces, was irradiated with a 532 nm laser (10 Hz, 16 – 19 mL) until the band of Au^{3+} at 300 nm was not observable and the H_2O_2 band at 240 nm decreased close to the absorbance of the plasmon band at 520 – 525 nm. The mixture was diluted with water (2:1 H_2O:AuNPs) the excess of H_2O_2 was removed by irradiating for 20 min with an UV-lamp [291].

3.5 Experimental conditions

3.5.1 UV-vis spectroscopy

Dissolved nitrogen determinations

The nitrate measurements were performed by the three different UV-vis instruments described in the **Table 14**. The signal was registered at 220 nm. Also, a signal correction to compensate the presence of organic matter and was done by registering the signal at 275 nm and subtracted twice to the 220 nm signal ($A_{220} – 2 \cdot A_{275}$) [292].

The nitrite determination was carried out using the Griess colorimetric sensor method [293]. The sensor was added to 0.5mL of citric acid and 0.5

mL of working standard solutions of nitrite (up to 1.5 $mg \cdot L^{-1}$) or water samples. After 10 min, the absorbance was measured at 540 nm and registered the spectrum between 400 and 650 nm from a portable optical fiber instrument and a benchtop instrument.

For the ammonium determination, to 500 µL of standard solution or samples, 10 µL of NaOH 1 M and NaOCl 0.6 % were added in a glass vial. The mixture was manually stirred during 0.5 min for the monochloramine formation. Then, half disc cut in four pieces of PDMS-SL-NP discs were introduced in the solution and maintained 5 min for the indophenol formation [294,295]. Finally, the solution was measured with a portable optical fiber spectrometer at 690 nm, registering its spectrum between 400 and 800 nm.

Regarding the determination of amino acids by molecular fluorescence standard solutions of tryptophan (T) (up to 10 $mg \cdot L^{-1}$), tyrosine (TY) (up to 10 $mg \cdot L^{-1}$), and β-phenylalanine (PA) (up to 75 $mg \cdot L^{-1}$) or water samples were analyzed by means of a portable optical fiber probe and a benchtop fluorometer (see **Figure 15**). For both, the excitation wavelength was set at 255 nm and the signal was registered between 200 and 1100 nm.

Finally, the chemiluminescence determination of ammonium and organic amino nitrogen was carried using a sensor fabricated following the procedure described by [296]. 350 µL of standard or sample were mixed with 50 µL of 0.25 µM sodium hypochlorite for 1min. Then, the resulting 400 µL were placed in the measurement tube, which contained the luminol composite. The chemiluminescence signal was captured at 10 s after the addition of the indicated volume in the portable luminometer.

Metallic NPs assessments and transformations

To obtain the LSPR response of MNPs by means of UV-vis spectroscopy different volumes of sample or standard were mixed with 300 μL of ultrapure H_2O and 300 μL of MNPs. The Cary 60 UV-vis equipment was used, and the signal was registered between 300 – 800 nm.

To perform the acid aggregation assay, MNPs dispersions were added to different volumes of ultrapure H_2O and then acidified with adequate volume of a HAc solution. In the case of citrate and phosphate capped AuNPs 25 % (v/v) in HAc 10 % (v/v), 250 μL of AuNPs were added to 250 μL of water, and then 500 μL of HAc was added to the mixture, reaching a final volume of 1 mL. For citrate capped AgNPs 50 % (v/v) in 0.2 % HAc (v/v) the volumes of MNPs dispersion, water, and HAc 1 % (v/v) were 500 μL, 300 μL, and 200 μL respectively, for a total volume of 1 mL. Finally, for citrate capped AgNPs and AuNPs mixtures each diluted at 25 % (v/v) in HAc 0.7 % (v/v), the volumes for each MNPs, water, and HAc 1 % (v/v) were 150 μL, 220 μL, and 80 μL respectively, for a final volume of 600 μL.

As for the CFS AgNPs transformation study, the sulfide determination was carried out by means of a spectrophotometric assay based on the formation of methylene blue after the reaction of hydrogen sulfide with dimethyl-p-phenylenediamine and iron (III) in acidic media (**Figure 32**) [297]. After mixing the reagents, the solution was left to stand for 20 min until the stabilization of the blue colour. To avoid the oxidation and volatilization of HS^-, the plastic tubes in the collector were previously flushed with Ar^0 and closed quickly. The sulfide determination was performed immediately after collecting the sample.

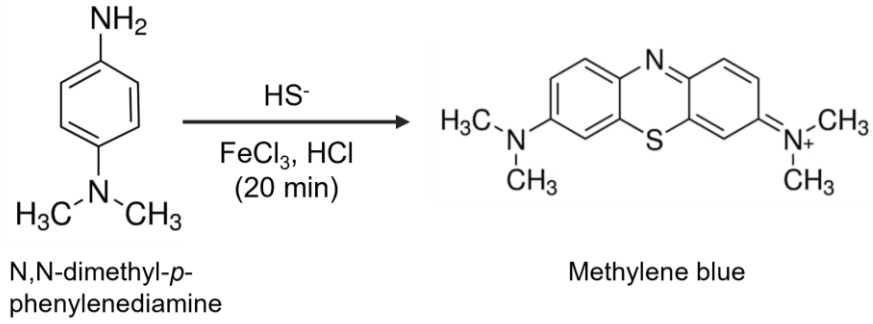

N,N-dimethyl-*p*-phenylenediamine

Methylene blue

Figure 32. Reaction between the N,N-dimethyl-*p*-phenylenediamine with hydrogen sulfide and iron (III) chloride to form methylene blue in acidic media.

3.5.2 DART-MS

For the analysis of the urine samples a DART interface coupled to MS was used. The ionization gas used during the measurements was grade 5 nitrogen (99.999 % purity) while for standby mode nitrogen from a generator (99.5 % purity) was used. The gas temperature and the sample speed were set at 350 °C and 0.5 mm·sec^{-1}. The mass spectrum was collected in the range of 90 – 1000 m/z in positive ionization mode. Before carrying out the analysis, the system was purged with grade 5 nitrogen for 10 min. Up to 12 samples were analysed at the same time with the QuickStrip sample holder. A total of 5 uL of methanolic samples extracts were deposited into the QuickStrip, allowing the solvent to evaporate prior to conducting the assay. Each sample was analysed in triplicate.

3.5.3 ICP-MS

To investigate the transformation of AgNPs, the following CFS diagrammed in **Figure 33** was employed. The system comprised two peristaltic pumps responsible for pushing the water and a Na_2S solution at a constant flow rate. The flow rate ratio between the two solvents was maintained at 1:9 H_2O:Na_2S. These solutions converged at a t-union and proceeded to the reactor, where the AgNPs are deposited and packed using various filters (see

Figure 34). Subsequently, the solution exited the reactor and was collected in metal-free polypropylene tubes using a fraction collector at specific time intervals. The collected samples were further acidified by adding 100 µL of HNO_3 (2 M) and stored until Ag^+ ICP-MS analysis. All the tubes and bottles containing sulfide were previously flushed with Ar^0 and kept closed as far as possible. The dissolved oxygen in the solution bottles was monitored by means of a electrochemical oxygen sensor. After each experiment, the system was cleaned with 0.02 M HNO_3 for 30 min and H_2O for another 30 min.

To avoid the interaction of the Ag^+ with the filters, a filter pre-treatment with Cu^{2+} was performed. Different solutions were flushed through the system and the filters without the sample: (1) Cu^{2+} 100 $mg \cdot L^{-1}$ for 10 min, (2) Cu^{2+} 1 $mg \cdot L^{-1}$ for 10 min, and (3) flushing with water or $NaNO_3$ 1 mM for 10 min. After undergoing pre-treatment, the filters were left to dry by passing air through the system for 15 min.

The plasma power was set at 1550 W, the plasma gas flow at 15 $L \cdot min^{-1}$, the nebulizer gas flow at 1.08 $mL \cdot min^{-1}$, and the auxiliary gas flow at 0.90 $mL \cdot min^{-1}$. The total ion content was quantified against an external calibration curve with a working range from 0.1 – 10 $\mu g \cdot L^{-1}$ prepared in 0.54 % nitric acid using 1000 $mg \cdot L^{-1}$ Ag^+ stock solutions in 5 % of nitric acid. A 10 $\mu g \cdot L^{-1}$ rhodium solution in 0.54 % nitric acid was used as internal standard, andwas prepared from a 1000 $mg \cdot L^{-1}$ ICP-MS stock solution. All the samples were analysed in triplicate. To avoid possible carry-over, between samples, the system was rinsed with 3 % and 6 % of nitric acid.

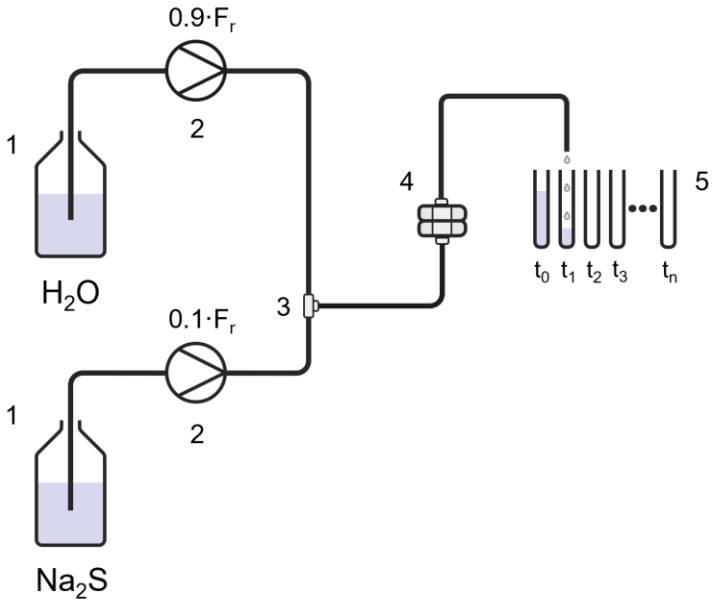

Figure 33. Diagram of the continuous flow system. 1. Reagent bottles, 2. peristaltic pumps, 3. t-union, 4. reactor, and 5. fraction collector.

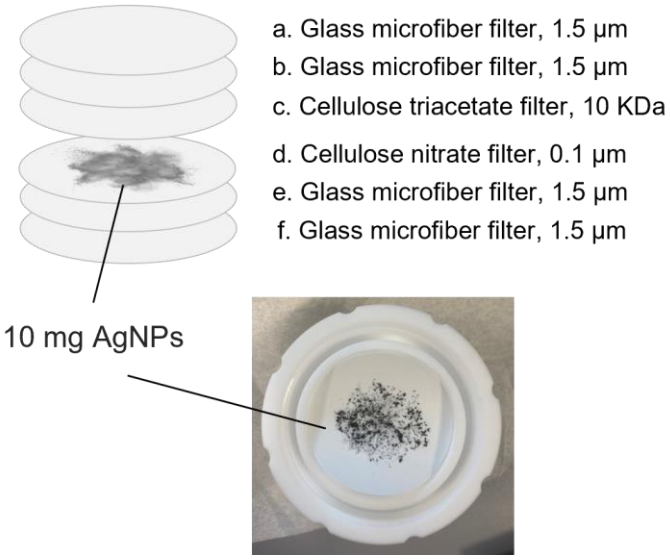

Figure 34. Filter distribution inside the reactor.

3.5.4 Chromatographic conditions

The **Tables 16**, **17**, **18**, and **19** show the chromatographic conditions used for the capLC, nanoLC, miniaturized portable LC, and the UHPLC-QTOF respectively. All the mobile phases were filtered through a 0.22 μm nylon filter and sonicated before use. Note that in the tables the injection volume is referred as the volume of sample that enters the chromatographic system (e.g., the sample loop volume) and must not be mistaken with the processed sample volume which is the sample volume passed through to the IT-SPME.

For the study of the capabilities of benchtop and portable minLC applied to the determination of environmental water samples, multicomponent solutions containing different analytes of interest, including pesticides, drugs, and other CEC were analysed. The multicomponent solutions were prepared in ultrapure water from the stock solutions of each analyte. The stock solutions were prepared from pure solid reagents (analytical grade) by dissolving a precisely known amount in MeOH. The concentration of each analyte in the multicomponent solution prepared for benchtop capLC and nanoLC and portable minLC are listed in the **Table 20**. All the solutions were filtered through a 0.22 μm nylon filter and refrigerated at 4 °C until analysis.

Table 16. Chromatographic conditions for capLC. Injection configuration, analytical column, mobile phase composition, flow rate (F_R), injection volume (I_V), and detection technique for the different studied analytes are shown.

Analyte	Injection configuration	Analytical column	Mobile phase composition	F_r	I_v	Detector
Acetaminophen Caffeine Dimethyl phthalate Fluometuron Imazalil Metribuzin O-phenyl phenol Potassium sorbate Proxyphylline Pyrimethanil Theobromine Theophylline Tribenuron methyl	IT-SPME 1-valve configuration. TEOS-MTEOS-SiO_2 NPs (0.075 mm i.d. x 150 mm length) and 50 µL of processed volume	ZORBAX 300SB-C18 (150 x 0.5 mm, 3.5 µm)	ACN:H_2O 7:93 % (t_0) 10:90 (1 min) 45:55 (2 min, kept 2 min) 70:30 (5 min, kept 2 min) 80:20 (8 min, kept 2 min) 95:5 (11 min, kept 3 min) 7:93 (14.2 min, kept 10 min)	10 µL min^{-1}	16 µL	DAD (230, 250, and 270 nm)
AgNPs AuNPs	IT-SPME 1-valve configuration. 35 % PDMS (200 mm length x 0.32 mm i.d.) and 16 µL of processed volume	Jupiter C18 (50 x 0.5 mm, 5 µm)	10 mM ammonium acetate + 10 mM SDS + 1 mM sodium thiosulfate	12 µL min^{-1}	16 µL	DAD (400 and 530 nm)

Table 17. Chromatographic conditions for nanoLC. Injection configuration, analytical column, mobile phase composition, flow rate (F_R), injection volume (I_V), and detection technique for the different studied analytes are shown.

Analyte	Injection configuration	Analytical column	Mobile phase composition	F_r	I_V	Detector
Acetaminophen Caffeine Dimethyl phthalate Fluometuron Imazalil Metribuzin O-phenyl phenol Potassium sorbate Proxyphylline Pyrimethanil Theobromine Theophylline Tribenuron methyl	IT-SPME 2-valve configuration. TEOS-MTEOS-SiO_2 NPs (0.075 mm i.d. x 100 mm length) and 50 µL of injection volume	ZORBAX 300SB-C18 (50 x 0.075 mm, 3.5 µm and 150 x 0.1 mm, 3.5 µm)	ACN:H_2O 7:93 (t_0) 10:90 (1 min) 45:55 (2 min, kept 2 min) 70:30 (5 min, kept 2 min) 80:20 (8 min, kept 2 min) 95:5 (11 min, kept 3 min) 7:93 (14.2 min, kept 10 min)	0.5 µL min^{-1}	440 nL	DAD (230, 250, and 270 nm)
Acetaminophen Acetaminophen glucuronide	IT-SPME 2-valve configuration. TEOS-MTEOS-SiO_2 NPs (0.075 mm i.d. x 10 mm length) and 50 µL of processed volume	ZORBAX 300SB-C18 (150 x 0.1 mm, 3.5 µm)	ACN:H_2O 5:95 (t_0, kept 5 min) 70:30 (5.5 min, kept 1.5 min) 5:95 (8 min, kept 10 min)	0.5 µL min^{-1}	440 nL	DAD (243 nm)
AgNPs AuNPs	IT-SPME 1-valve configuration. TEOS-MTEOS-SiO_2 NPs (15 mm lenght x 0.075 mm i.d.) and 20 µL of processed volume	ZORBAX 300SB-C18 (50 x 0.075 mm, 3.5 µm)	10 mM ammonium acetate + 10 mM SDS + 1 mM sodium thiosulfate	0.5 µL min^{-1}	660 nL	DAD (400 and 530 nm)

Table 18. Chromatographic conditions for portable minLC. Injection configuration, analytical column, mobile phase composition, flow rate (F_R), injection volume (I_V), and detection technique for the different studied analytes are shown.

Analyte	Injection configuration	Analytical column	Mobile phase composition	F_r	I_V	Detector
Acetaminophen Caffeine Dimethyl phthalate Diuron Fluometuron Metribuzin O-phenyl phenol Potassium sorbate Proxyphylline Pyrimethanil Theobromine Theophylline Tribenuron methyl	Direct injection	C18 packed (100 x 0.15 mm, 1,7 µm)	ACN:H_2O 5:95 (t_0) 20:80 (4 min) 60:40 (4.5 min, kept 1 min) 95:5 (6 min, kept 0.5 min)	1 mL min^{-1}	40 nL	On-column LED (255 nm)

Table 19. Chromatographic conditions for UHPLC-ESI-MS. Injection configuration, analytical column, mobile phase composition, flow rate (F_R), injection volume (I_V), and detection technique for the different studied analytes are shown.

Analyte	Injection configuration	Analytical column	Mobile phase composition	F_r	I_V	Detector
Acetaminophen Acetaminophen glu-curonide	Direct injection	Eclipse Plus C18 (50 x 2.1 mm, 1.8 µm) at 35 °C	ACN:H_2O (0.1 % formic acid) 5:95 (t_0) 10:90 (1 min) 90:10 (10 min, kept 1 min) 95:5 (6 min, kept 2 min)	0.4 mL min^{-1}	5 µL	QTOF (m/z: 152.0693, 328.1028)

Table 20. Concentration of the analytes for the different analysed multicomponent mixtures.

Analyte	Portable LC ($mg \cdot L^{-1}$)	CapLC ($\mu g \cdot L^{-1}$)	NanoLC[a] ($\mu g \cdot L^{-1}$)	NanoLC[b] ($\mu g \cdot L^{-1}$)
Potassium Sorbate	9.94	-	123.0	49.2
Theobromine	22.25	20	122.6	51.5
Acetaminophen	20.80	20	-	52.0
Theophylline	16.80	20	-	48.0
Caffein	12.00	10	120	48.8
Proxyphylline	12.00	10	100	50.0
Tribenuron-methyl	61.51	10	-	51.9
Metribuzin	26.63	20	95.1	47.6
Isoproturon	22.13	10	49.8	49.8
Dimethyl Phthalate	39.70	10	18.6	52.1
Fluometuron	15.56	10	46.7	46.7
Imazalil	-	-	-	51.9
O-phenyl phenol	16.83	20	46.8	52.1
Pyrimethanil	17.20	10	17.9	48.4

[a] 50 mm × 0.075 mm analytical column. [b] 150 mm × 0.10 mm analytical column

3.6 Analysed samples

3.6.1 Fruit washing residual water

Residual waters from fruit washing treatments were obtained from three different places. Samples were collected in clean 250 mL amber glass bottles and were stored in a refrigerator at 4 °C until its analysis. These waters can contain biocides such as potassium sorbate, imazalil, or pyrimethanil.

3.6.2 Well water and different surface waters

Well waters were obtained from the inlet to the water treatment plant coming from the “Pozo de la Concepción” (39.276081, -0.480150) in Alginet (Valencia, Spain). The samples were collected in clean 20 L HDPE jerrycans

and properly transported to the laboratory where these were stored in the dark at room temperature in suitable conditions of humidity.

Also, different surface water sources from the Comunidad Valenciana, Spain, such as transition, river, and lagoon water were collected in clean 250 mL amber glass bottles and stored in the refrigerator at 4 °C until its analysis.

3.6.3 Urine samples

For the APAP determination, urine samples were obtained from volunteers after intake of 1 g of acetaminophen. The volunteers did not take acetaminophen in the previous 48 h. Those were collected at different times (0 h, 2 h, 4 h, 5 h, and 7 h) after ingestion. Samples were collected in polystyrene sterile 120 mL urine containers. The APAP was extracted from samples carrying out the SPE described in **section 3.3.1**. Urine extracts were stored in 2 mL amber chromatographic vials at 4 °C until analysis.

In the case of the spermine analysis, urine was obtained from healthy volunteers aged from 22 to 30 years old and cancer patients aged from 40 to 70 years old. Before carrying out the plasmonic assays, spermine was extracted from samples by means of SPE (see **section 3.3.1**). The extracts were stored immediately in the refrigerator at 4 °C until analysis.

3.6.4 Noble metal nanoparticles dispersions

For the plasmonic aggregation assays naked AuNPs synthetized in lab and commercial AgNPs citrate capped and AuNPs with phosphate and citrate capping were used for the characterization studies. Those were stored in the refrigerator at 4 °C until its analysis.

For the CFS, commercial AgNPs (< 100 nm) were used. The collected fractions from the assay were saved in 15 mL polypropylene metal-free centrifuge tubes and stored at 4 °C until its analysis.

CHAPTER 4:

RESULTS AND DISCUSSION

4.1 Environmental samples

4.1.1 Benchtop and portable minLC

4.1.1.1 Optimization of chromatographic conditions

Two miniaturized benchtop LCs (capillary and nano) coupled on-line to IT-SPME with DAD and a portable minLC with a UV-LED detector were studied for the analysis of environmental pollutants such as pesticides and drugs. The chromatographic conditions of all three methodologies were first optimized in order to obtain the best results for each.

Based on previous works [63,89,298], chromatographic separation was carried out using mixtures of water and acetonitrile in different proportions as mobile phase and C18 RP analytical columns. Due to the wide range of polarities of the analytes ($logK_{ow}$ -0.78 - 3.52, see **Tables 9** and **10** in **section 1.4.1** for specific $logK_{ow}$ information), segmented gradient elution was chosen to reduce the separation time and improve resolution. The optimum results in terms of efficiency, resolution, and analysis time were obtained by starting with a low elution strength composition (low percentage of ACN) to retain the more polar compounds. Then, the percentage of ACN was gradually increased to elute the rest of compounds. Finally, a high percentage of ACN (95 %) was held for a few minutes (3 min and 0.5 min for benchtop and portable instrument respectively) to eliminate possible impurities retained in the column which could negatively affect the following injections and analytical column lifetime.

The flow rate of the mobile phase was optimized to resolve the maximum number of peaks in the shortest possible time and within the pressure limits of the instrument. The optimized flow rates were 0.5 $\mu L \cdot min^{-1}$ for nanoLC, 10 $\mu L \cdot min^{-1}$ for capLC, and 1 $\mu L \cdot min^{-1}$ for portable minLC. At these

flow rates, maximum pressures of 14 MPa for benchtop capLC and nanoLC and 20 MPa for portable minLC were generated.

To carry out the analytical separation, the performance of two ZORBAX 300SB-C18 packed with 3.5 μm particles with dimensions 150 mm × 0.1 mm and and 50 mm × 0.075 mm was studied for nanoLC. For capLC, the same column with dimensions 150 mm × 0.5 mm was used. Lastly, for the portable minLC, a C18 column packed with 1.7 μm diameter particles with 100 mm of length and 0.15 mm of i.d. was used.

For the benchtop instruments the IT-SPME step was optimized by testing capillaries with different extractive phases, lengths, and internal diameters. Also, different injection configurations were tested. As IT-SPME extractive phases, TRB-35 and TEOS-MTEOS-SiO_2 capillaries were studied. The last capillary was selected as it provided better analyte pre-concentration covering at the same time a wider range of polarities. Regarding the capillary i.d. and length, these were optimized to minimize its internal volume while maintaining operability conditions. In this sense, it was selected to work capillaries with 100 mm length and 0.075 mm i.d. for nanoLC and 150 mm length and 0.32 mm i.d. for capLC. Finally, different IT-SPME configurations were tested. For the capLC a single valve (6-way and 2-positions) configuration was used due to its simplicity (see **Figure 7 b**). In the case of nanoLC, a second injection valve (6-way and 2-positions) was needed to transfer the sample to the valve were the IT-SPME capillary was placed (10-ways and 2-positions) (see **Figure 31**). The use of a second valve is intended to minimise the pressures generated by injecting directly into the valve containing the IT-SPME. The volume of sample processed through the IT-SPME was 100 μL, beyond this point, no significant pre-concentration was achieved.

For benchtop nanoLC and capLC, the DAD was set scan at a wavelength range of 190 – 600 nm. The UV-vis spectra of each compound were obtained by UV-vis spectroscopy in order to select the best measurement

wavelength. The maximum absorbance wavelength of each compound was covered by monitoring the chromatographic signal at 220 nm, 250 nm, and 270 nm.

Chromatograms obtained for the several multicomponent solutions (**see Table 20**) for portable, and benchtop cap and nanoLCs under the optimized chromatographic conditions, are shown in **Figure 35** and **Figure 36** respectively. The optimized results of the chromatographic conditions are listed in **Tables 16 – 19** in **section 3.5.4**. Suitable separation of the analytes was achieved in 8 min for portable minLC, 15 min for capLC, and 20 min for nanoLC.

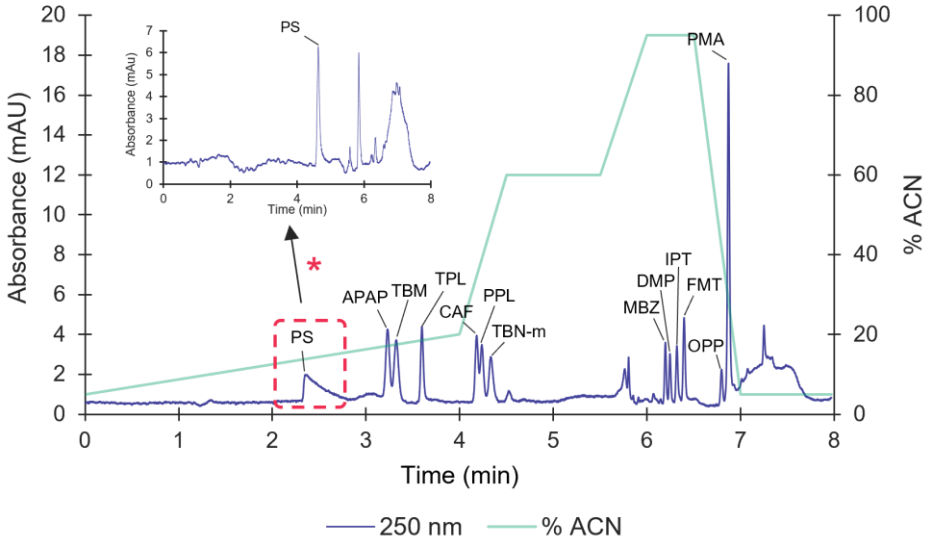

Figure 35. Chromatogram obtained for the multicomponent mixture for the portable minLC, the asterisk (*) shows the PS peak obtained for the analysis carried out using ACN and water with 0.1 % of formic acid as mobile phase solvents.

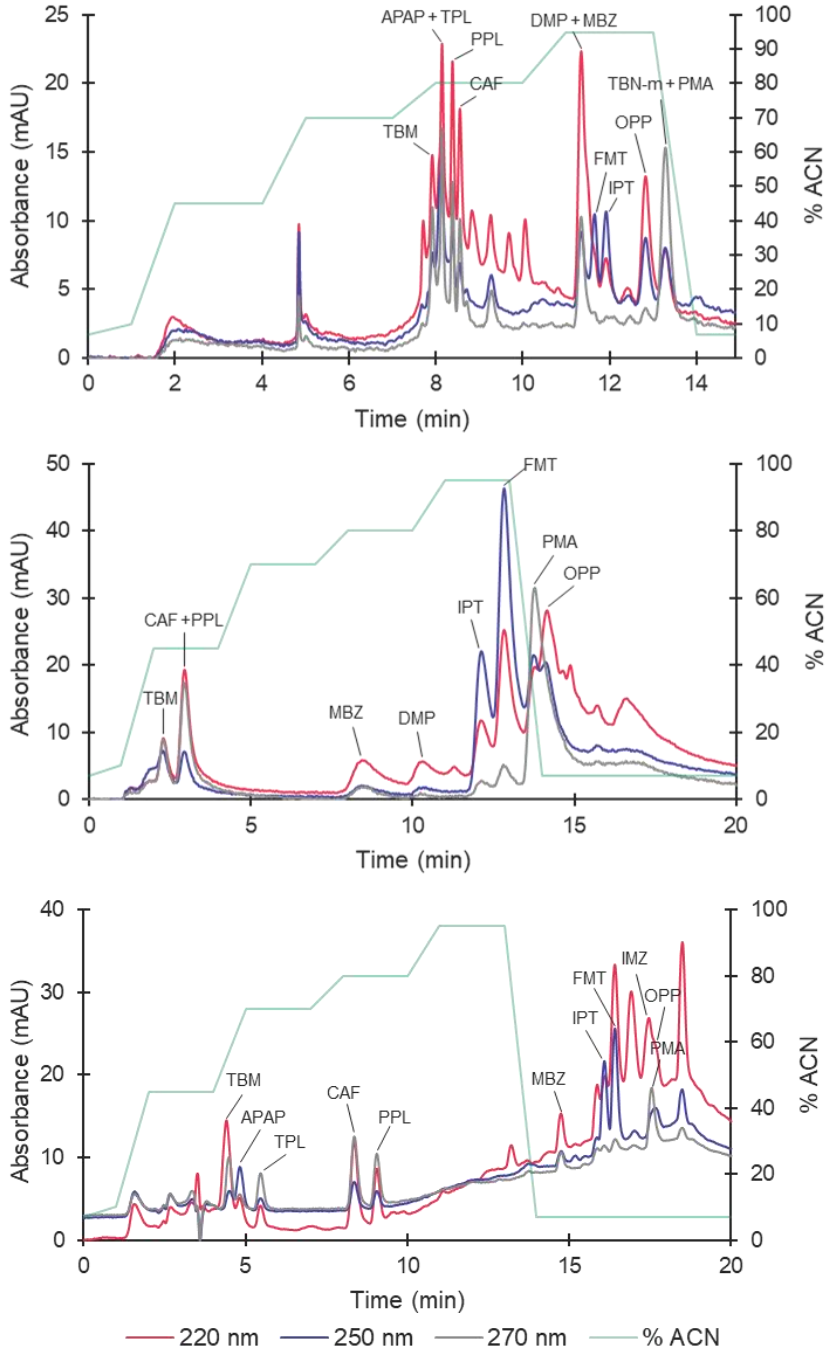

Figure 36. Chromatograms obtained for the multicomponent mixture with the benchtop capLC (a) and nanoLC with 50 mm × 0.075 mm column (b) and 150 mm × 0.1 mm column (c). The chromatograms were obtained at three different wavelengths.

4.1.1.2 Figures of merit

Figure 35 shows a good chromatographic resolution for the multicomponent solution achieved by the portable minLC, which only works at 255 nm by LED detection. The resolution achieved by the benchtop capLC (see **Figure 36 a**) was worse than that obtained by the portable minLC; several analytes provided overlapped chromatographic peaks. On the other hand, as **Figure 36 b** shows, working with the 50 × 0.075 mm column, the benchtop nanoLC gives lower performance than the obtained with the 150 × 0.1 column. The time window for the resolution of the assayed mixtures were different for the three systems as **Figure 35** and **Figure 36** shows: 8, 14 and 20 min for portable minLC, benchtop capLC and nanoLC with the longer column, respectively. As mentioned, capLC exhibit lower resolution for the multicomponent mixture separation compared to the other systems. On the other hand, both, the portable minLC and benchtop nanoLC demonstrated similar chromatographic profiles. However, it is worth noting that the portable LC system provided a higher overall resolution. This fact can be explained mainly by the particle sizes of the different columns employed (1.7 µm vs. 3.5 µm, for portable and nanoLC, respectively), which are limited by the maximum pressure that the LC tolerate. **Table 21** gives peak widths calculated from the software of each equipment as a measure of column performance in gradient elution. Achieved precision of the retention times for all LC systems and analytes were lower than 1 %. The mean peak widths and their standard deviations obtained from data given in **Table 21** are: 0.07 ± 0.01, 0.14 ± 0.05 and 0.18 ± 0.03 min for portable LC and benchtop capLC and nanoLC respectively. Peak capacity (P_C) is a measure of the separation power that includes the entire chromatographic space together with the variability of the peak width over the chromatogram. In the case where the peak width pattern remains relatively consistent, such as in most RP gradient separations and in this study, P_c can be calculated from **equation 3**, as described by U.D. Neue (2008) [299]:

$$P_C = 1 + \frac{t_G}{\bar{\omega}} \quad (3)$$

where $\bar{\omega}$ is the average peak width, and t_G is the gradient run time.

P_C can be used as a parameter for evaluating efficiency in gradient elution. The values calculated for portable LC and benchtop capLC and nanoLC were: 115, 101 and 112, respectively. The small differences can be explained by the dimensions of the analytical columns used and the particle sizes of the stationary phases (see **Table 21**). Note that the separation for the more polar compounds is achieved at higher water content for nanoLC than for capLC.

Table 21. Peak widths at 4σ ($\bar{\omega}$) obtained for the multicomponent mixtures by the software of the LC instruments used: portable LC (100 × 0.15 mm, 1.7 μm, loop volume 40 nL), benchtop capLC (150 × 0.5 mm, 5 μm, loop volume 16 μL), and benchtop nanoLC (150 × 0.1 mm, 3.5 μm, loop volume 440 nL).

Analyte	Portable LC		Benchtop capLC		Benchtop nanoLC	
	t_r (min)	$\bar{\omega}$ (min)	t_r (min)	$\bar{\omega}$ (min)	t_r (min)	$\bar{\omega}$ (min)
PS	2.35	-	4.60	-	3.10	0.24
TBM	3.32	0.10	7.93	0.11	4.54	0.20
APAP	3.13	0.10	8.11	0.08	4.79	0.20
TPL	3.51	0.08	8.15	-	5.47	0.21
CAF	4.18	0.07	8.57	0.09	9.86	0.20
PPL	4.24	0.07	8.40	0.09	8.91	0.20
TBN-m	4.30	0.08	13.30	-	-	-
MBZ	6.20	0.06	11.35	0.14	15.32	0.18
DMP	6.25	0.06	11.46	-	15.00	0.12
IPT	6.32	0.06	11.93	0.16	15.87	0.16
FMT	6.39	0.06	11.66	0.14	16.01	0.17
OPP	6.80	0.07	12.84	0.21	14.73	0.14
PMA	6.86	0.07	13.30	0.22	16.40	0.18

The cartridge performance of the portable minLC was evaluated throughout the number of injections. **Figure 37** shows the chromatograms

for 30 mg·L^{-1} of a) theophylline and b) theobromine as targets at different number of previous injections (new, 700 and 1000 previous ones). Compared with the chromatogram obtained from a new cartridge, for both analytes at 700 and 1000 injections the peak profiles were similar.

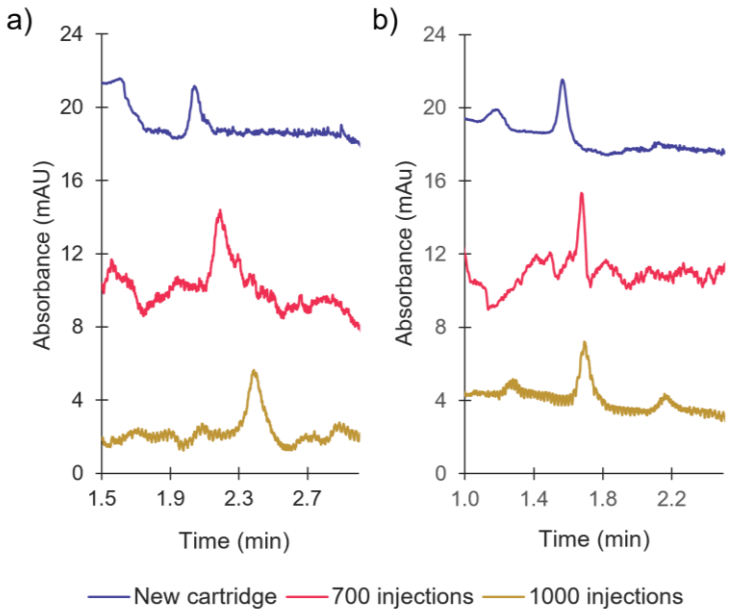

Figure 37. Chromatograms obtained for (a) theophylline and (b) theobromine at different number of injections.

Different analytical parameters such as linearity in the working range, precision, sensitivity, and recovery were determined for the portable minLC and compared with the ones obtained for the benchtop capLC and nanoLC. **Tables 22 – 24** show the results obtained. LODs were calculated as the concentration of analyte which gives a signal-to-noise ratio (s/n) equals 3. The limit of quantification (LOQ) was the concentration at the lower working linearity level (s/n = 10). Accuracy obtained from standards is expressed as relative error (E_r).

The instrumental detection limits for the portable LC, as indicated in **Table 22**, fall within the range of 0.4 – 10 mg·L^{-1}, enabling the determination of analytes at trace levels (mg·L^{-1}) but not ultra-trace (µg·L^{-1}). It is important

to note that no pre-concentration step was performed. As expected, benchtop cap LC and nanoLC provided lower LODs (around three order of magnitude lower), between 0.5 and 5 $\mu g \cdot L^{-1}$ (see **Tables 23 – 24**). These tables also include the LODs achieved at 250 nm to show the loss sensitivity in function of selected wavelength since the portable LC only includes a single LED detector at 255 nm. Accuracy values for portable LC and benchtop capLC and nanoLC provided suitable values for environmental analysis (Er < |15%|) [300].

Matrix effect was evaluated by spiking with several analytes (TPL, CAF, FMT, IPT) a well water, which contained the analytes below their LODs. The recovery values are shown in **Tables 22 – 24**. As it can be seen, the obtained values for the three LC techniques are statistically similar. No matrix effect was observed.

Table 22. Figures of merit obtained for determination of target analytes by means of a portable minLC. Regression line, regression coefficient (R^2), working range, limit of detection (LOD), relative error (Er) and recovery (R) are shown. * Solvents A and B of the mobile phase contained 0.1% of formic acid.

Compound	Working range ($mg \cdot L^{-1}$)	Regression line and coefficient $y = (a \pm sa) + (b \pm sb) \cdot (L \cdot mg^{-1}) \cdot x$, R^2	LOD ($mg \cdot L^{-1}$)	E_r (%)	R (%) (n = 3)
PS*	1.0 – 1.6	y = (-0.1 ± 0.1) + (1.584 ± 0.012)·x, 0.9999	0.4	-1	90 ± 10
TBM	3.0 – 22	y = (0.48 ± 0.01) + (0.53 ± 0.09)·x, 0.9996	1	-2	
APAP	3.0 – 23	y = (0.0 ± 0.3) + (0.58 ± 0.02)·x, 0.997	1	-5	
TPL	1.8 – 12	y = (0.2 ± 0.1) + (0.521 ± 0.014)·x, 0.998	0.6	4	90 ± 10
PPL	3.0 – 10	y = (0.33 ± 0.05) + (0.580 ± 0.008)·x, 0.9998	1	-1	
CAF	3.0 – 24	y = (0.3 ± 0.5) + (0.69 ± 0.03)·x, 0.9990	1	5	85 ± 7
TBN-m	30 – 115	y = (0.2 ± 0.3) + (0.075 ± 0.004)·x, 0.994	10	1	
IPT	2.0 – 20	y = (-0.3 ± 0.2) + (0.53 ± 0.02)·x, 0.995	0.8	10	85 ± 10
FMT	3.0 – 19	y = (0.2 ± 0.3) + (0.42 ± 0.03)·x, 0.990	1	-7	85 ± 10
PMA	0.3 – 29	y = (1.8 ± 1.8) + (3.32 ± 0.10)·x, 0.998	0.1	-4	70 ± 8

Table 23. Figures of merit obtained for determination of target analytes by means of a benchtop capLC. Regression line, regression coefficient (R^2), working range, limit of detection (LOD), relative error (Er) and recovery (R) are shown. *LOD estimated at 255 nm.

Compound / λ (nm)	**Working range ($\mu g \cdot L^{-1}$)**	**Regression line and coefficient $y = (a \pm sa) + (b \pm sb) \cdot (L \cdot \mu g^{-1}) \cdot x$, R^2**	**LOD ($\mu g \cdot L^{-1}$)**	**E_r (%)**	**R (%) (n = 3)**
PS / 250	15 – 500	y = (60 ± 60) + (7.13 ± 0.012)·x, 0.990	5	2.0	95 ± 10
TBM / 270	3.0 – 50	y = (13 ± 3) + (2.60 ± 0.14)·x, 0.990	1, 5*	1.0	
CAF / 270	1.5 – 50	y = (2.5 ± 1.6) + (3.38 ± 0.05)·x, 0.998	0.5, 2*	-1.0	95 ± 10
TPL / 270	3.0 – 50	y = (4.8 ± 1.6) + (2.36 ± 0.05)·x, 0.995	1, 5*	-4.5	120 ± 10
APAP / 250	1.5 – 52	y = (4 ± 2) + (3.90 ± 0.07)·x, 0.997	0.5	3.0	
DMP / 220	5.0 – 50	y = (0 ± 2) + (3.13 ± 0.07)·x, 0.995	2, 25*	2.0	
MBZ / 270	5.0 – 50	y = (2.4 ± 1.0) + (2.28 ± 0.03)·x, 0.998	2, 10*	-5.0	
FMT / 250	3.0 – 50	y = (-0.5 ± 0.8) + (4.68 ± 0.03)·x, 0.997	1	6.0	110 ± 5
IPT / 250	3.0 – 50	y = (-3.6 ± 2.0) + (4.53 ± 0.07)·x, 0.998	1	4.0	109 ± 9
IMZ / 220	15 – 1000	y = (-70 ± 30) + (3.98 ± 0.07)·x, 0.998	5	-4.0	100 ± 5
PMA / 270	6.0 - 500	y = (-110 ± 60) + (10.6 ± 0.02)·x, 0.998	2, 10*	-5.0	100 ± 5

Table 24. Figures of merit obtained for determination of target analytes by means of a benchtop nanoLC. Regression line, regression coefficient (R^2), working range, limit of detection (LOD), relative error (Er) and recovery (R) are shown. *LOD estimated at 255 nm.

Compound / λ (nm)	Working range ($\mu g \cdot L^{-1}$)	Regression line and coefficient $y = (a \pm sa) + (b \pm sb) \cdot (L \cdot \mu g^{-1}) \cdot x$, R^2	LOD ($\mu g \cdot L^{-1}$)	E_r (%)	R (%) (n = 3)
PS / 250	15 – 60	y = (1.6 ± 0.7) + (7 ± 0.3)·x, 0.998	2	1.0	100 ± 5
TBM / 270	15 – 60	y = (1.249 ± 0.016) + (7 ± 0.3)·x, 0.9996	5, 12*	0.7	
APAP / 250	8 – 60	y = (-1.2 ± 1.9) + (1.76 ± 0.05)·x, 0.998	2.5	-6.2	
TPL / 270	3 – 60	y = (0 ± 1) + (1.04 ± 0.03)·x, 0.998	1, 4*	-4.4	120 ± 10
PPL / 270	3 – 60	y = (4.3 ± 0.6) + (1.750 ± 0.015)·x, 0.999	1, 6*	-0.2	
CAF / 270	15 – 60	y = (2 ± 1) + (2.541 ± 0.016)·x, 0.9999	0.5, 2*	1.3	120 ± 10
MBZ / 250	15 – 60	y = (-0.9 ± 1.4) + (1.19 ± 0.04)·x, 0.998	4	3.6	
DMP / 220	9 – 60	y = (-0.6 ± 1.4) + (0.89 ± 0.04)·x, 0.997	3	2.5	
IPT / 250	3 – 60	y = (14 ± 2) + (3.28 ± 0.06)·x, 0.9992	1	4.3	103 ± 9
FMT / 250	3 – 60	y = (6 ± 3) + (2.93 ± 0.01)·x, 0.998	1	6.2	96 ± 5
IMZ / 220	3 – 100	y = (0.6 ± 1.5) + (1.20 ± 0.03)·x, 0.9990	1, 10*	-12	98 ± 5
OPP / 220	6 – 60	y = (8.5 ± 1.9) + (0.76 ± 0.04)·x, 0.997	2, 12*	-3.3	
PMA / 270	6 – 80	y = (46 ± 12) + (7.1 ± 0.3)·x, 0.998	2, 10*	-7.6	100 ± 5

The increasing need for in-situ analysis carried out in the field makes portable equipment indispensable. In addition to the weight, size, and battery requirements, a liquid chromatograph intended for in-field applications must also provide reliable results in adverse conditions. Therefore, the analytical performance of portable minLC was evaluated in the field under different conditions of humidity, wind, and temperature. We selected caffeine as target analyte for testing the performance. **Figure 38** shows the chromatograms obtained for caffeine in laboratory and in-field conditions. Variation in humidity between measurements (45 – 80 % relative humidity) was not relevant. However, chromatograms baseline becomes slightly noisier with the decrease in temperature. Wind speed did not modify the response. In all cases, the chromatographic profile was maintained.

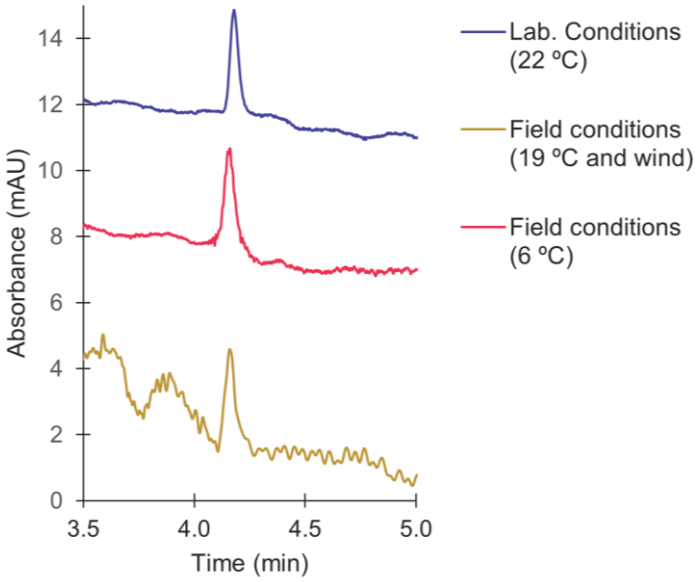

Figure 38. Chromatograms obtained for caffeine at laboratory conditions (a) 22 °C and 45% humidity, field conditions (b) 14 °C, 68% humidity and 25 km·h^{-1} wind (c) field conditions 7 °C, 73% humidity and 15 km/h wind.

4.1.1.3 Determination of biocides in wastewaters

Three residual waters from fruit washing treatment of three different places were analysed. The waters can contain biocides like potassium sorbate, imazalil or pyrimethanil. **Figures 39 – 41** show the obtained chromatograms, which were very clean in the interest time window. No matrix effect was observed (see **Tables 22 – 24**). The sample 1 contained PS and IMZ, at levels of concentration given in **Table 25**. Due to the portable minLC restricted measuring wavelength of 255 nm, the quantification of IMZ was not feasible, thereby allowing only the quantification of PMA in samples 2 and 3 (**Figures 40** and **41**, respectively). Similar results were obtained from the three LC systems for PMA as it can be shown in **Table 25**, although the sample dilutions carried out for sample processing were very different. IMZ can be quantified from the benchtop instruments providing similar results. **Figure 42** shows the normalized UV spectra of the chromatographic peaks in samples corresponding to the analytes of interest in comparison to the standard.

Table 25. Pesticide concentrations found in samples (mean ± IR 95%).

Instrument	**Sample**	**Found concentration ($mg \cdot L^{-1}$)**		
		Potassium sorbate	Imazalil	Pyrimethanil
Portable minLC	M1	1800 ± 140	n.d.	n.d.
	M2	n.d.	n.d.	3.2 ± 0.3
	M3	n.d.	n.d.	110 ± 20
Benchtop capLC	M1	1800 ± 120	180 ± 30	n.d.
	M2	n.d.	480 ± 60	3.3 ± 0.2
	M3	n.d.	450 ± 20	120 ± 10
Benchtop nanoLC	M1	1750 ± 20	150 ± 30	n.d.
	M2	n.d.	480 ± 20	3.6 ± 0.14
	M3	n.d.	450 ± 20	130 ± 20

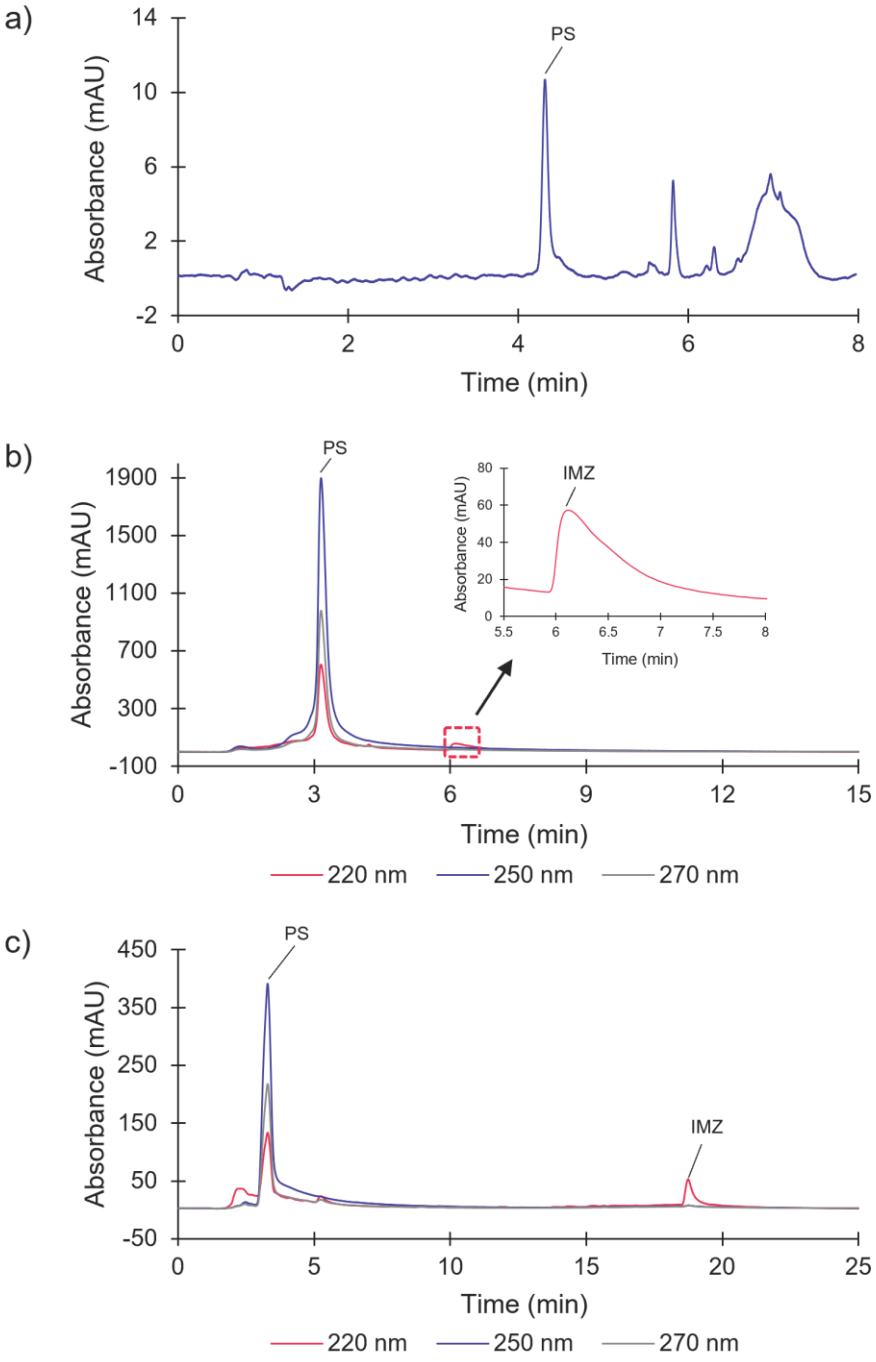

Figure 39. Chromatograms obtained for “sample 1” using the portable LC (a), benchtop capLC (b) and benchtop nanoLC (150 mm × 0.1 mm, 35 µm column) (c).

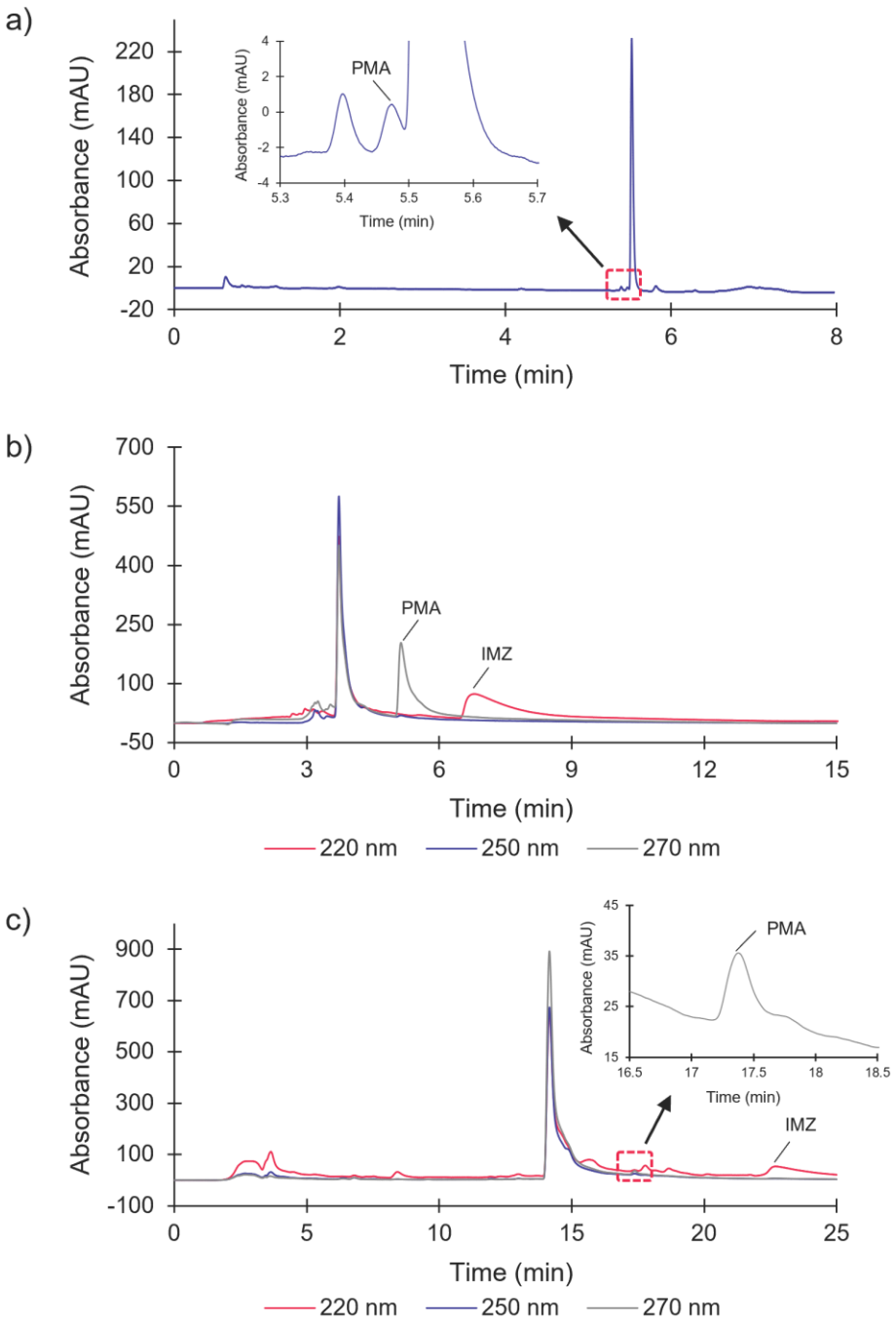

Figure 40. Chromatograms obtained for “sample 2” using the portable LC (a), benchtop capLC (b) and benchtop nanoLC (150 mm × 0.1 mm, 35 µm column) (c).

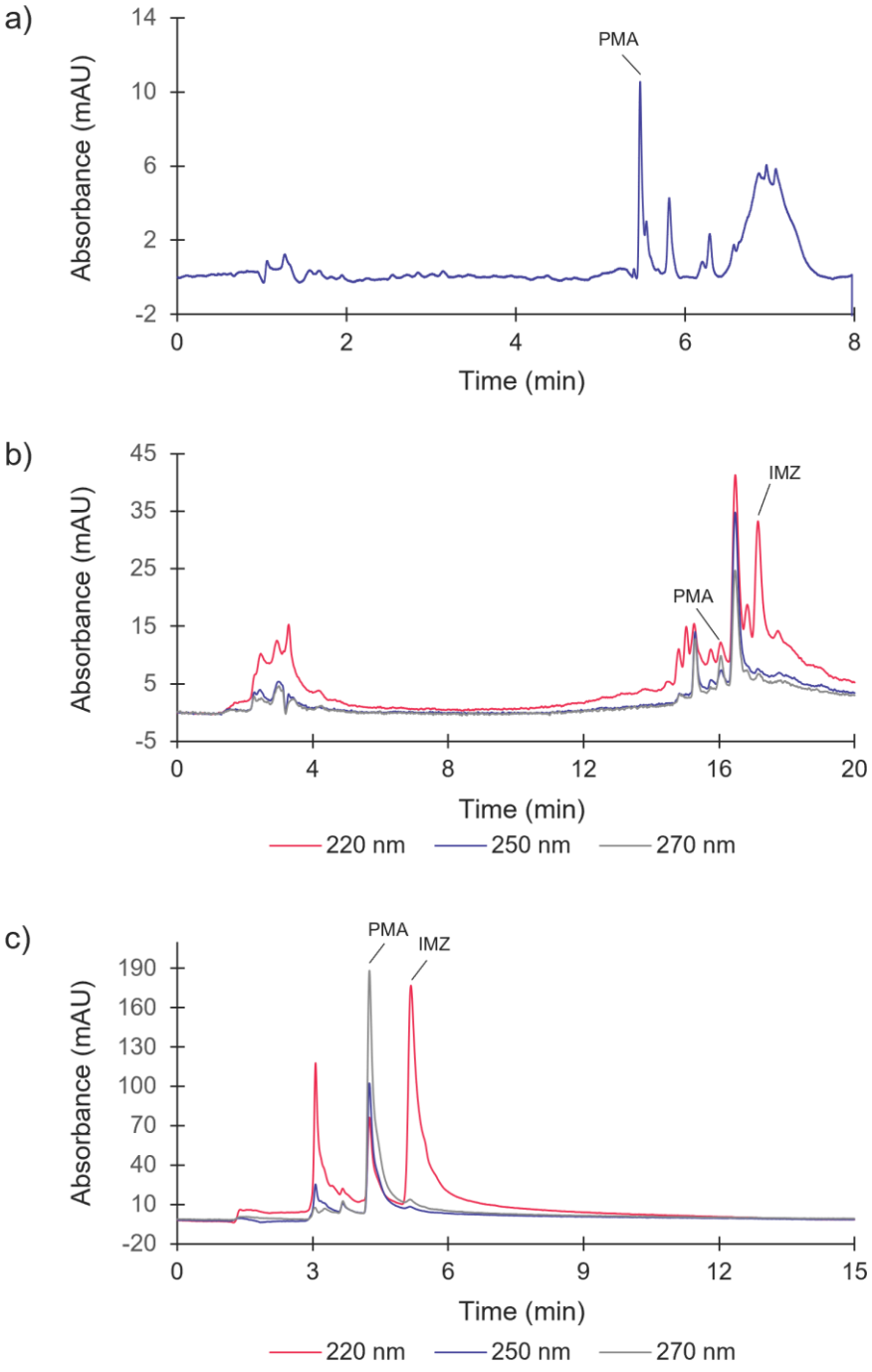

Figure 41. Chromatograms obtained for "sample 3" using the portable LC (a), benchtop capLC (b) and benchtop nanoLC (150 mm × 0.1 mm, 35 µm column) (c).

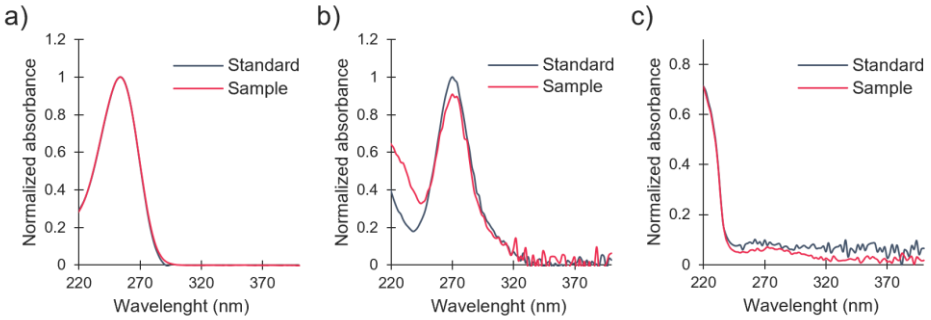

Figure 42. Normalized UV spectra for observed peaks in samples analysed by means of the benchtop nanoLC (see Figures 38, 39, and 40). The spectra correspond to a) potassium sorbate (t_r = 3.3 min) found in sample 1, b) pyrimethanil (t_r = 17.4 min) found in sample 2, and c) imazalil (t_r = 22.9 min) found in sample 2.

4.1.1.4 Evaluation tools for benchtop and portable miniaturized liquid chromatography

To evaluate capacities of the Axcend Focus LC, the BETTER assessments defined by Rahimi et al. [301] were used. BETTER grade levels (each ranging from 1 to 5) are selected both to represent the current range of developments, and community goals. To date, portable LC systems meet some of the grade 2 and 3 criteria [46,133]. The grade 4 and 5 criteria are deemed a challenge to be met by next generation devices; indeed, no instrument reported to date reaches Grade 5 in any category. Various non-chromatographic and chromatographic characteristics (system cost, cost/test, weight, and performance) and other requirements for in-field analysis (portability, robustness, sample introduction) are considered.

The system cost of the Axcend Focus LC is in the average in relation to other portable chromatographic systems [301]. However, due to the low solvent consumption (approximately 16 µL per chromatographic run) the cost/test is notably low. If it is only considered the solvent usage, the cost per test is approximately 0.0005 €. Assuming an average price of electricity of 0.15 Kw·h^{-1} the Axcend Focus LC will cost 0.02 €·h^{-1} which is less than 0.01

€·run^{-1}. Because of the low solvent usage and injection volume, waste production is minimal (50 µL per run). The system weight is 8 kg without the cartridge, which is slightly higher than the maximum weight to consider an instrument as portable (7 kg) [302], nevertheless, it can be easily hand-transported. Regarding to the operation time, the system can work away from main power for an average of 12 h, which is similar to the battery duration of the latest portable chromatographs (see **Table 5**). The chromatograph autonomy is enough to last a full working day. The equipment shown suitable robustness at the climate conditions tested.

Chromatographic performance is classified in accordance with the operation pressure. The portable minLC was able to operate at 410 bar, which aligns with the values reported in the majority of portable LC systems described in the literature [46]. The sample introduction consists of a closed injection system, restricting any possible modification by the operator. In general, the sample introduction is a simple procedure that does not require a highly specialized operators. Pretreatment should be included if the sample clean-up and/or preconcentration steps are needed. **Figure 43** sum up the different BETTER assessments in a table and a radar chart in accordance with [46]. BETTER grade levels (ranging from 1 to 5) describe the advancement of a given characteristic. Further grade classification can be found in [132].

	BETTER grade				
Criteria	1	2	3	4	5
System cost		■			
Cost per test					■
Weight			■		
Portability				■	
Operation time		■			
Robustness				■	
Performance			■		
Sample injection			■		
Waste production				■	

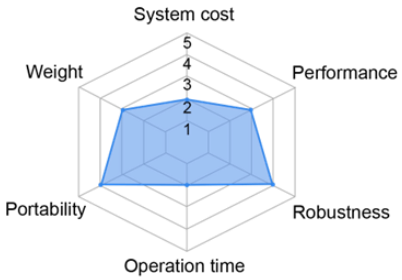

Figure 43. Table and radar chart with the different assessments of BETTER criteria (higher grades means better results).

The HEXAGON tool was employed for evaluating and quantifying the associated features of an analytical methodology, in reference to its figures of merit, greenness and sustainability. The tool metrics are defined in [12]. Lower penalization score corresponds to a better adaptation to provide reliable results for the different method aspects [12,122]. An overall penalization ranking from 0 to 4 scale is indicated in a hexagon pictogram where variables such as figures of merit, health and safety, environmental impact, sustainability, and cost-benefit relation are shown. Eventually, the arithmetic mean (Sav) of the 0–4 scale is computed in order to compare different analytical methods [122].

Firstly, the penalty points (PPs) of the figures of merit 1 were assigned. It is considered that the proposed methodology has successfully resolved the quantification of biocides at $mg \cdot L^{-1}$ levels in washing waters. Water sample processing involved filtering (0.45 µm pore size nylon filter) and dilution with distilled water for all the analytical techniques studied, thus, similar penalization score was obtained for the sample treatment evaluation within figures of merit 1, as represented in **Figure 44**. Regarding calibration, portable minLC exhibited higher penalization scores because of the higher limits of detection reached with respect to the other lab techniques.

Toxicity and safety evaluation were performed by collecting reagents pictograms assigning them its corresponding penalty points [12]. Generally, acetonitrile and methanol were employed as organic solvents, both implying health severe toxicity and flammable physical hazard. The amount of waste generated was also considered and penalized within the residue variable of the HEXAGON tool. Solvent amount used and residue production were negligible for portable minLC in reference to benchtop LCs. This fact influences PPs for toxicity and safety estimations and residues as it is shown in **Figure**

44. The environmental impact was also quantified by the so-called carbon footprint and expressed by kilograms of CO_2 equivalent. In this regard, electricity consumption is the main factor to be considered. The portable minLC showed the best adaptation to reduce environmental impact (**Figure 44**). Finally, the cost-effectiveness of the analytical methodologies was analysed according to the instrumentation needed, electricity consumption, salary of qualified personnel and reagents and materials costs. The obtained results demonstrated that the portable minLC was the most economical option (as depicted in **Figure 44**) due to its cheaper instrumentation and the lower electrical consumption, the reagent usage, and analysis time.

Final overall qualification in a 0–4 scale is indicated in the hexagon pictogram illustrated in **Figure 45**. The arithmetic mean is also calculated, which allows to rank the analytical methods according to greenness and sustainability aspects. In this regard, the portable minLC (Sav = 1.0) has demonstrated to be superior to the capLC and nanoLC (Sav = 1.57) for solving the planned problem.

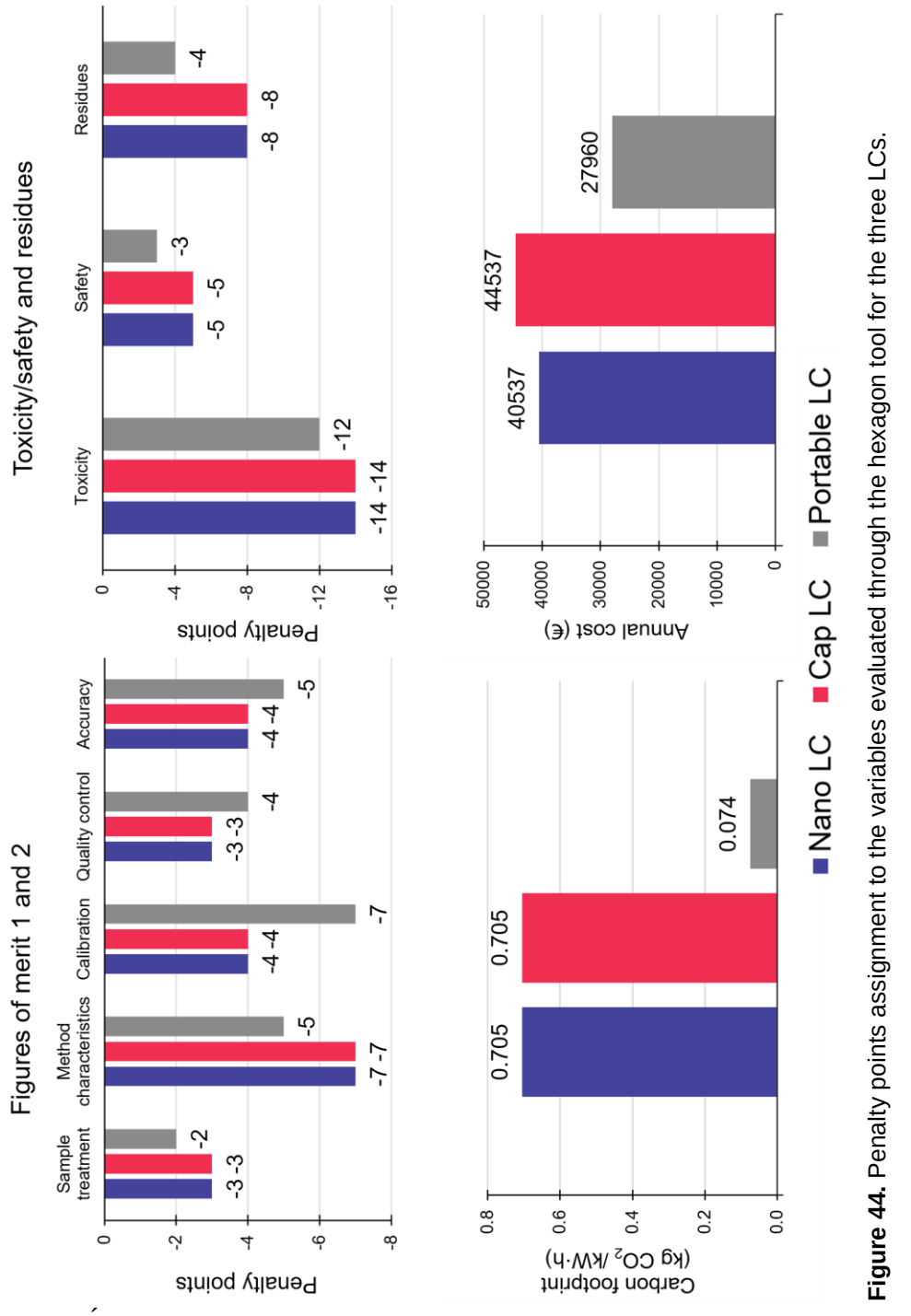

Figure 44. Penalty points assignment to the variables evaluated through the hexagon tool for the three LCs.

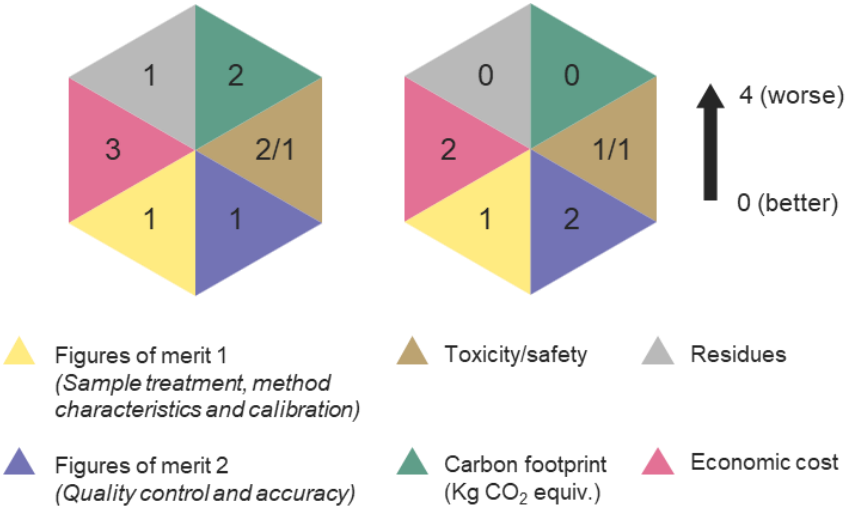

Figure 45. Hexagon tool for capLC nanoLC (left) and Portable minLC (right).

4.1.1.5 Conclusions

In this study it has been evaluated the figures of merit of a commercial portable minLC-LED-UV in comparison with a capLC-DAD and nanoLC-DAD coupled to IT-SPME for the analysis of different substances of analytical interest. The portable minLC achieved suitable separation with good chromatographic resolution and a short analysis time. Also, the system maintained the chromatographic profile in different in-field conditions. One of the flaws of the portable minLC was its limited sensibility, with LODs in the order of low $mg \cdot L^{-1}$. Nevertheless, these LODs were enough for its application in the determination biocides in fruit washing residual waters, obtaining adequate quantification with similar results to those obtained by the benchtop systems. Finally, two evaluation tools, the BETTER criteria and HEXAGON were used to objectively compare its portability and method characteristics. Regarding the BETTER criteria, the results were comparable to those achieved by other recently developed portable LCs. The HEXAGON tool was used to compare the benchtop and portable LC, obtaining favourable results for the latter in terms of waste generated, carbon footprint, safety and toxicity, and economic cost.

4.1.2 Determination of legislated nitrogen compounds by portable instruments in different water sources

4.1.2.1 Determination of nitrate, nitrite, and ammonium

Figures of merit for the determination of nitrates based on its native absorbance (at 220 nm) were evaluated for the different instruments (see **Table 26**). Lower slope of the calibration graph was obtained by using the in-place analyzer. This is in accordance with its specifications which indicates a concentration range of measurement up to 100 $mg \cdot L^{-1}$. The inter and intra-day precision achieved were similar in all cases with RSDs below 3 %. **Figure 46** compares the absorbance spectrum of a nitrate calibration measured on the benchtop spectrophotometer, the portable optical fiber spectrophotometer, and the analyzer.

Table 26. Figures of merit of the studied instruments (benchtop spectrophotometer, portable optical fiber probe, and nitrate analyzer) including the regression line equation ($y = a + b \cdot x$), regression coefficient, LOD, and LOQ for the analysis of different analytes.

Analyte	Instrument	b ± sb (L·mg-1)	a ± sa	R^2	LOD (mg·L-1)	LOQ (mg·L-1)
NO_3^-	Benchtop	0.0563 ± 0.0016	0.010 ± 0.014	0.998	0.5	1.5
	Probe	0.0542 ± 0.0017	0.012 ± 0.014	0.998	0.5	1.5
	Analyzer	0.0154 ± 0.0009	0.010 ± 0.014	0.998	3.0	9.0
NO_2^-	Benchtop	00.661 ± 0.017	0.010 ± 0.014	0.9998	0.01	0.03
	Probe	0.654 ± 0.017	0.012 ± 0.014	0.9998	0.01	0.03
NH_4^+	Probe	0.717 ± 0.017	0.003 ± 0.015	0.9983	0.01	0.03

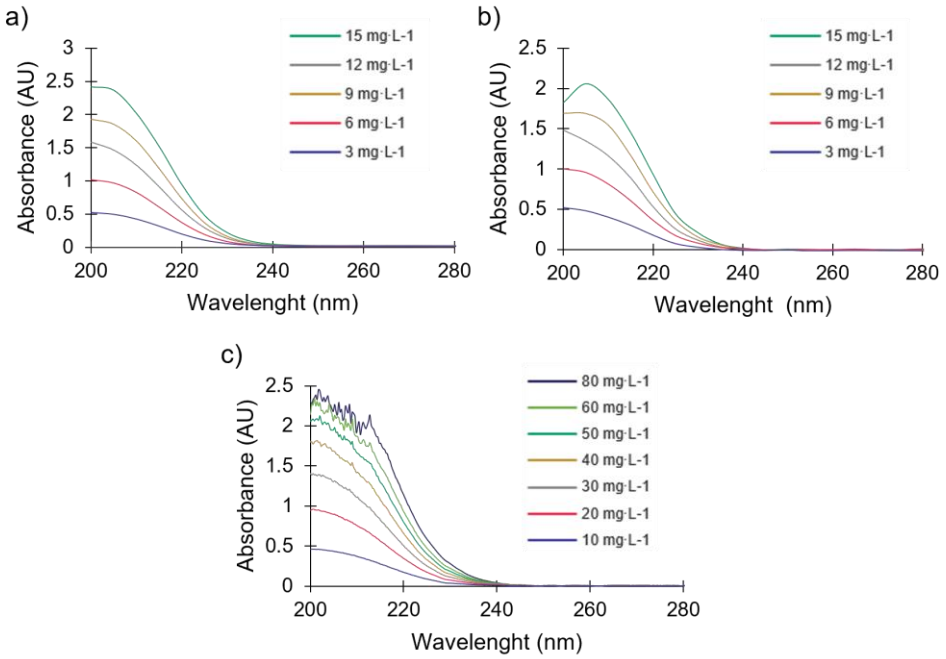

Figure 46. UV spectra of nitrate standard solutions in a) analyzer, b) benchtop spectrophotometer, and c) portable optical fiber spectrophotometer

The influence of turbidity and presence of humic acids were studied due to their possible contribution to the nitrate response. Different stock solutions of nitrate 15 mg·L^{-1} with 5, 10, 20, 30 and 40 UNT of turbidity or 2, 4, 6, 8 and 10 mg/L of humic acids were measured. Turbidity values below 10 UNT may be considered negligible when analyzing nitrate concentration at 220 nm, and even up to 20 UNT. By using the analyzer, turbidity < 40 UNT can be tolerated. Humic acid concentration could affect markedly accuracy in the estimation of nitrate for concentrations over 2 mg·L^{-1} even when utilizing the A_{220}-2·A_{275} correction [292] (see **Figure 47**).

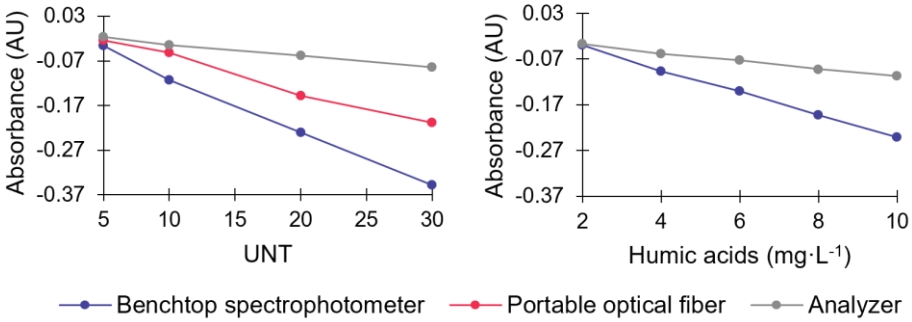

Figure 47. Impact of different levels of turbidity (left) and humic acids (right) on the absorbance measurement (A_{220}-2·A_{270}) of a 15 mg·L^{-1} nitrate solution.

Concerning the determination of nitrite, the Griess reaction was used. Besides to the conventional laboratory spectrophotometer, the portable optical fiber probe was employed. The calibration parameters are given in **Table 26**. Similar sensitivity was obtained for both instruments with LODs of 0.01 mg·L^{-1}. The inter and intra-day precision was higher for the portable optical fiber but in all cases the values were maintained below the 7 %.

Ammonium was determined by colorimetry using the Berteloth's reaction registering the spectra by means of the portable optical fiber probe. The calibration curve is shown in **Table 26**. Good sensitivity was obtained, with a LOD of 0.01 mg·L^{-1} which is in accordance with the legislated values given in **Table 11**. The RSD values for the intra-day precision were 1.5 % and 0.7 % for the portable optical fiber and the conventional lab spectrophotometer.

Environmental water samples from various sources within the Valencia Community, an agricultural region where high NO_3^- concentrations can be expected, were subjected to analysis (see **Table 27**). To assess the potential matrix effect, the samples were fortified with known analyte concentrations. It was observed that all tested methodologies exhibited recoveries close to 100%, indicating the absence of any significant matrix effect. All the

concentrations found are in accordance with the regulatory limits specified in previous sections.

The analyzer was used as well in a real drinking water osmosis treatment plant during a period of seven days in a continuous mode registering the NO3⁻ concentration each 30 min. As can be seen in the **Figure 48 a,** small variations associated to the different NO_3^- content in the water were observed. In addition, this equipment was utilized to monitor the removal of NO_3^- from well water in the treatment plant. The amount of NO_3^- that was left in water was estimated in place by using the analyzer. Also, discrete samples were collected and analyzed using the optical fiber probe The comparative results are shown in **Figure 48 b**. As can be observed, similar results were obtained, keeping in mind that the optical fiber probe works within a linear range of up to 50 $mg \cdot L^{-1}$, while the analyzer is calibrated up to 100 $mg \cdot L^{-1}$, as indicated in the experimental section.

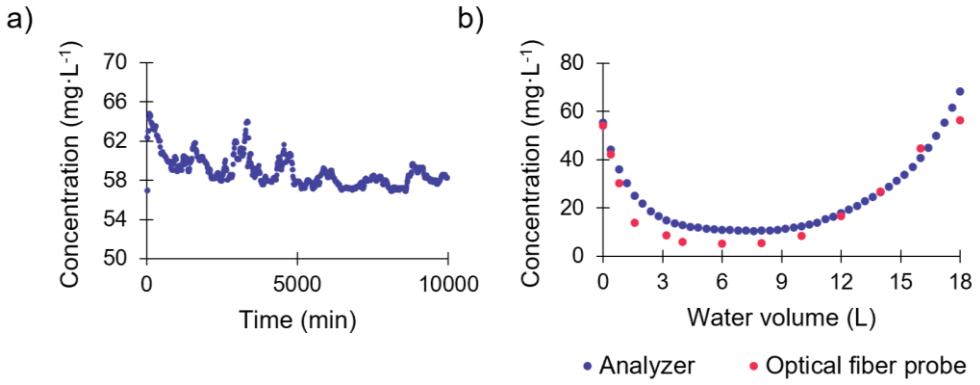

Figure 48. a) Estimated NO_3^- concentration over time obtained by means of the NO_3^- analyzer in a treatment plant of drinking water in continuous mode. b) Estimated NO_3^- concentrations found in treated water to remove NO_3^- by means of the analyzer in continuous mode and the optical fiber probe in collected samples.

Table 27. Found nitrate concentrations in different well waters sources with the nitrate analyzer and the benchtop spectrophotometer M1: Sea water; M2: Well water; M3: Transition water; M4: Fountain water; M5: Well water (2); M6: Lagoon water.

Sample	NH_4^+ and NH_4^+ as N ($mg \cdot L^{-1}$)	NO_2^- and NO_2^- as N ($mg \cdot L^{-1}$)	NO_3^- and NO_3^- as N ($mg \cdot L^{-1}$)		NH_4^+ + DON / DON as N ($mg \cdot L^{-1}$)
	Probe	Probe	Analyzer	Benchtop spectrophotometer	Portable luminometer
M1	< LOD	0.035 ± 0.01 0.010 ± 0.003	15.8 ± 0.1 3.56 ± 0.02	15.5 ± 0.5 3.5 ± 0.1	0.16 ± 0.03 0.16
M2	-	-	2.9 ± 0.1 0.66 ± 0.02	2.9 ± 0.1 0.66 ± 0.02	-
M3	0.28 ± 0.02 0.22 ± 0.01	LOD	35.4 ± 0.1 7.99 ± 0.02	38.7 ± 0.5 8.7 ± 0.1	0.7 ± 0.003 0.5
M4	0.12 ± 0.02 0.09 ± 0.01	0.10 ± 0.01 0.030 ± 0.003	21.6 ± 0.1 4.87 ± 0.02	19.8 ± 0.3 4.47 ± 0.07	0.16 ± 0.04 0.07
M5	< LOD	< LOD	45.8 ± 0.1 10.34 ± 0.02	42.7 ± 0.1 9.64 ± 0.02	-
M6	2.5 ± 0.1 1.9 ± 0.1	LOD	30.6 ± 0.1 6.90 ± 0.02	31.7 ± 0.1 7.15 ± 0.02	3.43 ± 0.20 1.5

4.1.2.2 Determination of dissolved organic nitrogen

The determination of nitrogen organic compounds such as amino acids, more precisely tryptophan like fluorescent can be used to indicate the size and activity of a microbial community [303] and it can be correlated with the bioavailable organic material present [304,305]. Other amino acids like tyrosine and β-phenylalanine as aromatic compounds also present fluorescence. **Figure 49** shows the excitation vs emission wavelengths for the three amino acids obtained by the lab instrument, the emission wavelengths were: 355, 300 and 280 nm for T, TY, and PA, respectively. Signals were followed by using the fluorescent optical probe and by the lab spectrofluorometer. For

the optical probes, parameters like the deep of the probe in the solution, the type of container of the solution, the solution agitation and the size of the container were studied.

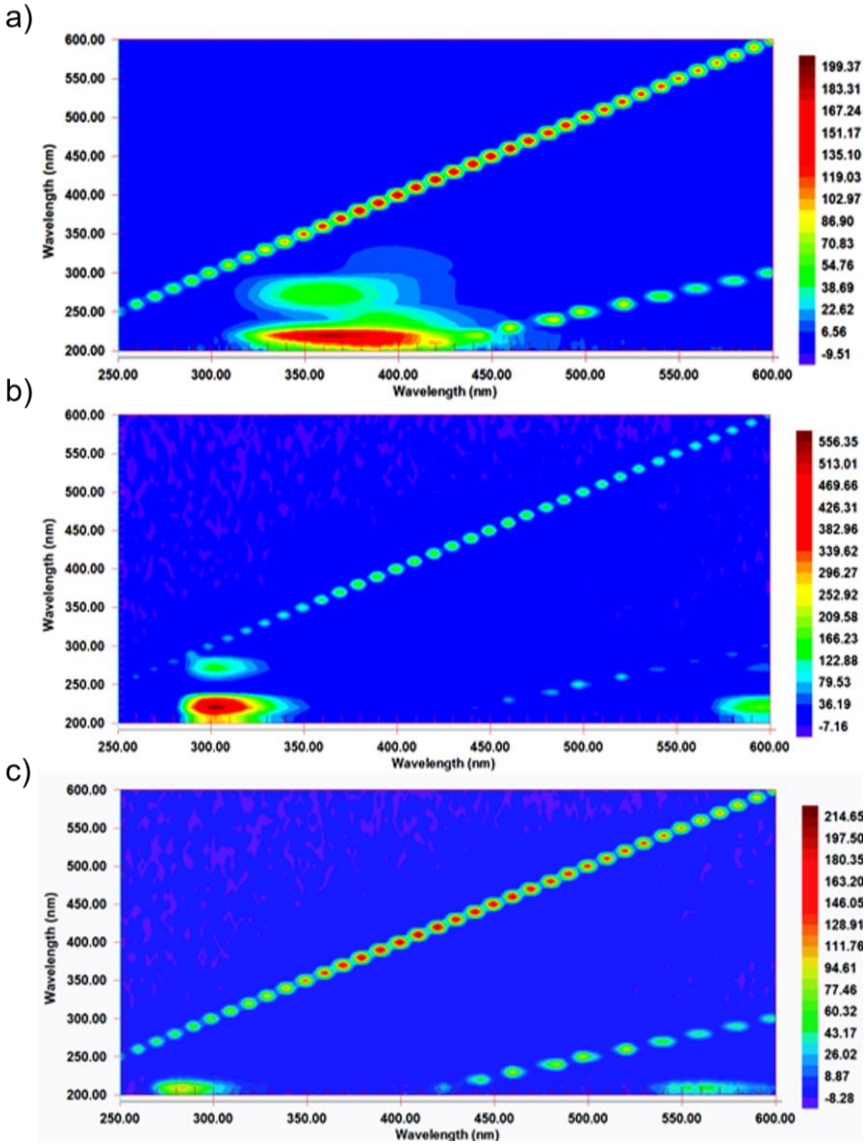

Figure 49.Excitation vs. emission wavelengths obtained by the benchtop fluorescence instrument for: a) tryptophan 1 mg·L^{-1}, b) tyrosine 10 mg·L^{-1}, and c) β-phenylalanine 10 mg·L^{-1}.

When bottles of 100 mL were employed, similar results were achieved between placing the probe on the top or at 8 cm from the bottom. The containers were topaz colour. No influence of the size of the container (up to 5 mL) was observed. Better results were obtained with low or not agitation of the sample. Fluorescent signal was unaffected by the turbidity for values below 10 UNT. To evaluate the interference of organic matter, humic acid was used, and no modification of the amino acid signal was observed since the emission occurs between 425 and 460 nm. **Table 28** shows the figures of merit of the different used instruments. Although similar detection limits can be reached by both instruments the S/N ratio provided by the optic fiber probe was lower than that provided by conventional spectrofluorometer (4.6 and 14.6 respectively). Similar LOQs were obtained by using portable instrumentation than those provided by the benchtop instrument.

Table 28. Figures of merit of the studied benchtop fluorometer and the portable optical fiber probe, including the regression line equation ($y = a + b \cdot x$), regression coefficient, LOD, and LOQ for the analysis of different amino acids.

Instrument	**Aa**	**b ± sb ($L \cdot mg^{-1}$)**	**a ± sa**	**R^2**	**LOD ($mg \cdot L^{-1}$)**	**LOQ ($mg \cdot L^{-1}$)**
Benchtop fluorimeter	T	97 ± 2	3 ± 5	0.998	0.3	0.9
	TY	92 ± 3	-2 ± 3	0.997	0.4	1
	PA	13 ± 1	3 ± 5	0.995	3	9
Portable optical fiber p**robe**	T	1517 ± 80	2 ± 5	0.998	0.4	1
	TY	1260 ± 70	3 ± 3	0.995	0.4	1
	PA	125 ± 5	-1 ± 4	0.995	3	9

Portable instrumentation has also been used to register the chemiluminescence signal emitted by luminol in presence of HClO and amine nitrogen or ammonia. It is an indirect determination of organic nitrogen compounds plus ammonia. Compared to conventional laboratory instrument, the calibration sensitivity obtained by the portable luminometer was higher, and

lower LODs can be reached (see **Table 28**). This is a sustainable and green alternative that can substitute the Kjeldahl method for a variety of samples [306]. This method can be designed for an in-situ methodology, through embedding of luminol in a TEOS-MTEOS sol gel in a measurement tub [296]. Delivering of luminol is around 90 %. The lectures were performed at 10 s. The slope values obtained for ammonium and organic amino groups were statistically similar expressed as μM^{-1} of N: $(5.5 \pm 0.5) \cdot 10^4$, the LOD was 0.8 µM, and the RSD was below 5 %. The quantification results for the portable luminometer for the NH_4^+ + DON and DON as total N is shown in **Table 27.** In the analyzed samples, none of the studied amino acids were found; therefore, not contributing to the DON.

4.1.2.3 Determination of phenylurea pesticides by portable miniaturized liquid chromatography

Two phenylurea pesticides, diuron and isoproturon, which can contribute to DON, were determined and quantified in different water samples, including river water, lagoon water, well water, and transitional water, using the portable LC and performing a previous preconcentration step based on SPE with a C18 cartridge (for more information see **section 3.3.1**).

For the optimisation of the SPE step different volumes of sample and elution solvent were passed through the cartridge. For the loading step, 25 mL of sample was selected for achieving a suitable preconcentration factor. For the elution step, various volumes of MeOH down to 100 µL were tested. Finally, The elution of the analytes was done using 3 individual portions of 100, 50, and 50 µL of MeOH, which were separately filtered and analysed by portable minLC. **Figure 50** shows the chromatograms obtained for the three separate fractions obtained from the optimized SPE for a 20 $\mu g \cdot L^{-1}$ mixture

of isoproturon and diuron. As can be seen, the second fraction had the highest analyte concentration, and therefore, it was selected for the analysis of the samples. For this fraction, the recovery obtained was (60 ± 4) %.

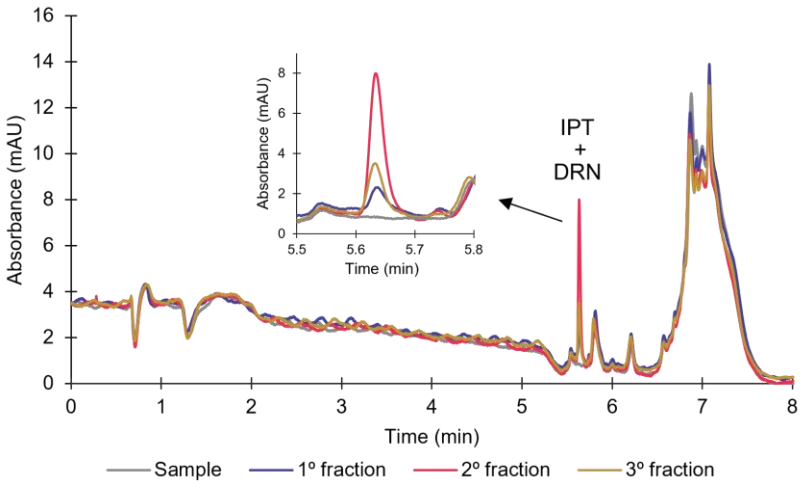

Figure 50. Chromatograms obtained for the different elution fractions for a spiked water sample with 10 µg·L^{-1} of IPT and 10 µg·L^{-1} of DRN.

The LODs for diuron and isoproturon were 0.25 µg·L^{-1} and 0.5 µg·L^{-1} respectively, both below the legal concentration limits. The pesticides were not detected in any sample, hence, not having any contribution in the DON. As an example, **Figure 51 a** shows the chromatogram obtained using the portable minLC for a fortified well water sample containing concentrations corresponding to the LODs of both pesticides. Finally, the results obtained were confirmed using UHPLC-QTOF and IT-SPME-nanoLC-DAD (**Figures 51 b** and **c** respectively)

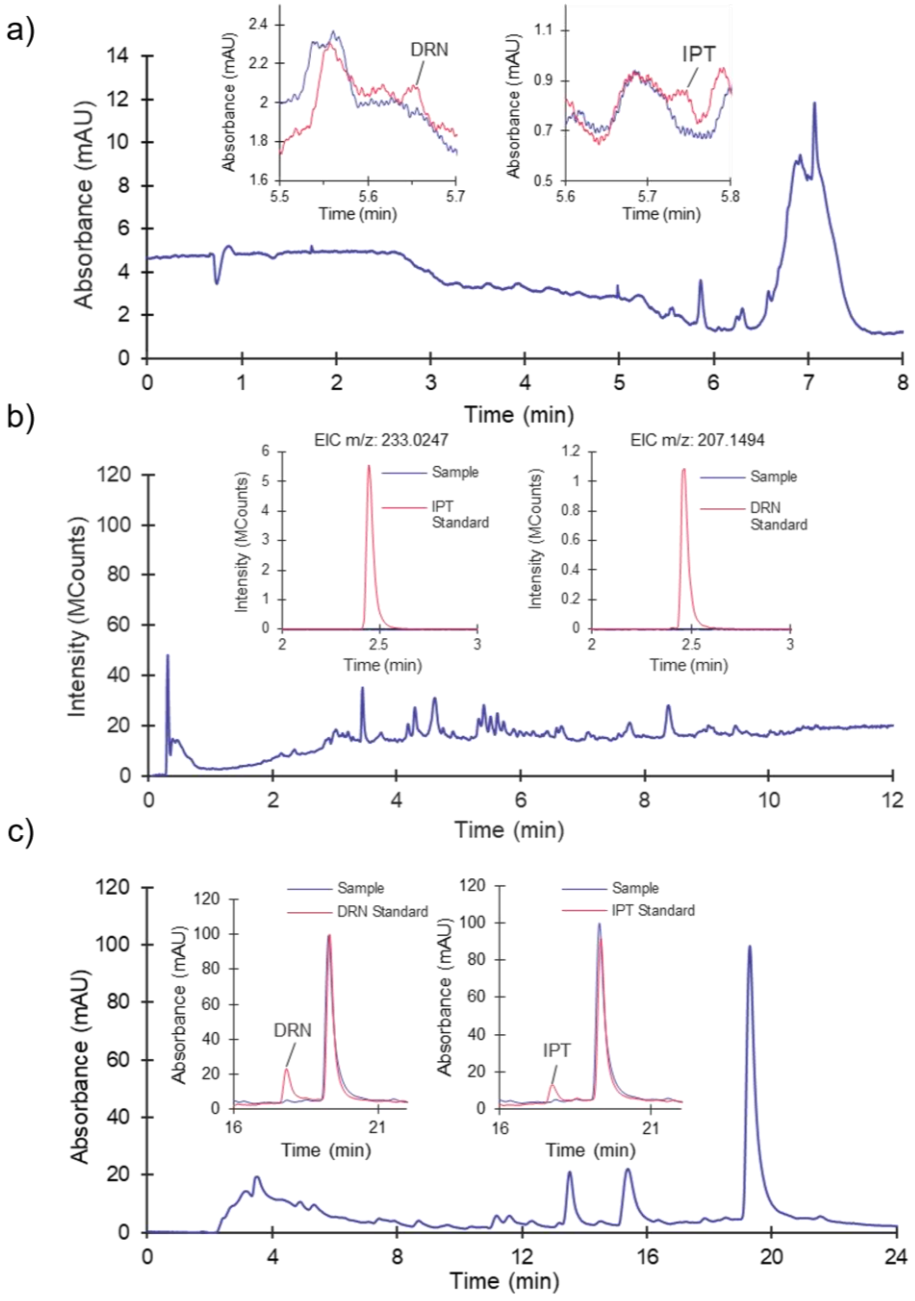

Figure 51. a) Chromatogram obtained for a well sample with and without fortification of DRN and IPT at 0.25 and 0.5 $\mu g \cdot L^{-1}$ by portable minLC. b) TIC and EIC at m/z: 233.0247 and 208.1494 for a well water sample with and without DRN and IPT fortification. (250 $\mu g \cdot L^{-1}$ for each analyte) by UHPLC-MS. c) Chromatograms obtained at 250 nm for a well water sample with and without DRN and IPT fortification (50 $\mu g \cdot L^{-1}$ of each analyte) by IT-SPME coupled on-line with nanoLC-DAD.

4.1.2.4 Conclusions

Traditionally, the determination of the different forms of dissolved nitrogen are carried out in laboratory with benchtop instrumentation; however, current demands require to develop new analysis strategies that allow in-situ analysis in real-time. In this work, the capabilities of an analyzer for the determination of nitrate based in its native absorbance were evaluated in comparison with a conventional laboratory spectrophotometer and a portable optical fiber portable spectrophotometer. Also, other N forms, including nitrites, ammonium, and amino acids were determined by the portable optical fiber probe and the benchtop spectrophotometer. Finally, a portable minLC was used for the determination of two legislated phenylurea pesticides.

The nitrate analyzer provided good sensibility and reproducibility, comparable to the obtained by the benchtop and portable spectrophotometer. Minimal influence of turbidity and humic acid was observed in the tested conditions. The quantification of real water environmental samples was suitable with similar results to those obtained by the benchtop spectrophotometer. Finally, it was demonstrated that the monitoring of nitrates in a water treatment plant was feasible, validating the results with the obtained by the portable optical fiber spectrophotometer.

On the other hand, the portable minLC was used for the determination of two regulated phenylurea pesticides, DRN and IPS, in various water sources. A minimal sample pre-treatment based on a C18 cartridge SPE was used. The results obtained were validated by means of IT-SPME-nanoLC-DAD and UHPLC-QTOF. The portable minLC demonstrated to be able to achieve the LODs required by the legislation being an adequate option for monitoring of priority nitrogen environmental pollutants.

4.2 Biological samples

4.2.1 Determination of acetaminophen in urine

Acetaminophen is a widely used over the counter medication to treat fever and mild pain. However, its easy access and lack of knowledge of its toxicological information has caused to be one of the main causes of liver injuries. The rapid diagnosis of overdose is key to avoid more severe consequences, therefore, new analytical strategies for its determination need to be developed.

In this work, IT-SPME-nanoLC-DAD was presented as a cost-effective, rapid, and sensitive technique for the analysis of APAP in urine samples. The results were compared to those provided by UHPLC-QTOF and DART-QTOF. To compare the methodologies considering greenness and sustainability, the HEXAGON tool was employed.

4.2.1.1 Optimization of chromatographic conditions and figures of merit of IT-SPME-nanoLC-DAD

A mobile phase consisting of ACN and water mixtures was used in isocratic mode. As analytical column, a RP ZORBAX 300SB-C18 (0.1 mm × 150 mm, 3.5 μm) was used. Due to the high polarity of APAP ($logK_{ow}$ = 0.46), a low proportion of ACN was required to ensure its retention in the analytical column. At the end of the chromatographic run, the percentage of ACN was increased to remove potential contaminants from the urine that could be retrained in the column. Lowering the initial percentage of ACN increased the retention, but also increased the time needed for the column to return to its initial state (re-equilibration time). As **Figure 52** shows, good results were obtained with H_2O:ACN compositions of 95:5 without prolonging the re-equilibration time in the analytical column. The flow rate of the mobile phase was

set to 0.5 μL·min^{-1} to obtain the fastest separation within the maximum pressure limits.

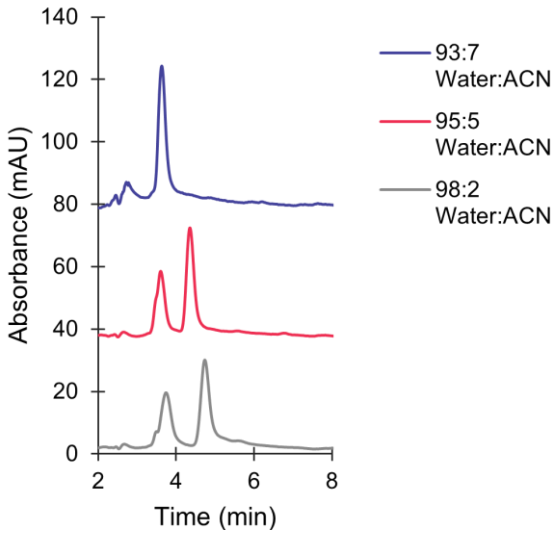

Figure 52. Chromatograms corresponding to a 200 μg·L^{-1} APAP standard solution with different initial mobile phase compositions and a re-equilibration time of 10 min.

Since the percentage of ACN was raised to 70 % for clean-up, there must be a period after each analysis to ensure that the initial composition of the mobile phase is flowing through the analytical column. The delay time (the time needed for the mobile phase to reach the head column from the mixing valve) affects directly to the re-equilibration time, as well as the nature of stationary phase, the column dimensions, and the initial and final composition of the mobile phase. The effect of re-equilibration time on the chromatographic profile was studied and optimized to obtain a suitable separation in a lesser analysis time. As can be seen in the **Figure 53**, an increase in the re-equilibration time also increases the retention of APAP getting, therefore, a better separation. A re-equilibration time of 10 min was selected since it provides a suitable separation of the analyte from the solvent front with acceptable retention time variation (RSD < 1 %) (**Figure 53**) in a short time. The total chromatographic analysis time, including the re-equilibration time was 18 min.

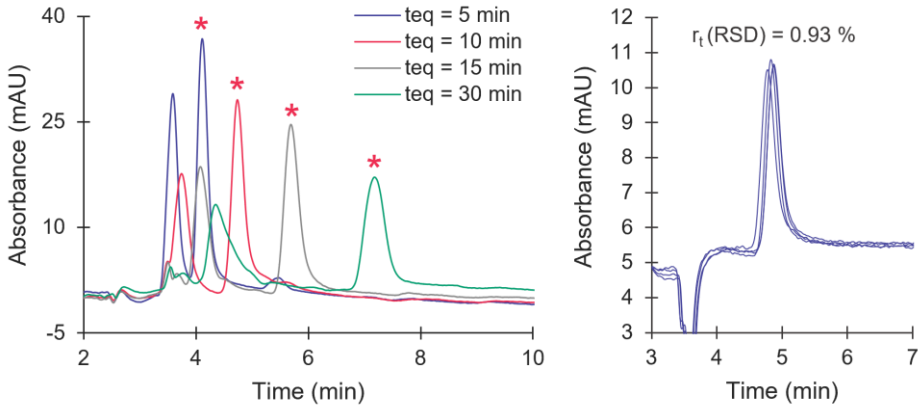

Figure 53. Effect of re-equilibration time on the chromatographic profile for a 0 h urine sample fortified with 234 µg·L^{-1} of APAP (left). Comparison of the retention time for successive injections of 32 µg·L^{-1} of APAP working at 10 min of re-equilibration time (right). APAP peak is marked with an asterisk (*) in the figure.

For the IT-SPME, a 10 cm segment of fused silica capillary with 0.075 mm of i.d. and filled with TEOS-METOS-SiO_2 NPs was used in a two-valve configuration (see **Figure 31**). The volume of sample processed through the IT-SPME was 100 µL. The IT-SPME capillary was cleaned after each analysis with ACN to avoid contaminations from run to run.

To study the potential matrix effect (ME) in samples, external and standard addition calibration were carried out. The parameters of the calibration curves are shown in **Table 29.** The ME was calculated comparing the slopes of the calibration curves in solvent and in each sample [307], as expressed in **equation 5** :

$$\%ME = \frac{Slope_{matrix}}{Slope_{solvent}} \cdot 100 \qquad (5)$$

No significant matrix effect was observed for the different urine samples (ME ranging from 83 % - 96 %), so no standard addition calibration was needed. The LOD was obtained by visual evaluation injecting decreasing concentration of solutions of APAP using the 0 h urine as matrix till the peak

signal was approximately 3 times the signal of the baseline. The obtained LOD was 0.45 $\mu g \cdot L^{-1}$ (**Figure 54**).

Table 29. Standard addition calibration curve parameters (slope (b) and its standard deviation (s_b), y-intercept (a) and its standard deviation (s_a) and coefficient of determination (R^2)) for the APAP determination by means of the IT-SPME-nanoLC-DAD. The working range is comprised between 15 to 100 $\mu g \cdot L^{-1}$ (n = 5).

Sample	b ($L \cdot mg^{-1}$)	s_b ($L \cdot mg^{-1}$)	a	s_a	R^2
Water	2.57	0.06	-10	3	0.998
0 h urine	2.10	0.04	3	2	0.9990
2 h urine	2.11	0.07	53	4	0.997
5 h urine	2.47	0.04	48	2	0.9991
6 h urine	2.18	0.06	19	2	0.9990
7 h urine	2.23	0.10	12	5	0.997

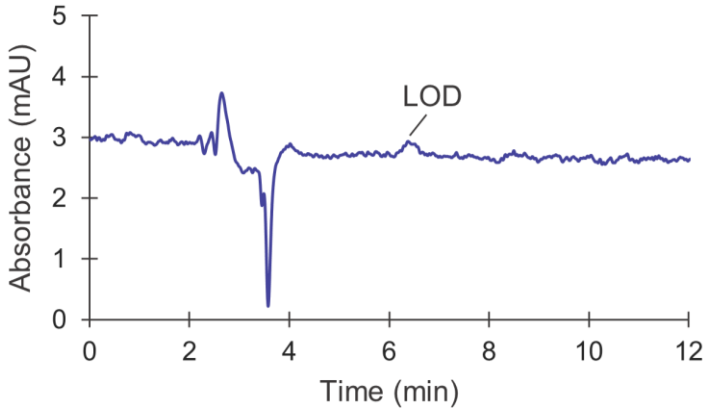

Figure 54. Chromatogram obtained for 0.47 $\mu g \cdot L^{-1}$ of APAP in 0 h urine sample.

4.2.1.2 Optimization of chromatographic conditions and figures of merit of UHPLC-ESI-QTOF

Regarding the UHPLC-ESI-QTOF, mixtures of H2O:ACN both containing 0.1 % of formic acid were used as the mobile phase. The initial mobile phase composition was 95:5 H_2O:ACN and was gradually increased up to 95% of ACN to clean the system. For detection, positive ionization mode was

selected. Different capillary voltages were tested from 1000 to 3500 v, obtaining the highest sensitivity for 3500 v.

The calibration curve parameters for the UHPLC-ESI-QTOF are shown in the **Table 30.** As can be seen, there was no significant matrix effect (from 87 to 109 % for 2 h and 7 h urine samples) and hence the quantification can be done by external calibration. The LOD was obtained by visual evaluation in the same way that for the IT-SPME-nanoLC-DAD. The LOD for this method was 1.1 $\mu g \cdot L^{-1}$.

Table 30. Standard addition calibration curve parameters (slope (b) and its standard deviation (s_b), y-intercept (a) and its standard deviation (s_a) and coefficient of determination (R^2)) for the APAP determination by means of the UHPLC-ESI-QTOF. The working range is comprised between 8 to 64 $\mu g \cdot L^{-1}$ (n = 6).

Sample	**b ($L \cdot mg^{-1}$)**	**s_b ($L \cdot mg^{-1}$)**	**a**	**s_a**	**R^2**
Water	$4.21 \cdot 10^3$	$0.09 \cdot 10^3$	$0.017 \cdot 10^5$	$0.04 \cdot 10^5$	0.999
0 h urine	$4.06 \cdot 10^3$	$0.16 \cdot 10^3$	$0.00 \cdot 10^5$	$0.05 \cdot 10^5$	0.995
2 h urine	$3.9 \cdot 10^3$	$0.3 \cdot 10^3$	$1.89 \cdot 10^5$	$0.09 \cdot 10^5$	0.990
5 h urine	$3.67 \cdot 10^3$	$0.18 \cdot 10^3$	$1.95 \cdot 10^5$	$0.06 \cdot 10^5$	0.993
6 h urine	$4.12 \cdot 10^3$	$0.12 \cdot 10^3$	$0.12 \cdot 10^5$	$0.04 \cdot 10^5$	0.998
7 h urine	$4.57 \cdot 10^3$	$0.10 \cdot 10^3$	$0.182 \cdot 10^5$	$0.018 \cdot 10^5$	0.993

4.2.1.3 Optimization of method conditions and figures of merit of DART-QTOF

The DART-QTOF method conditions were also optimized. Different gas temperatures were tested from 150 to 450 °C, obtaining best ionization of APAP at 350 °C. Different sampling velocities from 0.2 to 0.5 $mm \cdot min^{-1}$ were studied obtaining suitable results with minimum analysis time for 0.5 $mm \cdot min^{-1}$.

The **Figure 55** shows the extracted ion chromatogram for APAP (152.0693 m/z) for the urine just before APAP dosage and after 2, 6 and 7 hours with and without APAP fortification. Despite the concentration of APAP

added is the same, it can be seen how the urine sample exhibits different influence on the analyte signal since the increment in the areas for 6 and 7 hours are higher than the ones for 0 and 2 hours, thus matrix effect must be considered for quantifying. **Table 31** shows the analytical parameters of the standard addition calibration. LODs were calculated as $3 \cdot s_{yx} \cdot b^{-1}$ showing similar values for all samples with a mean value of 2.8 mg·L^{-1}.

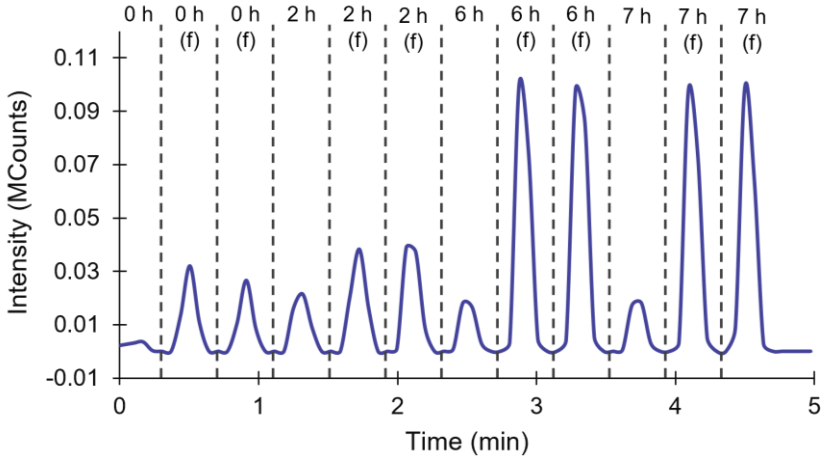

Figure 55. Extracted ion chromatogram (152.0693 m/z) for urine samples just before (0 h) and 2, 6 and 7 hours after APAP intake with (f) and without 18·mg·L^{-1} APAP fortification.

Table 31. Standard addition calibration curve parameters (slope (b) and its standard deviation (s_b), y-intercept (a) and its standard deviation (s_a) and coefficient of determination (R^2)) for the APAP determination by means of the DART-QTOF. The working range is comprised between 10 to 35 mg·L^{-1} (n = 5).

Sample	b (L·mg^{-1})	s_b (L·mg^{-1})	a	s_a	R^2
0 h urine	3.6 · 104	0.08 · 104	-1.4 · 104	1.6 · 104	0.990
2 h urine	2.1 · 104	0.13 · 104	5.6 · 105	3 · 104	0.992
5 h urine	3.96 · 104	0.19 · 104	7.8 · 105	0.3 · 104	0.990
6 h urine	8.37 · 104	0.10 · 104	13 · 104	13 · 104	0.9998
7 h urine	8.74 · 104	0.15 · 104	8 · 104	3 · 104	0.998

4.2.1.4 Analysis of urine samples

Prior to the analysis of the urine samples, a SPE to eliminate possible interferences was carried out (see **section 3.3.1**). The recovery of the SPE was calculated by adding a known concentration of APAP to the 0 h urine before the extraction and then obtaining the concentration in the methanolic solution by interpolation in the regression curve. The recovery obtained was 71 ± 4 % which is an acceptable value for this kind of extraction. It was verified that there was not major analyte loss during the washing step.

The five samples of urine at different times (0, 2, 5, 6, and 7 h) were analysed by IT-SPME-nanoLC-DAD and APAP was detected in all of them but the 0 hours (just before administration of APAP) like it was expected (**Figure 56**). Acetaminophen glucoronide (APAP-glu), the major APAP metabolite, was also found in samples, however, due to its high polarity, it is not enough retained in the column coeluting with the solvent peak and, hence, making quantification not possible. It is noteworthy that the retention of APAP-glu could be increase working with higher re-equilibration times, allowing thus its quantification.

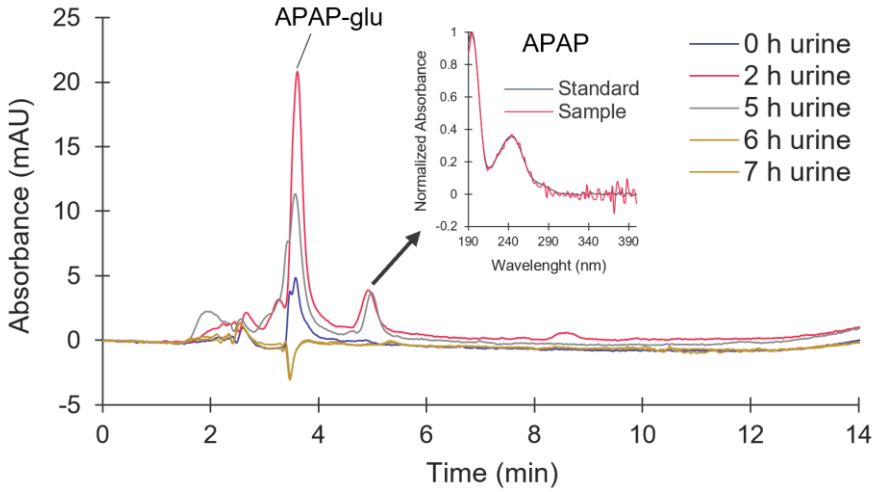

Figure 56. Urine sample chromatograms for 0, 2, 5, 6 and 7 h after 1 g of APAP intake. The normalized UV spectra for APAP chromatographic peak in sample and standard is shown.

The results obtained by the IT-SPME-nanoLC-DAD were compared to those obtained by UHPLC-ESI-QTOF and DART-QTOF to validate the methodology. Both techniques were able to determine APAP in the urine samples, however, only the UHPLC-ESI-QTOF was able to detect APAP-glu (m/z: 328.1028). As an example of chromatogram, **Figure 57** shows the results for urine 2 h after the intake of APAP. The DART registers for the analysis of the urine samples are shown in **Figure 58**.

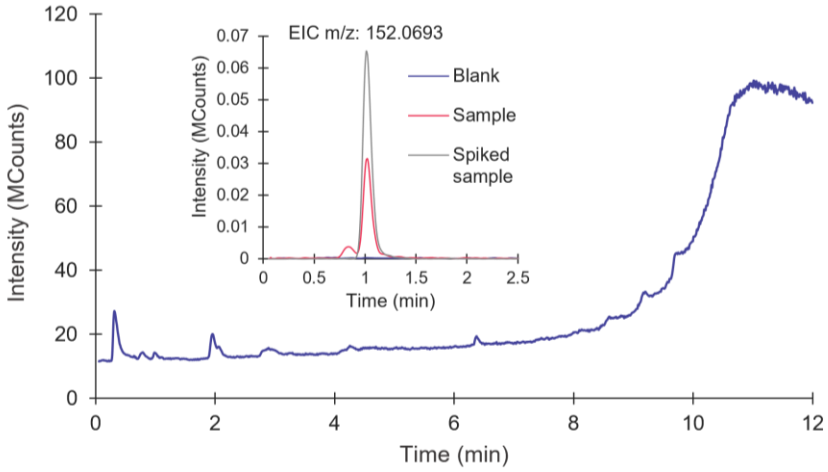

Figure 57. TIC for 2 h urine sample and its EIC compared to blank and APAP spiked sample at m/z: 152.0693.

The **Table 32** shows the quantification results for the urine samples by the proposed methodologies. As expected, for the urine at 0 h, APAP was not detected. After the first 2 hours maximum concentration was obtained, decreasing slightly for 5 h. For the 6 and 7 h almost no APAP was found in samples. The observed trend of excreted APAP was similar for all three methods (see **Figure 59**), only having a slightly concentration variation for the 5 h urine sample. These results are in line with those found in the literature, where for healthy subjects most of the APAP is excreted in the first 9 hours [308]. It should be noted that most of the APAP is metabolized by hepatic route and excreted in the urine as APAP-glucuronide (50 %) and APAP-sulfate (30 %) [309], while free APAP is minority [310].

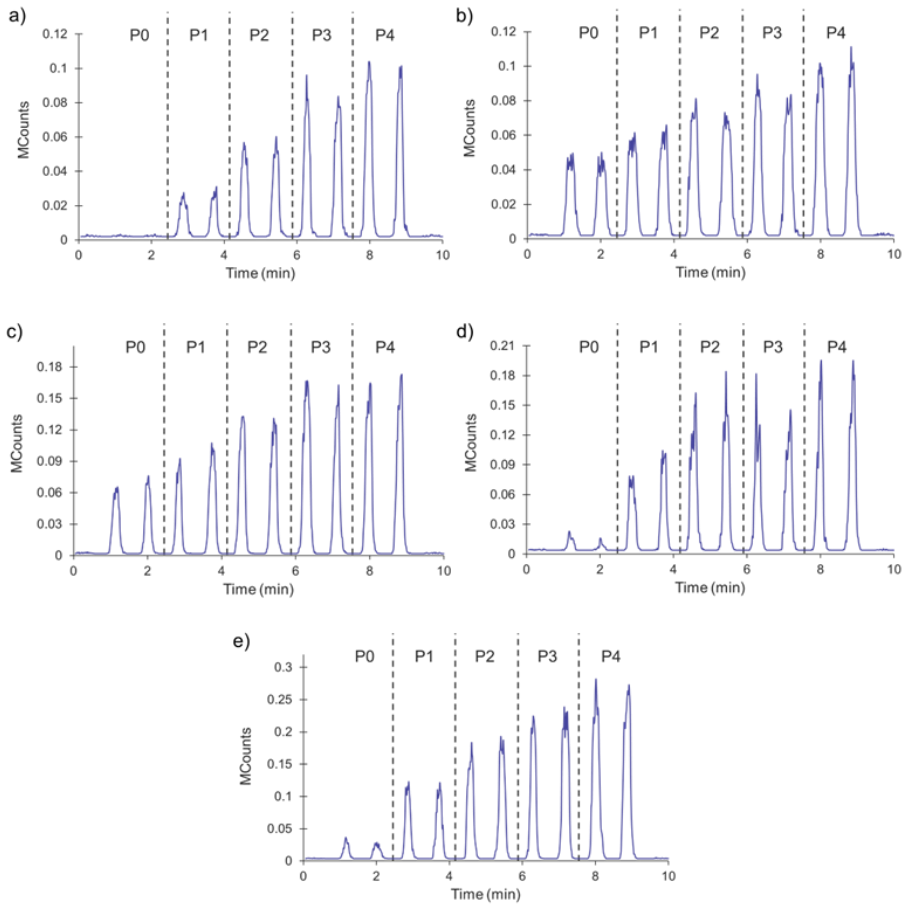

Figure 58. DART records for standar additions of 0 (P0), 9 (P1), 18 (P2), 26 (P3) and 32 (P4) mg·L^{-1} of APAP on 0 h (a), 2 h (b), 5 h (c), 6 h (d) and 7 h (e) urine samples. Each solution is measured twice.

Table 32. Quantification results of urine samples using the IT-SPME-nLC-DAD, UHPLC-ESI-MS, and DART-MS (n = 3).

Hours after APAP intake	**IT-SPME-nLC-DAD**		**UHPLC-ESI-QTOF**		**DART-QTOF**	
	APAP (mg·L^{-1})	RSD (%)	APAP (mg·L^{-1})	RSD (%)	APAP (mg·L^{-1})	RSD (%)
0 h	< LOD	-	< LOD	-	< LOD	-
2 h	217	4.2	190	5.2	205	13.1
5 h	196	2.8	200	5.4	180	7.2
6 h	16.09	0.90	11.1	4.3	8.7	2.1
7 h	16.51	0.34	15.4	5.4	7.2	4.0

To the date, there is no study that indicates an approximate concentration of APAP in urine from which it can be considered overdose. It should be noted that the concentration of APAP in urine is approximately 10 times the concentration in serum [311], and taking in to account the Rumack-Matthew nomogram [312], it can be approximated that the range of concentration for a possible case of hepatoxicity in urine is between 2000 to 50 $mg \cdot L^{-1}$ in the 0 h to 24 h respectively. However, this cannot be directly extrapolated to overdose cases where the normal metabolism of APAP is altered, and hence it is hard to state an absolute value above which can indicate a case of overdose. Despite that, urinary APAP determination by IT-SPME-nanoLC might be used to rapidly discard a negative result of overdose avoiding the use of serum test

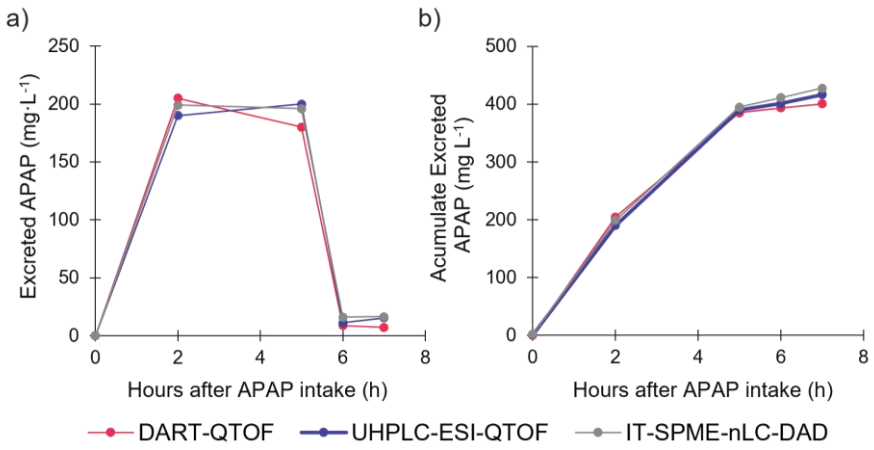

Figure 59. a) Found APAP concentration and b) accumulated concentration for the samples at different times after dosage.

4.2.1.5 Evaluation tool

The HEXAGON tool was used to objectively compare the different method features (see **Figures 60** and **61**). As can be observed from the previous results, DART-QTOF provided the lowest LODs, capable of detecting APAP at concentrations of $mg \cdot L^{-1}$. In contrast, the LODs obtained by IT-

SPME-nanoLC-DAD and UHPLC-ESI-QTOF were several orders of magnitude lower (low $\mu g \cdot L^{-1}$), implying the possibility of diluting the sample to mitigate potential column fouling, matrix effects, and ion suppression in the ESI. The repeatability for all three techniques was acceptable with RSDs below 10 %. Regarding the analysis time, DART is the fastest technique being able to analyse up to 12 samples in less than 10 minutes. Even when only one sample is determined at once, the analysis time is below the other techniques.

The environmental perspective of the methods was evaluated from the waste generated and the carbon footprint. The amount of organic solvent used by the UHPLC-ESI-QTOF (approximately 100 mL per working day) were notably higher than the used by the IT-SPME-nanoLC-DAD and the DART-QTOF which produces negligible or no waste respectively. Furthermore, the high electricity consumption of MS detectors significantly contributes to a larger carbon footprint associated with the UHPLC-ESI-QTOF and DART-QTOF techniques, as opposed to the IT-SPME-nanoLC-DAD. The minimal waste generation and low carbon footprint make IT-SPME-nanoLC-DAD a superior choice from the perspective of green analytical chemistry.

Another key aspect to consider is the monthly economic cost, which includes the instrument price (amortized over 10 years), necessary reagents and materials, electricity cost, and specialized analysts. In this regard, the approximate cost for IT-SPME-nanoLC-DAD is €40,000 per year, which is half the cost compared to the other two methods.

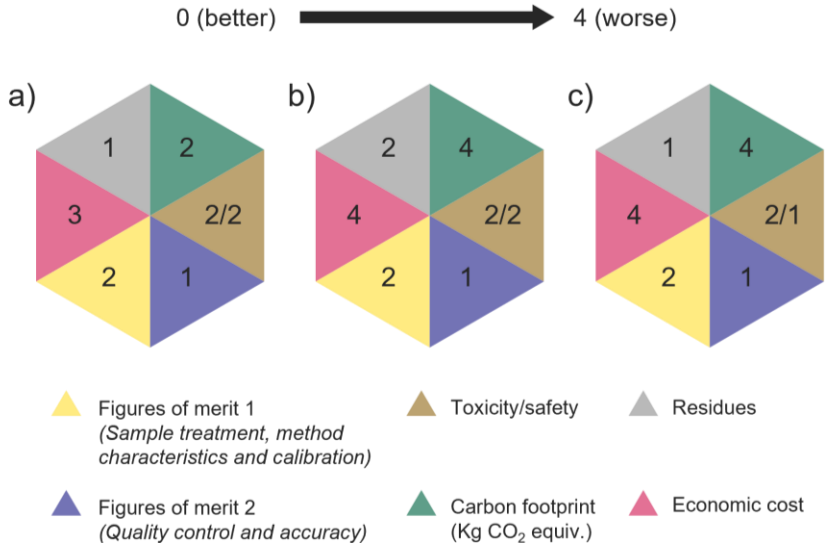

Figure 60. HEXAGON tool for a) IT-SPME-nanoLC-DAD, b) UHPLC-ESI-QTOF, and c) DART-QTOF.

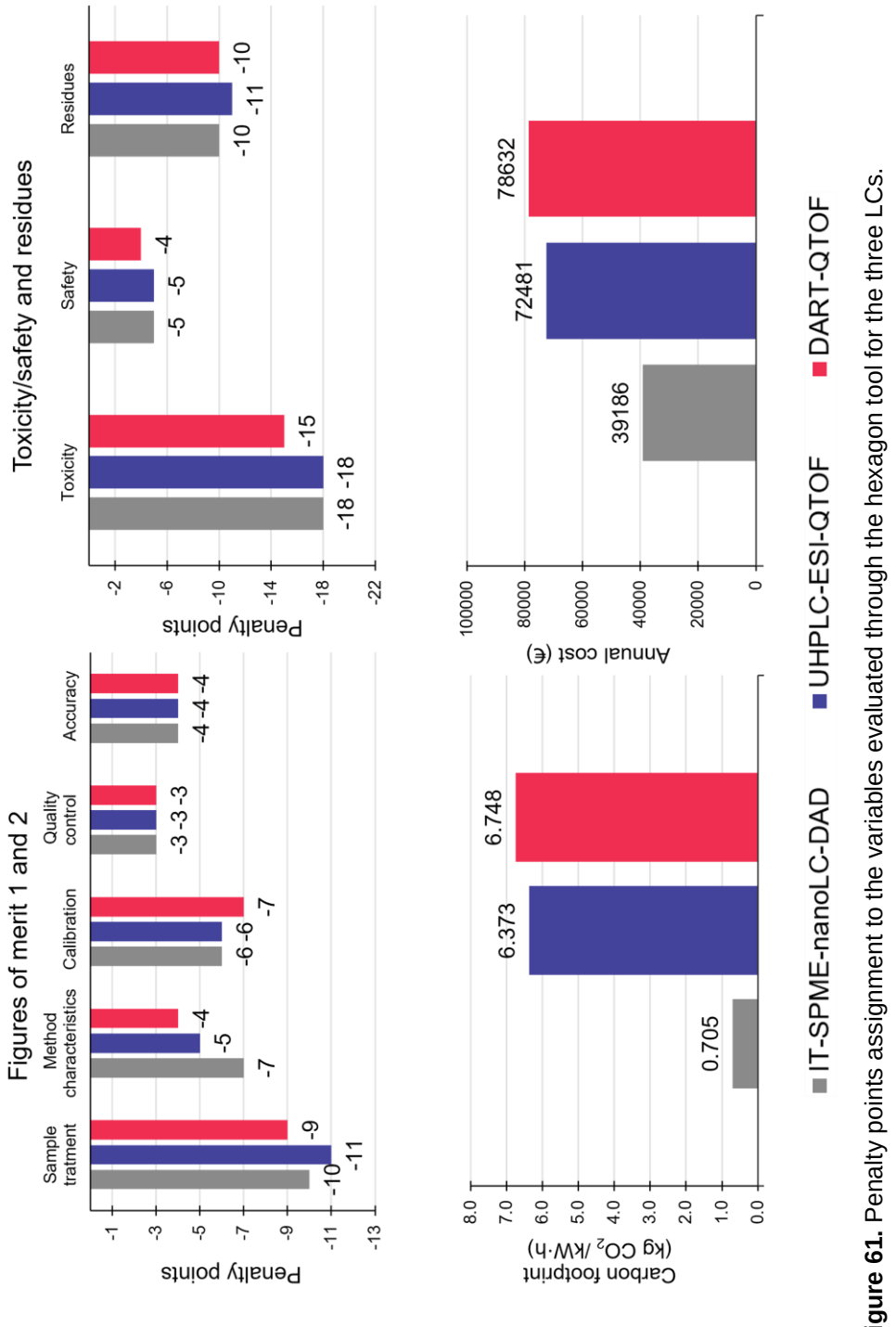

Figure 61. Penalty points assignment to the variables evaluated through the hexagon tool for the three LCs.

4.2.1.6 Conclusions

APAP overdose is one of the main causes of induced injury. The early poisoning diagnose is the key for successful treatment preventing a possible hepatoxicity. In this regard, new rapid, reliable, and cost-effective analysis strategies are required. In this work, IT-SPME-nanoLC-DAD was used for this purpose and the results were compared to those obtained by UHPLC-ESI-QTOF and DART-QTOF. The HEXAGON tool was used for the objective method comparison.

The IT-SPME-nanoLC-DAD allowed the determination of APAP in different urine samples, including the sample pretreatment, in less than 25 min. The high sensitivity offered by this technique allowed to dilute the sample avoiding potential matrix effect and impurities which could affect the analytical column. Similar results were obtained for the UHPLC-ESI-QTOF, at the cost of increasing the residue generated, solvent usage, carbon footprint, and price. The main advantage of the DART-QTOF was its real-time feedback and rapidity, however, it provided lower sensitivity, reproducibility at a higher economic cost and carbon footprint The HEXAGON tool highlighted the IT-SPME-nanoLC-DAD in terms of sustainability, greenness and economic cost.

4.3 Nanoparticles samples

4.3.1 IT-SPME-minLC-DAD for the assessment of MNPs dispersions and plasmonic assays

Over the course of the thesis, the IT-SPME-nanoLC-DAD was used to assess AgNPs and AuNPs based on its chromatographic profile. The results obtained from the NMNPs evaluation were used to select the more suitable NPs dispersions for aggregation based plasmonic assays. Acid and spermine induced aggregation were studied on commercial capped (citrate

and phosphate) Au and AgNPs and lab synthetized naked AuNPs respectively.

4.3.1.1 Characterization of MNPs dispersions by IT-SPME-minLC-DAD

The IT-SPME which influences the chromatographic profile was studied by coupling it on-line with capLC-DAD. **Figure 62** shows the chromatogram for 1:8 diluted AgNPs of 20 nm core and capped with citrate. The first chromatographic peak (t_r = 2.8 min) corresponds with the polarized group of NPs while the second chromatographic peak (t_r = 4.5 min) corresponds to the non-polarized NPs and require higher volumes of mobile phase to leave the IT-SPME capillary. These results are in accordance with the separation mechanism studied by Gonzalez-Fuenzalida (2016) [235]. When performing direct injection by means of a conventional stainless-steel loop instead of IT-SPME capillary only one population is observed by capLC. The obtained signal in this case is similar than the obtained in the literature [235]. The weaker interactions of the polarized population with the film phase in the IT-SPME makes them elute first. The same phenomenon is observed, but in opposite manner, for the non-polarized population, which elutes later due to its stronger interactions with the IT-SPME phase.

The chromatographic profiles of commercial citrate capped NPs with different sizes obtained by IT-SPME-capLC-DAD are depicted in **Figure 65 a**. MinLC enhances the sensitivity and resolution due to the lower sample dilution and diffusion effects in comparison with conventional LC. Moreover, the IT-SPME allows to detect differences in the NPs distribution (polarized and non-polarized) in the dispersion. The different interactions and elution times for both populations can be explained based on size exclusion and hydrophobic effects. The group of NPs with lower retention exhibited minimal interaction with the IT-SPME extractive phase, thus suggesting that the separation mechanism was primarily attributed to size exclusion interactions

within the analytical column [235]. On the other hand, the second peak is characterized by stronger interactions with the IT-SPME extractive phase, and the separation can be explained by the hydrophobic effect. In the light of these results, IT-SPME-minLC-DAD demonstrated the ability to differentiate NMNPs bulk dispersions.

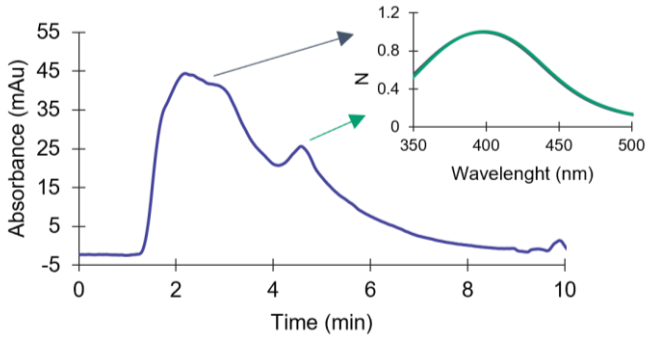

Figure 62. Chromatogram obtained by IT-SPME-capLC-DAD for 20 nm citrate capped AgNPs diluted 1:8 (inset: normalized (N) UV-vis spectra obtained for each chromatographic peak).

4.3.1.2 Study of the MNPs degradation overtime by IT-SPME-minLC-DAD

The study of the degradation over time of the AgNPs and AuNPs was carried out using 20 nm core of citrate capped NPs, diluting the stock dispersions with ultrapure water, and obtaining the chromatogram immediately after preparing the dilution (t_0), after 1 h, and after 24 h. In the case of the AgNPs, the chromatographic profile was maintained for the first hour, however, a significant decrease of the SPR signal is observed after 24 h as **Figure 63** illustrates. On the other hand, as can be seen in the **Figure 64**, the chromatographic profile for the AuNPs dilutions is predominantly maintained with time, indicating that the citrate capped AuNPs will remain relatively unchanged throughout the experimental duration.

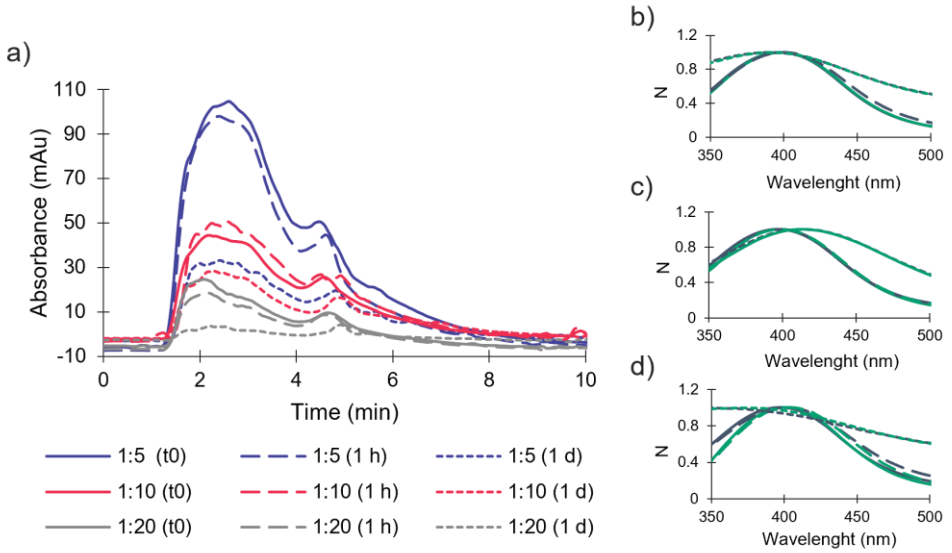

Figure 63. a) Degradation with time for different dilutions of 20 nm citrate capped AgNPs. The normalized SPR for the two chromatographic peaks at t_0 (continuous line) and after 1 h and 1 d (dotted line) for 1:5, 1:10 and 1:20 dilutions are shown in figures (b), (c), and (d) respectively

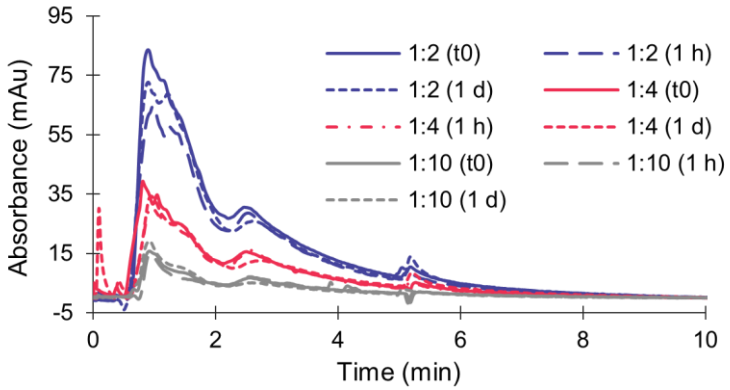

Figure 64. Degradation with time for different dilutions of 20 nm citrate capped AuNPs.

4.3.1.3 MNPs assessment and plasmonic assays monitored by IT-SPME-minLC-DAD

Acetic acid (HAc) was selected as analyte to study the aggregation profiles of 20 nm size NPs in acidic media. **Figure 65 b – e** shows the UV-

vis spectra over time for different commercial NMNPs. For citrate capping NPs, the AuNPs provide lower sensitivity to acetic acid induced aggregation than AgNPs, which agglomerate quickly with low acid concentrations. Also, when AgNPs and AuNPs where mixed together the response was additive (see **Figure 65 e**). It is worth noting that the grade of aggregation is highly affected by the nature of the capping as **Figures 65 c** and **d** demonstrate.

The acid aggregation was also studied by IT-SPME-nanoLC-DAD. Commercial citrate 20 nm AgNPs and AuNPs were assayed. The **Figure 66** show the acid aggregation chromatographic profiles for citrate capped AuNPs and AgNPs. As discussed before, faster kinetic process was observed for citrate capped AgNPs 20 nm than for AuNPs 20 nm. In comparison with AuNPs, the AgNPs are more sensitive to the acid aggregation being completely aggregated with acetic acid concentrations of 0.2 % (v/v) (**Figure 66 b** and **d**). **Figures 66 d** and **67** show the UV-vis spectra of AuNPs 20 nm with citrate and phosphate capping respectively and its aggregation in acid media. Spectra differences can be observed between both, indicating the influence of the NPs capping on the SPR band.

An intermediate sensitivity is obtained for mixtures of AgNPs and AuNPs using HAc concentrations of 0.67 % as **68** demonstrates. The chromatograms were obtained at 400 nm and 530 nm corresponding with the SPR bands of AgNPs and AuNPs respectively. From these studies can be derived that the aggregation assay can be optimized in function of the need concentration of acetic acid to test.

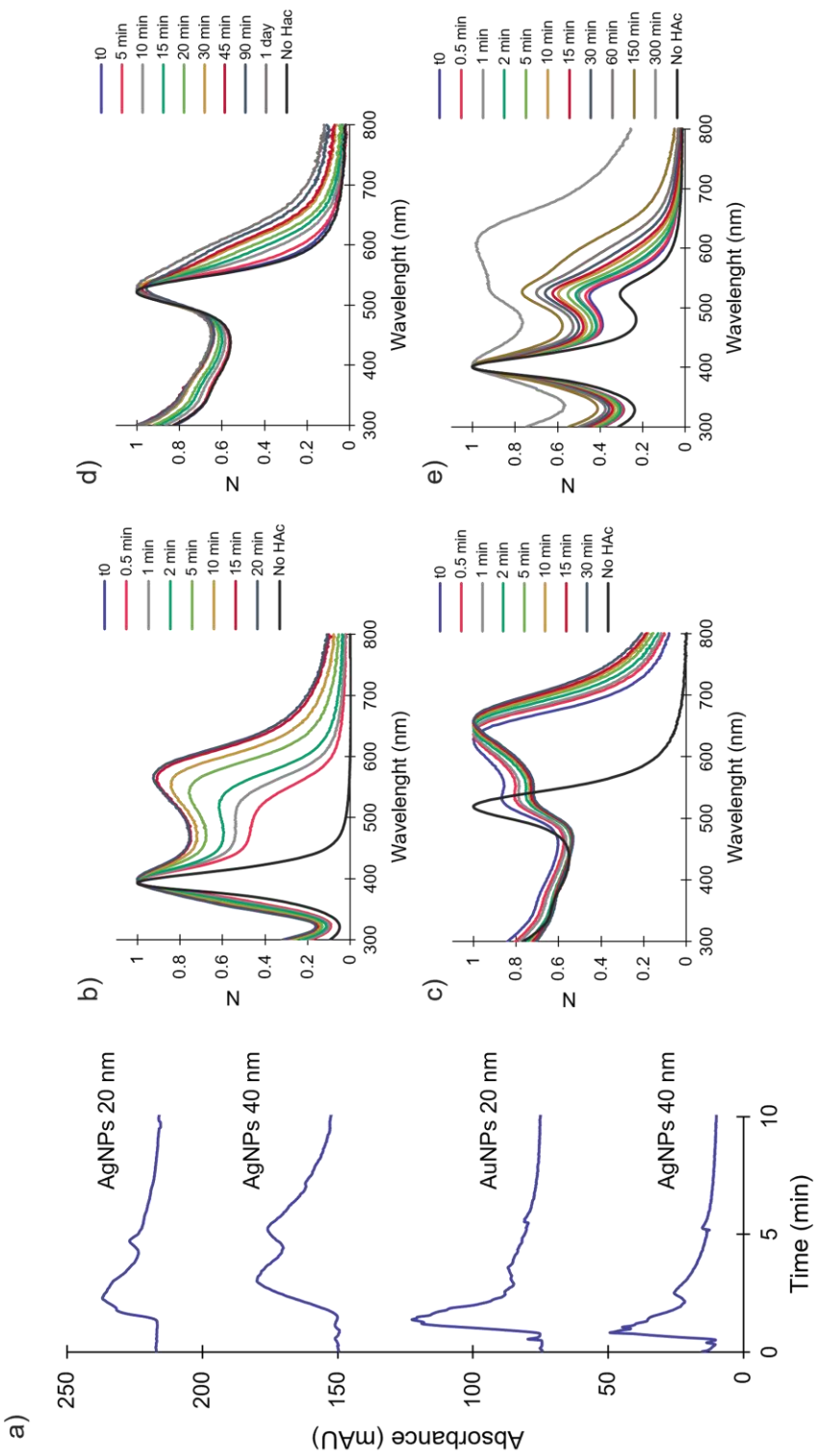

Figure 65. a) Chromatographic profile obtained by IT-SPME-capLC for commercial citrate capped AgNPs with different core sizes and acetic acid induced aggregation profiles as function of time for b) citrate capped AgNPs 20 nm diluted 1:2 in HAc 0.2 % (v/v), c) citrate capped AuNPs 20 nm diluted 1:4 in HAc 10 % (v/v), d) phosphate capped AuNPs 20 nm diluted 1:4 in 0.2 HAc (v/v), and e) a mixture of citrate capped AuNPs and AgNPs 20 nm diluted 1:4 in HAc 0.7 % (v/v) obtained by UV-vis spectroscopy .

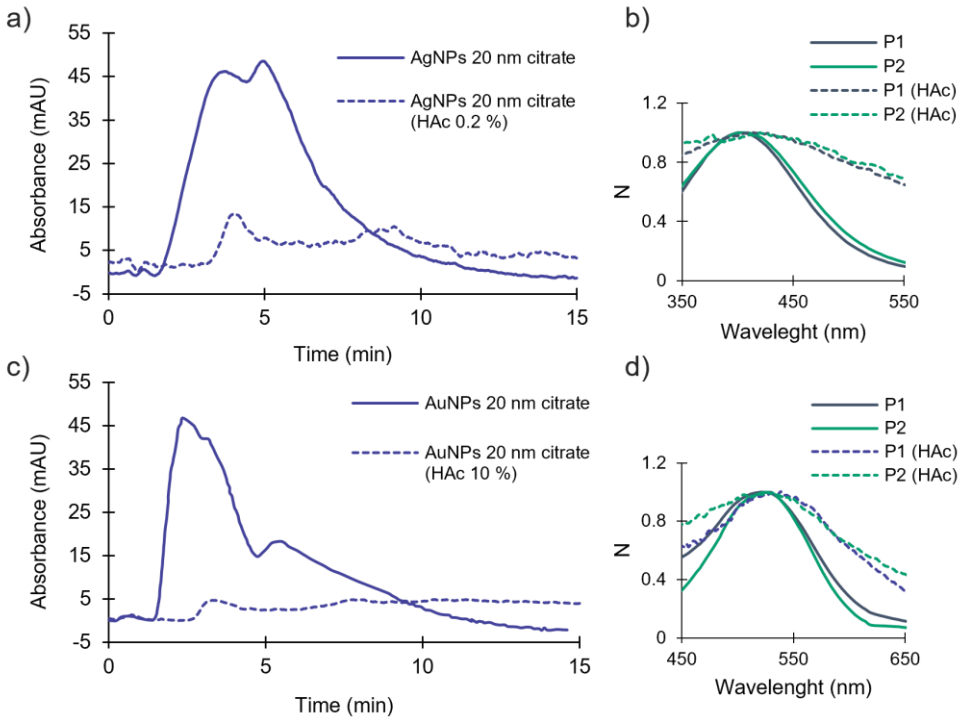

Figure 66. Chromatographic aggregation profiles obtained by IT-SPME-nanoLC-DAD for AgNPs 20 nm core with citrate capping and HAc concentration of 0.2 % (v/v) (a) and its UV-vis spectra for peak 1 (t_r = 3.6 min) and peak 2 (t_r = 5.0 min) (b), and for AuNPs 20 nm core with citrate capping and HAc concentration of 10 % (v/v) (c) and its UV-vis spectra for peak 1 (t_r = 2.7 min) and peak 2 (5.0 min) (d).

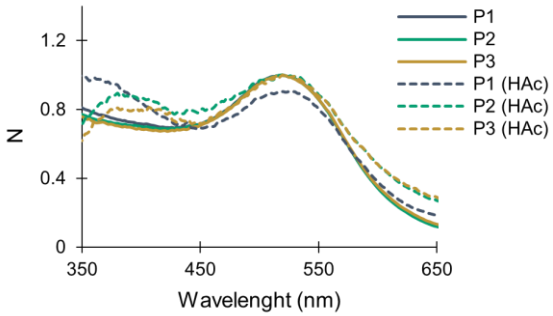

Figure 67. UV-vis spectra for AuNPs 20 nm with phosphate capping and HAc concentration of 10 % (v/v). P1, P2, and P3 corresponds to the chromatographic peaks at 3.8 min, 5.0 min, and 7.9 min.

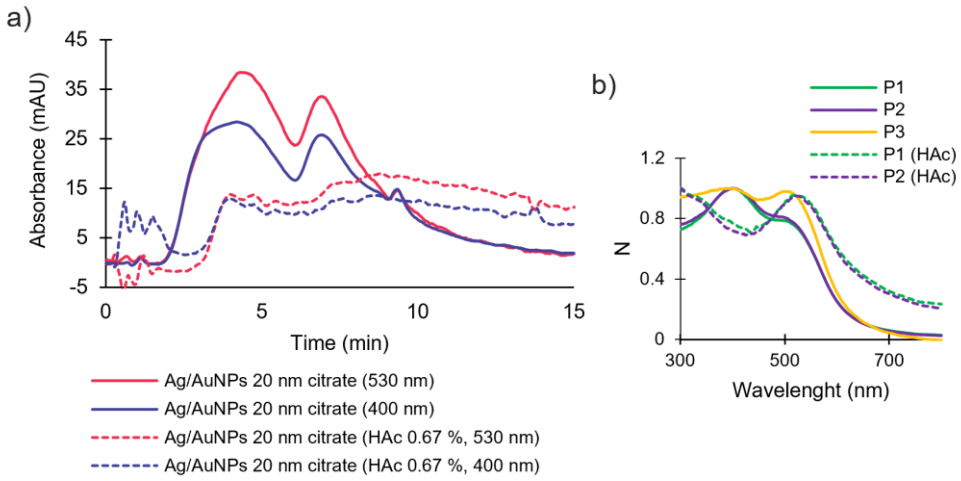

Figure 68. Chromatographic aggregation profiles obtained by IT-SPME-nanoLC-DAD for a mixture of AgNPs and AuNPs 20 nm core with citrate capping and HAc concentration of 0.67 % (v/v) (a) and its UV-vis spectra for peak 1 (t_r = 4.3 min), peak 2 (t_r = 7.0 min), and peak 3 (t_r = 9.3 min) (b). The chromatograms were registered at both SPR band maximum wavelengths, 400 nm, and 530 nm respectively for AgNPs and AuNPs.

Spermine induced aggregation was studied with commercial NMNPs, however, no aggregation was observed at the concentration levels assayed. The aggregation of NPs is largely influenced by the surface accessibility, obtaining higher sensitivities for more naked NPs . Based on this, spermine and acetic acid induced aggregation were studied using naked lab synthetized naked AuNPs. Six batches of naked AuNPs were diluted 1:1 with ultrapure water and analyzed by IT-SPME-capLC-DAD. The obtained chromatographic profiles exhibited significant differences among them, allowing for their classification into two distinct groups: (1) the AuNPs I which possess a similar distribution of polarized and non-polarized populations and (2) AuNPs II in which the polarized population prevails over non-polarized (**see Figures 69 a** and **b** respectively). In this regard, IT-SPME-capLC-DAD proved to be effective to distinguish different batches. In the other hand, the UV-vis spectra for all six batches did not show significant differences being not possible to discriminate them.

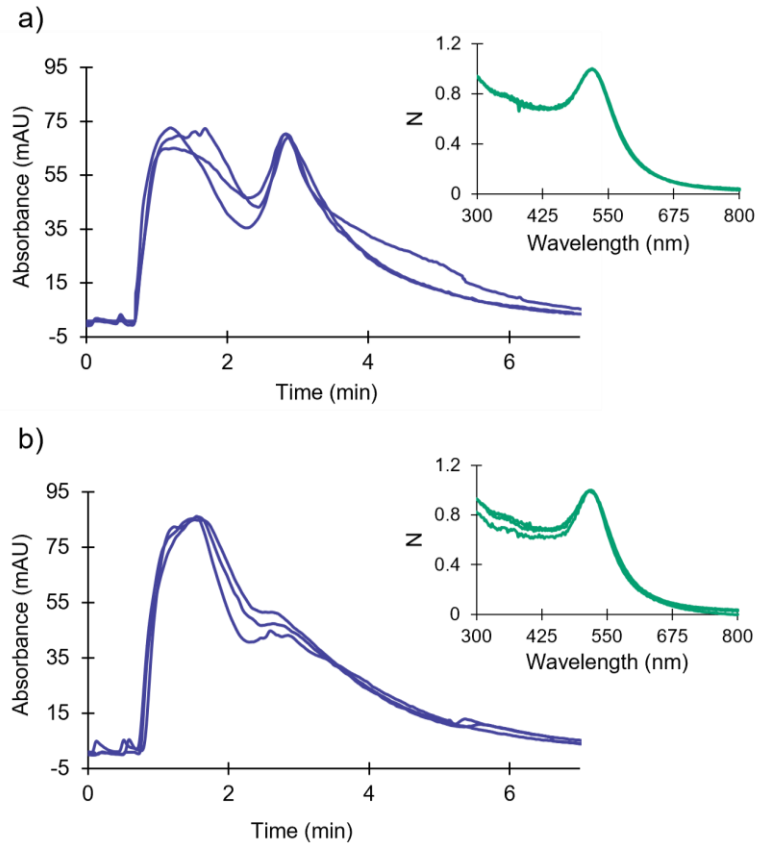

Figure 69. Chromatographic profiles obtained for the different batches of naked AuNPs corresponding to AuNPs I (a) and AuNPs II (b)

The chromatograms obtained for the acetic acid and spermine induced aggregation using naked AuNPs by IT-SPME-capLC-DAD are shown in the **Figures 70** and **71** for the groups I and II respectively. The assays are based on the absence of a competitive organic capping on the naked AuNPs together with the affinity of the amine groups of spermine with the NPs. The presence of HAc or spermine in the AuNPs dispersion resulted in batho-chromic shift of the SPR band evidenced by a colour change from red to blue which is indicative of an aggregation process.

For the AuNPs I the successive analyte additions (41, 66, and 82 $\mu g \cdot L^{-1}$) resulted in a reduction in the chromatographic peak areas. The UV-vis spectra show the SPR shift to higher wavelengths demonstrating that the

reduction of the peak signal is related to an aggregation phenomenon. Also, the relative peak area between the first and second chromatographic peak varies with the addition of analyte. As can be seen in **Figure 70 a**, the peak corresponding to the polarized group of AuNPs (t_r = 1.2 min) shows lower sensitivity than the second one to the spermine induced aggregation, being only appreciable the area reduction at spermine concentrations over 66 $\mu g \cdot L^{-1}$. For non-polarized group of NPs (t_r = 3.0 min) a correlation can be observed between the spermine concentration and the peak area with a slope of (7600 ± 700)$L \cdot \mu g^{-1}$, a intercept of 670 ± 54, and a coefficient of determination of 0.99. In the case of the HAc aggregation, bot chromatographic peaks decrease proportionally to the HAc successive additions (0.35, 0.50, and 0.60 mM), thus the relative area between both remains constant (**Figure 70 b**).

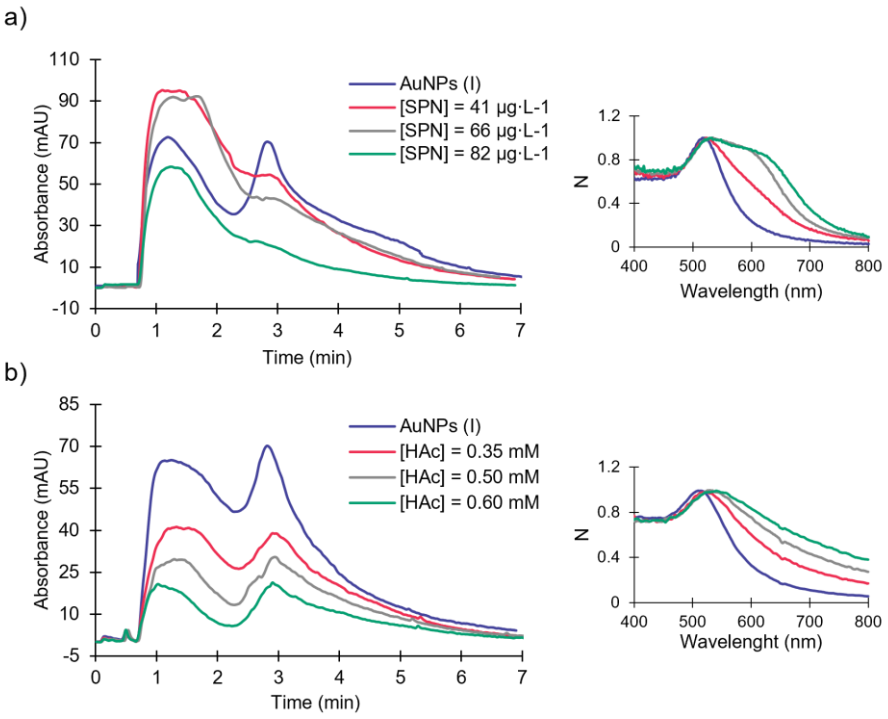

Figure 70. Chromatograms obtained for naked AuNPs I in function of: a) the added spermine and b) the added acetic acid. Insents: variations of the LSPR of the second chromatographic peak (t_r = 3.0 min).

On the other hand, for the AuNPs II the addition of low spermine concentration (41 $\mu g \cdot L^{-1}$) produced nearly total NPs aggregation limiting its capacity to discern different spermine concentration levels and shorten its working interval (see **Figure 71 a**). The acid aggregation was observed for the different concentration levels of HAc (0.35, 0.40, and 0.50 mM) as **Figure 71 b** shows.

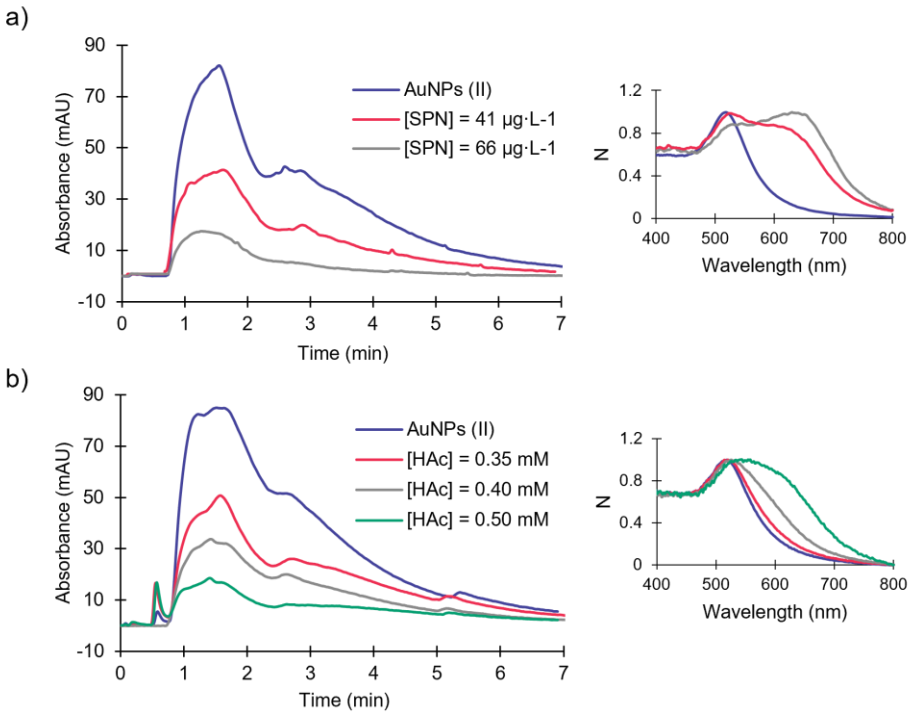

Figure 71. Chromatograms obtained for naked AuNPs I in function of: a) the added spermine and b) the added acetic acid. Insents: variations of the LSPR of the second chromatographic peak (t_r = 3.0 min).

In order to assess the practical application of the chromatographic method for monitoring plasmonic assays, urine samples from both healthy volunteers and cancer patients were analysed. The study is based in the previous work of Jornet-Martinez et al. [266], who demonstrated that the extracted spermine can be selectively detected by aggregation of naked AuNPs, and can be used as an biomarker of cancerous processes. In the

plasmonic assay used in this study the spermine is extracted using acetic acid through SPE. Consequently, it is essential to consider the contributions of both compounds. The extracted analyte was subsequently combined with the dispersion of AuNPs to generate the LSPR analytical signal using chromatographic analysis.

From the information provided by the chromatographic profiles obtained for healthy volunteers and cancer patients (**Figure 72**) differences in the aggregation was observed. For healthy volunteers the aggregation was lower and no difference in the peak area ratio was detected. On the other hand, the LSPR obtained for cancer patients show variations related with the spermine concentration which was correlated to the presence of a cancerous process.

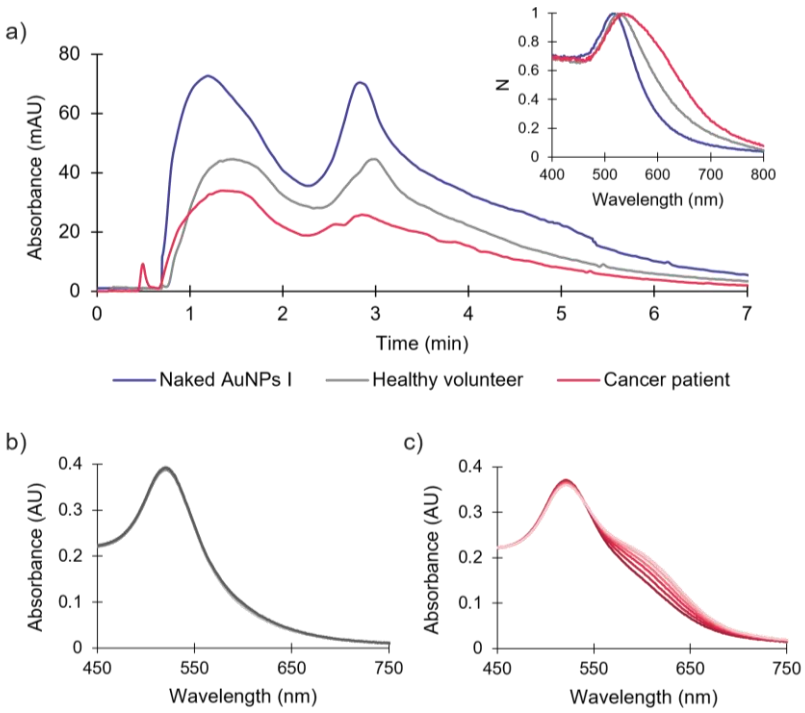

Figure 72. a) Chromatographic profiles of AuNPs I for a healthy volunteer and cancer patient. Inset: normalized UV-vis spectra at chromatographic peak (t_r = 3.0 min). b) and c) normalized UV-vis spectra showing the LSPR variation at the chromatographic peak (t_r = 3.0 min) for healthy volunteer and cancer patient respectively.

Naked AuNPs I was added to urine samples from healthy volunteers and cancer patients and were analysed by UV-vis spectrophotometry recording the signal every 20 s over 3 min in order to understand the differences between both. Spectroscopic signal provided a lower sensitivity than chromatographic signal. Indeed, no aggregation was observed for healthy volunteers, even at reaction times comparable to the retention times obtained in the chromatographic system (**Figure 72 b**). However, in the case of cancer patients, aggregation was observed as a function of the contact time when using spectroscopy (**Figure 72 c**), albeit with lower sensitivity compared to the analytical response achieved with chromatography

Finally, spermine was determined in cancer patients urine samples by means of IT-SPME-capLC-DAD. **Figure 73** shows the chromatograms obtained for the naked AuNPs I in the: blank acidic extract, and urine sample with 0, 16, and 26 $\mu g \cdot L^{-1}$ of spermine. As expected, the addition of spermine to the urine samples resulted in the reduction the chromatographic peak as a consequence of the NPs aggregation. From the fortified samples, the following calibration equation was obtained: $A = (-3 \pm 8) + (8.4 \pm 0.5) \cdot 10^3 \cdot C$, where A is the absorbance in mAU, and C is the spermine concentration in $\mu g \cdot L^{-1}$, being the coefficient of determination of 0.997. From this, the spermine concentration was estimated in the urine sample, which was found to be 83 $mg \cdot L^{-1}$, consistent with the results obtained in previous studies [266].

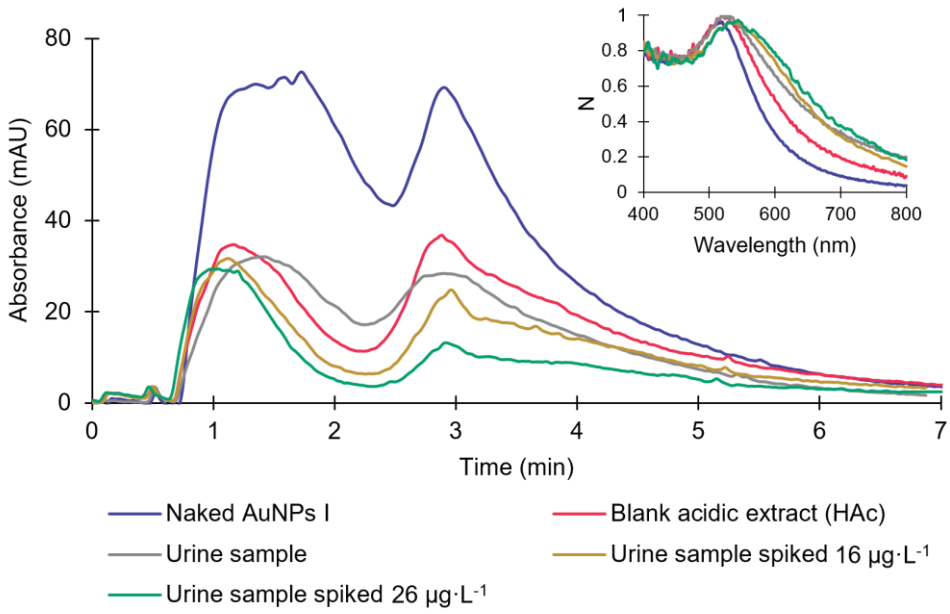

Figure 73. Chromatographic profiles obtained for the naked AuNPs I, for the blank acidic extract, urine sample, and spiked urine sample.

4.3.1.4 Conclusions

In this study, the IT-SPME-minLC-DAD was used as a characterization tool of AgNPs and AuNPs dispersion to guarantee solid results in further plasmonic assays. The characterization was based on the distribution of the NPs in two groups, polarized and non-polarized NPs, which were observed in the chromatogram as two separated peaks attending to its interactions with the extractive phase of the IT-SPME. Furthermore, the induced acid and spermine aggregation was followed by IT-SPME-nanoLC-DAD. Finally, the technique was successfully applied to the determination of spermine in urine samples as a cancer biomarker.

The time degradation of the NPs dispersions was studied, showing higher stability of the AuNPs over the AgNPs. The induced aggregation of naked AuNPs in presence of acid and spermine was studied by IT-SPME-nanoLC-DAD. The decreasing of the chromatographic peaks in presence of

acid and spermine was linked to the shift of the LSPR to higher wavelengths, indicating a aggregation process. Also, the concentration of spermine was linearly correlated with the peak area decrease, allowing for its quantification. As a practical application, spermine, which was previously proposed as a cancer biomarker, was determined in urine samples of health volunteers and cancer patients with satisfactory results. In comparison to UV-spectroscopy, IT-SPME-nanoLC-DAD offered higher sensitivity and sensibility.

4.3.2 Sulfidation transformation study of solid AgNPs

The sulfidation and dissolution of solid AgNPs nanoparticles were studied under different experimental conditions. A CFS with a double circuit was used to conduct the study under aerobic and anaerobic conditions (flushing with Ar), with varying concentrations of sulfide (see **Figure 33**). The ratio between the flow rate of the sulfide solution and water was 1:10, meaning that the concentration of this solution should be 10 times higher than the desired concentration in the system. The aliquots from the outlet of the system were collected over time and the silver concentration was determined by by ICP-MS. Also, the sulfide concentration was determined by the colorimetric assay described in the **Section 3.5.3**.

To carry out the assay cellulose triacetate and polyethersulfone filters both with 10 KDa of pore size were used. There were no significative differences in the silver dissolution; however, the triacetate cellulose filter was preferred over the polyethersulfone to avoid possible interferences due to the sulphur.

The results for the sulfidation assay under anaerobic conditions are plotted in the **Figure 74**. Theoretically, the presence of oxygen in the medium produces an outer layer of Ag_2O that subsequently interacts with bisulfide to form a nearly insoluble layer of Ag_2S. In the obtained results, the presence of bisulfide in the media produces an increase of the solubility of the AgNPs

which contrast with the sulfidation theory described. One possible explanation to this phenomenon is that, similarly to what occurs with other NPs such as CuNPs [313,314], before forming the crystalline Ag_2S layer, an initial layer of amorphous Ag_2S may form, which exhibits a faster dissolution kinetics (**Figure 75**). In the **Figures 74 b** and **c** is shown the sulfide concentration variation with time in the collected samples and in the initial solution. In the samples, the concentration of sulfide gradually increases until it reaches a point where it stabilizes, which coincides with the saturation of the AgNPs. It is also observed that the sulfide concentration in the solution decreases by approximately 20% compared to the initial concentration.

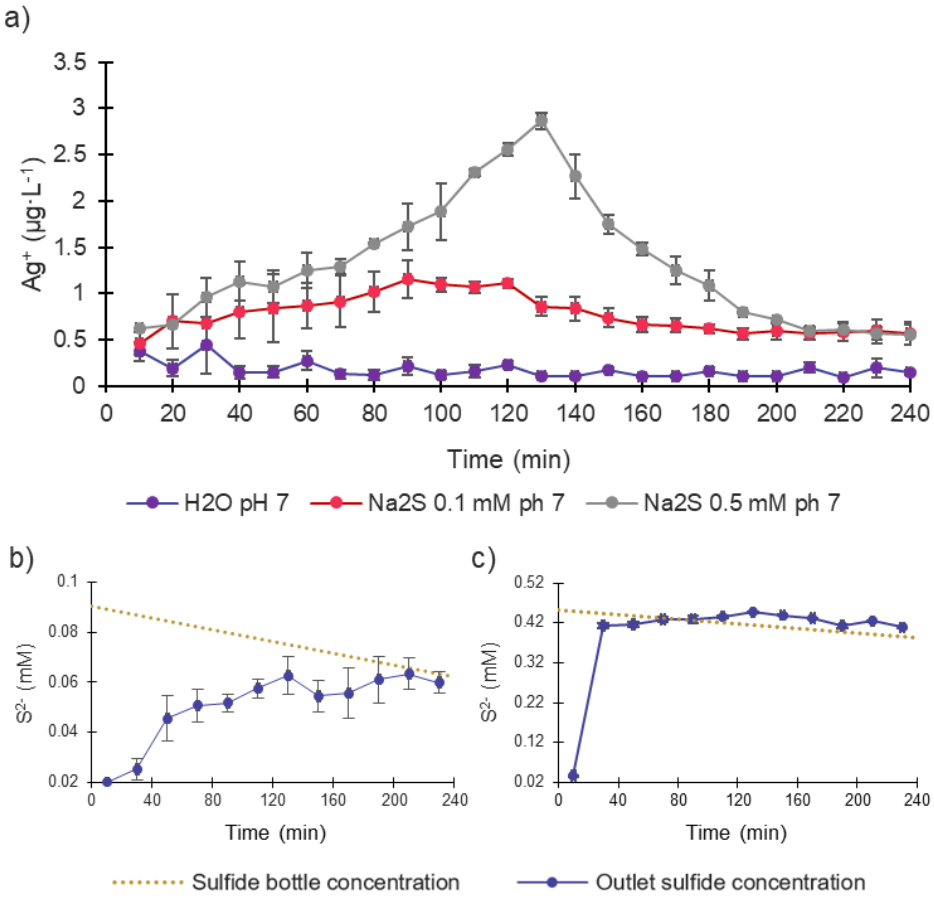

Figure 74. a) Silver dissolution profile at 1 mL·min^{-1} at different Na_2S concentrations in anaerobic conditions. b) and c) variation of the concentration of sulfide in samples and in the initial solution for 0.1 mM and 0.5 mM of Na_2S respectively.

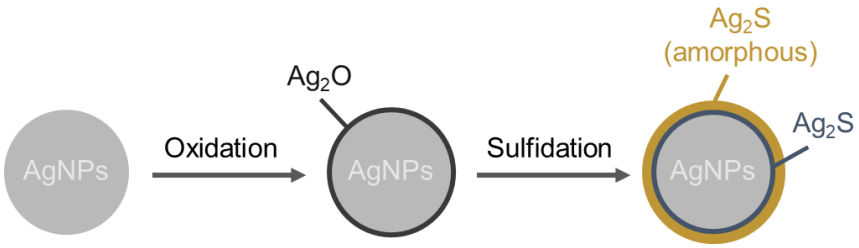

Figure 75. Schematic representation of the proposed sulfidation process with the formation of an amorphous Ag_2S previous the formation of the crystalline Ag_2S layer.

The presence and absence of oxygen in the media was studied by performing the assay with H_2O with and without Ar^0 flushing. The dissolved oxygen concentration in the bottles was monitored throughout the experiment by means of a , obtaining a mean concentration of O_2 of (0.26 ± 0.04) $mg \cdot L^{-1}$ and (8.4 ± 0.3) $mg \cdot L^{-1}$ for Ar^0 purged and non-purged solvent bottles respectively. The **Figure 76** shows the AgNPs dissolution profile at different Na_2S concentrations in both, aerobic and anaerobic conditions. In all cases, the dissolution profile is maintained, however, the dissolved silver increases drastically when there is oxygen in the system proving its importance in the oxidation step. Also, it can be seen the proportional dependence of initial Na_2S with the total dissolved silver.

To avoid the possible interaction of the silver ions with the filter, a pre-treatment of the filter with Cu^{2+} was performed (described in **Section 3.5.3**). In this pre-treatment, the filter is saturated with copper ions preventing the further interaction with silver. At the same time, the effect of the ionic strength on the media was studied comparing the obtained results with different $NaNO_3$ concentration in the media. The **Figure 77** show the results related to the filter treatment and ionic strength influence on the silver concentration. When the assay is carried out with the Cu^{2+} pre-treatment an initial Ag^+ peak can be observed in comparison to the assay with no pre-treatment. Confirming the interaction of the Ag^+ ions with the filter. Also, the increase in ionic

strength resulted in a reduction of the solubility of the AgNPs due to the compression of the electrical double layer which produces a reduction of the zeta potential favouring the AgNPs aggregation.

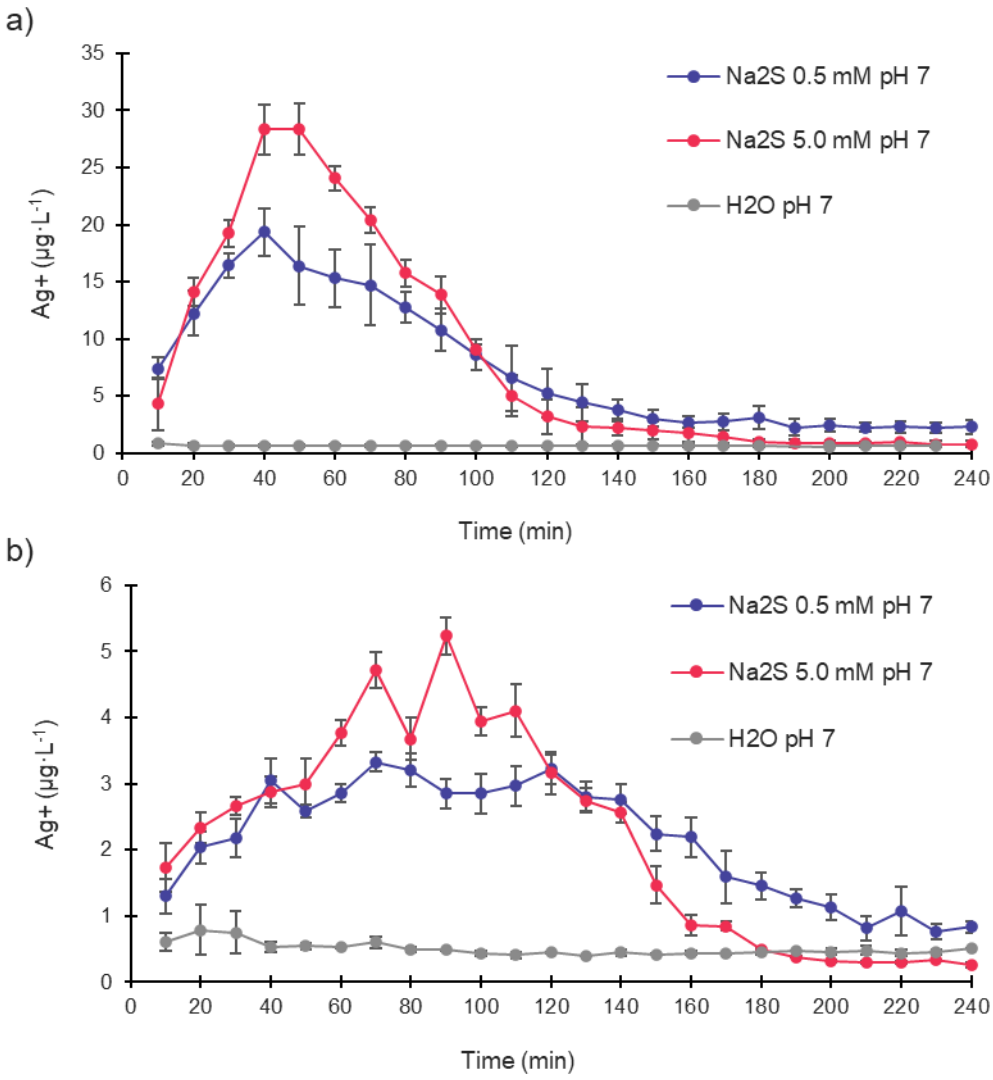

Figure 76. AgNPs dissolution profile at different Na_2S concentrations in aerobic (a) and anaerobic (b) conditions,

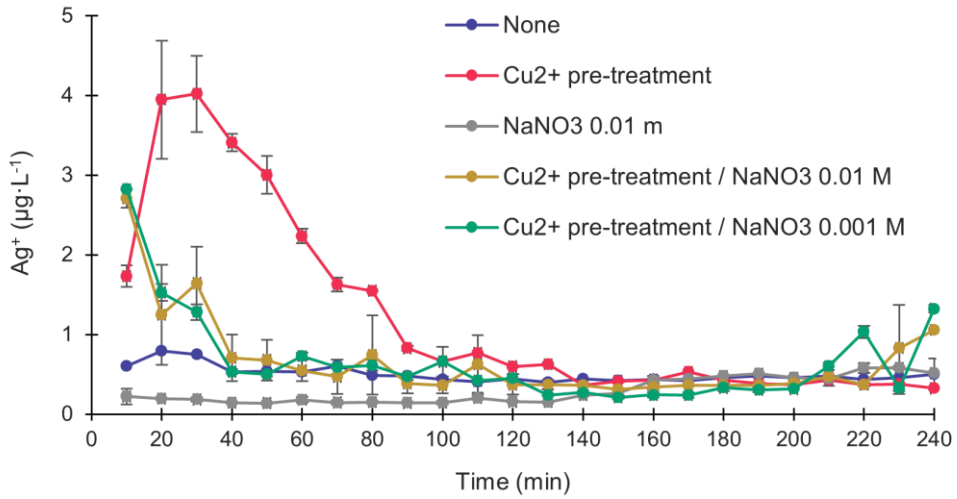

Figure 77. Effect of the filter pre-treatment with Cu^{2+} and the $NaNO_3$ concentration on the dissolution profile of AgNPs. The assay was carried out at pH = 7 and aerobic conditions.

The experimental conditions were fixed as follows: pH = 7, aerobic conditions, $NaNO_3$ 10 mM, and filter pre-treatment with Cu^{2+}. Under these conditions, the dissolution of the AgNPs was studied at different flow rates (0.2 µL·min^{-1}, 1 µL·min^{-1}, and 5 µL·min^{-1}) and the results are depicted in **Figure 78**. To properly evaluate the effect of flow on the dissolution of AgNPs, the results were normalized for each flow-rate, representing the dissolution rate as a function of the total collected volume. As can be observed, there is a positive correlation between the dissolution rate and the flow (**Figure 78 b**).

Finally, the different flow-rates were assayed in sulfide media conditions (**Figure 79**). As discussed earlier, the presence of sulfide in the medium leads to an increase in AgNPs dissolution due to the formation of an amorphous Ag_2S layer. However, in this case, for flow rates of 1 mL·min^{-1} and 5 mL·min^{-1}, it can be observed that after a certain time, the concentration of Ag^+ ions in the presence of sulfide is lower than in its absence. This could be attributed to the gradual formation of crystalline Ag_2S, which has negligible

solubility. It is worth noting that this point is reached earlier for higher flow rates, indicating that the total volume of the medium interacting with AgNPs has a significant effect on the amorphous Ag_2S layer life-time. Therefore, for a flow rate of 0.2 $mL \cdot min^{-1}$, longer times would be required to observe the formation of crystalline Ag_2S.

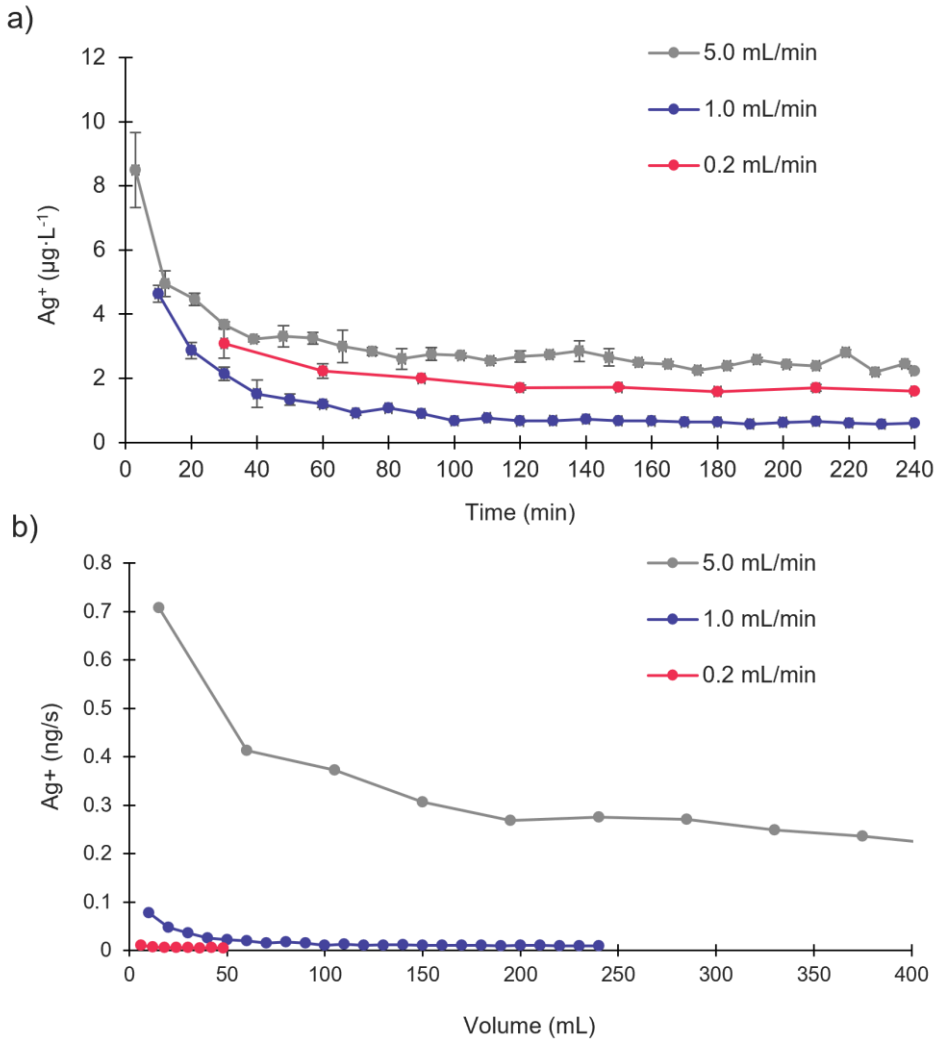

Figure 78. a) AgNPs dissolution profile for different flow-rates. b) Normalized results showing the dissolution rate in function of the total volume. The assays were carried out at pH = 7, aerobic conditions, $NaNO_3$ 0.01 M in the media, and filter pre-treatment.

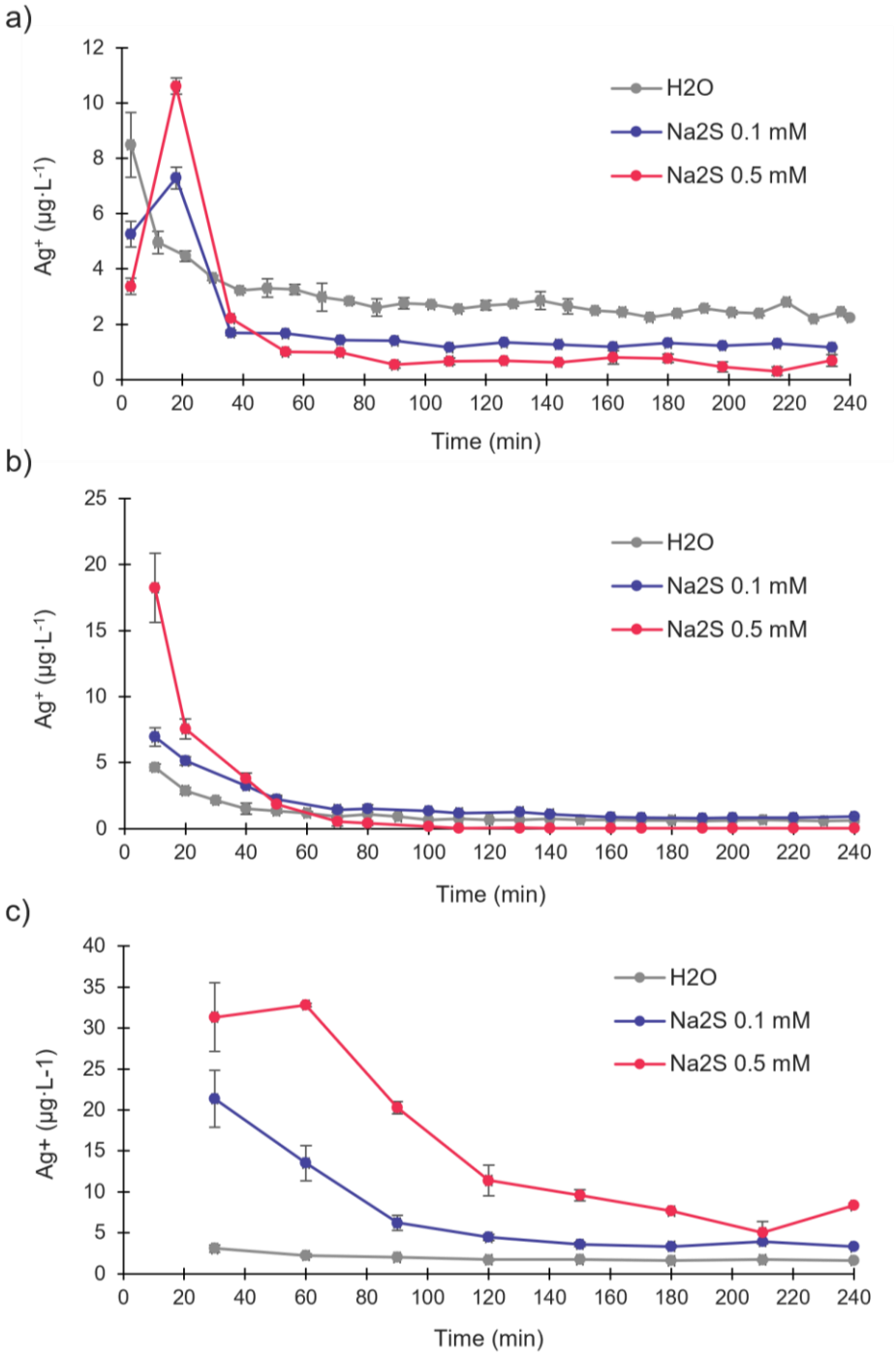

Figure 79. AgNPs dissolution profile at different sulfide concentrations at: a) 5.0 $mL \cdot min^{-1}$, b) 1.0 $mL \cdot min^{-1}$, and c) 0.2 $mL \cdot min^{-1}$. The assays were carried out at pH = 7, aerobic conditions, $NaNO_3$ 0.01 M in the media, and filter pre-treatment.

The results presented in this section are derived from the work conducted during the doctoral stay at the Centre for Microbiology and Environmental System Science in the Department of Environmental Geosciences at the University of Vienna.

4.3.2.1 Conclusions

In the environment, NPs undergo transformations in multiple ways, modifying their properties and consequently affecting its toxicity, accumulation, and other adverse effects. In this sense, gaining insight into the NPs transformations is crucial for comprehending their fate, transport, and potential effects in the environment. In this study, the transformations of AgNPs in presence of sulfide were studied in a CFS under different conditions. The fractions were collected over time and the Ag^+ concentration was determined by means of ICP-MS.

As expected, the presence of oxygen resulted in increased solubility due to the formation of an Ag_2O layer with higher dissolution rates that the AgNPs itself. The effect of ionic strength was investigated by introducing various concentrations of $NaNO_3$ into the medium. Increasing the ionic strength caused the reduction in the concentration of silver ions. This reduction can be explained by the compression of the double layer, which hinders the formation of small AgNPs clusters. Furthermore, different flow rates were tested, observing a positive correlation with the Ag^+ concentration in the collected fractions. Finally, The presence of sulfide in the solution led to an increase in the solubility of AgNPs. This increase can be attributed to the formation of an amorphous Ag_2S layer, which possesses higher solubility. The further formation of the crystalline Ag_2S layer was observed when worked with higher flow rates, evidenced as a decrease in Ag+ concentration after a certain period, compared to the assay conducted without sulfide in the medium.

CHAPTER 5:

GENERAL CONCLUSIONS

The present thesis aims to provide new knowledge about minLC as greener alternative to conventional LC. Furthermore, it explores the possibilities of portability in LC as a tool to overcome the analytical challenges of in-situ analysis. New strategies of analysis based on miniaturized and portable LC were applied to different matrices of analytical interest, including environmental, biological, and nanoparticles samples (**Table 33**).

Table 33. Matrices studied throughout the thesis: selected samples, determined analytes, and analysis techniques employed.

Matrix	Sample	Analyte	Techniques
Environmental	Fruit washing, well, and different superficial waters	Pesticides Drugs Nitrates Nitrites Ammonium Amino acids	IT-SPME-nanoLC-DAD IT-SPME-capLC-DAD UHPLC-QTOF Portable minLC Portable optical fiber Nitrate Analyzer Lab spectrophotometer Lab fluorometer Portable luminometer
Biological	Urine	APAP Spermine	IT-SPME-nanoLC-DAD DART-QTOF UHPLC-QTOF UV-vis spectroscopy
Nanoparticles	NPs dispersions	AgNPs AuNPs Acetic acid Spermine	IT-SPME-nanoLC-DAD IT-SPME-capLC-DAD ICP-MS UV-vis spectroscopy

Environmental samples: Different drugs and pesticides with a wide range of polarities ($\log K_{ow}$ ranging from -1.72 – 3.82) were selected as targeted analytes to study the capabilities of portable minLC for in-field analysis. The figures of merit obtained were compared to those provided by benchtop IT-SPME-cap/nanoLC-DAD. The portable minLC provided chromatogram with greater peak resolution in a lower analysis allowing to detect a higher

number of analytes in a lower analysis time. However, its sensitivity was limited, with LODs range of $mg \cdot L^{-1}$ in comparison to benchtop instruments in the order of low $\mu g \cdot L^{-1}$. Two evaluation tools were employed to objectively evaluate the instrument and method characteristics. Firstly, the BETTER criteria allowed to assess the characteristics related to portability. In this regard, the portable minLC provided suitable results, in line with other portable LC developed. In the other hand, the HEXAGON tool was employed to compare the method characteristics related to greenness and sustainability providing better results for the portable minLC in comparison to the benchtop cap/nanoLC. As practical application, fruit washing residual waters with high concentration levels of different biocides were suitably determined by all three techniques with comparable results.

Different in-situ instrumentation was used for the determination of various legislated nitrogen compounds. An analyzer was tested for the in-situ monitoring of nitrate and its results were compared to those obtained by a benchtop spectrophotometer and a spectrophotometric probe. Higher LODs were obtained by means of the nitrate analyzer (3.0 $mg \cdot L^{-1}$ vs. 0.5 $mg \cdot L^{-1}$) but in accordance with its specifications working range. Low or no influence of turbidity and humic acids was observed at regular concentrations of these. Different forms of inorganic and organic dissolved N were successfully quantified in several water bodies. For all samples, the results obtained by means of the analyzer, portable optical fiber probe, and benchtop instrumentation were comparable in terms of sensitivity and precision. The analyzer was also employed for the monitoring of nitrates in a well water treatment plant obtaining similar results to those obtained by the spectrophotometric probe.

Finally, a portable minLC was used for the determination of DRN and IPT, two legislated phenylurea pesticides. By performing a previous SPE, the instrument was able to achieve the required LODs showing reliable results for the environmental monitoring of these compounds.

Biological samples: Acetaminophen was determined by IT-SPME-nanoLC-DAD in urine samples and the results were compared and validated with those provided by UHPLC-ESI-QTOF and DART-QTOF. A minimal sample pretreatment consisting of a acid deproteinization, centrifugation and filtration was performed prior to the determination. For the IT-SPME-nanoLC-DAD, the sample analysis was carried out in 25 min with good sensitivity and reproducibility. The low LODs obtained allowed to greatly dilute the sample minimizing the potential interferences and matrix effect. The acetaminophen glucoronide was detected and could be also determined if needed increasing the equilibrium time. The objective comparison of all three methodologies was carried out by means of the HEXAGON tool. It revealed superior results for the IT-SPME-nanoLC-DAD in terms of toxicity/safety, residues, and carbon footprint. Additionally, it exhibited significantly lower annual economic costs, amounting to roughly half of those associated with the DART-QTOF and UHPLC-ESI-QTOF methodologies. Overall, the IT-SPME-nanoLC-DAD demonstrated to be a good alternative for the acetaminophen overdose diagnosis in clinical centres.

Nanoparticles samples: The IT-SPME-minLC-DAD has proven to be an effective tool for the assessment of NMNPs, ensuring reliable results in further plasmonic assays. The use of IT-SPME allowed to separate the NMNPs in two groups (polarized and non-polarized NPs) based on the different interactions with the extractive phase. This made possible the monitoring of the LSPR of naked AuNPs in function of the ratio of both peaks. It demonstrated that the functionality of a given NPs dispersion can be ensured from its chromatographic profile in less than 10 min. Induced aggregation plasmonic assays were carried out using citrate and phosphate capping AuNPs and naked AuNPs and spermine and acetic acid as analytes. The variations in the chromatographic peak areas and ratios were successfully related to the presence of these target analytes. In comparison with UV-vis

spectroscopy, the IT-SPME-minLC-DAD provided higher sensitivity. As practical applications, spermine which was proposed as a cancer biomarker, was determined in urine samples of cancer patients and healthy volunteers with adequate results. The spermine concentration was linearly correlated with the chromatographic peak areas in urine samples allowing the quanitifcation. A concentration of 83 $\mu g \cdot L^{-1}$ of spermine was found in cancer patient urine, which is in accordance with the literature [266]

Finally, AgNPs sulfidation and dissolution transformations were studied by means of a CFS under different conditions of flow rate, ionic strength, oxygen, and sulfide concentration. These studies aim to shed light on the transformations that AgNPs can undergo in continuous flow environmental systems such as rivers. The presence of sulfide in the solution produced an increase in the AgNPs solubility which was attributed to the formation of a former Ag_2S amorphous layer with higher solubility which is gradually transformed to crystalline Ag_2S with negligible solubility. As expected, the presence of oxygen produced an increase in the solubility as a consequence of the formation of a Ag_2O layer which further dissolves in Ag^+ ions. The effect of ionic strength by adding different concentrations of $NaNO_3$ the medium. The increasing ionic strength produced a reduction in the concentration of silver ions due to the compression of the double layer which hinders the formation of small AgNPs clusters. Different flow rates were tested showing a positive correlation with the Ag^+ ions. Furthermore, in the presence of sulfide, when higher flow rates are employed, the formation of a crystalline Ag2S layer becomes apparent after a certain assay time. This is evidenced by a decrease in the Ag^+ concentration below that observed in the assay carried out without sulfide in the medium.

REFERENCES

[1] O. Hutzinger, The greening of chemistry — Is it sustainable?, Environ. Sci. Pollut. Res. 6 (1999) 123–123. https://doi.org/10.1007/BF02987605.

[2] Maja, R. Fowkes, Planetary Forecast: The Roots of Sustainability in the Radical Art of the 1970s, Third Text. 23 (2009) 669–674. https://doi.org/10.1080/09528820903189277.

[3] G. Brundtland, Report of the World Commision on Environement and Development: Our Common Future. United Nations General Assembly document A/42/42, 1987.

[4] I.T. Horváth, Introduction: Sustainable Chemistry, Chem. Rev. 118 (2018) 369–371. https://doi.org/10.1021/acs.chemrev.7b00721.

[5] P.T. Anastas, J.C. Warner, Green chemistry: theory and practice, Oxford University Press, Oxford; New York, 1998.

[6] P.M. Nowak, R. Wietecha-Posłuszny, J. Pawliszyn, White Analytical Chemistry: An approach to reconcile the principles of Green Analytical Chemistry and functionality, TrAC Trends Anal. Chem. 138 (2021) 116223. https://doi.org/10.1016/j.trac.2021.116223.

[7] A. Gałuszka, Z. Migaszewski, J. Namieśnik, The 12 principles of green analytical chemistry and the SIGNIFICANCE mnemonic of green analytical practices, TrAC Trends Anal. Chem. 50 (2013) 78–84. https://doi.org/10.1016/j.trac.2013.04.010.

[8] L.H. Keith, L.U. Gron, J.L. Young, Green analytical methodologies, Chem. Rev. 107 (2007) 2695–2708. https://doi.org/10.1021/cr068359e.

[9] A. Gałuszka, Z.M. Migaszewski, P. Konieczka, J. Namieśnik, Analytical Eco-Scale for assessing the greenness of analytical procedures, TrAC Trends Anal. Chem. 37 (2012) 61–72. https://doi.org/10.1016/j.trac.2012.03.013.

[10] J. Płotka-Wasylka, A new tool for the evaluation of the analytical procedure: Green Analytical Procedure Index, Talanta. 181 (2018) 204–209. https://doi.org/10.1016/j.talanta.2018.01.013.

[11] P.M. Nowak, P. Kościelniak, What Color Is Your Method? Adaptation of the RGB Additive Color Model to Analytical Method Evaluation, Anal. Chem. 91 (2019) 10343–10352. https://doi.org/10.1021/acs.analchem.9b01872.

[12] A. Ballester-Caudet, P. Campíns-Falcó, B. Pérez, R. Sancho, M.

Lorente, G. Sastre, C. González, A new tool for evaluating and/or selecting analytical methods: Summarizing the information in a hexagon, TrAC Trends Anal. Chem. 118 (2019) 538–547. https://doi.org/10.1016/j.trac.2019.06.015.

[13] S. Cortés-Bautista, R. Navarro-Utiel, A. Ballester-Caudet, P. Campíns-Falcó, Towards in field miniaturized liquid chromatography: Biocides in wastewater as a proof of concept, J. Chromatogr. A. 1673 (2022) 463119. https://doi.org/10.1016/j.chroma.2022.463119.

[14] A. Ballester-Caudet, R. Navarro-Utiel, I. Campos-Hernández, P. Campíns-Falcó, Evaluation of the sample treatment influence in green and sustainable assessment of liquid chromatography methods by the HEXAGON tool: Sulfonate-based dyes determination in meat samples, Green Anal. Chem. 3 (2022). https://doi.org/10.1016/j.greeac.2022.100024.

[15] F. Pena-Pereira, W. Wojnowski, M. Tobiszewski, AGREE—Analytical GREEnness Metric Approach and Software, Anal. Chem. 92 (2020) 10076–10082. https://doi.org/10.1021/acs.analchem.0c01887.

[16] W.S. Trimer, Micromechanics and MEMS: Classic and Seminal Papers to 1990, 1st ed., Wiley-IEEE Press, 1997.

[17] N. Convery, N. Gadegaard, 30 years of microfluidics, Micro Nano Eng. 2 (2019) 76–91. https://doi.org/10.1016/j.mne.2019.01.003.

[18] N. Jornet-Martínez, Y. Moliner-Martínez, C. Molins-Legua, P. Campíns-Falcó, Trends for the Development of In Situ Analysis Devices, Encycl. Anal. Chem. (2017) 1–23. https://doi.org/10.1002/9780470027318.a9593.

[19] C. Duan, J. Li, Y. Zhang, K. Ding, X. Geng, Y. Guan, Portable instruments for on-site analysis of environmental samples, TrAC Trends Anal. Chem. 154 (2022) 116653. https://doi.org/10.1016/j.trac.2022.116653.

[20] L.F. Capitán-Vallvey, A.J. Palma, Recent developments in handheld and portable optosensing—A review, Anal. Chim. Acta. 696 (2011) 27–46. https://doi.org/10.1016/j.aca.2011.04.005.

[21] H. Eren, Recent technological progress in portable instruments, in: 2nd ISA/IEEE Sensors Ind. Conf., ISA, 2003: pp. 78–83. https://doi.org/10.1109/SFICON.2002.1159811.

[22] T.K. With, A portable source of woods light in Porphyrin Analysis,

Scand. J. Clin. Lab. Invest. 9 (1957) 208–209. https://doi.org/10.3109/00365515709101227.

[23] J.P. Grinias, The Potential for Portable Capillary Liquid Chromatography, Recent Dev. Column Technol. 6 (2020) 15–24.

[24] M. Tswett, 51. M. Tswett: Physikalisch-chemische Studien über das Chlorophyll. Die Adsorptionen, Ber. Dtsch. Bot. Ges. 24 (1906) 316–323. https://doi.org/10.1111/j.1438-8677.1906.tb06524.x.

[25] J.P. Chervet, M. Ursem, J.P. Salzmann, Instrumental Requirements for Nanoscale Liquid Chromatography, Anal. Chem. 68 (1996) 1507–1512. https://doi.org/10.1021/ac9508964.

[26] S.R. Wilson, T. Vehus, H.S. Berg, E. Lundanes, Nano-LC in proteomics: recent advances and approaches, Bioanalysis. 7 (2015) 1799–1815. https://doi.org/10.4155/bio.15.92.

[27] C.G. Horvath, B.A. Preiss, S.R. Lipsky, Fast liquid chromatography. Investigation of operating parameters and the separation of nucleotides on pellicular ion exchangers, Anal. Chem. 39 (1967) 1422–1428. https://doi.org/10.1021/ac60256a003.

[28] C. Horvath, S.R. Lipsky, Rapid Analysis of Ribonucleosides and Bases at the Picomole Level Using Pellicular Cation Exchange Resin in Narrow Bore Columns, Anal. Chem. 41 (1969) 1227–1234. https://doi.org/10.1021/ac60279a024.

[29] T. Tsuda, G. Nakagawa, Open-tubular liquid chromatography with 5–10-μm I.D. Columns, J. Chromatogr. A. 268 (1983) 369–374. https://doi.org/10.1016/S0021-9673(01)95435-4.

[30] R.T. Kennedy, J.W. Jorgenson, Preparation and evaluation of packed capillary liquid chromatography columns with inner diameters from 20 to 50 micrometers, Anal. Chem. 61 (1989) 1128–1135. https://doi.org/10.1021/ac00185a016.

[31] S. Hsieh, J.W. Jorgenson, Preparation and Evaluation of Slurry-Packed Liquid Chromatography Microcolumns with Inner Diameters from 12 to 33 μm, Anal. Chem. 68 (1996) 1212–1217. https://doi.org/10.1021/ac950682m.

[32] J.H. Knox, J.F. Parcher, Effect of Column to Particle Diameter Ratio on the Dispersion of Unsorbed Solutes in Chromatography, Anal. Chem. 41 (1969) 1599–1606. https://doi.org/10.1021/ac60281a009.

[33] C.E.D. Nazario, M.R. Silva, M.S. Franco, F.M. Lanças, Evolution in

miniaturized column liquid chromatography instrumentation and applications: An overview, J. Chromatogr. A. 1421 (2015) 18–37. https://doi.org/10.1016/j.chroma.2015.08.051.

[34] T. Tsuda, M. Novotny, Band-broadening phenomena in microcapillary tubes under the conditions of liquid chromatography, Anal. Chem. 50 (1978) 632–634. https://doi.org/10.1021/ac50026a023.

[35] F. Gritti, G. Guiochon, On the minimization of the band-broadening contributions of a modern, very high pressure liquid chromatograph, J. Chromatogr. A. 1218 (2011) 4632–4648. https://doi.org/10.1016/j.chroma.2011.05.024.

[36] A. Prüß, C. Kempter, J. Gysler, T. Jira, Extracolumn band broadening in capillary liquid chromatography, J. Chromatogr. A. 1016 (2003) 129–141. https://doi.org/10.1016/S0021-9673(03)01290-1.

[37] J. Grinias, B. Bunner, M. Gilar, J. Jorgenson, Measurement and Modeling of Extra-Column Effects Due to Injection and Connections in Capillary Liquid Chromatography, Chromatography. 2 (2015) 669–690. https://doi.org/10.3390/chromatography2040669.

[38] T. Werres, T.C. Schmidt, T. Teutenberg, The influence of injection volume on efficiency of microbore liquid chromatography columns for gradient and isocratic elution, J. Chromatogr. A. 1641 (2021) 461965. https://doi.org/10.1016/j.chroma.2021.461965.

[39] T. Werres, T.C. Schmidt, T. Teutenberg, Peak broadening caused by using different micro–liquid chromatography detectors, Anal. Bioanal. Chem. 414 (2022) 6107–6114. https://doi.org/10.1007/s00216-022-04170-9.

[40] E.-J. Sneekers, L. Rieux, R. Swart, Nano LC: Principles, Evolution, and State-of-the-Art of the Technique, LCGC NA. 29 (2011) 926–934. https://doi.org/[Online] https://www.chromatographyonline.com/view/nano-lc-principles-evolution-and-state-art-technique.

[41] J.P.C. Vissers, H.A. Claessens, C.A. Cramers, Microcolumn liquid chromatography: instrumentation, detection and applications, J. Chromatogr. A. 779 (1997) 1–28. https://linkinghub.elsevier.com/retrieve/pii/S0021967397004226.

[42] A. Iliuk, K. Jayasundera, R. Schluttenhofer, W.A. Tao, Nanoproteomics, Humana Press, Totowa, NJ, 2011. https://doi.org/10.1007/978-1-61779-319-6.

[43] P. Kucera, Micro-column high performance liquid chromatography, 1st ed., Elsevier Ltd, Amsterdam, Netherlands, 2000.

[44] F. Pena-Pereira, 1 From Conventional to Miniaturized Analytical Systems, in: Miniaturization Sample Prep., De Gruyter Open Poland, 2014: pp. 1–28. https://doi.org/10.2478/9783110410181.1.

[45] J. Šesták, D. Moravcová, V. Kahle, Instrument platforms for nano liquid chromatography, J. Chromatogr. A. 1421 (2015) 2–17. https://doi.org/10.1016/j.chroma.2015.07.090.

[46] F. Rahimi, S. Chatzimichail, A. Saifuddin, A.J. Surman, S.D. Taylor-Robinson, A. Salehi-Reyhani, A Review of Portable High-Performance Liquid Chromatography: the Future of the Field?, Chromatographia. 83 (2020) 1165–1195. https://doi.org/10.1007/s10337-020-03944-6.

[47] E. Vasconcelos Soares Maciel, A.L. de Toffoli, E. Sobieski, C.E. Domingues Nazário, F.M. Lanças, Miniaturized liquid chromatography focusing on analytical columns and mass spectrometry: A review, Anal. Chim. Acta. 1103 (2020) 11–31. https://doi.org/10.1016/j.aca.2019.12.064.

[48] S.R. Wilson, C. Olsen, E. Lundanes, Nano liquid chromatography columns, Analyst. 144 (2019) 7090–7104. https://doi.org/10.1039/C9AN01473J.

[49] H. Roberg-Larsen, S.R. Wilson, E. Lundanes, Recent advances in on-line upfront devices for sensitive bioanalytical nano LC methods, TrAC Trends Anal. Chem. 136 (2021) 116190. https://doi.org/10.1016/j.trac.2021.116190.

[50] L. Yi, P.D. Piehowski, T. Shi, R.D. Smith, W.-J. Qian, Advances in microscale separations towards nanoproteomics applications, J. Chromatogr. A. 1523 (2017) 40–48. https://doi.org/10.1016/j.chroma.2017.07.055.

[51] K.L. Sanders, J.L. Edwards, Nano-liquid chromatography-mass spectrometry and recent applications in omics investigations, Anal. Methods. 12 (2020) 4404–4417. https://doi.org/10.1039/D0AY01194K.

[52] C. Fanali, L. Dugo, P. Dugo, L. Mondello, Capillary-liquid chromatography (CLC) and nano-LC in food analysis, TrAC - Trends Anal. Chem. 52 (2013) 226–238. https://doi.org/10.1016/j.trac.2013.05.021.

[53] C. Aydoğan, Nanoscale separations based on LC and CE for food analysis: A review, TrAC - Trends Anal. Chem. 121 (2019). https://doi.org/10.1016/j.trac.2019.115693.

[54] Z. Aturki, A. Rocco, S. Rocchi, S. Fanali, Current applications of miniaturized chromatographic and electrophoretic techniques in drug analysis, J. Pharm. Biomed. Anal. 101 (2014) 194–220. https://doi.org/10.1016/j.jpba.2014.03.041.

[55] M.R. Gama, C.H. Collins, C.B.G. Bottoli, Nano-Liquid Chromatography in Pharmaceutical and Biomedical Research, J. Chromatogr. Sci. 51 (2013) 694–703. https://doi.org/10.1093/chromsci/bmt023.

[56] D. Moreno-González, J. Alcántara-Durán, S.M. Addona, M. Beneito-Cambra, Multi-residue pesticide analysis in virgin olive oil by nanoflow liquid chromatography high resolution mass spectrometry, J. Chromatogr. A. 1562 (2018) 27–35. https://doi.org/10.1016/j.chroma.2018.05.053.

[57] C. Tejada-Casado, M. del Olmo-Iruela, A.M. García-Campaña, F.J. Lara, Green and simple analytical method to determine benzimidazoles in milk samples by using salting-out assisted liquid-liquid extraction and capillary liquid chromatography, J. Chromatogr. B. 1091 (2018) 46–52. https://doi.org/10.1016/j.jchromb.2018.05.024.

[58] J. Alcántara-Durán, D. Moreno-González, J.F. García-Reyes, A. Molina-Díaz, Use of a modified QuEChERS method for the determination of mycotoxin residues in edible nuts by nano flow liquid chromatography high resolution mass spectrometry, Food Chem. 279 (2019) 144–149. https://doi.org/10.1016/j.foodchem.2018.11.149.

[59] M.E. Salih, A. Aqel, B.Y. Abdulkhair, Z.A. Alothman, M.A. Abdulaziz, A.Y. Badjah-Hadj-Ahmed, Simultaneous Determination of Paracetamol and Chlorzoxazone in Their Combined Pharmaceutical Formulations by Reversed-phase Capillary Liquid Chromatography Using a Polymethacrylate Monolithic Column, J. Chromatogr. Sci. 56 (2018) 819–827. https://doi.org/10.1093/chromsci/bmy058.

[60] S.W. Foster, X. Xie, M. Pham, P.A. Peaden, L.M. Patil, L.T. Tolley, P.B. Farnsworth, H.D. Tolley, M.L. Lee, J.P. Grinias, Portable capillary liquid chromatography for pharmaceutical and illicit drug analysis, J. Sep. Sci. 43 (2020) 1623–1627. https://doi.org/10.1002/jssc.201901276.

[61] J. Pla-Tolós, P. Serra-Mora, L. Hakobyan, C. Molins-Legua, Y. Moliner-Martinez, P. Campins-Falcó, A sustainable on-line CapLC method for quantifying antifouling agents like irgarol-1051 and diuron in water samples: Estimation of the carbon footprint, Sci. Total Environ. 569–570 (2016) 611–618. https://doi.org/10.1016/j.scitotenv.2016.06.181.

[62] A. Celma, J. V. Sancho, N. Salgueiro-González, S. Castiglioni, E. Zuccato, F. Hernández, L. Bijlsma, Simultaneous determination of new psychoactive substances and illicit drugs in sewage: Potential of micro-liquid chromatography tandem mass spectrometry in wastewater-based epidemiology, J. Chromatogr. A. 1602 (2019) 300–309. https://doi.org/10.1016/j.chroma.2019.05.051.

[63] H.D. Ponce-Rodríguez, J. Verdú-Andrés, R. Herráez-Hernández, P. Campíns-Falcó, Exploring hand-portable nano-liquid chromatography for in place water analysis: Determination of trimethylxanthines as a use case, Sci. Total Environ. 747 (2020) 140966. https://doi.org/10.1016/j.scitotenv.2020.140966.

[64] D. Liu, X. Han, X. Liu, M. Cheng, M. He, G. Rainer, H. Gao, X. Zhang, Measurement of ultra-trace level of intact oxytocin in plasma using SALLE combined with nano-LC–MS, J. Pharm. Biomed. Anal. 173 (2019) 62–67. https://doi.org/10.1016/j.jpba.2019.04.023.

[65] A. Cattaneo, G. Martano, U. Restuccia, L. Tronci, M. Bianchi, A. Bachi, V. Matafora, Opti-nQL: An Optimized, Versatile and Sensitive Nano-LC Method for MS-Based Lipidomics Analysis, Metabolites. 11 (2021) 720. https://doi.org/10.3390/metabo11110720.

[66] D. Raynie, Trends in Sample Preparation, LCGC North Am. 34 (2016) 174–188.

[67] P. Anastas, N. Eghbali, Green Chemistry : Principles and Practice, Chem Soc Rev. 19 (2010) 301–312. https://doi.org/10.1039/b918763b.

[68] D.A. Vargas Medina, D.M. Sartore, E.V.S. Maciel, Á.J. Santos-Neto, F.M. Lanças, Microextraction columns for automated sample preparation. A review focusing on fully miniaturized column switching and bioanalytical applications, Adv. Sample Prep. 3 (2022) 100031. https://doi.org/10.1016/j.sampre.2022.100031.

[69] Y. Moliner-Martínez, P. Serra-Mora, J. Verdú-Andrés, R. Herráez-Hernández, P. Campíns-Falcó, Analysis of polar triazines and

degradation products in waters by in-tube solid-phase microextraction and capillary chromatography: an environmentally friendly method, Anal. Bioanal. Chem. 407 (2015) 1485–1497. https://doi.org/10.1007/s00216-014-8366-7.

[70] P. Serra-Mora, Y. Moliner-Martínez, C. Molins-Legua, R. Herráez-Hernández, J. Verdú-Andrés, P. Campíns-Falcó, Trends in Online Intube Solid Phase Microextraction, in: Compr. Anal. Chem., 2017: pp. 427–461. https://doi.org/10.1016/bs.coac.2017.01.002.

[71] Y. Moliner-Martínez, H. Prima-Garcia, A. Ribera, E. Coronado, P. Campíns-Falcó, Magnetic In-Tube Solid Phase Microextraction, Anal. Chem. 84 (2012) 7233–7240. https://doi.org/10.1021/ac301660k.

[72] H.D. Ponce-Rodríguez, J. Verdú-Andrés, R. Herráez-Hernández, P. Campíns-Falcó, Innovations in Extractive Phases for In-Tube Solid-Phase Microextraction Coupled to Miniaturized Liquid Chromatography: A Critical Review, Molecules. 25 (2020) 2460. https://doi.org/10.3390/molecules25102460.

[73] H. Kataoka, In-tube solid-phase microextraction: Current trends and future perspectives, J. Chromatogr. A. 1636 (2021). https://doi.org/10.1016/j.chroma.2020.461787.

[74] R. González-Fuenzalida, Y. Moliner-Martínez, H. Prima-Garcia, A. Ribera, P. Campins-Falcó, R. Zaragozá, Evaluation of Superparamagnetic Silica Nanoparticles for Extraction of Triazines in Magnetic in-Tube Solid Phase Microextraction Coupled to Capillary Liquid Chromatography, Nanomaterials. 4 (2014) 242–255. https://doi.org/10.3390/nano4020242.

[75] P. Serra-Mora, N. Jornet-Martinez, Y. Moliner-Martinez, P. Campíns-Falcó, In tube-solid phase microextraction-nano liquid chromatography: Application to the determination of intact and degraded polar triazines in waters and recovered struvite, J. Chromatogr. A. 1513 (2017) 51–58. https://doi.org/10.1016/j.chroma.2017.07.053.

[76] P. Serra-Mora, R. Herráez-Hernández, P. Campíns-Falcó, Bimodal copper oxide nanoparticles doped phase for the extraction of highly polar compounds by in-tube solid-phase microextraction coupled on-line to nano-liquid chromatography, J. Chromatogr. A. 1617 (2020) 460819. https://doi.org/10.1016/j.chroma.2019.460819.

[77] M.C. Prieto-Blanco, S. Peñafiel Barba, Y. Moliner-Martínez, P.

Campíns-Falcó, Footprint of carbonyl compounds in hand scent by in-tube solid-phase microextraction coupled to nano-liquid chromatography/diode array detection, J. Chromatogr. A. 1596 (2019) 241–249. https://doi.org/10.1016/j.chroma.2019.03.007.

[78] M.C. Prieto-Blanco, Y. Moliner-Martínez, P. López-Mahía, P. Campíns-Falcó, Determination of carbonyl compounds in particulate matter PM2.5 by in-tube solid-phase microextraction coupled to capillary liquid chromatography/mass spectrometry, Talanta. 115 (2013) 876–880. https://doi.org/10.1016/j.talanta.2013.07.003.

[79] N. Jornet-Martínez, M. Muñoz-Ortuño, Y. Moliner-Martínez, R. Herráez-Hernández, P. Campíns-Falcó, On-line in-tube solid phase microextraction-capillary liquid chromatography method for monitoring degradation products of di-(2-ethylhexyl) phthalate in waters, J. Chromatogr. A. 1347 (2014) 157–160. https://doi.org/10.1016/j.chroma.2014.04.074.

[80] Y. Moliner-Martinez, Y. Vitta, H. Prima-Garcia, R.A. González-Fuenzalida, A. Ribera, P. Campíns-Falcó, E. Coronado, Silica supported Fe3O4 magnetic nanoparticles for magnetic solid-phase extraction and magnetic in-tube solid-phase microextraction: application to organophosphorous compounds, Anal. Bioanal. Chem. 406 (2014) 2211–2215. https://doi.org/10.1007/s00216-013-7379-y.

[81] M.C. Prieto-Blanco, A. Argente-García, P. Campíns-Falcó, A capillary liquid chromatography method for benzalkonium chloride determination as a component or contaminant in mixtures of biocides, J. Chromatogr. A. 1431 (2016) 176–183. https://doi.org/10.1016/j.chroma.2015.12.073.

[82] N. Jornet-Martínez, C. Antón-Soriano, P. Campíns-Falcó, Estimation of the presence of unmetabolized dialkyl phthalates in untreated human urine by an on-line miniaturized reliable method, Sci. Total Environ. 532 (2015) 239–244. https://doi.org/10.1016/j.scitotenv.2015.05.124.

[83] A. Argente-García, Y. Moliner-Martínez, E. López-García, P. Campíns-Falcó, R. Herráez-Hernández, Application of Carbon Nanotubes Modified Coatings for the Determination of Amphetamines by In-Tube Solid-Phase Microextraction and Capillary Liquid Chromatography, Separations. 3 (2016) 7. https://doi.org/10.3390/chromatography3010007.

[84] M.C. Prieto-Blanco, S. Peñafiel Barba, Y. Moliner-Martínez, P.

Campíns-Falcó, Footprint of carbonyl compounds in hand scent by in-tube solid-phase microextraction coupled to nano-liquid chromatography/diode array detection, J. Chromatogr. A. 1596 (2019) 241–249. https://doi.org/10.1016/j.chroma.2019.03.007.

[85] R.A. González-Fuenzalida, L. Sanjuan-Navarro, Y. Moliner-Martínez, P. Campíns-Falcó, Quantitative study of the capture of silver nanoparticles by several kinds of soils, Sci. Total Environ. 630 (2018) 1226–1236. https://doi.org/10.1016/j.scitotenv.2018.02.307.

[86] A. Argente-García, L. Hakobyan, C. Guillem, P. Campíns-Falcó, Estimating Diphenylamine in Gunshot Residues from a New Tool for Identifying both Inorganic and Organic Residues in the Same Sample, Separations. 6 (2019) 16. https://doi.org/10.3390/separations6010016.

[87] P. Serra-Mora, R. Herráez-Hernández, P. Campíns-Falcó, Minimizing the impact of sample preparation on analytical results: In-tube solid-phase microextraction coupled on-line to nano-liquid chromatography for the monitoring of tribenuron methyl in environmental waters, Sci. Total Environ. 721 (2020). https://doi.org/10.1016/j.scitotenv.2020.137732.

[88] L. Sanjuan-Navarro, S. Cortés-Bautista, Y. Moliner-Martínez, P. Campíns-Falcó, In-tube solid phase microextraction coupled to miniaturized liquid chromatography for both, noble metal nanoparticle assessment and sensitive plasmonic assay development, Anal. Chim. Acta. 1171 (2021) 338665. https://doi.org/10.1016/j.aca.2021.338665.

[89] M.F. Mirabelli, J.-C. Wolf, R. Zenobi, Pesticide analysis at ppt concentration levels: coupling nano-liquid chromatography with dielectric barrier discharge ionization-mass spectrometry, Anal. Bioanal. Chem. 408 (2016) 3425–3434. https://doi.org/10.1007/s00216-016-9419-x.

[90] K. Murtada, F. de Andrés, Á. Ríos, M. Zougagh, A simple poly(styrene-co-divinylbenzene)-coated glass blood spot method for monitoring of seven antidepressants using capillary liquid chromatography-mass spectrometry, Talanta. 188 (2018) 772–778. https://doi.org/10.1016/j.talanta.2018.06.059.

[91] N. Danne-Rasche, C. Coman, R. Ahrends, Nano-LC/NSI MS Refines Lipidomics by Enhancing Lipid Coverage, Measurement Sensitivity, and Linear Dynamic Range, Anal. Chem. 90 (2018) 8093–8101. https://doi.org/10.1021/acs.analchem.8b01275.

[92] E.J. Carrasco-Correa, F. Vela-Soria, O. Ballesteros, G. Ramis-Ramos, J.M. Herrero-Martínez, Sensitive determination of parabens in human urine and serum using methacrylate monoliths and reversed-phase capillary liquid chromatography–mass spectrometry, J. Chromatogr. A. 1379 (2015) 65–73. https://doi.org/10.1016/j.chroma.2014.12.053.

[93] N. Albekairi, A. Aqel, Z.A. ALOthman, Simultaneous Capillary Liquid Chromatography Determination of Drugs in Pharmaceutical Preparations Using Tunable Platforms of Polymethacrylate Monolithic Columns Modified with Octadecylamine, Chromatographia. 82 (2019) 1003–1015. https://doi.org/10.1007/s10337-019-03739-4.

[94] S. Sharma, H.D. Tolley, P.B. Farnsworth, M.L. Lee, LED-Based UV Absorption Detector with Low Detection Limits for Capillary Liquid Chromatography, Anal. Chem. 87 (2015) 1381–1386. https://doi.org/10.1021/ac504275m.

[95] Y. Tang, N. Zhang, B. Zhang, X. Lei, X. Wu, On-line coupling of hydrophilic ionic liquids-based polymer monolith microextraction to capillary liquid chromatography with amperometric detection: An ultrasensitive residue analysis method for glycopeptide antibiotics, J. Chromatogr. A. 1556 (2018) 10–20. https://doi.org/10.1016/j.chroma.2018.04.063.

[96] V. Kahle, Fiber optic z-cell for cze, Biomed. Chromatogr. 13 (1999) 93–94. https://doi.org/10.1002/(SICI)1099-0801(199902)13:1<93::AID-BMC786>3.0.CO;2-9.

[97] J.P. Chervet, R.E.J. Van Soest, M. Ursem, Z-shaped flow cell for UV detection in capillary electrophoresis, J. Chromatogr. A. 543 (1991) 439–449. https://doi.org/10.1016/S0021-9673(01)95795-4.

[98] M. Macka, T. Piasecki, P.K. Dasgupta, Light-Emitting Diodes for Analytical Chemistry, Annu. Rev. Anal. Chem. 7 (2014) 183–207. https://doi.org/10.1146/annurev-anchem-071213-020059.

[99] Y. Li, M. Dvořák, P.N. Nesterenko, N. Nuchtavorn, M. Macka, High power deep UV-LEDs for analytical optical instrumentation, Sensors Actuators B Chem. 255 (2018) 1238–1243. https://doi.org/10.1016/j.snb.2017.08.085.

[100] Y. Li, P.N. Nesterenko, R. Stanley, B. Paull, M. Macka, High sensitivity deep-UV LED-based z-cell photometric detector for capillary liquid chromatography, Anal. Chim. Acta. 1032 (2018) 197–202.

https://doi.org/10.1016/j.aca.2018.06.005.

[101] A.-N. Neagu, M. Jayathirtha, E. Baxter, M. Donnelly, B.A. Petre, C.C. Darie, Applications of Tandem Mass Spectrometry (MS/MS) in Protein Analysis for Biomedical Research, Molecules. 27 (2022) 2411. https://doi.org/10.3390/molecules27082411.

[102] I. Manisali, D.D.Y. Chen, B.B. Schneider, Electrospray ionization source geometry for mass spectrometry: past, present, and future, TrAC Trends Anal. Chem. 25 (2006) 243–256. https://doi.org/10.1016/j.trac.2005.07.007.

[103] J.S. Page, I. Marginean, E.S. Baker, R.T. Kelly, K. Tang, R.D. Smith, Biases in ion transmission through an electrospray ionization-mass spectrometry capillary inlet, J. Am. Soc. Mass Spectrom. 20 (2009) 2265–2272. https://doi.org/10.1016/j.jasms.2009.08.018.

[104] M.S. Wilm, M. Mann, Electrospray and Taylor-Cone theory, Dole's beam of macromolecules at last?, Int. J. Mass Spectrom. Ion Process. 136 (1994) 167–180. https://doi.org/10.1016/0168-1176(94)04024-9.

[105] M.R. Emmett, R.M. Caprioli, Micro-electrospray mass spectrometry: Ultra-high-sensitivity analysis of peptides and proteins, J. Am. Soc. Mass Spectrom. 5 (1994) 605–613. https://doi.org/10.1016/1044-0305(94)85001-1.

[106] A.D. Lesiak, J.R. Shepard, Recent advances in forensic drug analysis by DART-MS, Bioanalysis. 6 (2014) 819–842. https://doi.org/10.4155/bio.14.31.

[107] J. Ji, J. Wang, Y. Zhang, Rapid screening of 23 synthetic cannabinoids in blood by direct analysis in real time - Tandem mass spectrometry, Int. J. Mass Spectrom. 469 (2021) 116667. https://doi.org/10.1016/j.ijms.2021.116667.

[108] W.L. Shelver, S. Chakrabarty, D.J. Smith, Rapid Screening Method for β-Adrenergic Agonist Residues Incurred in Animal Urine Using Direct Analysis in Real-Time Mass Spectrometry, ACS Food Sci. Technol. 2 (2022) 195–205. https://doi.org/10.1021/acsfoodscitech.1c00427.

[109] G.I. Baram, M.A. Grachev, N.I. Komarova, M.P. Perelroyzen, Y.A. Bolvanov, S. V. Kuzmin, V. V. Kargaltsev, E.A. Kuper, Micro-column liquid chromatography with multi-wave-length photometric detection. I. The OB-4 micro-column liquid chromatograph, J. Chromatogr. A. 264 (1983) 69–90. https://doi.org/10.1016/S0021-9673(01)95007-1.

[110] T. Otagawa, J.R. Stetter, S. Zaromb, Portable liquid chromatograph for analysis of primary aromatic amines in coal-derived materials, J. Chromatogr. A. 360 (1986) 252–259. https://doi.org/10.1016/S0021-9673(00)91671-6.

[111] G.I. Baram, Portable liquid chromatograph for mobile laboratories I. Aims, J. Chromatogr. A. 728 (1996) 387–399. https://doi.org/10.1016/0021-9673(95)01271-0.

[112] V.M. Tulchinsky, D.E. St. Angelo, A practical portable HPLC system?MINICHROM, a new generation for field HPLC, F. Anal. Chem. Technol. 2 (1998) 281–285. https://doi.org/10.1002/(SICI)1520-6521(1998)2:5<281::AID-FACT5>3.0.CO;2-V.

[113] C.B. Boring, P.K. Dasgupta, A. Sjögren, Compact, field-portable capillary ion chromatograph, J. Chromatogr. A. 804 (1998) 45–54. https://doi.org/10.1016/S0021-9673(98)00139-3.

[114] S. Sharma, A. Plistil, H.E. Barnett, H.D. Tolley, P.B. Farnsworth, S.D. Stearns, M.L. Lee, Hand-Portable Gradient Capillary Liquid Chromatography Pumping System, Anal. Chem. 87 (2015) 10457–10461. https://doi.org/10.1021/acs.analchem.5b02583.

[115] Y. Li, M. Dvořák, P.N. Nesterenko, R. Stanley, N. Nuchtavorn, L.K. Krčmová, J. Aufartová, M. Macka, Miniaturised medium pressure capillary liquid chromatography system with flexible open platform design using off-the-shelf microfluidic components, Anal. Chim. Acta. 896 (2015) 166–176. https://doi.org/10.1016/j.aca.2015.09.015.

[116] A. Ishida, M. Fujii, T. Fujimoto, S. Sasaki, I. Yanagisawa, H. Tani, M. Tokeshi, A portable liquid chromatograph with a battery-operated compact electroosmotic pump and a microfluidic chip device with a reversed phase packed column, Anal. Sci. 31 (2015) 1163–1169. https://doi.org/10.2116/analsci.31.1163.

[117] K.B. Lynch, A. Chen, Y. Yang, J.J. Lu, S. Liu, High-performance liquid chromatographic cartridge with gradient elution capability coupled with UV absorbance detector and mass spectrometer for peptide and protein analysis, J. Sep. Sci. 40 (2017) 2752–2758. https://doi.org/10.1002/jssc.201700185.

[118] S. Chatzimichail, D. Casey, A. Salehi-Reyhani, Zero electrical power pump for portable high-performance liquid chromatography, Analyst. 144 (2019) 6207–6213. https://doi.org/10.1039/C9AN01302D.

[119] S.C. Lam, L.J. Coates, M. Hemida, V. Gupta, P.R. Haddad, M. Macka, B. Paull, Miniature and fully portable gradient capillary liquid chromatograph, Anal. Chim. Acta. 1101 (2020) 199–210. https://doi.org/10.1016/j.aca.2019.12.014.

[120] D. Li, H. Chen, S. Ren, Y. Zhang, Y. Yang, H. Chang, Portable liquid chromatography for point-of-care testing of glycated haemoglobin, Sensors Actuators, B Chem. 305 (2020) 127484. https://doi.org/10.1016/j.snb.2019.127484.

[121] C. Fitzhenry, L. Jowett, P. Roche, K. Harrington, B. Moore, B. Paull, E. Murray, Portable analyser using two-dimensional ion chromatography with ultra-violet light-emitting diode-based absorbance detection for nitrate monitoring within both saline and freshwaters, J. Chromatogr. A. 1652 (2021) 462368. https://doi.org/10.1016/j.chroma.2021.462368.

[122] P.M. Nowak, P. Kościelniak, M. Tobiszewski, A. Ballester-Caudet, P. Campíns-Falcó, Overview of the three multicriteria approaches applied to a global assessment of analytical methods, TrAC Trends Anal. Chem. 133 (2020) 116065. https://doi.org/10.1016/j.trac.2020.116065.

[123] T. Otagawa, J.R. Stetter, S. Zaromb, Portable liquid chromatograph for analysis of primary aromatic amines in coal-derived materials, J. Chromatogr. A. 360 (1986) 252–259. https://doi.org/10.1016/S0021-9673(00)91671-6.

[124] G.I. Baram, Portable liquid chromatograph for mobile laboratories: I. Aims, J. Chromatogr. A. 728 (1996) 387–399. https://doi.org/10.1016/0021-9673(95)01271-0.

[125] V.M. Tulchinsky, D.E.S. Angelo, A Practical Portable HPLC System - MINICHROM, a New Generation for Field HPLC, F. Anal. Chem. Technol. 2 (1998) 281–285. https://doi.org/10.1002/(SICI)1520-6521(1998)2:5<281::AID-FACT5>3.0.CO;2-V.

[126] C.B. Boring, P.K. Dasgupta, A. Sjögren, Compact, field-portable capillary ion chromatograph, J. Chromatogr. A. 804 (1998) 45–54. https://doi.org/10.1016/S0021-9673(98)00139-3.

[127] S. Sharma, A. Plistil, H.E. Barnett, H.D. Tolley, P.B. Farnsworth, S.D. Stearns, M.L. Lee, Hand-Portable Gradient Capillary Liquid Chromatography Pumping System, Anal. Chem. 87 (2015) 10457–10461. https://doi.org/10.1021/acs.analchem.5b02583.

[128] K.B. Lynch, A. Chen, Y. Yang, J.J. Lu, S. Liu, High-performance liquid chromatographic cartridge with gradient elution capability coupled with UV absorbance detector and mass spectrometer for peptide and protein analysis, J. Sep. Sci. 40 (2017) 2752–2758. https://doi.org/10.1002/jssc.201700185.

[129] S. Chatzimichail, D. Casey, A. Salehi-Reyhani, Zero electrical power pump for portable high-performance liquid chromatography, Analyst. 144 (2019) 6207–6213. https://doi.org/10.1039/c9an01302d.

[130] S.W. Foster, X. Xie, M. Pham, P.A. Peaden, L.M. Patil, L.T. Tolley, P.B. Farnsworth, H.D. Tolley, M.L. Lee, J.P. Grinias, Portable capillary liquid chromatography for pharmaceutical and illicit drug analysis, J. Sep. Sci. 43 (2020) 1623–1627. https://doi.org/10.1002/jssc.201901276.

[131] S.C. Lam, L.J. Coates, M. Hemida, V. Gupta, P.R. Haddad, M. Macka, B. Paull, Miniature and fully portable gradient capillary liquid chromatograph, Anal. Chim. Acta. 1101 (2020) 199–210. https://doi.org/10.1016/j.aca.2019.12.014.

[132] F. Rahimi, S. Chatzimichail, A. Saifuddin, BETTER-HPLC, (2020). https://github.com/BETTER-HPLC/better-hplc.github.io (accessed May 23, 2023).

[133] S. Chatzimichail, F. Rahimi, A. Saifuddin, A.J. Surman, S.D. Taylor-Robinson, A. Salehi-Reyhani, Hand-portable HPLC with broadband spectral detection enables analysis of complex polycyclic aromatic hydrocarbon mixtures, Commun. Chem. 4 (2021) 17. https://doi.org/10.1038/s42004-021-00457-7.

[134] Y. Moliner-Martinez, A. Ballester-Caudet, J. Verdú-Andrés, R. Herráez-Hernández, C. Molins-Legua, P. Campíns-Falcó, In-tube solid-phase microextraction in Solid-Phase Extraction. A volume in Handbooks in Separation Science (Chapter 14), Elsevier, Amsterdam, Netherlands, 2019. https://doi.org/10.1016/B978-0-12-816906-3.00014-5.

[135] G. Rozing, Micropillar array columns for advancing nanoflow HPLC, Microchem. J. 170 (2021) 106629. https://doi.org/10.1016/j.microc.2021.106629.

[136] M. Hemida, A. Ghiasvand, V. Gupta, L.J. Coates, A.A. Gooley, H.-J. Wirth, P.R. Haddad, B. Paull, Small-Footprint, Field-Deployable LC/MS System for On-Site Analysis of Per- and Polyfluoroalkyl

Substances in Soil, Anal. Chem. 93 (2021) 12032–12040. https://doi.org/10.1021/acs.analchem.1c02193.

[137] A.N. Kozitsina, T.S. Svalova, N.N. Malysheva, A. V. Okhokhonin, M.B. Vidrevich, K.Z. Brainina, Sensors based on bio and biomimetic receptors in medical diagnostic, environment, and food analysis, Biosensors. 8 (2018) 1–34. https://doi.org/10.3390/bios8020035.

[138] S. Vashist, Point-of-Care Diagnostics: Recent Advances and Trends, Biosensors. 7 (2017) 62. https://doi.org/10.3390/bios7040062.

[139] N. Jornet-Martínez, S. Bocanegra-Rodríguez, R.A. González-Fuenzalida, C. Molins-Legua, P. Campíns-Falcó, In Situ Analysis Devices for Estimating the Environmental Footprint in Beverages Industry, Elsevier Inc., 2019. https://doi.org/10.1016/b978-0-12-815259-1.00009-4.

[140] J. V. Abonamah, B.A. Eckenrode, M. Moini, On-site detection of fentanyl and its derivatives by field portable nano-liquid chromatography-electron lonization-mass spectrometry (nLC-EI-MS), Forensic Chem. 16 (2019) 100180. https://doi.org/10.1016/j.forc.2019.100180.

[141] M.C. May, D.C. Pavone, I.S. Lurie, The separation and identification of synthetic cathinones by portable low microflow liquid chromatography with dual capillary columns in series and dual wavelength ultraviolet detection, J. Sep. Sci. 43 (2020) 3756–3764. https://doi.org/10.1002/jssc.202000767.

[142] C. Soto, H.D. Ponce-Rodríguez, J. Verdú-Andrés, R. Herráez-Hernández, P. Campíns-Falcó, Determination of caffeine in dietary supplements by miniaturized portable liquid chromatography, J. Chromatogr. A. 1664 (2022) 462770. https://doi.org/10.1016/j.chroma.2021.462770.

[143] C. Soto, H.D. Ponce-Rodríguez, J. Verdú-Andrés, P. Campíns-Falcó, R. Herráez-Hernández, Hand-Portable Miniaturized Liquid Chromatography for the Determination of Chlorogenic Acids in Dietary Supplements, Antioxidants. 11 (2022) 2408. https://doi.org/10.3390/antiox11122408.

[144] N. Jornet-Martínez, R. Herráez-Hernández, P. Campíns-Falcó, Scopolamine analysis in beverages: Bicolorimetric device vs portable nano liquid chromatography, Talanta. 232 (2021). https://doi.org/10.1016/j.talanta.2021.122406.

[145] M. Pham, S.W. Foster, S. Kurre, R.A. Hunter, J.P. Grinias, Use of Portable Capillary Liquid Chromatography for Common Educational Demonstrations Involving Separations, J. Chem. Educ. 98 (2021) 2444–2448. https://doi.org/10.1021/acs.jchemed.1c00342.

[146] N. Zhu, K.-W. Schramm, T. Wang, B. Henkelmann, X. Zheng, J. Fu, Y. Gao, Y. Wang, G. Jiang, Environmental fate and behavior of persistent organic pollutants in Shergyla Mountain, southeast of the Tibetan Plateau of China, Environ. Pollut. 191 (2014) 166–174. https://doi.org/10.1016/j.envpol.2014.04.031.

[147] D. Megson, E.J. Reiner, K.J. Jobst, F.L. Dorman, M. Robson, J.-F. Focant, A review of the determination of persistent organic pollutants for environmental forensics investigations, Anal. Chim. Acta. 941 (2016) 10–25. https://doi.org/10.1016/j.aca.2016.08.027.

[148] J. Aravind kumar, T. Krithiga, S. Sathish, A.A. Renita, D. Prabu, S. Lokesh, R. Geetha, S.K.R. Namasivayam, M. Sillanpaa, Persistent organic pollutants in water resources: Fate, occurrence, characterization and risk analysis, Sci. Total Environ. 831 (2022) 154808. https://doi.org/10.1016/j.scitotenv.2022.154808.

[149] European Union Council, Directive 2013/39/EU Of The European Parliment and of The Council of 12 August 2013 amending Directives 2000/60/EC and 2008/105/EC as regards priority substances in the field of water policy (Text, Hart Publishing, 2016. https://doi.org/10.5040/9781782258674.0032.

[150] Y. Abdulrazaq, A. Abdulsalam, A. Larayetan Rotimi, A. Aliyu Abdulbasit, O. Clifford, O. Abdulazeez Abdulsalam, O. Nayo Racheal, A. Akor Joy, F. Omale Victor, Z. Mbese Johannes, M. Bilal, S. Umar M, Classification, Potential Routes and Risk of Emerging Pollutants/Contaminant, in: Emerg. Contam., IntechOpen, 2021: p. 13. https://doi.org/10.5772/intechopen.94447.

[151] M. Salimi, A. Esrafili, M. Gholami, A. Jonidi Jafari, R. Rezaei Kalantary, M. Farzadkia, M. Kermani, H.R. Sobhi, Contaminants of emerging concern: a review of new approach in AOP technologies, Environ. Monit. Assess. 189 (2017) 414. https://doi.org/10.1007/s10661-017-6097-x.

[152] V.L.R. Pullagurala, S. Rawat, I.O. Adisa, J.A. Hernandez-Viezcas, J.R. Peralta-Videa, J.L. Gardea-Torresdey, Plant uptake and translocation of contaminants of emerging concern in soil, Sci. Total Environ. 636 (2018) 1585–1596.

https://doi.org/10.1016/j.scitotenv.2018.04.375.

[153] Y. Tang, Y. Zhong, H. Li, Y. Huang, X. Guo, F. Yang, Y. Wu, Contaminants of emerging concern in aquatic environment: Occurrence, monitoring, fate, and risk assessment, Water Environ. Res. 92 (2020) 1811–1817. https://doi.org/10.1002/wer.1438.

[154] A. Xabadia, E. Esteban, Y. Martinez, I. Ortuzar, Contaminants of Emerging Concern: A Review of Biological and Economic Principles to Guide Water Management Policies, Int. Rev. Environ. Resour. Econ. 15 (2021) 387–430. https://doi.org/10.1561/101.00000138.

[155] H. Sousa, C.A. Sousa, L.C. Simões, M. Simões, Microalgal-based removal of contaminants of emerging concern, J. Hazard. Mater. 423 (2022) 127153. https://doi.org/10.1016/j.jhazmat.2021.127153.

[156] T.M. Adeniji, K.J. Stine, Nanostructure Modified Electrodes for Electrochemical Detection of Contaminants of Emerging Concern, Coatings. 13 (2023) 381. https://doi.org/10.3390/coatings13020381.

[157] W. Aktar, D. Sengupta, A. Chowdhury, Impact of pesticides use in agriculture: their benefits and hazards, Interdiscip. Toxicol. 2 (2009) 1–12. https://doi.org/10.2478/v10102-009-0001-7.

[158] O. Tiryaki, C.T. Cinar, The fate of pesticide in the environment, J. Biol. Environ. Sci. 4 (2010) 29–38.

[159] V.I. Lushchak, T.M. Matviishyn, V. V. Husak, J.M. Storey, K.B. Storey, Pesticide toxicity: A mechanistic approach, EXCLI J. 17 (2018) 1101–1136. https://doi.org/10.17179/excli2018-1710.

[160] Official Journal of the European Union, Council Directive 98/83/EC of, Cambridge University Press, 2006. https://doi.org/10.1017/CBO9780511610851.055.

[161] European Union Council, Directive 2006/118/EC of the European Parliment and of the Council of 12 December 2006 on the protection of groundwater against pollution and deterioration, 2008. https://doi.org/10.5040/9781782258674.0025.

[162] European Union Council, Directive 2009/128/EC of the European Parliment and of the Council of 21 October 2009 establishing a framework for Community action to achieve the sustainable use of pesticides, 2009.

[163] M. Patel, R. Kumar, K. Kishor, T. Mlsna, C.U. Pittman, D. Mohan, Pharmaceuticals of Emerging Concern in Aquatic Systems:

Chemistry, Occurrence, Effects, and Removal Methods, Chem. Rev. 119 (2019) 3510–3673. https://doi.org/10.1021/acs.chemrev.8b00299.

[164] T. aus der Beek, F.-A. Weber, A. Bergmann, S. Hickmann, I. Ebert, A. Hein, A. Küster, Pharmaceuticals in the environment-Global occurrences and perspectives, Environ. Toxicol. Chem. 35 (2016) 823–835. https://doi.org/10.1002/etc.3339.

[165] K. FENT, A. WESTON, D. CAMINADA, Ecotoxicology of human pharmaceuticals, Aquat. Toxicol. 76 (2006) 122–159. https://doi.org/10.1016/j.aquatox.2005.09.009.

[166] A. Courtier, A. Cadiere, B. Roig, Human pharmaceuticals: Why and how to reduce their presence in the environment, Curr. Opin. Green Sustain. Chem. 15 (2019) 77–82. https://doi.org/10.1016/j.cogsc.2018.11.001.

[167] European Union Council, Directive 2008/105/EC of the European Parliment and of the Council of 16 December 2008 on environmental quality standards in the field of water policy, amending and subsequently repealing Council Directives 82/176/EEC, 83/513/EEC, 84/156/EEC, 84/491/EEC, 2007.

[168] Oficial Journal of th European Commission, Communication from the Commission to the European Parliament, the Council, and the European Economic and Social Committee: European Union Strategic Approach to Pharmaceuticals in the Environment, 2019.

[169] W. Koagouw, N.A. Stewart, C. Ciocan, Long-term exposure of marine mussels to paracetamol: is time a healer or a killer?, Environ. Sci. Pollut. Res. 28 (2021) 48823–48836. https://doi.org/10.1007/s11356-021-14136-6.

[170] H. Jeong, J. Park, H. Kim, Determination of NH 4 + in Environmental Water with Interfering Substances Using the Modified Nessler Method, J. Chem. 2013 (2013) 1–9. https://doi.org/10.1155/2013/359217.

[171] L.O.C. Šraj, M.I.G.S. Almeida, S.E. Swearer, S.D. Kolev, I.D. McKelvie, Analytical challenges and advantages of using flow-based methodologies for ammonia determination in estuarine and marine waters, TrAC Trends Anal. Chem. 59 (2014) 83–92. https://doi.org/10.1016/j.trac.2014.03.012.

[172] Bijay-Singh, E. Craswell, Fertilizers and nitrate pollution of surface and ground water: an increasingly pervasive global problem, SN Appl. Sci.

3 (2021) 1–24. https://doi.org/10.1007/s42452-021-04521-8.

[173] P.M. Glibert, J. Harrison, C. Heil, S. Seitzinger, Escalating Worldwide use of Urea – A Global Change Contributing to Coastal Eutrophication, Biogeochemistry. 77 (2006) 441–463. https://doi.org/10.1007/s10533-005-3070-5.

[174] R.W. Howarth, Coastal nitrogen pollution: A review of sources and trends globally and regionally, Harmful Algae. 8 (2008) 14–20. https://doi.org/10.1016/j.hal.2008.08.015.

[175] M. Parvizishad, A. Dalvand, A.H. Mahvi, F. Goodarzi, A Review of Adverse Effects and Benefits of Nitrate and Nitrite in Drinking Water and Food on Human Health, Heal. Scope. In Press (2017). https://doi.org/10.5812/jhealthscope.14164.

[176] M. Ward, R. Jones, J. Brender, T. de Kok, P. Weyer, B. Nolan, C. Villanueva, S. van Breda, Drinking Water Nitrate and Human Health: An Updated Review, Int. J. Environ. Res. Public Health. 15 (2018) 1557. https://doi.org/10.3390/ijerph15071557.

[177] K. Venkatesan, N. Deo, Biochemical Aspects, in: W.H. Organization (Ed.), IAL Textb. Lepr., 4th ed., Jaypee Brothers Medical Publishers (P) Ltd., Geneva, 2010: pp. 87–87. https://doi.org/10.5005/jp/books/11431_8.

[178] European Union Council, Council Directive 91/676/EEC of 12 December 1991 concerning the protection of waters against pollution caused by nitrates from agricultural sources, 1991.

[179] European Union Council, Directive 2000/60/EC Of The European Parliament And Of The Council of 23 October 2000 establishing a framework for Community action in the field of water policy, 2000. https://eur-lex.europa.eu/legal-content/EN/TXT/?uri=CELEX:32000L0060.

[180] Ministerio de Agricultura Alimentación y Medio ambiente, Real Decreto 817/2015, de 11 de septiembre, por el que se establecen los criterios de seguimiento y evaluación del estado de las aguas superficiales y las normas de calidad ambiental, 2015.

[181] J.B. Vaught, M.K. Henderson, Biological sample collection, processing, storage and information management., IARC Sci. Publ. (2011) 23–42.

[182] Parinya Panuwet, Ronald E. Hunter, P.E. D'Souza, X. Chen, J.R.C.

Samantha A. Radford, K.K. M. Elizabeth Marder, P.B. Ryan, Dana Boyd Barr, Biological Matrix Effects in Quantitative Tandem Mass Spectrometry-Based Analytical Methods: Advancing Biomonitoring, Physiol. Behav. 92 (2016) 135–140. https://doi.org/10.1080/10408347.2014.980775.Biological.

[183] K. Persona, K. Madej, P. Knihnicki, W. Piekoszewski, Analytical methodologies for the determination of benzodiazepines in biological samples, J. Pharm. Biomed. Anal. 113 (2015) 239–264. https://doi.org/10.1016/j.jpba.2015.02.017.

[184] J. Peng, F. Tang, R. Zhou, X. Xie, S. Li, F. Xie, P. Yu, L. Mu, New techniques of on-line biological sample processing and their application in the field of biopharmaceutical analysis, Acta Pharm. Sin. B. 6 (2016) 540–551. https://doi.org/10.1016/j.apsb.2016.05.016.

[185] B. Hu, B. Zheng, D. Rickert, G.A. Gómez-Ríos, B. Bojko, J. Pawliszyn, Z.P. Yao, Direct coupling of solid phase microextraction with electrospray ionization mass spectrometry: A Case study for detection of ketamine in urine, Anal. Chim. Acta. 1075 (2019) 112–119. https://doi.org/10.1016/j.aca.2019.05.044.

[186] E. Dmitrieva, A. Temerdashev, A. Azaryan, E. Gashimova, Quantification of steroid hormones in human urine by DLLME and UHPLC-HRMS detection, J. Chromatogr. B. 1159 (2020) 122390. https://doi.org/10.1016/j.jchromb.2020.122390.

[187] A.A. Matin, P. Biparva, M. Gheshlaghi, E.M. Khosrowshahi, K. Farhadi, Monolithic mixed matrix membrane based on polyethersulfone/functionalized MWCNTs nanocomposite as an SPME fiber: Application to extract chlorophenols from human urine and serum samples followed by GC-ECD, J. Chromatogr. B. 1150 (2020) 122190. https://doi.org/10.1016/j.jchromb.2020.122190.

[188] C. Ghosh, C.P. Shinde, B.S. Chakraborty, Influence of ionization source design on matrix effects during LC–ESI-MS/MS analysis, J. Chromatogr. B. 893–894 (2012) 193–200. https://doi.org/10.1016/j.jchromb.2012.03.012.

[189] W. Bernal, G. Auzinger, A. Dhawan, J. Wendon, Acute liver failure, Lancet. 376 (2010) 190–201. https://doi.org/10.1016/S0140-6736(10)60274-7.

[190] M.L. Alvarellos, E.M. McDonagh, S. Patel, H.L. McLeod, R.B. Altman, T.E. Klein, PharmGKB summary, Pharmacogenet. Genomics. 25

(2015) 622–630. https://doi.org/10.1097/FPC.0000000000000170.

[191] M.J. Hodgman, A.R. Garrard, A Review of Acetaminophen Poisoning, Crit. Care Clin. 28 (2012) 499–516. https://doi.org/10.1016/j.ccc.2012.07.006.

[192] P. Nagaraja, K.C. Srinivasa Murthy, K.S. Rangappa, Spectrophotometric method for the determination of paracetamol and phenacetin, J. Pharm. Biomed. Anal. 17 (1998) 501–506. https://doi.org/10.1016/S0731-7085(97)00237-9.

[193] F. Shihana, D. Dissanayake, P. Dargan, A. Dawson, A modified low-cost colorimetric method for paracetamol (acetaminophen) measurement in plasma, Clin. Toxicol. 48 (2010) 42–46. https://doi.org/10.3109/15563650903443137.

[194] F. Pourkarim, E. Rahimpour, M. Khoubnasabjafari, V. Jouyban-Gharamaleki, A. Gharakhani, A. Jouyban, Validation of a colorimetric method for determination of paracetamol in exhaled breath condensate, Chem. Pap. 75 (2021) 2901–2906. https://doi.org/10.1007/s11696-021-01520-2.

[195] Sirajuddin, A.R. Khaskheli, A. Shah, M.I. Bhanger, A. Niaz, S. Mahesar, Simpler spectrophotometric assay of paracetamol in tablets and urine samples, Spectrochim. Acta Part A Mol. Biomol. Spectrosc. 68 (2007) 747–751. https://doi.org/10.1016/j.saa.2006.12.055.

[196] L.B. Lyndgaard, F. van den Berg, A. de Juan, Quantification of paracetamol through tablet blister packages by Raman spectroscopy and multivariate curve resolution-alternating least squares, Chemom. Intell. Lab. Syst. 125 (2013) 58–66. https://doi.org/10.1016/j.chemolab.2013.03.014.

[197] M. DELOSAOLIVA, R. OLSINA, A. MASI, Selective spectrofluorimetric method for paracetamol determination through coumarinic compound formation, Talanta. 66 (2005) 229–235. https://doi.org/10.1016/j.talanta.2004.11.015.

[198] T. Madrakian, A. Afkhami, M. Mohammadnejad, Second-order advantage applied to simultaneous spectrofluorimetric determination of paracetamol and mefenamic acid in urine samples, Anal. Chim. Acta. 645 (2009) 25–29. https://doi.org/10.1016/j.aca.2009.05.002.

[199] F. Tadayon, S. Vahed, H. Bagheri, Au-Pd/reduced graphene oxide composite as a new sensing layer for electrochemical determination of ascorbic acid, acetaminophen and tyrosine, Mater. Sci. Eng. C. 68

(2016) 805–813. https://doi.org/10.1016/j.msec.2016.07.039.

[200] S. Sharifian, A. Nezamzadeh-Ejhieh, Modification of carbon paste electrode with Fe(III)-clinoptilolite nano-particles for simultaneous voltammetric determination of acetaminophen and ascorbic acid, Mater. Sci. Eng. C. 58 (2016) 510–520. https://doi.org/10.1016/j.msec.2015.08.071.

[201] Z. Jiang, G. Li, M. Zhang, A novel electrochemical sensor based on SH-β-cyclodextrin functionalized gold nanoparticles/reduced-graphene oxide nanohybrids for ultrasensitive electrochemical sensing of acetaminophen and ofloxacin, Int. J. Electrochem. Sci. 12 (2017) 5157–5173. https://doi.org/10.20964/2017.06.28.

[202] H. Montaseri, P.B.C. Forbes, Analytical techniques for the determination of acetaminophen: A review, TrAC Trends Anal. Chem. 108 (2018) 122–134. https://doi.org/10.1016/j.trac.2018.08.023.

[203] P. Soysa, S. Kolambage, Rapid HPLC/UV method for analysis of urinary and plasma/serum paracetamol concentrations, J. Natl. Sci. Found. Sri Lanka. 38 (2010) 131. https://doi.org/10.4038/jnsfsr.v38i2.2039.

[204] R.K.T. Kam, M.H.M. Chan, H.T. Wong, A. Ghose, A.M. Dondorp, K. Plewes, J. Tarning, Quantitation of paracetamol by liquid chromatography-mass spectrometry in human plasma in support of clinical trial, Futur. Sci. OA. 4 (2018). https://doi.org/10.4155/fsoa-2018-0039.

[205] W. Lu, S. Zhao, M. Gong, L. Sun, L. Ding, Simultaneous determination of acetaminophen and oxycodone in human plasma by LC–MS/MS and its application to a pharmacokinetic study, J. Pharm. Anal. 8 (2018) 160–167. https://doi.org/10.1016/j.jpha.2018.01.006.

[206] D. Vilas, S. Reddy, A Rapid LC-MS/MS Method for Quantification of Acetaminophen in Human Whole Blood, 11 (2020) 1–6. https://doi.org/10.35248/2157-7064.20.11.432.Copyright.

[207] D.N. Ingram, G.N. Bosse, E.P. Womack, S. Jortani, Evaluation of a urine screen for acetaminophen., J. Med. Toxicol. 4 (2008) 96–100. https://doi.org/10.1007/BF03160962.

[208] A.A. Yaqoob, H. Ahmad, T. Parveen, A. Ahmad, M. Oves, I.M.I. Ismail, H.A. Qari, K. Umar, M.N. Mohamad Ibrahim, Recent Advances in Metal Decorated Nanomaterials and Their Various Biological Applications: A Review, Front. Chem. 8 (2020) 1–23.

https://doi.org/10.3389/fchem.2020.00341.

[209] N. Venkatesh, Metallic Nanoparticle: A Review, Biomed. J. Sci. Tech. Res. 4 (2018) 3765–3775. https://doi.org/10.26717/BJSTR.2018.04.0001011.

[210] A. Schröfel, G. Kratošová, I. Šafařík, M. Šafaříková, I. Raška, L.M. Shor, Applications of biosynthesized metallic nanoparticles - A review, Acta Biomater. 10 (2014) 4023–4042. https://doi.org/10.1016/j.actbio.2014.05.022.

[211] P.G. Jamkhande, N.W. Ghule, A.H. Bamer, M.G. Kalaskar, Metal nanoparticles synthesis: An overview on methods of preparation, advantages and disadvantages, and applications, J. Drug Deliv. Sci. Technol. 53 (2019) 101174. https://doi.org/10.1016/j.jddst.2019.101174.

[212] S. Putta, R.K. Sharma, P. Khandelwal, Metal Nanoparticles: Synthesis, Characterization, and Biomedical Applications, in: Nanomaterials, Springer Nature Singapore, Singapore, 2023: pp. 85–102. https://doi.org/10.1007/978-981-19-7963-7_4.

[213] V. Chandrakala, V. Aruna, G. Angajala, Review on metal nanoparticles as nanocarriers: current challenges and perspectives in drug delivery systems, Emergent Mater. 5 (2022) 1593–1615. https://doi.org/10.1007/s42247-021-00335-x.

[214] S. Das, R. Kotcherlakota, C.R. Patra, Noninvasive Imaging Techniques of Metal Nanoparticles and Their Future Diagnostic Applications, in: Med. Imaging Methods, Springer Singapore, Singapore, 2019: pp. 119–141. https://doi.org/10.1007/978-981-13-9121-7_5.

[215] D.N. Păduraru, D. Ion, A.-G. Niculescu, F. Mușat, O. Andronic, A.M. Grumezescu, A. Bolocan, Recent Developments in Metallic Nanomaterials for Cancer Therapy, Diagnosing and Imaging Applications, Pharmaceutics. 14 (2022) 435. https://doi.org/10.3390/pharmaceutics14020435.

[216] A. Gupta, M. Tandon, A. Kaur, Role of metallic nanoparticles in water remediation with special emphasis on sustainable synthesis: a review, Nanotechnol. Environ. Eng. 5 (2020) 27. https://doi.org/10.1007/s41204-020-00092-y.

[217] L. H Madkour, Ecofriendly green biosynthesized of metallic nanoparticles: Bio-reduction mechanism, characterization and

pharmaceutical applications in biotechnology industry, Glob. Drugs Ther. 3 (2017) 1–11. https://doi.org/10.15761/GDT.1000144.

[218] N. Narayan, A. Meiyazhagan, R. Vajtai, Metal nanoparticles as green catalysts, Materials (Basel). 12 (2019) 1–12. https://doi.org/10.3390/ma12213602.

[219] A.J. Shnoudeh, I. Hamad, R.W. Abdo, L. Qadumii, A.Y. Jaber, H.S. Surchi, S.Z. Alkelany, Synthesis, Characterization, and Applications of Metal Nanoparticles, in: Biomater. Bionanotechnol., Elsevier, 2019: pp. 527–612. https://doi.org/10.1016/B978-0-12-814427-5.00015-9.

[220] S. Mourdikoudis, R.M. Pallares, N.T.K. Thanh, Characterization techniques for nanoparticles: comparison and complementarity upon studying nanoparticle properties, Nanoscale. 10 (2018) 12871–12934. https://doi.org/10.1039/C8NR02278J.

[221] J. Jana, M. Ganguly, T. Pal, Enlightening surface plasmon resonance effect of metal nanoparticles for practical spectroscopic application, RSC Adv. 6 (2016) 86174–86211. https://doi.org/10.1039/c6ra14173k.

[222] T. Yu, Q. Wei, Plasmonic molecular assays: Recent advances and applications for mobile health, Nano Res. 11 (2018) 5439–5473. https://doi.org/10.1007/s12274-018-2094-9.

[223] G. Pasparakis, Recent developments in the use of gold and silver nanoparticles in biomedicine, WIREs Nanomedicine and Nanobiotechnology. 14 (2022) 1–22. https://doi.org/10.1002/wnan.1817.

[224] S. Unser, I. Bruzas, J. He, L. Sagle, Localized Surface Plasmon Resonance Biosensing: Current Challenges and Approaches, Sensors. 15 (2015) 15684–15716. https://doi.org/10.3390/s150715684.

[225] Y.-C. Yeh, B. Creran, V.M. Rotello, Gold nanoparticles: preparation, properties, and applications in bionanotechnology, Nanoscale. 4 (2012) 1871–1880. https://doi.org/10.1039/C1NR11188D.

[226] T.A. El-Brolossy, T. Abdallah, M.B. Mohamed, S. Abdallah, K. Easawi, S. Negm, H. Talaat, Shape and size dependence of the surface plasmon resonance of gold nanoparticles studied by Photoacoustic technique, Eur. Phys. J. Spec. Top. 153 (2008) 361–364. https://doi.org/10.1140/epjst/e2008-00462-0.

[227] E. Ringe, J. Zhang, M.R. Langille, K. Sohn, C. Cobley, L. Au, Y. Xia, C.A. Mirkin, J. Huang, L.D. Marks, R.P. Van Duyne, Effect of Size, Shape, Composition, and Support Film on Localized Surface Plasmon Resonance Frequency: A Single Particle Approach Applied to Silver Bipyramids and Gold and Silver Nanocubes, MRS Proc. 1208 (2009) 1208-O10-02. https://doi.org/10.1557/PROC-1208-O10-02.

[228] D.H. Anjum, Characterization of nanomaterials with transmission electron microscopy, IOP Conf. Ser. Mater. Sci. Eng. 146 (2016) 012001. https://doi.org/10.1088/1757-899X/146/1/012001.

[229] A.E. Vladár, V.-D. Hodoroaba, Characterization of nanoparticles by scanning electron microscopy, in: V.D. Hodoroaba, W. Unger, A. Shard (Eds.), Charact. Nanoparticles, 1st ed., Elsevier, Amsterdam, Netherlands, 2020: pp. 7–27. https://doi.org/10.1016/B978-0-12-814182-3.00002-X.

[230] C.F. Holder, R.E. Schaak, Tutorial on Powder X-ray Diffraction for Characterizing Nanoscale Materials, ACS Nano. 13 (2019) 7359–7365. https://doi.org/10.1021/acsnano.9b05157.

[231] P.M. Carvalho, M.R. Felício, N.C. Santos, S. Gonçalves, M.M. Domingues, Application of light scattering techniques to nanoparticle characterization and development, Front. Chem. 6 (2018) 1–17. https://doi.org/10.3389/fchem.2018.00237.

[232] S. Behzadi, F. Ghasemi, M. Ghalkhani, A.A. Ashkarran, S.M. Akbari, S. Pakpour, M.R. Hormozi-Nezhad, Z. Jamshidi, S. Mirsadeghi, R. Dinarvand, F. Atyabi, M. Mahmoudi, Determination of nanoparticles using UV-Vis spectra, Nanoscale. 7 (2015) 5134–5139. https://doi.org/10.1039/c4nr00580e.

[233] M.M. Eid, Characterization of Nanoparticles by FTIR and FTIR-Microscopy, in: Handb. Consum. Nanoproducts, Springer Nature Singapore, Singapore, 2022: pp. 645–673. https://doi.org/10.1007/978-981-16-8698-6_89.

[234] R. Bellotti, G.B. Picotto, L. Ribotta, AFM Measurements and Tip Characterization of Nanoparticles with Different Shapes, Nanomanufacturing Metrol. 5 (2022) 127–138. https://doi.org/10.1007/s41871-022-00125-x.

[235] R.A. González-Fuenzalida, Y. Moliner-Martínez, C. Molins-Legua, V. Parada-Artigues, J. Verdú-Andrés, P. Campins-Falcó, New Tools for Characterizing Metallic Nanoparticles: AgNPs, A Case Study, Anal.

Chem. 88 (2016) 1485–1493. https://doi.org/10.1021/acs.analchem.5b04751.

[236] R.A. González-Fuenzalida, Y. Moliner-Martínez, C. Molins-Legua, P. Campíns-Falcó, Miniaturized liquid chromatography coupled on-line to in-tube solid-phase microextraction for characterization of metallic nanoparticles using plasmonic measurements. A tutorial, Anal. Chim. Acta. 1045 (2019) 23–41. https://doi.org/10.1016/j.aca.2018.07.073.

[237] C.C. Novoa, G. Tortella, A.B. Seabra, M.C. Diez, O. Rubilar, Cotton Textile with Antimicrobial Activity and Enhanced Durability Produced by L-Cysteine-Capped Silver Nanoparticles, Processes. 10 (2022) 958. https://doi.org/10.3390/pr10050958.

[238] P. Velmurugan, J. Shim, K.-S. Bang, B.-T. Oh, Gold nanoparticles mediated coloring of fabrics and leather for antibacterial activity, J. Photochem. Photobiol. B Biol. 160 (2016) 102–109. https://doi.org/10.1016/j.jphotobiol.2016.03.051.

[239] A. Istiqola, A. Syafiuddin, A review of silver nanoparticles in food packaging technologies: Regulation, methods, properties, migration, and future challenges, J. Chinese Chem. Soc. 67 (2020) 1942–1956. https://doi.org/10.1002/jccs.202000179.

[240] S. Paidari, S.A. Ibrahim, Potential application of gold nanoparticles in food packaging: a mini review, Gold Bull. 54 (2021) 31–36. https://doi.org/10.1007/s13404-021-00290-9.

[241] W.T.J. Ong, K.L. Nyam, Evaluation of silver nanoparticles in cosmeceutical and potential biosafety complications, Saudi J. Biol. Sci. 29 (2022) 2085–2094. https://doi.org/10.1016/j.sjbs.2022.01.035.

[242] M. Ben Haddada, E. Gerometta, R. Chawech, J. Sorres, A. Bialecki, S. Pesnel, J. Spadavecchia, A.-L. Morel, Assessment of antioxidant and dermoprotective activities of gold nanoparticles as safe cosmetic ingredient, Colloids Surfaces B Biointerfaces. 189 (2020) 110855. https://doi.org/10.1016/j.colsurfb.2020.110855.

[243] Y. Yuan, S. Zhang, J. Hwang, I. Kong, Silver Nanoparticles Potentiates Cytotoxicity and Apoptotic Potential of Camptothecin in Human Cervical Cancer Cells, Oxid. Med. Cell. Longev. 2018 (2018) 1–21. https://doi.org/10.1155/2018/6121328.

[244] S. Prabhu, S. Vinodhini, C. Elanchezhiyan, D. Rajeswari, Retracted : Evaluation of antidiabetic activity of biologically synthesized silver nanoparticles using Pouteria sapota in streptozotocin-induced

diabetic rats, J. Diabetes. 10 (2018) 28–42. https://doi.org/10.1111/1753-0407.12554.

[245] M. Yafout, A. Ousaid, Y. Khayati, I.S. El Otmani, Gold nanoparticles as a drug delivery system for standard chemotherapeutics: A new lead for targeted pharmacological cancer treatments, Sci. African. 11 (2021) e00685. https://doi.org/10.1016/j.sciaf.2020.e00685.

[246] B. Klębowski, J. Depciuch, M. Parlińska-Wojtan, J. Baran, Applications of noble metal-based nanoparticles in medicine, Int. J. Mol. Sci. 19 (2018). https://doi.org/10.3390/ijms19124031.

[247] P. Tan, H. Li, J. Wang, S.C.B. Gopinath, Silver nanoparticle in biosensor and bioimaging: Clinical perspectives, Biotechnol. Appl. Biochem. 68 (2020) bab.2045. https://doi.org/10.1002/bab.2045.

[248] G. Doria, J. Conde, B. Veigas, L. Giestas, C. Almeida, M. Assunção, J. Rosa, P. V. Baptista, Noble Metal Nanoparticles for Biosensing Applications, Sensors. 12 (2012) 1657–1687. https://doi.org/10.3390/s120201657.

[249] M. Bouché, J.C. Hsu, Y.C. Dong, J. Kim, K. Taing, D.P. Cormode, Recent Advances in Molecular Imaging with Gold Nanoparticles, Bioconjug. Chem. 31 (2020) 303–314. https://doi.org/10.1021/acs.bioconjchem.9b00669.

[250] S. Slomkowski, J. V Alemán, R.G. Gilbert, M. Hess, K. Horie, R.G. Jones, P. Kubisa, I. Meisel, W. Mormann, S. Penczek, R.F.T. Stepto, Terminology of polymers and polymerization processes in dispersed systems (IUPAC Recommendations 2011), Pure Appl. Chem. 83 (2011) 2229–2259. https://doi.org/10.1351/PAC-REC-10-06-03.

[251] P. van der Schoot, Nanoparticle dispersions: A colloid and polymer solution perspective, in: J. Lagerwall, G. Scalia (Eds.), Liq. Cryst. with Nano Microparticles, World Scientific Publishing, Singapore, 2016: pp. 95–133. https://doi.org/10.1142/9789814619264_0003.

[252] F. Matter, A.L. Luna, M. Niederberger, From colloidal dispersions to aerogels: How to master nanoparticle gelation, Nano Today. 30 (2020) 100827. https://doi.org/10.1016/j.nantod.2019.100827.

[253] A.R. Studart, E. Amstad, L.J. Gauckler, Colloidal stabilization of nanoparticles in concentrated suspensions, Langmuir. 23 (2007) 1081–1090. https://doi.org/10.1021/la062042s.

[254] A. Heuer-Jungemann, N. Feliu, I. Bakaimi, M. Hamaly, A. Alkilany, I.

Chakraborty, A. Masood, M.F. Casula, A. Kostopoulou, E. Oh, K. Susumu, M.H. Stewart, I.L. Medintz, E. Stratakis, W.J. Parak, A.G. Kanaras, The Role of Ligands in the Chemical Synthesis and Applications of Inorganic Nanoparticles, Chem. Rev. 119 (2019) 4819–4880. https://doi.org/10.1021/acs.chemrev.8b00733.

[255] M. Pan, J. Yang, K. Liu, Z. Yin, T. Ma, S. Liu, L. Xu, S. Wang, Noble Metal Nanostructured Materials for Chemical and Biosensing Systems, Nanomaterials. 10 (2020) 209. https://doi.org/10.3390/nano10020209.

[256] H.K. Choi, M.-J. Lee, S.N. Lee, T.-H. Kim, B.-K. Oh, Noble Metal Nanomaterial-Based Biosensors for Electrochemical and Optical Detection of Viruses Causing Respiratory Illnesses, Front. Chem. 9 (2021) 1–9. https://doi.org/10.3389/fchem.2021.672739.

[257] A. Gautam, P. Komal, P. Gautam, A. Sharma, N. Kumar, J.P. Jung, Recent Trends in Noble Metal Nanoparticles for Colorimetric Chemical Sensing and Micro-Electronic Packaging Applications, Metals (Basel). 11 (2021) 329. https://doi.org/10.3390/met11020329.

[258] V. Montes-García, M.A. Squillaci, M. Diez-Castellnou, Q.K. Ong, F. Stellacci, P. Samorì, Chemical sensing with Au and Ag nanoparticles, Chem. Soc. Rev. 50 (2021) 1269–1304. https://doi.org/10.1039/D0CS01112F.

[259] H. Singh, A. Bamrah, S.K. Bhardwaj, A. Deep, M. Khatri, R.J.C. Brown, N. Bhardwaj, K.-H. Kim, Recent advances in the application of noble metal nanoparticles in colorimetric sensors for lead ions, Environ. Sci. Nano. 8 (2021) 863–889. https://doi.org/10.1039/D0EN00963F.

[260] L. Tan, M. Wei, L. Shang, Y. Yang, Cucurbiturils-Mediated Noble Metal Nanoparticles for Applications in Sensing, SERS, Theranostics, and Catalysis, Adv. Funct. Mater. 31 (2021) 2007277. https://doi.org/10.1002/adfm.202007277.

[261] A. Scroccarello, F. Della Pelle, M. Del Carlo, D. Compagnone, Optical plasmonic sensing based on nanomaterials integrated in solid supports. A critical review, Anal. Chim. Acta. 1237 (2023) 340594. https://doi.org/10.1016/j.aca.2022.340594.

[262] V. Amendola, R. Pilot, M. Frasconi, O.M. Maragò, M.A. Iatì, Surface plasmon resonance in gold nanoparticles: a review, J. Phys. Condens. Matter. 29 (2017) 203002. https://doi.org/10.1088/1361-648X/aa60f3.

[263] L. Guo, Y. Xu, A.R. Ferhan, G. Chen, D.-H. Kim, Oriented Gold Nanoparticle Aggregation for Colorimetric Sensors with Surprisingly High Analytical Figures of Merit, J. Am. Chem. Soc. 135 (2013) 12338–12345. https://doi.org/10.1021/ja405371g.

[264] M. Nilam, A. Hennig, W.M. Nau, K.I. Assaf, Gold nanoparticle aggregation enables colorimetric sensing assays for enzymatic decarboxylation, Anal. Methods. 9 (2017) 2784–2787. https://doi.org/10.1039/C7AY00642J.

[265] L. Zou, R. Shen, L. Ling, G. Li, Sensitive DNA detection by polymerase chain reaction with gold nanoparticles, Anal. Chim. Acta. 1038 (2018) 105–111. https://doi.org/10.1016/j.aca.2018.07.006.

[266] N. Jornet-Martínez, M. Gonzállez-Béjar, Y. Moliner-Martínez, P. Capíns-Falcó, J. Pérez-Prieto, Sensitive and Selective Plasmonic Assay for Spermine as Biomarker in Human Urine, Anal. Chem. 86 (2014) 1347–1351. https://doi.org/dx.doi.org/10.1021/ac404165j.

[267] M. Shellaiah, T. Simon, P. Venkatesan, K.W. Sun, F.-H. Ko, S.-P. Wu, Nanodiamonds conjugated to gold nanoparticles for colorimetric detection of clenbuterol and chromium(III) in urine, Microchim. Acta. 185 (2018) 74. https://doi.org/10.1007/s00604-017-2611-7.

[268] G. Liu, X. Yang, T. Li, H. Yu, X. Du, Y. She, J. Wang, S. Wang, F. Jin, M. Jin, H. Shao, L. Zheng, Y. Zhang, P. Zhou, Spectrophotometric and visual detection of the herbicide atrazine by exploiting hydrogen bond-induced aggregation of melamine-modified gold nanoparticles, Microchim. Acta. 182 (2015) 1983–1989. https://doi.org/10.1007/s00604-015-1531-7.

[269] N. Gao, P. Huang, F. Wu, Colorimetric detection of melamine in milk based on Triton X-100 modified gold nanoparticles and its paper-based application, Spectrochim. Acta Part A Mol. Biomol. Spectrosc. 192 (2018) 174–180. https://doi.org/10.1016/j.saa.2017.11.022.

[270] K. Mousapour, S. Hajizadeh, K. Farhadi, Colorimetric speciation analysis of chromium using 2-thiobarbituric acid capped silver nanoparticles, Anal. Methods. 12 (2020) 2484–2490. https://doi.org/10.1039/D0AY00160K.

[271] J. Zhu, L. Yin, W. Zhang, M. Chen, D. Feng, Y. Zhao, Y. Zhu, Colorimetric Measurement of Deltamethrin Pesticide Using a Paper Sensor Based on Aggregation of Gold Nanoparticles, Coatings. 12 (2021) 38. https://doi.org/10.3390/coatings12010038.

[272] S. Smita, S.K. Gupta, A. Bartonova, M. Dusinska, A.C. Gutleb, Q. Rahman, Nanoparticles in the environment: assessment using the causal diagram approach, Environ. Heal. 11 (2012) S13. https://doi.org/10.1186/1476-069X-11-S1-S13.

[273] S.M. Louie, R. Ma, G. V. Lowry, Transformations of Nanomaterials in the Environment, Front. Nanosci. 7 (2014) 55–87. https://doi.org/10.1016/B978-0-08-099408-6.00002-5.

[274] Q. Abbas, B. Yousaf, Amina, M.U. Ali, M.A.M. Munir, A. El-Naggar, J. Rinklebe, M. Naushad, Transformation pathways and fate of engineered nanoparticles (ENPs) in distinct interactive environmental compartments: A review, Environ. Int. 138 (2020) 105646. https://doi.org/10.1016/j.envint.2020.105646.

[275] S. Das, D. Ghosh, K. Kerkar, M. Tiwari, D.K. Tiwari, Effects of the Transformation of Metallic Nanoparticles in the Environment and Its Toxicity on Aquatic and Terrestrial Life Forms, in: Mol. Integr. Toxicol., 2021: pp. 43–71. https://doi.org/10.1007/978-3-030-83446-3_3.

[276] S.-J. Chao, C.P. Huang, C.-C. Lam, L.-C. Hua, S.-H. Chang, C. Huang, Transformation of copper oxide nanoparticles as affected by ionic strength and its effects on the toxicity and bioaccumulation of copper in zebrafish embryo, Ecotoxicol. Environ. Saf. 225 (2021) 112759. https://doi.org/10.1016/j.ecoenv.2021.112759.

[277] S. Lekamge, A.F. Miranda, A. Abraham, V. Li, R. Shukla, V. Bansal, D. Nugegoda, The toxicity of silver nanoparticles (AgNPs) to three freshwater invertebrates with different life strategies: Hydra vulgaris, Daphnia carinata, and Paratya australiensis, Front. Environ. Sci. 6 (2018) 1–13. https://doi.org/10.3389/fenvs.2018.00152.

[278] Z. Ferdous, A. Nemmar, Health impact of silver nanoparticles: A review of the biodistribution and toxicity following various routes of exposure, 2020. https://doi.org/10.3390/ijms21072375.

[279] M.A. Kakakhel, F. Wu, W. Sajjad, Q. Zhang, I. Khan, K. Ullah, W. Wang, Long-term exposure to high-concentration silver nanoparticles induced toxicity, fatality, bioaccumulation, and histological alteration in fish (Cyprinus carpio), Environ. Sci. Eur. 33 (2021). https://doi.org/10.1186/s12302-021-00453-7.

[280] E. Navarro, F. Piccapietra, B. Wagner, F. Marconi, R. Kaegi, N. Odzak, L. Sigg, R. Behra, Toxicity of Silver Nanoparticles to Chlamydomonas reinhardtii, Environ. Sci. Technol. 42 (2008) 8959–

8964. https://doi.org/10.1021/es801785m.

[281] J. Jiravova, K.B. Tomankova, M. Harvanova, L. Malina, J. Malohlava, L. Luhova, A. Panacek, B. Manisova, H. Kolarova, The effect of silver nanoparticles and silver ions on mammalian and plant cells in vitro, Food Chem. Toxicol. 96 (2016) 50–61. https://doi.org/10.1016/j.fct.2016.07.015.

[282] A.-J. Miao, Z. Luo, C.-S. Chen, W.-C. Chin, P.H. Santschi, A. Quigg, Intracellular Uptake: A Possible Mechanism for Silver Engineered Nanoparticle Toxicity to a Freshwater Alga Ochromonas danica, PLoS One. 5 (2010) e15196. https://doi.org/10.1371/journal.pone.0015196.

[283] F. Piccapietra, C.G. Allué, L. Sigg, R. Behra, Intracellular Silver Accumulation in Chlamydomonas reinhardtii upon Exposure to Carbonate Coated Silver Nanoparticles and Silver Nitrate, Environ. Sci. Technol. 46 (2012) 7390–7397. https://doi.org/10.1021/es300734m.

[284] C. Zhang, Z. Hu, B. Deng, Silver nanoparticles in aquatic environments: Physiochemical behavior and antimicrobial mechanisms, Water Res. 88 (2016) 403–427. https://doi.org/10.1016/j.watres.2015.10.025.

[285] X. Zhang, Z. Xu, A. Wimmer, H. Zhang, J. Wang, Q. Bao, Z. Gu, M. Zhu, L. Zeng, L. Li, Mechanism for sulfidation of silver nanoparticles by copper sulfide in water under aerobic conditions, Environ. Sci. Nano. 5 (2018) 2819–2829. https://doi.org/10.1039/C8EN00651B.

[286] C. Levard, E.M. Hotze, B.P. Colman, A.L. Dale, L. Truong, X.Y. Yang, A.J. Bone, G.E. Brown, R.L. Tanguay, R.T. Di Giulio, E.S. Bernhardt, J.N. Meyer, M.R. Wiesner, G. V. Lowry, Sulfidation of silver nanoparticles: Natural antidote to their toxicity, Environ. Sci. Technol. 47 (2013) 13440–13448. https://doi.org/10.1021/es403527n.

[287] C. Levard, S. Mitra, T. Yang, A.D. Jew, A.R. Badireddy, G. V. Lowry, G.E. Brown, Effect of chloride on the dissolution rate of silver nanoparticles and toxicity to E. coli, Environ. Sci. Technol. 47 (2013) 5738–5745. https://doi.org/10.1021/es400396f.

[288] S. Garg, H. Rong, C.J. Miller, T.D. Waite, Oxidative Dissolution of Silver Nanoparticles by Chlorine: Implications to Silver Nanoparticle Fate and Toxicity, Environ. Sci. Technol. 50 (2016) 3890–3896. https://doi.org/10.1021/acs.est.6b00037.

[289] Y. Yin, X. Yang, X. Zhou, W. Wang, S. Yu, J. Liu, G. Jiang, Water

chemistry controlled aggregation and photo-transformation of silver nanoparticles in environmental waters, J. Environ. Sci. 34 (2015) 116–125. https://doi.org/10.1016/j.jes.2015.04.005.

[290] Z. Zhang, X. Yang, M. Shen, Y. Yin, J. Liu, Sunlight-driven reduction of silver ion to silver nanoparticle by organic matter mitigates the acute toxicity of silver to Daphnia magna, J. Environ. Sci. 35 (2015) 62–68. https://doi.org/10.1016/j.jes.2015.03.007.

[291] G.L. Hallett-Tapley, C. D'Alfonso, N.L. Pacioni, C.D. McTiernan, M. González-Béjar, O. Lanzalunga, E.I. Alarcon, J.C. Scaiano, Gold nanoparticle catalysis of the cis–trans isomerization of azobenzene, Chem. Commun. 49 (2013) 10073. https://doi.org/10.1039/c3cc41669k.

[292] B.G. Ribeiro, P.R.D.B.S. David, T.P.P. Daltro, L.V.C. Charamba, M.F. de Andrade, D.C. Napoleão, Performance verification of methodology for determination of nitrate ion in drinking water samples, Rev. Eletrônica Em Gestão, Educ. e Tecnol. Ambient. 22 (2018) 2. https://doi.org/10.5902/2236117031383.

[293] L. Hakobyan, B. Monforte-Gómez, Y. Moliner-Martínez, C. Molins-Legua, P. Campíns-Falcó, Improving Sustainability of the Griess Reaction by Reagent Stabilization on PDMS Membranes and ZnNPs as Reductor of Nitrates: Application to Different Water Samples, Polymers (Basel). 14 (2022) 464. https://doi.org/10.3390/polym14030464.

[294] M.C. Prieto-Blanco, N. Jornet-Martínez, Y. Moliner-Martínez, C. Molins-Legua, R. Herráez-Hernández, J. Verdú Andrés, P. Campins-Falcó, Development of a polydimethylsiloxane–thymol/nitroprusside composite based sensor involving thymol derivatization for ammonium monitoring in water samples, Sci. Total Environ. 503–504 (2015) 105–112. https://doi.org/10.1016/j.scitotenv.2014.07.077.

[295] M.C. Prieto-Blanco, A. Ballester-Caudet, F.J. Souto-Varela, P. López-Mahía, P. Campíns-Falcó, Rapid evaluation of ammonium in different rain events minimizing needed volume by a cost-effective and sustainable PDMS supported solid sensor, Environ. Pollut. 265 (2020) 114911. https://doi.org/10.1016/j.envpol.2020.114911.

[296] S. Bocanegra-Rodríguez, C. Molins-Legua, P. Campíns-Falcó, Luminol Doped Silica-Polymer Sensor for Portable Organic Amino Nitrogen and Ammonium Determination in Water, Separations. 8 (2021) 149. https://doi.org/10.3390/separations8090149.

[297] J.D. Cline, Spectrophotometric determination of nitrogen sulfide in natural waters, Limnol. Oceanogr. 14 (1969) 454–458. https://doi.org/10.4319/lo.1969.14.3.0454.

[298] D. Moreno-González, P. Pérez-Ortega, B. Gilbert-López, A. Molina-Díaz, J.F. García-Reyes, A.R. Fernández-Alba, Evaluation of nanoflow liquid chromatography high resolution mass spectrometry for pesticide residue analysis in food, J. Chromatogr. A. 1512 (2017) 78–87. https://doi.org/10.1016/j.chroma.2017.07.019.

[299] J. Pla-Tolós, Y. Moliner-Martínez, C. Molins-Legua, R. Herráez-Hernández, J. Verdú-Andrés, P. Campíns-Falcó, Selective and sentivive method based on capillary liquid chromatography with in-tube solid phase microextraction for determination of monochloramine in water, J. Chromatogr. A. 1388 (2015) 17–23. https://doi.org/10.1016/j.chroma.2015.02.024.

[300] A. Gustavo González, M. Ángeles Herrador, A practical guide to analytical method validation, including measurement uncertainty and accuracy profiles, TrAC - Trends Anal. Chem. 26 (2007) 227–238. https://doi.org/10.1016/j.trac.2007.01.009.

[301] F. Rahimi, S. Chatzimichail, A. Saifuddin, A.J. Surman, S.D. Taylor-Robinson, A. Salehi-Reyhani, A Review of Portable High-Performance Liquid Chromatography: the Future of the Field?, Springer Berlin Heidelberg, 2020. https://doi.org/10.1007/s10337-020-03944-6.

[302] S. Sharma, L.T. Tolley, H.D. Tolley, A. Plistil, S.D. Stearns, M.L. Lee, Hand-portable liquid chromatographic instrumentation, J. Chromatogr. A. 1421 (2015) 38–47. https://doi.org/10.1016/j.chroma.2015.07.119.

[303] J.P.R. Sorensen, A. Baker, S.A. Cumberland, D.J. Lapworth, A.M. MacDonald, S. Pedley, R.G. Taylor, J.S.T. Ward, Real-time detection of faecally contaminated drinking water with tryptophan-like fluorescence: defining threshold values, Sci. Total Environ. 622–623 (2018) 1250–1257. https://doi.org/10.1016/j.scitotenv.2017.11.162.

[304] N. Hudson, A. Baker, D. Ward, D.M. Reynolds, C. Brunsdon, C. Carliell-Marquet, S. Browning, Can fluorescence spectrometry be used as a surrogate for the Biochemical Oxygen Demand (BOD) test in water quality assessment? An example from South West England, Sci. Total Environ. 391 (2008) 149–158. https://doi.org/10.1016/j.scitotenv.2007.10.054.

[305] J.S.T. Ward, D.J. Lapworth, D.S. Read, S. Pedley, S.T. Banda, M. Monjerezi, G. Gwengweya, A.M. MacDonald, Tryptophan-like fluorescence as a high-level screening tool for detecting microbial contamination in drinking water, Sci. Total Environ. 750 (2021) 141284. https://doi.org/10.1016/j.scitotenv.2020.141284.

[306] S. Meseguer-Lloret, C. Molins-Legua, J. Verdú-Andrés, P. Campíns-Falcó, Chemiluminescent Method for Detection of Eutrophication Sources by Estimation of Organic Amino Nitrogen and Ammonium in Water, Anal. Chem. 78 (2006) 7504–7510. https://doi.org/10.1021/ac0604437.

[307] S.J. Lehotay, K.A. Son, H. Kwon, U. Koesukwiwat, W. Fu, K. Mastovska, E. Hoh, N. Leepipatpiboon, Comparison of QuEChERS sample preparation methods for the analysis of pesticide residues in fruits and vegetables, J. Chromatogr. A. 1217 (2010) 2548–2560. https://doi.org/10.1016/j.chroma.2010.01.044.

[308] A.J. Cummings, M.L. King, B.K. Martin, a Kinetic Study of Drug Elimination: the Excretion of Paracetamol and Its Metabolites in Manmetabolites in Man, Br. J. Pharmacol. Chemother. 29 (1967) 150–157. https://doi.org/10.1111/j.1476-5381.1967.tb01948.x.

[309] L.S. Jensen, J. Valentine, R.W. Milne, A.M. Evans, The quantification of paracetamol, paracetamol glucuronide and paracetamol sulphate in plasma and urine using a single high-performance liquid chromatography assay, J. Pharm. Biomed. Anal. 34 (2004) 585–593. https://doi.org/10.1016/S0731-7085(03)00573-9.

[310] M.C. Bhowmik, M. Misbahuddin, H.A. Bhuiyan, Estimation of paracetamol in urine to assess the diurnal variation, Bangabandhu Sheikh Mujib Med. Univ. J. 11 (2018) 193. https://doi.org/10.3329/bsmmuj.v11i2.36780.

[311] D. Kietzmann, K.W. Bock, B. Krähmer, D. Kettler, J. Bircher, Paracetamol test: Modification by renal function, urine flow and pH, Eur. J. Clin. Pharmacol. 39 (1990) 245–251. https://doi.org/10.1007/BF00315104.

[312] B.H. Rumack, H. Matthew, Acetaminophen Poisoning and Toxicity, Pediatrics. 55 (1975) 871–876.

[313] R. Ma, J. Stegemeier, C. Levard, J.G. Dale, C.W. Noack, T. Yang, G.E. Brown, G. V. Lowry, Sulfidation of copper oxide nanoparticles and properties of resulting copper sulfide, Environ. Sci. Nano. 1 (2014)

347–357. https://doi.org/10.1039/C4EN00018H.

[314] A. Gogos, B. Thalmann, A. Voegelin, R. Kaegi, Sulfidation kinetics of copper oxide nanoparticles, Environ. Sci. Nano. 4 (2017) 1733–1741. https://doi.org/10.1039/C7EN00309A.

ANNEXES

A1. Abbreviations

Abbreviation	Definition
Aa	Amino acid
ACN	Acetonitrile
AD	Amperometric detection
AFM	Atomic force microscopy
AgNPs	Silver nanoparticles
APAP	Acetaminophen
APAP-glu	Acetaminophen glucoronide
APAP-sulf	Acetaminophen sulfate
API	Atmospheric pressure ionization
AuNPs	Gold nanoparticles
BETTER	portaBle fiEld Testing sTandard framEwoRk
C18	Octadecylsilane
C8	Octylsilane
CAF	Caffein
CapLC	Capillary liquid chromatography
CEC	Contaminant of emerging concern
CFS	Continuous flow system
CTAB	Cetyltrimethylammonium bromide
D.c.	Direct current
DAD	Diode array detector
DART	Direct analysis in real time
DBDI	Dielectric barrier discharge ionization
DIN	Dissolved inorganic nitrogen
DLLME	Dispersive liquid-liquid microextraction

Abbreviation	Definition
DLS	Dynamic light scattering
DMP	Dimethyl Phthalate
DOM	Dissolved organic matter
DPV	Differential pulse voltammetry
DRN	Diuron
EIC	Extracted ion chromatogram
EMP	Electrolysis micropump
Er	Relative error
ESI	Electrospray ionization
FLD	Fluorescence detector
FMT	Fluometuron
FTIR	Fourier transformation infrared
GC	Gas chromatography
HAc	Acetic acid
HPLC	High performance liquid chromatography
HSSE	Head-space sorptive extraction
I.d.	Internal diameter
ICP	Inductively coupled plasma
IMZ	Imazalil
IPT	Isoproturon
IT-SPME	In-tube solid phase microextraction
LC	Liquid chromatography
LED	Light emitting diode
LLE	Liquid-liquid extraction
LOD	Limit of detection

Abbreviation	Definition
LOQ	Limit of quantification
LSPR	Localized surface plasmon of resonance
μESI	Micro electrospray ionization
μPAC	Micropillar array column
MBZ	Metribuzin
MeOH	Methanol
MinLC	Miniaturized liquid chromatography
MIT-SPME	Magnetic in-tube solid phase microextraction
MNPs	Metallic nanoparticles
MS	Mass detector
MS/MS	Tandem mass spectrometry
MTEOS	Methyltriethoxysilane
MWCNTs	Multi-wall carbon nanotubes
N.a.	Not available
N.d.	Not detected
NanoLC	Nano liquid chromatography
NAPQI	N acetil-p-benzoquinona imina
nESI	Nano electrospray ionization
NMNPs	Noble metal nanoparticles
NPs	Nanoparticles
$\bar{\omega}$	Average peak width
OPP	O-phenyl phenol
PA	β-phenylalanine
PAH	Polycyclic aromatic compound
PBS	Phosphate buffered-saline

Abbreviation	Definition
PC	Peak capacity
PDMS	Polydimethylsiloxane
PEG	Polyethylene glycol
PMA	Pyrimethanil
POC	Point of care
PP	Penalty point
PPL	Proxyphylline
PS	Potassium Sorbate
PVA	Polyvinyl alcohol
PVP	Polyvinylpyrrolidone
QqQ	Triple quadrupole
QTOF	Quadrupole time-of-flight
R	Recovery
R^2	Determination coefficient
ROS	Reactive oxygen specie
RP	Reverse phase
Sav	Arithmetic mean of HEXAGON 0 - 4 scale
SBSE	Stir bar sorptive extraction
SDME	Single-drop microextraction
SDS	Sodium dodecyl sulfate
SEM	Scanning electron microscopy
SPE	Solid phase extraction
SPME	Solid phase microextracction
SPN	Spermine
SPR	Surface plasmon of resonance

Abbreviation	Definition
SWCNTs	Single-wall carbon nanotubes
SWV	Square wave voltammetry
T	Tyrosine
TBM	Theobromine
TBN-m	Tribenuron-methyl
TEM	Transmission electronic microscopy
TEOS	Tetraethyl orthosilicate
t_G	Gradient run time
TIC	Total ion chromatogram
TPL	Theophylline
t_r	Retention time
TY	Tryptophan
UHPLC	Ultra high-performance liquid chromatography
UV-vis	Ultraviolet-visible
WHO	World Health Organization
XRD	X-ray diffraction

A2. List of figures

p.

Figure 1. Number of publications in the Web of Science database in the last 25 years with topics “green chemistry” and “sustainable chemistry”. Consulted in June 2023. 3

Figure 2. Evolution of the number of publications (a) and number of citations (b) for the topic “portable instrumentation” using the Web of Science database. Consulted in June 2023. 8

Figure 3. Evolution (a) and total number of publications (b) in the last 10 years with the topic “liquid chromatography”, “spectrometry”, “spectroscopy”, and “electrochemical” and refined by “portable”. Consulted in June 2023. 9

Figure 4. Size comparison of analytical columns for the different levels of miniaturization. 11

Figure 5. Number of publications reported over the last 45 years with the search topic “Capillary LC” and “Nano LC”. Source: Scopus database. 12

Figure 6. Percentage of publications reported in the Scopus database according to the field of application for the topics a) capillary LC, b) nano LC, and c) HPLC. 12

Figure 7. Schematic representation of switching column configurations using a) trap column and b) IT-SPME capillary. 19

Figure 8. Different flow-cells for UV-vis detection. a) Z-shaped, b) U-shaped, and c) on-column detection. 23

Figure 9. Schematic representation of a DART-MS system where a) is the DART ion source, b) is the sample mesh holder, and c) is the MS detector. 25

Figure 10. Timeline with the different developed portable LC and its main features. 26

Figure 11. Size comparison between a benchtop (left) and portable LC (right) 35

Figure 12. Schematic representation of a portable LC platform showing the different possibilities for injector, pumping system, analytical columns, power supply, and detection system. 36

Figure 13. Percentage of different applications for portable instrumentation. Source: Web of Science, consulted in January 2023. 45

Figure 14. Schematic representation of the Axcend Focus LC (left) and the interchangeable cartridge (right). 1) Interchangeable cartridge, 2) Syringe pumps, 3) battery, 4) injection valve, 5) mixing valve, 6) waste vial, 7) solvent vial, 8) analytical column, 9) on-column UV-LED detector, and 10) to waste capillary. 46

Figure 15. Schematic representation of the APAP main metabolic pathways. 56

Figure 16. Evolution of the number of publications with time using the following searching topics in the Web of Science database: “AgNPs” or “silver nanoparticles” (blue bars) and “AuNPs” or “gold nanoparticles” (red bars). 60

Figure 17. Schematic representation of the LSPR showing the oscillation of the free conduction electron in metallic nanoparticles under resonant excitation of electromagnetic radiation. 60

Figure 18. Schematic representation of the AuNPs induced aggregation by spermine. The spermine stabilizes the aggregation thanks to the affinity of its amino groups for the nanoparticle surface. The aggregation produces a shift in the AuNPs LSPR resulting in a colour change from red to blue [247]. 63

Figure 19. Tree diagram of the different NPs transformations in the environment. 64

Figure 20. Graphical resume of the main AgNPs transformations in the environment. 65

Figure 21. Hazard pictograms according to the CLP regulation (EC) No 1268/2008 75

Figure 22. a) Ocean Optics optical fiber portable spectrophotometer, b) Thesthys UV500 nitrate analyzer, and c) Agilent Cary60 UV-vis spectrophotometer 80

Figure 23. Benchtop Agilent Cary Eclipse fluorescence spectrometer. 81

Figure 24. a) Ion Sense DART SVP ion source interface and b) Quick Strip sample holder. 82

Figure 25. Agilent 7900 ICP-MS detector with an ASX-500 autosampler. 83

Figure 26. Agilent 1260 infinity series capillary LC equipped with a Rheodyne 7721-I injection valve for sample injection. 84

Figure 27. Axcend Focus portable miniaturized LC. 85

Figure 28. Agilent 6546 LC/QTOF equipped with an ESI interface. The analytical separation was carried out using an Agilent 1290 Infinity II series UHPLC. 86

Figure 29. Schematic representation of the APAP sample collection and treatment. 87

Figure 30. a) Two-valve injection system where a first valve is used for trespassing the sample to the second valve where the IT-SPME takes place and b) close-up of the second valve where the IT-SPME capillary can be seen. 88

Figure 31. Schematic representation of the two-valve configuration IT-SPME used. V1 and V2 are 6 – port and 2 – way, and 10 – port and 2 – way injection valves respectively. The extractive phase for the IT-SPME consist of a TEOS-MTEOS polymer enhanced with SiO_2 nanoparticles. 89

Figure 32. Reaction between the N,N-dimethyl-p-phenylenediamine with hydrogen sulfide and iron (III) chloride to form methylene blue in acidic media. 93

Figure 33. Diagram of the continuous flow system. 1. Reagent bottles, 2. peristaltic pumps, 3. t-union, 4. reactor, and 5. fraction collector. 95

Figure 34. Filter distribution inside the reactor. 95

Figure 35. Chromatogram obtained for the multicomponent mixture for the portable minLC, the asterisk (*) shows the PS peak obtained for the analysis carried out using ACN and water with 0.1 % of formic acid as mobile phase solvents. 107

Figure 36. Chromatograms obtained for the multicomponent mixture with the benchtop capLC (a) and nanoLC with 50 mm × 0.075 mm column (b) and 150 mm × 0.1 mm column (c). The chromatograms were obtained at three different wavelengths. 108

Figure 37. Chromatograms obtained for (a) theophylline and (b) theobromine at different number of injections. 111

Figure 38. Chromatograms obtained for caffeine at laboratory conditions (a) 22 °C and 45% humidity, field conditions (b) 14 °C, 68% humidity and 25 $km \cdot h^{-1}$ wind (c) field conditions 7 °C, 73% humidity and 15 km/h wind. 116

Figure 39. Chromatograms obtained for “sample 1” using the portable LC (a), benchtop capLC (b) and benchtop nanoLC (150 mm × 0.1 mm, 35 µm column) (c). 118

Figure 40. Chromatograms obtained for “sample 2” using the portable LC (a), benchtop capLC (b) and benchtop nanoLC (150 mm × 0.1 mm, 35 µm column) (c). 119

Figure 41. Chromatograms obtained for “sample 3” using the portable LC (a), benchtop capLC (b) and benchtop nanoLC (150 mm × 0.1 mm, 35 µm column) (c). 120

Figure 42. Normalized UV spectra for observed peaks in samples analysed by means of the benchtop nanoLC (see Figures 38, 39, and 40). The spectra correspond to a) potassium sorbate (t_r = 3.3 min) found in sample 1, b) pyrimethanil (t_r = 17.4 min) found in sample 2, and c) imazalil (t_r = 22.9 min) found in sample 2. 121

Figure 43. Table and radar chart with the different assessments of BETTER criteria (higher grades means better results). 123

Figure 44. Penalty points assignment to the variables evaluated through the hexagon tool for the three LCs. 125

Figure 45. Hexagon tool for capLC nanoLC (left) and Portable minLC (right). 126

Figure 46. UV spectra of nitrate standard solutions in a) analyzer, b) benchtop spectrophotometer, and c) portable optical fiber spectrophotometer 128

Figure 47. Impact of different levels of turbidity (left) and humic acids (right) on the absorbance measurement (A_{220}-2·A_{270}) of a 15 mg·L^{-1} nitrate solution. 129

Figure 48. a) Estimated NO_3^- concentration over time obtained by means of the NO_3^- analyzer in a treatment plant of drinking water in continuous mode. b) Estimated NO_3^- concentrations found in treated water to remove NO_3^- by means of the analyzer in continuous mode and the optical fiber probe in collected samples. 130

Figure 49.Excitation vs. emission wavelengths obtained by the benchtop fluorescence instrument for: a) tryptophan 1 mg·L^{-1}, b) tyrosine 10 mg·L^{-1}, and c) β-phenylalanine 10 mg·L^{-1}. 132

Figure 50. Chromatograms obtained for the different elution fractions for a spiked water sample with 10 µg·L^{-1} of IPT and 10 µg·L^{-1} of DRN. 135

Figure 51. a) Chromatogram obtained for a well sample with and without fortification of DRN and IPT at 0.25 and 0.5 $\mu g \cdot L^{-1}$ by portable minLC. b) TIC and EIC at m/z: 233.0247 and 208.1494 for a well water sample with and without DRN and IPT fortification. (250 $\mu g \cdot L^{-1}$ for each analyte) by UHPLC-MS. c) Chromatograms obtained at 250 nm for a well water sample with and without DRN and IPT fortification (50 $\mu g \cdot L^{-1}$ of each analyte) by IT-SPME coupled on-line with nanoLC-DAD. 136

Figure 52. Chromatograms corresponding to a 200 $\mu g \cdot L^{-1}$ APAP standard solution with different initial mobile phase compositions and a re-equilibration time of 10 min. 139

Figure 53. Effect of re-equilibration time on the chromatographic profile for a 0 h urine sample fortified with 234 $\mu g \cdot L^{-1}$ of APAP (left). Comparison of the retention time for successive injections of 32 $\mu g \cdot L^{-1}$ of APAP working at 10 min of re-equilibration time (right). APAP peak is marked with an asterisk (*) in the figure. 140

Figure 54. Chromatogram obtained for 0.47 $\mu g \cdot L^{-1}$ of APAP in 0 h urine sample. 141

Figure 55. Extracted ion chromatogram (152.0693 m/z) for urine samples just before (0 h) and 2, 6 and 7 hours after APAP intake with (f) and without 18·$mg \cdot L^{-1}$ APAP fortification. 143

Figure 56. Urine sample chromatograms for 0, 2, 5, 6 and 7 h after 1 g of APAP intake. The normalized UV spectra for APAP chromatographic peak in sample and standard is shown. 144

Figure 57. TIC for 2 h urine sample and its EIC compared to blank and APAP spiked sample at m/z: 152.0693. 145

Figure 58. DART records for standar additions of 0 (P0), 9 (P1), 18 (P2), 26 (P3) and 32 (P4) $mg \cdot L^{-1}$ of APAP on 0 h (a), 2 h (b), 5 h (c), 6 h (d) and 7 h (e) urine samples. Each solution is measured twice. 146

Figure 59. a) Found APAP concentration and b) accumulated concentration for the samples at different times after dosage. 147

Figure 60. HEXAGON tool for a) IT-SPME-nanoLC-DAD, b) UHPLC-ESI-QTOF, and c) DART-QTOF. 149

Figure 61. Penalty points assignment to the variables evaluated through the hexagon tool for the three LCs. 150

Figure 62. Chromatogram obtained by IT-SPME-capLC-DAD for 20 nm citrate capped AgNPs diluted 1:8 (inset: normalized (N) UV-vis spectra obtained for each chromatographic peak). 153

Figure 63. a) Degradation with time for different dilutions of 20 nm citrate capped AgNPs. The normalized SPR for the two chromatographic peaks at t_0 (continuous line) and after 1 h and 1 d (dotted line) for 1:5, 1:10 and 1:20 dilutions are shown in figures (b), (c), and (d) respectively 154

Figure 64. Degradation with time for different dilutions of 20 nm citrate capped AuNPs. 154

Figure 65. a) Chromatographic profile obtained by IT-SPME-capLC for commercial citrate capped AgNPs with different core sizes and acetic acid induced aggregation profiles as function of time for b) citrate capped AgNPs 20 nm diluted 1:2 in HAc 0.2 % (v/v), c) citrate capped AuNPs 20 nm diluted 1:4 in HAc 10 % (v/v), d) phosphate capped AuNPs 20 nm diluted 1:4 in 0.2 HAc (v/v), and e) a mixture of citrate capped AuNPs and AgNPs 20 nm diluted 1:4 in HAc 0.7 % (v/v) obtained by UV-vis spectroscopy . 156

Figure 66. Chromatographic aggregation profiles obtained by IT-SPME-nanoLC-DAD for AgNPs 20 nm core with citrate capping and HAc concentration of 0.2 % (v/v) (a) and its UV-vis spectra for peak 1 (t_r = 3.6 min) and peak 2 (t_r = 5.0 min) (b), and for AuNPs 20 nm core with citrate capping and HAc concentration of 10 % (v/v) (c) and its UV-vis spectra for peak 1 (t_r = 2.7 min) and peak 2 (5.0 min) (d). 157

Figure 67. UV-vis spectra for AuNPs 20 nm with phosphate capping and HAc concentration of 10 % (v/v). P1, P2, and P3 corresponds to the chromatographic peaks at 3.8 min, 5.0 min, and 7.9 min. 157

Figure 68. Chromatographic aggregation profiles obtained by IT-SPME-nanoLC-DAD for a mixture of AgNPs and AuNPs 20 nm core with citrate capping and HAc concentration of 0.67 % (v/v) (a) and its UV-vis spectra for peak 1 (t_r = 4.3 min), peak 2 (t_r = 7.0 min), and peak 3 (t_r = 9.3 min) (b). The chromatograms were registered at both SPR band maximum wavelengths, 400 nm, and 530 nm respectively for AgNPs and AuNPs. 158

Figure 69. Chromatographic profiles obtained for the different batches of naked AuNPs corresponding to AuNPs I (a) and AuNPs II (b) 159

Figure 70. Chromatograms obtained for naked AuNPs I in function of: a) the added spermine and b) the added acetic acid. Insents: variations of the LSPR of the second chromatographic peak (t_r = 3.0 min). 160

Figure 71. Chromatograms obtained for naked AuNPs I in function of: a) the added spermine and b) the added acetic acid. Insents: variations of the LSPR of the second chromatographic peak (t_r = 3.0 min). 161

Figure 72. a) Chromatographic profiles of AuNPs I for a healthy volunteer and cancer patient. Inset: normalized UV-vis spectra at chromatographic peak (t_r = 3.0 min). b) and c) normalized UV-vis spectra showing the LSPR variation at the chromatographic peak (t_r = 3.0 min) for healthy volunteer and cancer patient respectively. 162

Figure 73. Chromatographic profiles obtained for the naked AuNPs I, for the blank acidic extract, urine sample, and spiked urine sample. 164

Figure 74. a) Silver dissolution profile at 1 $mL \cdot min^{-1}$ at different Na_2S concentrations in anaerobic conditions. b) and c) variation of the concentration of sulfide in samples and in the initial solution for 0.1 mM and 0.5 mM of Na_2S respectively. 166

Figure 75. Schematic representation of the proposed sulfidation process with the formation of an amorphous Ag_2S previous the formation of the crystalline Ag_2S layer. 167

Figure 76. AgNPs dissolution profile at different Na_2S concentrations in aerobic (a) and anaerobic (b) conditions, 168

Figure 77. Effect of the filter pre-treatment with Cu^{2+} and the $NaNO_3$ concentration on the dissolution profile of AgNPs. The assay was carried out at pH = 7 and aerobic conditions. 169

Figure 78. a) AgNPs dissolution profile for different flow-rates. b) Normalized results showing the dissolution rate in function of the total volume. The assays were carried out at pH = 7, aerobic conditions, $NaNO_3$ 0.01 M in the media, and filter pre-treatment. 170

Figure 79. AgNPs dissolution profile at different sulfide concentrations at: a) 5.0 $mL \cdot min^{-1}$, b) 1.0 $mL \cdot min^{-1}$, and c) 0.2 $mL \cdot min^{-1}$. The assays were carried out at pH = 7, aerobic conditions, $NaNO_3$ 0.01 M in the media, and filter pre-treatment. 171

A3. List of tables

p.

Table 1. Liquid chromatography denominations attending to the analytical column internal diameter and flow rate [25]. 11

Table 2. Main reviews with the topic of miniaturized liquid chromatography instrumentation and applications in the last 10 years 17

Table 3. Conditions of the reported applications of IT-SPME coupled to Cap/NanoLC in the last 10 years (from 2013 to 2023) 21

Table 4. Examples of different detection systems for miniaturized LC. 22

Table 5. Portability related characteristics of developed portable LC 33

Table 6. Pumping system specifications for portable LC. 38

Table 7. Injectors specifications for portable LC. 40

Table 8. Column and detector specifications for the different portable LC. 44

Table 9. Classification, octanol-water partition coefficient, and structure of the studied pesticides. LogK_{ow} were obtained from PubChem database. 49

Table 10. Classification, octanol-water partition coefficient, and structure of the studied drugs. LogK_{ow} were obtained from PubChem database. 51

Table 11. European legislation concerning the N compounds in water 52

Table 12. Main techniques used for nanoparticle characterization. 59

Table 13. List of the chemicals used during the thesis, supplier, and hazard identification. The suppliers are the following: Merck (Rahway, NJ, USA), Panreac (Barcelona, España), Scharlau (Barcelona, España), Sigma (St. Louis, MO, USA), and VWR Chemicals (Radnor, PA, USA). 76

Table 14. Working conditions for the different UV-vis spectrophotometer. 80

Table 15. Working conditions for the different UV-vis spectrophotometer. 81

Table 16. Chromatographic conditions for capLC. Injection configuration, analytical column, mobile phase composition, flow rate (F_R), injection volume (I_V), and detection technique for the different studied analytes are shown. 97

Table 17. Chromatographic conditions for nanoLC. Injection configuration, analytical column, mobile phase composition, flow rate (F_R), injection volume (I_V), and detection technique for the different studied analytes are shown. 98

Table 18. Chromatographic conditions for portable minLC. Injection configuration, analytical column, mobile phase composition, flow rate (F_R), injection volume (I_V), and detection technique for the different studied analytes are shown. 99

Table 19. Chromatographic conditions for UHPLC-ESI-MS. Injection configuration, analytical column, mobile phase composition, flow rate (F_R), injection volume (I_V), and detection technique for the different studied analytes are shown. 99

Table 20. Concentration of the analytes for the different analysed multicomponent mixtures. 100

Table 21. Peak widths at 4σ (ω) obtained for the multicomponent mixtures by the software of the LC instruments used: portable LC (100 × 0.15 mm, 1.7 µm, loop volume 40 nL), benchtop capLC (150 × 0.5 mm, 5 µm, loop volume 16 µL), and benchtop nanoLC (150 × 0.1 mm, 3.5 µm, loop volume 440 nL). 110

Table 22. Figures of merit obtained for determination of target analytes by means of a portable minLC. Regression line, regression coefficient (R^2), working range, limit of detection (LOD), relative error (Er) and recovery (R) are shown. * Solvents A and B of the mobile phase contained 0.1% of formic acid. 113

Table 23. Figures of merit obtained for determination of target analytes by means of a benchtop capLC. Regression line, regression coefficient (R^2), working range, limit of detection (LOD), relative error (Er) and recovery (R) are shown. *LOD estimated at 255 nm. 114

Table 24. Figures of merit obtained for determination of target analytes by means of a benchtop nanoLC. Regression line, regression coefficient (R^2), working range, limit of detection (LOD), relative error (Er) and recovery (R) are shown. *LOD estimated at 255 nm. 115

Table 25. Pesticide concentrations found in samples (mean ± IR 95%). 117

Table 26. Figures of merit of the studied instruments (benchtop spectrophotometer, portable optical fiber probe, and nitrate analyzer) including the regression line equation ($y = a + b \cdot x$), regression coefficient, LOD, and LOQ for the analysis of different analytes. 127

Table 27. Found nitrate concentrations in different well waters sources with the nitrate analyzer and the benchtop spectrophotometer M1: Sea water; M2: Well water; M3: Transition water; M4: Fountain water; M5: Well water (2); M6: Lagoon water. 131

Table 28. Figures of merit of the studied benchtop fluorometer and the portable optical fiber probe, including the regression line equation ($y = a + b \cdot x$), regression coefficient, LOD, and LOQ for the analysis of different amino acids. 133

Table 29. Standard addition calibration curve parameters (slope (b) and its standard deviation (s_b), y-intercept (a) and its standard deviation (s_a) and coefficient of determination (R^2)) for the APAP determination by means of the IT-SPME-nanoLC-DAD. The working range is comprised between 15 to 100 $\mu g \cdot L^{-1}$ (n = 5). 141

Table 30. Standard addition calibration curve parameters (slope (b) and its standard deviation (s_b), y-intercept (a) and its standard deviation (s_a) and coefficient of determination (R^2)) for the APAP determination by means of the UHPLC-ESI-QTOF. The working range is comprised between 8 to 64 $\mu g \cdot L^{-1}$ (n = 6). 142

Table 31. Standard addition calibration curve parameters (slope (b) and its standard deviation (s_b), y-intercept (a) and its standard deviation (s_a) and coefficient of determination (R^2)) for the APAP determination by means of the DART-QTOF. The working range is comprised between 10 to 35 $mg \cdot L^{-1}$ (n = 5). 143

Table 32. Quantification results of urine samples using the IT-SPME-nLC-DAD, UHPLC-ESI-MS, and DART-MS (n = 3). 146

Table 33. Matrices studied throughout the thesis: selected samples, determined analytes, and analysis techniques employed. 175

A4. PhD contribution to publications

- Sanjuan-Navarro, L., **Cortés-Bautista, S.**, Moliner-Martínez, Y., Campíns-Falcó, P. In-tube solid phase microextraction coupled to miniaturized liquid chromatography for both, noble metal nanoparticles assessment and sensitive plasmonic assay development. Anal. Chem. 1171, 338665 (2021). **Contribution 50%**
- **S. Cortés-Bautista**, R. Navarro-Utiel, A. Ballester-Caudet y P. Campins-Falcó. Towards in field miniaturized liquid chromatography: Biocides in wastewaters as proof of concept. J. Cromatogr. A. 1673, 463119 (2022)**. Contribution 50 %**
- **S. Cortés-Bautista**, H. R. Robles-Jimárez, I. Carrero-Ferrer, C. Molins-Legua, P. Campins-Falcó. Portable determination for legislated dissolved nitrogen forms in several environmental water samples as a study case. Sci. Total Environ. 864, 161131 (2023). **Contribution 50 %**
- **S. Cortés-Bautista**, P. Campins-Falcó. Portable liquid chromatography, in: Encyclopaedia of Analytical Chemistry, Wiley. (In edition). **Contribution 100 %**
- **S. Cortés-Bautista**, C. Molins-Legua, P. Campins-Falcó. Miniaturized liquid chromatography in environmental analysis. A review. (In preparation). **Contribution 100 %**
- **S. Cortés-Bautista**, R. Navarro-Utiel, P. Campins-Falcó. Direct analysis in in real-time mass mass spectrometry for rapid determination of acetaminophen in urine samples. (In preparation) **Contribution 50 %**